

**THE SURFACE CRACK PROBLEM
FOR A FUNCTIONALLY GRADED COATING
BONDED TO A HOMOGENEOUS LAYER**

**Fazil Erdogan
and
Maheendra Kasmalkar**

**Lehigh University
Bethlehem, PA 18015**

October 2000

**AIR FORCE OFFICE OF SCIENTIFIC RESEARCH
GRANT F49620-98-1-0028**

DISTRIBUTION STATEMENT A
Approved for Public Release
Distribution Unlimited

20010419 098

DTIC CONVERSATION RECORD FOR DISTRIBUTION STATEMENT REQUEST

DTIC Personnel Making Call

JACK RIKE

Date

17 April 02

Time

1436

Authorizing Official

F. Erdogan

Phone

Agency

LEHIGH UNIV. MECH. Engineering : Mechanics

Title

Internet Document URL (if applicable)

Distribution Statement (Please check one box)

- ☒ DISTRIBUTION STATEMENT A: Approved for public release. Distribution is unlimited.
- ☐ DISTRIBUTION STATEMENT B: Distribution authorized to U.S. Government Agencies only.
- ☐ DISTRIBUTION STATEMENT C: Distribution authorized to U.S. Government Agencies and their contractors.
- ☐ DISTRIBUTION STATEMENT D: Distribution authorized to U.S. Department of Defense (DoD) and U.S DoD contractors only.
- ☐ DISTRIBUTION STATEMENT E: Distribution authorized to U.S. Department of Defense (DoD) components only.
- ☐ DISTRIBUTION STATEMENT F: Further dissemination only as directed by the controlling DoD office indicated below or by higher authority.
- ☐ DISTRIBUTION STATEMENT X: Distribution authorized to U.S. Government agencies and private individuals or enterprises eligible to obtain export-controlled technical data in accordance with DoD Directive 5230.25, Withholding of Unclassified Technical Data from Public Disclosure, 6 Nov 84.

Reason for the above identified distribution statement (in accordance with DoD Directive 5230.24)

Controlling Office

Date of Distribution Statement Determination

AQ Number (For DTIC-OCA Use Only)

**THE SURFACE CRACK PROBLEM
FOR A FUNCTIONALLY GRADED COATING
BONDED TO A HOMOGENEOUS LAYER**

**Fazil Erdogan
and
Maheendra Kasmalkar**

**Lehigh University
Bethlehem, PA 18015**

October 2000

**AIR FORCE OFFICE OF SCIENTIFIC RESEARCH
GRANT F49620-98-1-0028**

ABSTRACT

In the continuing search for materials which can withstand the grueling requirements of modern day applications, Functionally Graded Materials (FGMs) seem to be a promising alternative to conventional materials. These nonhomogeneous materials offer better interfacial properties by improving bond strength and reducing thermal mismatch. Before putting these materials into application, an important step in the design of FGMs is the stress analysis and fracture characterization. The fracture performance of FGM coatings on homogeneous substrates is the focus of this study.

In this study, various internal and surface crack configurations in the coating and the substrate are subjected to mechanical and thermal loads. The analysis is linear elastic. The thermo-mechanical properties of the FGM coating are assumed to vary exponentially with the spatial coordinate. The equilibrium equations are solved using integral transforms. The resulting singular integral equations are solved using numerical integration. The results of interest for this mode I formulation are the stress intensity factors and the crack opening displacements. The effects of the nonhomogeneity parameter and various dimensionless length parameters are studied.

One of the most important outcomes of this study is the theoretical proof that "kink" in material property at the interface does not introduce any singularity. In the numerical results it is observed that generally the stress intensity factors tend to increase with material nonhomogeneity. Also, it is observed that the substrate thickness tends to suppress cracking in the coating. In pure thermal loading, the surface cracks may either be arrested or there might be crack closure. The stress intensity factors from different loadings can be added up to obtain the resultant stress intensity factor for multiple loading.

Results in this study have wide-ranging applications. They can be applied to thermal barrier coatings on turbine components, combustion chambers, parts of the

airframe for the "Space Plane", soil mechanics, bone fractures and many more applications where the material is macroscopically nonhomogeneous. Thus this study solves a basic problem common to a variety of applications in diverse fields.

CHAPTER 1

INTRODUCTION

1.1 Introduction

In modern engineering applications, the requirements on materials are becoming more and more strict. The materials are subjected to grueling conditions. Conventional materials do not stand up to the high temperatures or corrosive environments. Hence there is always a need for new materials or new material systems. Most failure processes such as corrosion, wear and fatigue are surface related. Hence these failures can be controlled by controlling the material properties near and at the surface. Mere surface treatments such as surface hardening or introduction of residual compressive stresses to prevent fatigue crack initiation may not be sufficient in many applications. In such applications it is necessary either to use new materials to withstand the conditions or to provide the bulk material with a protective coating of a more resistant material. Examples of such applications include the blades in gas turbine engines which are subjected to high stresses and highly corrosive environment, machine tools undergoing excessive wear and combustion chambers which have to sustain very high temperatures upto 3000F. In all these applications it is necessary to develop new systems where conventional materials have failed.

Various attempts have been made in developing new materials for these applications[1]. The most promising ones are monolithic structural ceramics and fiber reinforced ceramics including carbon-carbon composites. The disadvantage of these ceramics is their brittle nature. This can be improved by introduction of fibers or whiskers to avoid catastrophic cracks. Carbon-carbon composites can sustain very high temperatures but have very low oxidation resistance and extraordinarily long manufacturing time.

All the new materials mentioned are essentially homogeneous. In today's demanding technological environment, these materials seem to be inadequate[2]. The main requirement is for materials to possess good thermomechanical as well as structural properties. In high temperature applications, the material is required to have high heat and corrosion resistance as well as high mechanical toughness and heat conductivity. Similarly in gears and bearings, a high degree of wear resistance and high toughness is required in the same material. Homogeneous materials seem to fail in one regard or another. Hence the idea of coating the substrate with a heat-resistant ceramic layer, called the thermal barrier coating, appears very attractive. Here is where composites seem to find widespread acceptance in industry.

One of the earliest applications of composites may have been in protection against corrosion by using a variety of coatings. Composite materials are designed to utilize the mechanical properties of the component materials so as to optimize certain physical bulk properties of the medium. In thermal barrier coatings, a ceramic coating is applied to the base substrate[3, 4]. Usually the substrate is some Ni based superalloy. The coating may be of Yttria-stabilized Zirconia on a bond coat of NiCoCrAlY. Zirconia makes the component heat resistant while the bond coat protects the substrate from oxidation. The mechanical strength is derived from the substrate. The disadvantage of such systems is the high thermal and residual stresses and relatively poor bonding strength.

A novel way of reducing the residual stresses and improving the bond strength between the coating and substrate is to layer the interfacial zone going from metal rich to ceramic rich compositions. For example, in joining tungsten to zirconia by introducing layers that contain 80/20, 60/40, 40/60 and 20/80 percent W/ZrO₂, it was shown that the peak value of the residual stress becomes approximately one-sixth of that obtained from direct W-ZrO₂ bonding[5]. The next logical step is the processing of fully tailored materials and interfacial zones with predetermined continuously varying volume fractions.

Such materials are referred to as "Functionally Graded Materials" (FGM). These are essentially nano-composites or fine composites having continuously varying rather than piecewise constant volume fractions. Apart from increasing the bond strength [6] and reducing the thermal stresses, grading also seems to improve the fracture toughness and fatigue and corrosion crack growth resistance parameters of thermal barrier coatings. With the advent of new techniques in powder metallurgy and in surface chemistry it is indeed possible to manufacture fully tailored functionally graded materials with varying volume fractions.

The philosophy of FGMs is different from any of the conventional materials[7]. FGMs are designed by an "Inverse Design Procedure" [8, 9] in which the material is tailored to suit the needs of any application. Various ingenious techniques are used in the synthesis of FGMs [10]. Vapor deposition techniques[11], centrifugal casting[12], combustion sintering[13, 14], plasma spraying[15] are a few of them. A good review of different manufacturing techniques can be found in [16]. Chemical and physical vapor deposition techniques can produce very clean FGMs but the processes are very slow for industrial applications. Plasma spraying is by far the most popular technique because of the relatively simple equipment and high deposition rate. The disadvantage of plasma spraying is the introduction of porosity at the substrate/coating boundary. Also, some oxide layers can form at the splat boundaries.

As the manufacturing of these materials can lead to some inherent flaws, it is important to carry out the fatigue and fracture characterization of FGMs. This requires the solution of some standard crack problems. Most flaws are surface related and under working conditions these flaws may give rise to surface cracks which can run through the component. Hence it is important to study the surface cracks and their growth under various loading conditions. This is the main problem investigated in this study.

Applications of this study are wide-ranging. The FGM layer may be the thermal barrier coating of a combustion chamber. It could be the thermal coating for microelectronic chips. A recent application is that of a "Space Plane" [17, 18]. The engine components and parts of the airframe of such a plane will be subjected to very high temperatures and FGMs are proposed as a possible material system. Nonhomogeneous materials with varying material properties also occur in various non-industrial applications. In Biomechanics, the cement line in secondary bones can be considered to be an FGM. In soil mechanics and rock fracture analysis, the results from this study could be readily applicable. Thermomechanical material nonhomogeneity may also be observed in components having highly temperature dependent properties and subjected to steep temperature profiles. The diffusion layer between two dissimilar materials is usually non-homogeneous[19]. Thus this study is attempting to solve a basic problem common to a variety of diverse fields.

1.2 Literature Survey

Literature on non homogenous materials can be classified into 3 periods. The early literature of 50s and 60s is mostly about nonhomogenous infinite or semi-infinite planes. In the 70s, emphasis was on layered structures. Here individual layers were homogenous. Interest in nonhomogeneous layers seems to have picked up in the mid-80s and is being vigorously pursued in present day research. Most of the research in FGMs is from this third period.

The early extension of the theory of elasticity to non-homogeneous bodies can be found in [20]. The early research of non-homogeneity in elasticity and plasticity can be found in the articles in [21]. Most of the articles derive equations for non-homogenous infinite or semi-infinite planes. Some solutions for displacements and stresses are found for specific forms of elastic modulus.[22]

In the 70s, the focus was on layered structures. With the advent of composites, a great deal of research was concentrated on ceramic coatings for metal substrates. These so-called cermets are precursors to the present day FGMs and hence are important for the purpose of comparison of performance with FGMs. The fracture characterization of layered structures can be found in many publications[for exg, 23 – 32]. Interface flaws[23 – 27], flaws perpendicular to the interface[27 – 31] and delamination[32] problems were extensively studied. The interest in layered structures is still continuing but is gradually being replaced by graded layers.

FGMs were looked into vigorously in the 90s. Most of the literature pertains to the design and manufacturing of FGMs. A good review of different manufacturing techniques is given in [16]. As these materials are macroscopically non-homogeneous, material characterization becomes an important issue. Thermomechanical characterization has been attempted with various different approaches. A review of the techniques on bounds of effective properties is given by Torquato[33]. Among these techniques is the variational approach developed largely by Hashin and Strickman[34]. The bounds on effective properties have been improved by various techniques such as simulation techniques, cell models and experimental techniques. Reader is referred to [33] for more references on each of these techniques.

There is still a considerable ambiguity regarding variation of properties within an FGM layer. The correlation between composition and properties is being studied extensively. Experiments using say indentation techniques to determine hardness show wide variations in results depending on the point of indentation[3]. Hence for analysis some suitable assumption has to be made for the variation of material properties. Another restriction on the analysis is that the governing equations for nonhomogeneous materials tend to be partial differential equations with variable coefficients. This has been explained in detail in Chapter 2. There is no known technique for solving such equations in a direct

way. The best approach is given by Varley et al[35]. This approach, though, is suitable only for a limited class of variations. From the foregoing discussion, it is obvious that the problem is analytically tractable only for specific variation of the material properties. A linear variation of material properties was considered in [36, 37]. Bakirtas[38] solved the problem of a rigid punch on a nonhomogeneous medium assuming an exponential variation. Exponential variation seems to be a more attractive assumption as the material property never goes to zero as in the linear case. This assumption is used in this study.

Before FGMs can be put to use in practical applications it is important to study the fracture properties of these materials to predict the service life of the components. Not much analytical work has been done in fracture mechanics of FGMs. Introduction of a crack in an infinite space was done by Konda and Erdogan[39]. The problem of an interface crack was solved by Delale and Erdogan[40]. Chen and Erdogan solved the interface crack problem for a coating[41]. Crack perpendicular to interface was first studied by Erdogan for Mode III loading[42]. Same problem was solved by Erdogan, Kaya and Joseph [43] for Mode I loading. Erdogan et al [44] also solved the problem for a nonhomogeneous diffusion layer between homogeneous half spaces. Erdogan and Ozturk [45] have studied the axisymmetric interfacial crack problem. The edge crack problem for an FGM layer was looked into by Wu and Erdogan [46]. It can be seen that the more practical problem of a crack perpendicular to the interface in an FGM coating on a substrate is yet to be solved for Mode I loading. This is the problem that is solved in this study.

Another important part of this investigation is the thermal loading and resulting thermal stresses in FGMs. This aspect has been studied in literature to some extent. Thermal stress analysis for layered cylindrical shells was done by Miller et al[47] while that for heterogeneous shells was done by Venkatarmana[48]. Numerical[49] and experimental[50] evaluation of thermal shock and thermal stresses in FGM plates have

been studied. Analytical techniques have mainly been limited to beam theory sort of approaches[51, 52]. The elasticity problem of an FGM layer under thermal loading was looked into by Wu and Erdogan[53]. Though, in most analyses, the temperature field has been separated from the displacement field, a coupled thermoelastic model has been developed by Zhang et al[54]. In this study, the temperature and displacement fields are uncoupled. Variations in both the modulus of elasticity and the coefficient of thermal expansion are considered to be exponential.

1.3 Outline of the dissertation

Chapter 1 of this study deals with the introduction of the problem, and the related literature survey.

Chapter 2 contains the statement of the problem and its formulation. The governing equations have been derived and boundary conditions stated.

In Chapter 3 the singular integral equations are derived. For different cases, the singularities and the stress intensity factors are derived.

Chapter 4 contains the numerical procedure to solve the singular integral equations. For various cases, the numerical procedures differ. These have been covered in this chapter.

Chapter 5 gives the results for some specific material properties. These results have been discussed and compared with previously published results.

In Chapter 6, conclusions drawn from this study have been listed and directions for future research are given.

The appendices A-F present some analytical details and material properties (Appendix E).

CHAPTER 2

FORMULATION OF THE PROBLEM

2.1 Geometry of the problem

The geometry of the plane elasticity problem described in the introduction is shown in Fig 2.1.

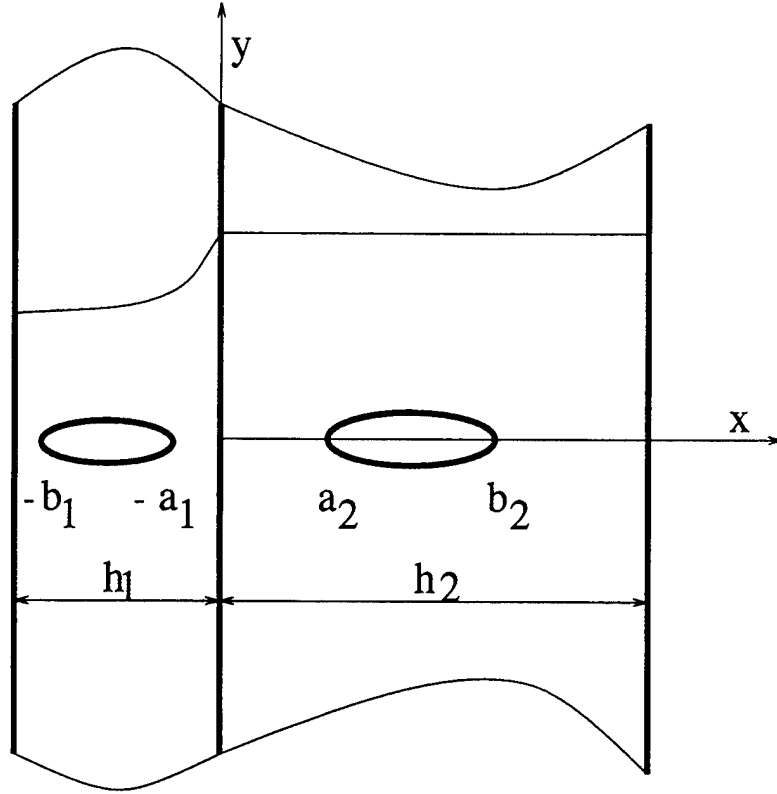


Figure 2.1 Geometry of the problem

The functionally graded coating lies to the left of the y -axis while the homogeneous substrate lies to the right. This figure shows the most general configuration. There can be various different configurations depending on the values of b_1, a_1, a_2 and b_2 . When $b_1 \neq a_1$ and $a_2 = b_2$, we obtain an internal crack in the nonhomogeneous coating only. When $b_1 = a_1$ and $a_2 \neq b_2$, we obtain an internal crack in the homogeneous

substrate only. When both $b_1 \neq a_1$ and $a_2 \neq b_2$, we obtain internal cracks in both the coating as well as in substrate. When $a_2 = b_2$, $b_1 = h_1$ and $0 < a_1 < h_1$, we obtain an edge crack in the nonhomogeneous coating. When $b_1 = h_1$ and $a_1 = 0$, $a_2 = 0$ and $0 < b_2 < h_2$, we obtain an edge crack crossing the interface. Another case would be when $0 < b_1 < h_1$, $a_1 = 0$, $a_2 = 0$ and $0 < b_2 < h_2$. In this case, there is an internal crack crossing the interface. All these cases have been considered in this study.

2.2 Solution procedure

The solution procedure involves finding the governing equations for the nonhomogeneous part as well as those for the homogeneous part. These governing equations are then solved to obtain displacements subject to the boundary conditions at the boundaries and the interface.

The displacements for the cracked nonhomogeneous strip and the cracked homogeneous strip are determined by a superimposition technique. For example, the superimposition technique for the nonhomogeneous strip is depicted in Fig 2.2.

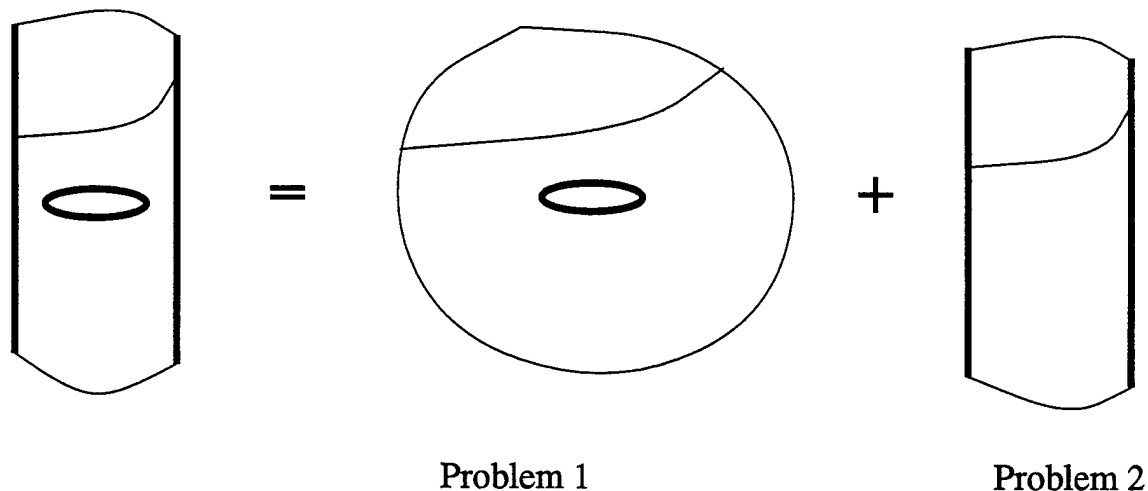


Figure 2.2 Superposition for the nonhomogeneous part

The strip is considered to be a combination of a cracked infinite space and an uncracked strip with appropriate boundary conditions applied at the boundaries. This is not the conventional superposition method as the geometries of the two problems are different. But the logic here is that, as long as the governing equations are satisfied within a domain and the boundary conditions are satisfied along the boundaries, the solution is valid. Hence the problem reduces to finding the solution of two simpler problems and adding up the solutions. Similar procedure is applied for the homogeneous strip.

2.3 Governing equations

The governing equations for the elasticity problem are the equilibrium equations. For the homogeneous part the development is straightforward. For the nonhomogeneous part, though, the shear modulus is a function of x . Hence certain assumptions need to be made to make the problem analytically tractable.

2.3.1 Navier's equations for nonhomogeneous elastic medium

The equilibrium equations for a two-dimensional elasticity problem can be expressed as

$$\frac{\partial \sigma_{xx}}{\partial x} + \frac{\partial \tau_{xy}}{\partial y} = 0, \quad (2.1)$$

$$\frac{\partial \tau_{xy}}{\partial x} + \frac{\partial \sigma_{yy}}{\partial y} = 0. \quad (2.2)$$

The relation between stresses and displacements is given by Hooke's law which can be stated as

$$\sigma_{xx} = \frac{\mu(x)}{\kappa-1} \left\{ (3-\kappa) \frac{\partial u}{\partial x} + (1+\kappa) \frac{\partial v}{\partial y} \right\}, \quad (2.3)$$

$$\sigma_{yy} = \frac{\mu(x)}{\kappa-1} \left\{ (3-\kappa) \frac{\partial u}{\partial x} + (1+\kappa) \frac{\partial v}{\partial y} \right\}, \quad (2.4)$$

$$\tau_{xy} = \mu(x) \left\{ \frac{\partial u}{\partial y} + \frac{\partial v}{\partial x} \right\} \quad (2.5)$$

where $\mu(x)$ is the shear modulus and κ is given as

$$\kappa = \begin{cases} 3-4\nu & \text{for plane strain} \\ \frac{3-\nu}{1+\nu} & \text{for generalized plane stress} \end{cases} \quad (2.6)$$

Substituting (2.3 – 2.5) into (2.1) and (2.2) and assuming that κ is constant we obtain

Navier's equations for a two-dimensional elasticity problem,

$$\begin{aligned} \mu(1+\kappa) \frac{\partial^2 u}{\partial x^2} + \mu(\kappa-1) \frac{\partial^2 u}{\partial y^2} + 2\mu \frac{\partial^2 v}{\partial x \partial y} + \frac{\partial \mu}{\partial x} (1+\kappa) \frac{\partial u}{\partial x} \\ + \frac{\partial \mu}{\partial x} (3-\kappa) \frac{\partial v}{\partial y} = 0, \end{aligned} \quad (2.7)$$

$$\begin{aligned} \mu(\kappa-1) \frac{\partial^2 v}{\partial x^2} + \mu(1+\kappa) \frac{\partial^2 v}{\partial y^2} + 2\mu \frac{\partial^2 u}{\partial x \partial y} + \frac{\partial \mu}{\partial x} (\kappa-1) \frac{\partial v}{\partial x} \\ + \frac{\partial \mu}{\partial x} (\kappa-1) \frac{\partial u}{\partial y} = 0. \end{aligned} \quad (2.8)$$

It can be seen that equations (2.7) and (2.8) are coupled partial differential equations of the second order with variable coefficients as μ is an arbitrary function of x . There is no direct analytical way to solve these differential equations. As discussed in the introduction, attempts have been made in the past to solve such equations using specific functions for $\mu(x)$. In this study it has been assumed that the shear modulus has an exponential behavior, namely,

$$\mu(x) = \mu_0 e^{(\beta x)} \quad \text{for } -h_1 < x < 0 \quad (2.9)$$

where μ_0 is the shear modulus of the homogeneous substrate and β is the nonhomogeneity parameter defined as

$$\beta = \frac{1}{h_1} \ln \left(\frac{\mu_0}{\mu_1} \right). \quad (2.10)$$

Substituting (2.9) into (2.7) and (2.8) we obtain,

$$(1+\kappa) \frac{\partial^2 u}{\partial x^2} + (\kappa-1) \frac{\partial^2 u}{\partial y^2} + 2 \frac{\partial^2 v}{\partial x \partial y} + \beta(1+\kappa) \frac{\partial u}{\partial x} + \beta(3-\kappa) \frac{\partial v}{\partial y} = 0, \quad (2.11)$$

$$(\kappa-1) \frac{\partial^2 v}{\partial x^2} + (1+\kappa) \frac{\partial^2 v}{\partial y^2} + 2 \frac{\partial^2 u}{\partial x \partial y} + \beta(\kappa-1) \frac{\partial v}{\partial x} + \beta(\kappa-1) \frac{\partial u}{\partial y} = 0. \quad (2.12)$$

Equations (2.11) and (2.12) are partial differential equations with constant coefficients and can be solved analytically.

2.3.2 Navier's equations for homogeneous elastic medium

These equations can be immediately derived from equations (2.11) and (2.12) by letting β go to zero. The equations can then be obtained as

$$(1+\kappa) \frac{\partial^2 u}{\partial x^2} + (\kappa-1) \frac{\partial^2 u}{\partial y^2} + 2 \frac{\partial^2 v}{\partial x \partial y} = 0, \quad (2.13)$$

$$(\kappa-1) \frac{\partial^2 v}{\partial x^2} + (1+\kappa) \frac{\partial^2 v}{\partial y^2} + 2 \frac{\partial^2 u}{\partial x \partial y} = 0. \quad (2.14)$$

2.3.3 Superposition technique

As discussed earlier the problem is split into two problems, one with a cracked infinite plane and other with uncracked strip. The solutions for each of these problems are

obtained in this section. The nonhomogeneous and homogeneous parts are considered separately.

2.3.3.1 Nonhomogeneous part

The superimposition technique is shown in Fig 2.2. For problem 1 (cracked infinite plane) Fourier transform with respect to x is the natural choice. For problem 2 (uncracked strip), it should be noted that u is symmetric about the x -axis while v is antisymmetric about the x -axis. Hence Cosine transform is chosen for u while Sine transform is chosen for v . In the solutions, the subscript c denotes cracked infinite plane while subscript uc denotes uncracked strip.

Solution of Problem 1

Taking Fourier transform with respect to x , we can write the displacements as

$$u_{1c} = \frac{1}{2\pi} \int_{-\infty}^{\infty} f_1(y, \alpha) e^{-i\alpha x} d\alpha, \quad (2.15)$$

$$v_{1c} = \frac{1}{2\pi} \int_{-\infty}^{\infty} g_1(y, \alpha) e^{-i\alpha x} d\alpha. \quad (2.16)$$

Substituting into equation (2.11) and (2.12) and taking Fourier inversion we obtain

$$(\kappa-1)f_1'' - (\kappa+1)(\alpha^2 + \beta i\alpha)f_1 + (\beta(3-\kappa) - 2i\alpha)g_1' = 0, \quad (2.17)$$

$$(\kappa+1)g_1'' - (\kappa-1)(\alpha^2 + \beta i\alpha)g_1 + (\beta(\kappa-1) - 2i\alpha)f_1' = 0. \quad (2.18)$$

These are coupled second order differential equations. Hence there should be four arbitrary constants. The solutions for f_1 and g_1 can then be written as

$$g_1(y, \alpha) = \sum_{j=1}^4 D_j(\alpha) e^{n_j y}, \quad (2.19)$$

$$f_1(y, \alpha) = \sum_{j=1}^4 m_j D_j(\alpha) e^{n_j y}. \quad (2.20)$$

Substituting (2.19) and (2.20) into (2.17) we obtain

$$\sum_{j=1}^4 \left\{ (\kappa-1)m_j D_j(\alpha) n_j^2 - (\kappa+1)(\alpha^2 + \beta i \alpha) m_j D_j(\alpha) + (\beta(3-\kappa) - 2i\alpha) D_j(\alpha) n_j \right\} e^{n_j y} = 0. \quad (2.21)$$

Since $e^{n_j y}$ s are linearly independent, equation (2.21) should go to zero for each value of $j = 1, 2, 3, 4$. Hence we obtain m_j as

$$m_j = \frac{(2i\alpha - \beta(3-\kappa)) n_j}{(\kappa-1)n_j^2 - (\kappa+1)(\alpha^2 + \beta i \alpha)}, \quad j = 1, 2, 3, 4. \quad (2.22)$$

On the other hand substituting (2.19) and (2.20) into (2.18) gives,

$$\sum_{j=1}^4 \left\{ (\kappa+1) D_j(\alpha) n_j^2 - (\kappa-1)(\alpha^2 + \beta i \alpha) D_j(\alpha) + (\beta(\kappa-1) - 2i\alpha) m_j D_j(\alpha) n_j \right\} e^{n_j y} = 0. \quad (2.23)$$

Again using the linear independency condition, we obtain,

$$m_j = \frac{-(\kappa+1)n_j^2 + (\kappa-1)(\alpha^2 + \beta i \alpha)}{(\beta(\kappa-1) - 2i\alpha) n_j}, \quad j = 1, 2, 3, 4. \quad (2.24)$$

Equating (2.22) and (2.24) we obtain the characteristic equation as

$$\left(n_j^2 - (\alpha^2 + \beta i \alpha)\right)^2 - \delta^2 n_j^2 = 0 \quad (2.25)$$

where

$$\delta = \sqrt{\frac{3-\kappa}{\kappa+1}} \beta. \quad (2.26)$$

This gives 4 solutions of n_j as

$$n_1 = -\frac{\delta}{2} - \frac{1}{2} \sqrt{\delta^2 + 4(\alpha^2 + \beta i \alpha)}, \quad (2.27)$$

$$n_2 = \frac{\delta}{2} - \frac{1}{2} \sqrt{\delta^2 + 4(\alpha^2 + \beta i \alpha)}, \quad (2.28)$$

$$n_3 = \frac{\delta}{2} + \frac{1}{2} \sqrt{\delta^2 + 4(\alpha^2 + \beta i \alpha)}, \quad (2.29)$$

$$n_4 = -\frac{\delta}{2} + \frac{1}{2} \sqrt{\delta^2 + 4(\alpha^2 + \beta i \alpha)}. \quad (2.30)$$

As the problem is symmetric about the x -axis, we consider only the upper half plane. Now for u and v to be bounded as y goes to ∞ , n_1 and n_2 are the only acceptable solutions.

The expressions for displacements and stresses can then be given as

$$u_{1c} = \frac{1}{2\pi} \int_{-\infty}^{\infty} \sum_{j=1}^2 m_j D_j(\alpha) e^{n_j y} e^{-i\alpha x} d\alpha, \quad (2.31)$$

$$v_{1c} = \frac{1}{2\pi} \int_{-\infty}^{\infty} \sum_{j=1}^2 D_j(\alpha) e^{n_j y} e^{-i\alpha x} d\alpha, \quad (2.32)$$

$$\sigma_{xx1c} = \frac{\mu_0 e^{(\beta x)}}{\kappa - 1} \frac{1}{2\pi} \int_{-\infty}^{\infty} \sum_{j=1}^2 \left\{ -(\kappa + 1)m_j i\alpha + (3 - \kappa)n_j \right\} D_j(\alpha) e^{n_j y} e^{-i\alpha x} d\alpha, \quad (2.33)$$

$$\sigma_{yy1c} = \frac{\mu_0 e^{(\beta x)}}{\kappa - 1} \frac{1}{2\pi} \int_{-\infty}^{\infty} \sum_{j=1}^2 \left\{ -(3 - \kappa)m_j i\alpha + (\kappa + 1)n_j \right\} D_j(\alpha) e^{n_j y} e^{-i\alpha x} d\alpha, \quad (2.34)$$

$$\tau_{xy1c} = \mu_0 e^{(\beta x)} \frac{1}{2\pi} \int_{-\infty}^{\infty} \sum_{j=1}^2 \left\{ -i\alpha + m_j n_j \right\} D_j(\alpha) e^{n_j y} e^{-i\alpha x} d\alpha. \quad (2.35)$$

Solution of Problem 2

Considering the symmetries of u and v , we take Cosine transform of u with respect to y and Sine transform of v with respect to y .

$$u_{1uc} = \frac{2}{\pi} \int_0^{\infty} f_2(x, \alpha) \cos(\alpha y) d\alpha, \quad (2.36)$$

$$v_{1uc} = \frac{2}{\pi} \int_0^{\infty} g_2(x, \alpha) \sin(\alpha y) d\alpha. \quad (2.37)$$

Substituting into (2.11) and (2.12) and taking the respective inverse transforms we obtain,

$$(\kappa + 1)f_2'' + \beta(\kappa + 1)f_2' - (\kappa - 1)\alpha^2 f_2 + 2\alpha g_2' + \beta(3 - \kappa)\alpha g_2 = 0, \quad (2.38)$$

$$(\kappa - 1)g_2'' + \beta(\kappa - 1)g_2' - (\kappa + 1)\alpha^2 f_2 - 2\alpha f_2' - \beta(\kappa - 1)\alpha f_2 = 0. \quad (2.39)$$

These are coupled second order differential equations. Hence there will be 4 arbitrary constants. The solutions can be written as

$$g_2(x, \alpha) = \sum_{j=1}^4 A_j(\alpha) e^{p_j x}, \quad (2.40)$$

$$f_2(x, \alpha) = \sum_{j=1}^4 q_j A_j(\alpha) e^{p_j x}. \quad (2.41)$$

Substituting (2.40) and (2.41) into (2.38) we obtain,

$$\sum_{j=1}^4 \left\{ (\kappa+1)q_j p_j^2 - (\kappa-1)\alpha^2 q_j + 2\alpha p_j + \beta \left((3-\kappa)\alpha + (\kappa+1)q_j p_j \right) \right\} A_j(\alpha) e^{p_j x} = 0. \quad (2.42)$$

Since $e^{p_j x}$ s are linearly independent, equation (2.42) should go to zero for each value of $j = 1, 2, 3, 4$. Hence we obtain q_j as

$$q_j = \frac{-(3-\kappa)\beta\alpha - 2\alpha p_j}{(\kappa+1)(p_j^2 + \beta p_j) - (\kappa-1)\alpha^2}. \quad (2.43)$$

On the other hand substituting (2.40) and (2.41) into (2.39) gives

$$\sum_{j=1}^4 \left\{ (\kappa-1)p_j^2 - (\kappa+1)\alpha^2 - 2\alpha q_j p_j + \beta(\kappa-1)(p_j - \alpha q_j) \right\} A_j(\alpha) e^{p_j x} = 0. \quad (2.44)$$

Using the linear independency condition we obtain,

$$q_j = \frac{(\kappa-1)(p_j^2 + \beta p_j) - (\kappa+1)\alpha^2}{2\alpha p_j + (\kappa-1)\beta\alpha}. \quad (2.45)$$

Equating (2.43) and (2.45) we obtain the characteristic equation as

$$\left\{ (p_j^2 + \beta p_j) - \alpha^2 \right\}^2 + \delta^2 \alpha^2 = 0 \quad (2.46)$$

where δ is defined in (2.26). The 4 solutions for p_j are as follows

$$p_1 = -\frac{\beta}{2} - \frac{1}{2} \sqrt{\beta^2 + 4\alpha^2 + 4i\delta\alpha}, \quad (2.47)$$

$$p_2 = -\frac{\beta}{2} - \frac{1}{2} \sqrt{\beta^2 + 4\alpha^2 - 4i\delta\alpha}, \quad (2.48)$$

$$p_3 = -\frac{\beta}{2} + \frac{1}{2} \sqrt{\beta^2 + 4\alpha^2 + 4i\delta\alpha}, \quad (2.49)$$

$$p_4 = -\frac{\beta}{2} + \frac{1}{2} \sqrt{\beta^2 + 4\alpha^2 - 4i\delta\alpha}. \quad (2.50)$$

The displacements and stresses can then be expressed as

$$u_{1uc} = \frac{2}{\pi} \int_0^\infty \sum_{j=1}^4 q_j A_j(\alpha) e^{p_j x} \cos(\alpha y) d\alpha, \quad (2.51)$$

$$v_{1uc} = \frac{2}{\pi} \int_0^\infty \sum_{j=1}^4 A_j(\alpha) e^{p_j x} \sin(\alpha y) d\alpha, \quad (2.52)$$

$$\sigma_{xx1uc} = \frac{\mu_0 e^{(\beta x)}}{\kappa - 1} \frac{2}{\pi} \int_0^\infty \sum_{j=1}^4 \left\{ (\kappa + 1) q_j p_j + (3 - \kappa) \alpha \right\} A_j(\alpha) e^{p_j x} \cos(\alpha y) d\alpha, \quad (2.53)$$

$$\sigma_{yy1uc} = \frac{\mu_0 e^{(\beta x)}}{\kappa - 1} \frac{2}{\pi} \int_0^\infty \sum_{j=1}^4 \left\{ (3 - \kappa) q_j p_j + (\kappa + 1) \alpha \right\} A_j(\alpha) e^{p_j x} \cos(\alpha y) d\alpha, \quad (2.54)$$

$$\tau_{xy1uc} = \mu_0 e^{(\beta x)} \frac{2}{\pi} \int_0^\infty \sum_{j=1}^4 \{p_j - q_j \alpha\} A_j(\alpha) e^{p_j x} \sin(\alpha y) d\alpha. \quad (2.55)$$

By superimposing these two sets of solutions, we obtain the displacements and stresses in the nonhomogeneous cracked strip as follows:

$$u_1 = \frac{1}{2\pi} \int_{-\infty}^\infty \sum_{j=1}^2 m_j D_j(\alpha) e^{n_j y} e^{-i\alpha x} d\alpha + \frac{2}{\pi} \int_0^\infty \sum_{j=1}^4 q_j A_j(\alpha) e^{p_j x} \cos(\alpha y) d\alpha, \quad (2.56)$$

$$v_1 = \frac{1}{2\pi} \int_{-\infty}^\infty \sum_{j=1}^2 D_j(\alpha) e^{n_j y} e^{-i\alpha x} d\alpha + \frac{2}{\pi} \int_0^\infty \sum_{j=1}^4 A_j(\alpha) e^{p_j x} \sin(\alpha y) d\alpha, \quad (2.57)$$

$$\sigma_{xx1} = \frac{\mu_0 e^{(\beta x)}}{\kappa - 1} \frac{1}{2\pi} \int_{-\infty}^\infty \sum_{j=1}^2 \{-(\kappa + 1)m_j i\alpha + (3 - \kappa)n_j\} D_j(\alpha) e^{n_j y} e^{-i\alpha x} d\alpha + \frac{\mu_0 e^{(\beta x)}}{\kappa - 1} \frac{2}{\pi} \int_0^\infty \sum_{j=1}^4 \{(\kappa + 1)q_j p_j + (3 - \kappa)\alpha\} A_j(\alpha) e^{p_j x} \cos(\alpha y) d\alpha, \quad (2.58)$$

$$\sigma_{yy1} = \frac{\mu_0 e^{(\beta x)}}{\kappa - 1} \frac{1}{2\pi} \int_{-\infty}^\infty \sum_{j=1}^2 \{-(3 - \kappa)m_j i\alpha + (\kappa + 1)n_j\} D_j(\alpha) e^{n_j y} e^{-i\alpha x} d\alpha + \frac{\mu_0 e^{(\beta x)}}{\kappa - 1} \frac{2}{\pi} \int_0^\infty \sum_{j=1}^4 \{(3 - \kappa)q_j p_j + (\kappa + 1)\alpha\} A_j(\alpha) e^{p_j x} \cos(\alpha y) d\alpha, \quad (2.59)$$

$$\begin{aligned}\tau_{xy1} = & \mu_0 e^{(\beta x)} \frac{1}{2\pi} \int_{-\infty}^{\infty} \sum_{j=1}^2 \left\{ -i\alpha + m_j n_j \right\} D_j(\alpha) e^{n_j y} e^{-i\alpha x} d\alpha + \\ & \mu_0 e^{(\beta x)} \frac{2}{\pi} \int_0^{\infty} \sum_{j=1}^4 \left\{ p_j - q_j \alpha \right\} A_j(\alpha) e^{p_j x} \sin(\alpha y) d\alpha.\end{aligned}\quad (2.60)$$

2.3.3.2 Homogeneous part

The superposition in the homogeneous part is same as in the nonhomogeneous part and is shown in Figure 2.3. Again the subscripts *c* and *uc* denote cracked infinite plane and uncracked strip, respectively.

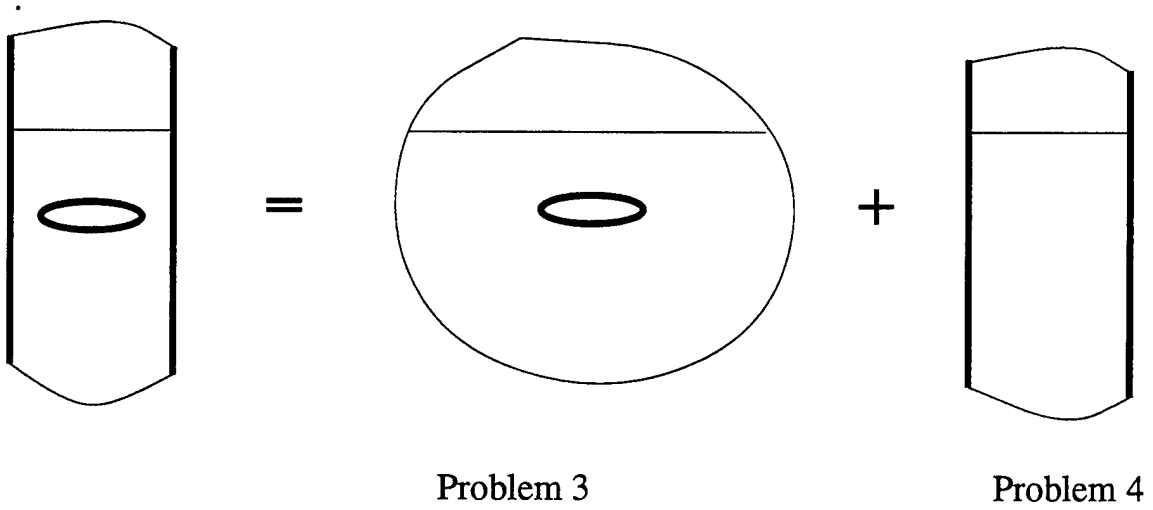


Figure 2.3 Superposition for the homogeneous part

Solution of Problem 3

Taking Fourier transform with respect to x

$$u_{2c} = \frac{1}{2\pi} \int_{-\infty}^{\infty} f_3(y, \alpha) e^{-i\alpha x} d\alpha, \quad (2.61)$$

$$v_{2c} = \frac{1}{2\pi} \int_{-\infty}^{\infty} g_3(y, \alpha) e^{-i\alpha x} d\alpha. \quad (2.62)$$

Substituting into equation (2.13) and (2.14) and taking Fourier inversion we obtain

$$(\kappa-1)f_3'' - (\kappa+1)(\alpha^2)f_3 - 2i\alpha g_3' = 0, \quad (2.63)$$

$$(\kappa+1)g_3'' - (\kappa-1)(\alpha^2)g_3 - 2i\alpha f_3' = 0. \quad (2.64)$$

These are coupled second order differential equations. By, for example, eliminating g_3 we can obtain a single 4th order differential equation in f_3 . The equation obtained is

$$f_3'''' - 2\alpha^2 f_3'' + \alpha^4 f_3 = 0. \quad (2.65)$$

If we assume

$$f_3 = e^{my} \quad (2.66)$$

we find that m has double roots at $\pm \alpha$. Hence the solution of f_3 can be written as

$$f_3 = C_1 e^{-|\alpha|y} + C_2 y e^{-|\alpha|y} + C_3 e^{|\alpha|y} + C_4 y e^{|\alpha|y}. \quad (2.67)$$

Considering the symmetry of the problem about the x -axis, we solve it only for the upper half plane. The displacements need to be bounded as y goes to ∞ . This necessitates C_3 and C_4 to be identically zero. Hence the solution can then be written as

$$f_3 = C_1 e^{-|\alpha|y} + C_2 y e^{-|\alpha|y}, \quad (2.68)$$

$$g_3 = -i \left(C_1 e^{-|\alpha|y} + C_2 y e^{-|\alpha|y} \left(\frac{\kappa}{\alpha} + y \right) \right). \quad (2.69)$$

The displacements and stresses are then given as

$$u_{2c} = \frac{1}{2\pi} \int_{-\infty}^{\infty} \left(C_1 e^{-|\alpha|y} + C_2 y e^{-|\alpha|y} \right) e^{-i\alpha x} d\alpha, \quad (2.70)$$

$$v_{2c} = -\frac{i}{2\pi} \int_{-\infty}^{\infty} \left(C_1 e^{-|\alpha|y} + C_2 e^{-|\alpha|y} \left(\frac{\kappa}{\alpha} + y \right) \right) e^{-i\alpha x} d\alpha, \quad (2.71)$$

$$\sigma_{xx2c} = \frac{\mu_0}{2\pi} \int_{-\infty}^{\infty} \left\{ -2i\alpha C_1 + iC_2 \left((3-\kappa) \frac{|\alpha|}{\alpha} - 2\alpha y \right) \right\} e^{-|\alpha|y} e^{-i\alpha x} d\alpha, \quad (2.72)$$

$$\sigma_{yy2c} = \frac{\mu_0}{2\pi} \int_{-\infty}^{\infty} \left\{ 2i\alpha C_1 + iC_2 \left((1+\kappa) \frac{|\alpha|}{\alpha} + 2\alpha y \right) \right\} e^{-|\alpha|y} e^{-i\alpha x} d\alpha, \quad (2.73)$$

$$\tau_{xy2c} = \frac{\mu_0}{2\pi} \int_{-\infty}^{\infty} \left\{ -2|\alpha| C_1 - C_2 \left(2|\alpha|y + \kappa - 1 \right) \right\} e^{-|\alpha|y} e^{-i\alpha x} d\alpha. \quad (2.74)$$

Solution of Problem 4

Considering the symmetries of u and v , we take Cosine transform of u with respect to y and Sine transform of v with respect to y and obtain,

$$u_{2uc} = \frac{2}{\pi} \int_0^{\infty} f_4(x, \alpha) \cos(\alpha y) d\alpha, \quad (2.75)$$

$$v_{2uc} = \frac{2}{\pi} \int_0^{\infty} g_4(x, \alpha) \sin(\alpha y) d\alpha. \quad (2.76)$$

Substituting into (2.13) and (2.14) and taking the respective inverse transforms we obtain,

$$(\kappa+1)f_4'' - (\kappa-1)\alpha^2 f_4 + 2\alpha g_4' = 0, \quad (2.77)$$

$$(\kappa-1)g_4'' - (\kappa+1)\alpha^2 f_4 - 2\alpha f_4' = 0. \quad (2.78)$$

These are coupled second order differential equations. By, for example, eliminating f_4 we can express this as one fourth order differential equation in g_4 . The equation thus obtained is

$$g_4'''' - 2\alpha^2 g_4'' + \alpha^4 g_4 = 0. \quad (2.79)$$

If we assume

$$g_4 = e^{ny} \quad (2.80)$$

we find that n has double roots at $\pm \alpha$. Hence the solution of g_4 and f_4 can be written as

$$g_4 = B_1 e^{\alpha x} + B_2 x e^{\alpha x} + B_3 e^{-\alpha x} + B_4 x e^{-\alpha x}, \quad (2.81)$$

$$f_4 = -B_1 e^{\alpha x} - B_2 \left(x - \frac{\kappa}{\alpha}\right) e^{\alpha x} + B_3 e^{-\alpha x} + B_4 \left(x + \frac{\kappa}{\alpha}\right) e^{-\alpha x}. \quad (2.82)$$

The displacements and stresses can then be written as

$$u_{2uc} = \frac{2}{\pi} \int_0^\infty \left\{ -B_1 e^{\alpha x} - B_2 \left(x - \frac{\kappa}{\alpha}\right) e^{\alpha x} + B_3 e^{-\alpha x} + B_4 \left(x + \frac{\kappa}{\alpha}\right) e^{-\alpha x} \right\} \cos(\alpha y) d\alpha, \quad (2.83)$$

$$v_{2uc} = \frac{2}{\pi} \int_0^\infty \left\{ B_1 e^{\alpha x} + B_2 x e^{\alpha x} + B_3 e^{-\alpha x} + B_4 x e^{-\alpha x} \right\} \sin(\alpha y) d\alpha \quad (2.84)$$

$$\sigma_{xx2uc} = -\frac{2\mu_0}{\pi} \int_0^\infty \left\{ 2\alpha B_1 e^{\alpha x} + B_2 (2\alpha x - \kappa - 1) e^{\alpha x} + 2\alpha B_3 e^{-\alpha x} + B_4 (2\alpha x + \kappa + 1) e^{-\alpha x} \right\} \cos(\alpha y) d\alpha, \quad (2.85)$$

$$\sigma_{yy2uc} = \frac{2\mu_0}{\pi} \int_0^\infty \left\{ 2\alpha B_1 e^{\alpha x} + B_2 (2\alpha x - \kappa + 3) e^{\alpha x} + 2\alpha B_3 e^{-\alpha x} + B_4 (2\alpha x + \kappa - 3) e^{-\alpha x} \right\} \cos(\alpha y) d\alpha, \quad (2.86)$$

$$\tau_{xy2uc} = \frac{2\mu_0}{\pi} \int_0^\infty \left\{ 2\alpha B_1 e^{\alpha x} + B_2(2\alpha x - \kappa + 1)e^{\alpha x} - 2\alpha B_3 e^{-\alpha x} - B_4(2\alpha x + \kappa - 1)e^{-\alpha x} \right\} \sin(\alpha y) d\alpha. \quad (2.87)$$

By superimposing these two sets of solutions, we obtain the displacements and stresses in the homogeneous cracked strip as

$$u_2 = \frac{1}{2\pi} \int_{-\infty}^\infty \left(C_1 e^{-|\alpha|y} + C_2 y e^{-|\alpha|y} \right) e^{-i\alpha x} d\alpha + \frac{2}{\pi} \int_0^\infty \left\{ -B_1 e^{\alpha x} - B_2 \left(x - \frac{\kappa}{\alpha} \right) e^{\alpha x} + B_3 e^{-\alpha x} + B_4 \left(x + \frac{\kappa}{\alpha} \right) e^{-\alpha x} \right\} \cos(\alpha y) d\alpha, \quad (2.88)$$

$$v_2 = -\frac{i}{2\pi} \int_{-\infty}^\infty \left(C_1 e^{-|\alpha|y} + C_2 e^{-|\alpha|y} \left(\frac{\kappa}{\alpha} + y \right) \right) e^{-i\alpha x} d\alpha + \frac{2}{\pi} \int_0^\infty \left\{ B_1 e^{\alpha x} + B_2 x e^{\alpha x} + B_3 e^{-\alpha x} + B_4 x e^{-\alpha x} \right\} \sin(\alpha y) d\alpha, \quad (2.89)$$

$$\sigma_{xx2} = \frac{\mu_0}{2\pi} \int_{-\infty}^\infty \left\{ -2i\alpha C_1 + iC_2 \left((3-\kappa) \frac{|\alpha|}{\alpha} - 2\alpha y \right) \right\} e^{-|\alpha|y} e^{-i\alpha x} d\alpha - \frac{2\mu_0}{\pi} \int_0^\infty \left\{ 2\alpha B_1 e^{\alpha x} + B_2(2\alpha x - \kappa - 1)e^{\alpha x} + 2\alpha B_3 e^{-\alpha x} + B_4(2\alpha x + \kappa + 1)e^{-\alpha x} \right\} \cos(\alpha y) d\alpha, \quad (2.90)$$

$$\sigma_{yy2} = \frac{\mu_0}{2\pi} \int_{-\infty}^\infty \left\{ 2i\alpha C_1 + iC_2 \left((1+\kappa) \frac{|\alpha|}{\alpha} + 2\alpha y \right) \right\} e^{-|\alpha|y} e^{-i\alpha x} d\alpha + \frac{2\mu_0}{\pi} \int_0^\infty \left\{ 2\alpha B_1 e^{\alpha x} + B_2(2\alpha x - \kappa + 3)e^{\alpha x} + 2\alpha B_3 e^{-\alpha x} + B_4(2\alpha x + \kappa - 3)e^{-\alpha x} \right\} \cos(\alpha y) d\alpha, \quad (2.91)$$

$$\begin{aligned}\tau_{xy2} = & \frac{\mu_0}{2\pi} \int_{-\infty}^{\infty} \left\{ -2|\alpha|C_1 - C_2 \left(2|\alpha|y + \kappa - 1 \right) \right\} e^{-|\alpha|y} e^{-i\alpha x} d\alpha + \\ & \frac{2\mu_0}{\pi} \int_0^{\infty} \left\{ 2\alpha B_1 e^{\alpha x} + B_2 (2\alpha x - \kappa + 1) e^{\alpha x} \right. \\ & \left. - 2\alpha B_3 e^{-\alpha x} - B_4 (2\alpha x + \kappa - 1) e^{-\alpha x} \right\} \sin(\alpha y) d\alpha. \quad (2.92)\end{aligned}$$

It should be noted that in equations (2.56 – 2.60) and in equations (2.88 – 2.92) there are totally 12 arbitrary constants. These will be evaluated with help of boundary conditions.

2.4 Boundary conditions

The homogeneous boundary conditions are given on the free surfaces and the interface. On the boundaries, the stresses are zero while on the interface stresses and displacements are continuous. These can be expressed as

$$\sigma_{xx1}(-h_1, y) = 0, \quad (2.93)$$

$$\tau_{xy1}(-h_1, y) = 0, \quad (2.94)$$

$$\sigma_{xx1}(0, y) = \sigma_{xx2}(0, y), \quad (2.95)$$

$$\tau_{xy1}(0, y) = \tau_{xy2}(0, y), \quad (2.96)$$

$$u_1(0, y) = u_2(0, y), \quad (2.97)$$

$$v_1(0, y) = v_2(0, y), \quad (2.98)$$

$$\sigma_{xx2}(h_2, y) = 0, \quad (2.99)$$

$$\tau_{xy2}(h_2, y) = 0. \quad (2.100)$$

On the plane of the crack we have symmetry conditions given by

$$\tau_{xy1}(x, 0) = 0, \quad -h_1 < x < 0 \quad (2.101)$$

$$\tau_{xy2}(x, 0) = 0, \quad 0 < x < h_2 \quad (2.102)$$

and the mixed boundary conditions given by

$$\sigma_{yy1}(x, 0) = p_1(x), \quad -b_1 < x < -a_1 \quad (2.103)$$

$$v_1(x, 0) = 0, \quad -h_1 < x < -b_1, -a_1 < x < 0 \quad (2.104)$$

$$\sigma_{yy2}(x, 0) = p_2(x), \quad a_2 < x < b_2 \quad (2.105)$$

$$v_2(x, 0) = 0, \quad 0 < x < a_2, b_2 < x < h_2. \quad (2.106)$$

The $p_1(x)$ and $p_2(x)$ are the negative of the stresses at the crack plane under external loading in an uncracked specimen. The mixed boundary conditions will give rise to the singular integral equations which will be derived in Chapter 3.

CHAPTER 3

SINGULAR INTEGRAL EQUATIONS AND STRESS INTENSITY FACTORS

In Chapter 2 the governing equations and the expressions for stresses and displacements were derived. The boundary conditions were also stated. In this chapter, we will use those expressions to derive the singular integral equations. Also, the singularities and the stress intensity factors at the crack tips will be discussed. In deriving these expressions, the variable x is replaced by x_1 and x_2 defined as,

$$x = \begin{cases} x_1, & x < 0 \\ x_2, & x > 0 \end{cases} \quad (3.1)$$

This is useful in distinguishing the non-homogeneous part from the homogeneous and hence the two singular integral equations.

3.1 Development of singular integral equations

3.1.1 Conditions along plane of symmetry $y = 0$

Using equations (2.101) and (2.60), it may be seen that

$$\begin{aligned} \mu_0 e^{(\beta x_1)} \frac{1}{2\pi} \int_{-\infty}^{\infty} \sum_{j=1}^2 \left\{ -i\alpha + m_j n_j \right\} D_j(\alpha) e^{n_j y} e^{-i\alpha x_1} d\alpha \Big|_{y \rightarrow 0} + \\ \mu_0 e^{(\beta x_1)} \frac{2}{\pi} \int_{-\infty}^{\infty} \sum_{j=1}^4 \left\{ p_j - q_j \alpha \right\} A_j(\alpha) e^{p_j x_1} \sin(\alpha y) d\alpha \Big|_{y \rightarrow 0} = 0. \end{aligned} \quad (3.2)$$

Taking now the Fourier inverse transform, we have,

$$D_1(\alpha) = - \frac{(m_2 n_2 - i\alpha)}{(m_1 n_1 - i\alpha)} D_2(\alpha). \quad (3.3)$$

Similarly from equations (2.102) and 2.92), it follows that,

$$\begin{aligned} & \left. \frac{\mu_0}{2\pi} \int_{-\infty}^{\infty} \left\{ -2|\alpha|C_1 - C_2 \left(2|\alpha|y + \kappa - 1 \right) \right\} e^{-|\alpha|y} e^{-i\alpha x_1} d\alpha \right|_{y \rightarrow 0} + \\ & \frac{2\mu_0}{\pi} \int_{-\infty}^{\infty} \left\{ 2\alpha B_1 e^{\alpha x_1} + B_2 (2\alpha x - \kappa + 1) e^{\alpha x_1} \right. \\ & \left. - 2\alpha B_3 e^{-\alpha x_1} - B_4 (2\alpha x + \kappa - 1) e^{-\alpha x_1} \right\} \sin(\alpha y) d\alpha \Big|_{y \rightarrow 0} = 0. \end{aligned} \quad (3.4)$$

By taking the Fourier inverse transform, we have,

$$C_1(\alpha) = \frac{1 - \kappa}{2|\alpha|} C_2(\alpha). \quad (3.5)$$

We now define the following new unknown functions

$$g_1(x_1) = \frac{\partial v_1}{\partial x_1}(x_1, 0) \quad -b_1 < x_1 < -a_1 \quad (3.6)$$

and

$$g_2(x_2) = \frac{\partial v_2}{\partial x_2}(x_2, 0) \quad a_2 < x_2 < b_2. \quad (3.7)$$

By taking Fourier inverse transform of (2.57), (2.89) and using (3.3), (3.5), (3.6), (3.7), we obtain

$$D_2(\alpha) = \frac{(m_1 n_1 - i\alpha)}{(m_1 n_1 - m_2 n_2)} \frac{i}{\alpha} \int_{-b_1}^{-a_1} g_1(t) e^{i\alpha t} dt \quad (3.8)$$

and

$$C_2(\alpha) = -\frac{2}{\kappa + 1} \int_{a_2}^{b_2} g_2(t) e^{i\alpha t} dt. \quad (3.9)$$

3.1.2 Homogeneous boundary conditions

By using the eight homogeneous boundary conditions (2.93 – 2.100) and the expressions from (2.56 – 2.60) and (2.88 – 2.92), after taking the appropriate Sine or Cosine transforms we can write a system of eight algebraic equations in eight unknowns . The system of equations we obtain is as follows:

$$\begin{aligned} \theta_1 A_1 e^{-p_1 h_1} + \theta_2 A_2 e^{-p_2 h_1} + \\ \theta_3 A_3 e^{-p_3 h_1} + \theta_4 A_4 e^{-p_4 h_1} \end{aligned} = R_1^*, \quad (3.10)$$

$$\begin{aligned} \Gamma_1 A_1 e^{-p_1 h_1} + \Gamma_2 A_2 e^{-p_2 h_1} + \\ \Gamma_3 A_3 e^{-p_3 h_1} + \Gamma_4 A_4 e^{-p_4 h_1} \end{aligned} = R_2^*, \quad (3.11)$$

$$\begin{aligned} \phi_1 A_1 + \phi_2 A_2 + \phi_3 A_3 + \phi_4 A_4 + \\ 2\alpha B_1 - (\kappa + 1)B_2 + 2\alpha B_3 + (\kappa + 1)B_4 \end{aligned} = R_3^*, \quad (3.12)$$

$$\begin{aligned} \Gamma_1 A_1 + \Gamma_2 A_2 + \Gamma_3 A_3 + \Gamma_4 A_4 - \\ 2\alpha B_1 + (\kappa - 1)B_2 + 2\alpha B_3 + (\kappa - 1)B_4 \end{aligned} = R_4^*, \quad (3.13)$$

$$\begin{aligned} q_1 A_1 + q_2 A_2 + q_3 A_3 + q_4 A_4 + \\ B_1 - B_2 \frac{\kappa}{\alpha} - B_3 - B_4 \frac{\kappa}{\alpha} \end{aligned} = R_5^*, \quad (3.14)$$

$$A_1 + A_2 + A_3 + A_4 - B_1 - B_3 = R_6^*, \quad (3.15)$$

$$\begin{aligned} 2\alpha B_1 e^{\alpha h_2} + (2\alpha h_2 - \kappa - 1)B_2 e^{\alpha h_2} + \\ 2\alpha B_3 e^{-\alpha h_2} + (2\alpha h_2 + \kappa + 1)B_4 e^{-\alpha h_2} \end{aligned} = R_7^*, \quad (3.16)$$

$$\begin{aligned}
& 2\alpha B_1 e^{\alpha h_2} + (2\alpha h_2 - \kappa + 1) B_2 e^{\alpha h_2} - \\
& 2\alpha B_3 e^{-\alpha h_2} + (2\alpha h_2 + \kappa - 1) B_4 e^{-\alpha h_2} = R_8^*. \quad (3.17)
\end{aligned}$$

The expressions for the variables used in these equations are given in Appendix A. It should be noted that while evaluating the right hand sides, some straightforward contour integrals have been evaluated. The system of equations in (3.10 – 3.17) can now be solved for the unknowns A_i and B_i ($i = 1, 2, 3, 4$) giving,

$$B_1 = R_{01}^* + e_1 B_3 + e_2 B_4, \quad (3.18)$$

$$B_2 = R_{02}^* + f_1 B_3 + f_2 B_4, \quad (3.19)$$

$$B_3 = R_{03}^* + A_1 \gamma_1 + A_2 \gamma_2 + A_3 \gamma_3 + A_4 \gamma_4, \quad (3.20)$$

$$B_4 = R_{04}^* + A_1 \delta_1 + A_2 \delta_2 + A_3 \delta_3 + A_4 \delta_4, \quad (3.21)$$

$$A_1 = R_{11}^* + A_3 \omega_3 + A_4 \omega_4, \quad (3.22)$$

$$A_2 = R_{12}^* + A_3 \rho_3 + A_4 \rho_4, \quad (3.23)$$

$$A_3 = R_{13}^*, \quad (3.24)$$

$$A_4 = R_{14}^*. \quad (3.25)$$

Again the expressions for the various variables that appear in (3.18 – 3.25) are given in Appendix A.

3.1.3 Mixed Boundary conditions

The First Singular Integral Equation

Using condition (2.103) and expression in (2.59) we obtain

$$\begin{aligned}
& \frac{\mu_0 e^{(\beta x_1)}}{\kappa - 1} \frac{1}{2\pi} \int_{-\infty}^{\infty} \sum_{j=1}^2 \left\{ -(3-\kappa)m_j i\alpha + (\kappa+1)n_j \right\} D_j(\alpha) e^{n_j y} e^{-i\alpha x_1} d\alpha \Big|_{y \rightarrow 0} + \\
& \frac{\mu_0 e^{(\beta x_1)}}{\kappa - 1} \frac{2}{\pi} \int_0^{\infty} \sum_{j=1}^4 \left\{ (3-\kappa)q_j p_j + (\kappa+1)\alpha \right\} A_j(\alpha) e^{p_j x_1} \cos(\alpha y) d\alpha \Big|_{y \rightarrow 0} \\
& = p_1(x_1). \tag{3.26}
\end{aligned}$$

Substituting from (3.3) and (3.22-3.25), from (3.26) we obtain,

$$\frac{1}{2\pi} \int_{-\infty}^{\infty} \Phi_1^* D_2 d\alpha + \frac{2}{\pi} \int_0^{\infty} R_{21}^* d\alpha = p_1(x_1) \frac{\kappa - 1}{\mu_0 e^{\beta x_1}} \tag{3.27}$$

where Φ_1^* and R_{21}^* are given in Appendix A. Using (3.8) we can write,

$$\begin{aligned}
& \frac{1}{2\pi} \int_{-\infty}^{\infty} \widehat{k}_1 e^{-i\alpha x_1} d\alpha \int_{-b_1}^{-a_1} g_1(t_1) e^{i\alpha t_1} dt_1 + \frac{2}{\pi} \int_0^{\infty} R_{21a}(\alpha, x_1, t_1) d\alpha \int_{-b_1}^{-a_1} g_1(t_1) dt_1 \\
& + \frac{2}{\pi} \int_0^{\infty} R_{21b}(\alpha, x_1, t_2) d\alpha \int_{a_2}^{b_2} g_2(t_2) dt_2 = p_1(x_1) \frac{\kappa - 1}{\mu_0 e^{\beta x_1}} \tag{3.28}
\end{aligned}$$

where the function \widehat{k}_1 and R_{21a} , R_{21b} are given in Appendix A. R_{21a} , R_{21b} are bounded.

\widehat{k}_1 , however, needs to be investigated further. Consider the first integral in (3.28). It can be written as,

$$\frac{1}{2\pi} \int_{-b_1}^{-a_1} g_1(t_1) dt_1 \int_{-\infty}^{\infty} \widehat{k}_1(\alpha, y) e^{i\alpha(t_1 - x_1)} d\alpha. \tag{3.29}$$

Separating $k_1(\alpha, y)$ into its real and imaginary parts and noting that

$$\widehat{k}_1(-\alpha, y) = \text{complex conjugate of } \widehat{k}_1(\alpha, y), \tag{3.30}$$

(3.29) may be expressed as

$$\begin{aligned} \frac{1}{\pi} \int_{-b_1}^{-a_1} g_1(t_1) dt_1 \int_0^\infty \left\{ \operatorname{Re}(\widehat{k}_1(\alpha, y)) \cos(\alpha(t_1 - x_1)) \right. \\ \left. - \operatorname{Im}(\widehat{k}_1(\alpha, y)) \sin(\alpha(t_1 - x_1)) \right\} d\alpha \end{aligned} \quad (3.31)$$

In (3.31) the dominant part of the kernel may be separated by taking the asymptotic expansion of $\widehat{k}_1(\alpha, y)$ as α tends to infinity. We find that,

$$\lim_{\alpha \rightarrow \infty} \widehat{k}_1(\alpha, y) = \widehat{k}_{1\infty} \quad (3.32)$$

where $\widehat{k}_{1\infty}$ is given as

$$\widehat{k}_{1\infty} = -4i \left(\frac{\kappa - 1}{\kappa + 1} \right) + \widehat{k}_{1\infty h} \quad (3.33)$$

where

$$\begin{aligned} \widehat{k}_{1\infty h} = & 2 \left(\frac{\beta}{\alpha} \right) \left(\frac{\kappa - 1}{\kappa + 1} \right) - i \left(\frac{\beta}{\alpha} \right)^2 \left(\frac{\kappa - 1}{\kappa + 1} \right)^2 \\ & - \frac{1}{2} \left(\frac{\beta}{\alpha} \right)^3 \left(\frac{\kappa - 1}{\kappa + 1} \right)^2 + \frac{i}{4} \left(\frac{\beta}{\alpha} \right)^4 \frac{(\kappa - 1)(\kappa^2 + 2\kappa - 5)}{(\kappa + 1)^3} \\ & + \frac{i}{8} \left(\frac{\beta}{\alpha} \right)^5 \frac{(\kappa - 1)(\kappa^2 + 6\kappa - 13)}{(\kappa + 1)^3} + O\left(\frac{1}{\alpha^6}\right). \end{aligned} \quad (3.34)$$

Subtracting the asymptotic limit in (3.32 – 3.34) from real and imaginary parts of $\widehat{k}_1(\alpha, y)$, (3.29) can be written as,

$$\begin{aligned}
& \frac{4}{\pi} \left(\frac{\kappa - 1}{\kappa + 1} \right) \int_{-b_1}^{-a_1} \frac{g_1(t_1)}{(t_1 - x_1)} dt_1 \\
& + \frac{1}{\pi} \int_{-b_1}^{-a_1} g_1(t_1) dt_1 \int_0^A \left\{ \operatorname{Re}(\widehat{k}_1(\alpha, y)) \cos(\alpha(t_1 - x_1)) \right. \\
& \quad \left. - \left(\operatorname{Im}(\widehat{k}_1(\alpha, y)) + 4 \left(\frac{\kappa - 1}{\kappa + 1} \right) \right) \sin(\alpha(t_1 - x_1)) \right\} d\alpha \\
& + \frac{1}{\pi} \int_{-b_1}^{-a_1} g_1(t_1) dt_1 \int_A^\infty \left\{ \left(\operatorname{Re}(\widehat{k}_1(\alpha, y)) - \operatorname{Re}(\widehat{k}_{1\infty h}(\alpha, y)) \right) \cos(\alpha(t_1 - x_1)) \right. \\
& \quad \left. - \left(\operatorname{Im}(\widehat{k}_1(\alpha, y)) + 4 \left(\frac{\kappa - 1}{\kappa + 1} \right) - \right. \right. \\
& \quad \left. \left. \operatorname{Im}(\widehat{k}_{1\infty h}(\alpha, y)) \right) \sin(\alpha(t_1 - x_1)) \right\} d\alpha \\
& + \frac{1}{\pi} \int_{-b_1}^{-a_1} g_1(t_1) dt_1 \int_A^\infty \left\{ \operatorname{Re}(\widehat{k}_{1\infty h}(\alpha, y)) \cos(\alpha(t_1 - x_1)) \right. \\
& \quad \left. - \operatorname{Im}(\widehat{k}_{1\infty h}(\alpha, y)) \sin(\alpha(t_1 - x_1)) \right\} d\alpha. \tag{3.35}
\end{aligned}$$

Thus we have separated the Cauchy singularity. Using (3.35) and putting all the bounded parts together, (3.28) may be expressed as

$$\begin{aligned}
& \frac{1}{\pi} \int_{-b_1}^{-a_1} \frac{g_1(t_1)}{(t_1 - x_1)} dt_1 + \frac{1}{\pi} \int_{-b_1}^{-a_1} g_1(t_1) K_{11}(x_1, t_1) dt_1 \\
& + \frac{1}{\pi} \int_{a_2}^{b_2} g_2(t_2) K_{12}(x_1, t_2) dt_2 = p_1(x_1) \frac{\kappa + 1}{4\mu_0 e^{\beta x_1}}. \tag{3.36}
\end{aligned}$$

The expressions for $K_{11}(x_1, t_1)$ and $K_{12}(x_1, t_2)$ are given in Appendix A. In (3.36), the first integral on the left has the Cauchy kernel whereas the other two integrals have Fredholm kernels.

The Second Singular Integral Equation

Using equations (2.105) and (2.91), we find,

$$\begin{aligned} & \frac{\mu_0}{2\pi} \int_{-\infty}^{\infty} \left\{ 2i\alpha C_1 + iC_2 \left((1+\kappa) \frac{|\alpha|}{\alpha} + 2\alpha y \right) \right\} e^{-|\alpha|y} e^{-i\alpha x_2} d\alpha \Big|_{y \rightarrow 0} + \\ & \frac{2\mu_0}{\pi} \int_0^{\infty} \left\{ 2\alpha B_1 e^{\alpha x_2} + B_2 (2\alpha x_2 - \kappa + 3) e^{\alpha x_2} \right. \\ & \left. + 2\alpha B_3 e^{-\alpha x_2} + B_4 (2\alpha x_2 + \kappa - 3) e^{-\alpha x_2} \right\} \cos(\alpha y) d\alpha \Big|_{y \rightarrow 0} = p_2(x_2) \end{aligned} \quad (3.37)$$

Also from (3.5) and (3.18-3.25) we obtain,

$$\frac{1}{2\pi} \int_{-\infty}^{\infty} \Phi_2^* C_2 d\alpha + \frac{2}{\pi} \int_0^{\infty} R_{22}^* d\alpha = \frac{p_2(x_2)}{\mu_0} \quad (3.38)$$

where Φ_2^* and R_{22}^* are given in Appendix A. By substituting from (3.9), (3.38) can be written as,

$$\begin{aligned} & \frac{1}{2\pi} \int_{-\infty}^{\infty} \hat{k}_2 e^{-i\alpha x_2} d\alpha \int_{a_2}^{b_2} g_2(t_2) e^{i\alpha t_2} dt_2 + \frac{2}{\pi} \int_0^{\infty} R_{21a}(\alpha, x_2, t_1) d\alpha \int_{-b_1}^{-a_1} g_1(t_1) dt_1 \\ & + \frac{2}{\pi} \int_0^{\infty} R_{21b}(\alpha, x_2, t_2) d\alpha \int_{a_2}^{b_2} g_2(t_2) dt_2 = \frac{p_2(x_2)}{\mu_0} \end{aligned} \quad (3.39)$$

where \hat{k}_2 is given in Appendix A. Consider the first integral in (3.39). It can be written as,

$$\frac{1}{2\pi} \int_{a_2}^{b_2} g_2(t_2) dt_2 \int_{-\infty}^{\infty} \hat{k}_2(\alpha, y) e^{i\alpha(t_2 - x_2)} d\alpha. \quad (3.40)$$

After some manipulations, the dominant part of (3.40) can be written as

$$\frac{1}{\pi} \left(\frac{4}{\kappa + 1} \right) \int_{a_2}^{b_2} \frac{g_2(t_2)}{(t_2 - x_2)} dt_2. \quad (3.41)$$

Substituting (3.41) back into (3.39) and rearranging we have,

$$\begin{aligned} & \frac{1}{\pi} \int_{a_2}^{b_2} \frac{g_2(t_2)}{(t_2 - x_2)} dt_2 + \frac{1}{\pi} \int_{-b_1}^{-a_1} g_1(t_1) K_{21}(x_2, t_1) dt_1 \\ & + \frac{1}{\pi} \int_{a_2}^{b_2} g_2(t_2) K_{22}(x_2, t_2) dt_2 = p_2(x_2) \frac{\kappa + 1}{4\mu_0}. \end{aligned} \quad (3.42)$$

Expressions for $K_{21}(x_2, t_1)$ and $K_{22}(x_2, t_2)$ are given in Appendix A. In (3.42), the first integral has the Cauchy kernel while the other two integrals have Fredholm kernels.

3.2 Asymptotic analysis of Fredholm kernels

The Fredholm kernels in (3.36) and (3.42) may contain generalized Cauchy kernels which are singular and play an important role in determination of the singularity in certain crack configurations. It is hence necessary to perform asymptotic analysis on the integrands of the Fredholm kernels as α tends to infinity.

$K_{11}(\alpha, x_1, t_1)$:

The expression for $K_{11}(\alpha, x_1, t_1)$ is given in Appendix A. For easy reference it has been reproduced here.

$$\begin{aligned}
K_{11}(\alpha, x_1, t_1) = & \left(\frac{\kappa + 1}{4(\kappa - 1)} \right) \left\{ \int_0^A \left\{ \text{Re}(\widehat{k}_1(\alpha, y)) \cos(\alpha(t_1 - x_1)) \right. \right. \\
& \left. \left. - \left(\text{Im}(\widehat{k}_1(\alpha, y)) + 4 \left(\frac{\kappa - 1}{\kappa + 1} \right) \right) \sin(\alpha(t_1 - x_1)) \right\} d\alpha \right. \\
& + \int_A^\infty \left\{ \left(\text{Re}(\widehat{k}_1(\alpha, y)) - \text{Re}(\widehat{k}_{1\infty h}(\alpha, y)) \right) \cos(\alpha(t_1 - x_1)) \right. \\
& \left. - \left(\text{Im}(\widehat{k}_1(\alpha, y)) + 4 \left(\frac{\kappa - 1}{\kappa + 1} \right) - \right. \right. \\
& \left. \left. \text{Im}(\widehat{k}_{1\infty h}(\alpha, y)) \right) \sin(\alpha(t_1 - x_1)) \right\} d\alpha \\
& + \int_A^\infty \left\{ \text{Re}(\widehat{k}_{1\infty h}(\alpha, y)) \cos(\alpha(t_1 - x_1)) \right. \\
& \left. - \text{Im}(\widehat{k}_{1\infty h}(\alpha, y)) \sin(\alpha(t_1 - x_1)) \right\} d\alpha \\
& \left. + 2 \int_0^\infty R_{21a}(\alpha, x_1, t_1) d\alpha \right\}. \tag{3.43}
\end{aligned}$$

It should be noted that the first three integrals do not lead to any singular term. The terms in these integrals are of order higher than $O(1)$. Hence the term that will give rise to a possible generalized Cauchy kernel is $R_{21a}(\alpha, x_1, t_1)$. After some very tedious asymptotic analysis, we find,

$$\begin{aligned}
R_{21a}(\alpha, x_1, t_1) \sim & \left(c_1^* \alpha^2 + c_2^* \alpha + c_3^* + \frac{c_4^*}{\alpha} \right) e^{-(x_1 + t_1 + 2h_1)\alpha} \\
& + \left(e_1^* \alpha + e_2^* + \frac{e_3^*}{\alpha} + \frac{e_4^*}{\alpha^2} \right) e^{(x_1 + t_1)\alpha} \tag{3.44}
\end{aligned}$$

where expressions for the variables appearing in (3.44) are given in Appendix B. It should be noted that c^* 's, and e^* 's are not constants but functions of x_1 and t_1 . Again here only the terms involving $O(\alpha^2)$, $O(\alpha)$ and $O(1)$ give rise to singular terms. Separating these singular terms from K_{11} we can write,

$$K_{11}(\alpha, x_1, t_1) = K_{11}^c(\alpha, x_1, t_1) + K_{11}^b(\alpha, x_1, t_1) \quad (3.45)$$

where

$$K_{11}^c(\alpha, x_1, t_1) = \left(\frac{\kappa + 1}{2(\kappa - 1)} \right) \int_0^\infty \left\{ \left(c_1^* \alpha^2 + c_2^* \alpha + c_3^* \right) e^{-(x_1 + t_1 + 2h_1)\alpha} \right. \\ \left. + \left(e_1^* \alpha + e_2^* \right) e^{(x_1 + t_1)\alpha} \right\} d\alpha \quad (3.46)$$

and

$$K_{11}^b(\alpha, x_1, t_1) = \left(\frac{\kappa + 1}{4(\kappa - 1)} \right) \left\{ \int_0^A \left\{ \operatorname{Re}(\widehat{k}_1(\alpha, y)) \cos(\alpha(t_1 - x_1)) \right. \right. \\ \left. \left. - \left(\operatorname{Im}(\widehat{k}_1(\alpha, y)) + 4 \left(\frac{\kappa - 1}{\kappa + 1} \right) \right) \sin(\alpha(t_1 - x_1)) \right\} d\alpha \right. \\ \left. + \int_A^\infty \left\{ \left(\operatorname{Re}(\widehat{k}_1(\alpha, y)) - \operatorname{Re}(\widehat{k}_{1\infty h}(\alpha, y)) \right) \cos(\alpha(t_1 - x_1)) \right. \right. \\ \left. \left. - \left(\operatorname{Im}(\widehat{k}_1(\alpha, y)) + 4 \left(\frac{\kappa - 1}{\kappa + 1} \right) - \operatorname{Im}(\widehat{k}_{1\infty h}(\alpha, y)) \right) \sin(\alpha(t_1 - x_1)) \right\} d\alpha \right. \\ \left. + \int_A^\infty \left\{ \operatorname{Re}(\widehat{k}_{1\infty h}(\alpha, y)) \cos(\alpha(t_1 - x_1)) \right. \right. \\ \left. \left. - \operatorname{Im}(\widehat{k}_{1\infty h}(\alpha, y)) \sin(\alpha(t_1 - x_1)) \right\} d\alpha \right. \\ \left. + 2 \int_0^\infty \left(R_{21a}(\alpha, x_1, t_1) - \left(c_1^* \alpha^2 + c_2^* \alpha + c_3^* \right) e^{-(x_1 + t_1 + 2h_1)\alpha} \right. \right. \\ \left. \left. - \left(e_1^* \alpha + e_2^* \right) e^{(x_1 + t_1)\alpha} \right) d\alpha \right\}. \quad (3.47)$$

Upon integration $K_{11}^c(\alpha, x_1, t_1)$ can be simplified as

$$K_{11}^c(\alpha, x_1, t_1) = \left(\frac{\kappa + 1}{2(\kappa - 1)} \right)$$

$$\left\{ \frac{2c_1^*}{(x_1 + t_1 + 2h_1)^3} + \frac{c_2^*}{(x_1 + t_1 + 2h_1)^2} + \frac{c_3^*}{(x_1 + t_1 + 2h_1)} + \frac{e_1^*}{(x_1 + t_1)^2} + \frac{e_2^*}{(x_1 + t_1)} \right\}. \quad (3.48)$$

This is the generalized Cauchy kernel in the sense that, even though bounded for $x_1 \neq 0$, $t_1 \neq 0$ and $x_1 \neq -h_1$, $t_1 \neq -h_1$, it becomes unbounded for $x_1 \rightarrow 0$, $t_1 \rightarrow 0$ or $x_1 \rightarrow -h_1$, $t_1 \rightarrow -h_1$ simultaneously. If we let β go to 0 in c_1^* , c_2^* , c_3^* we recover the following familiar form of the generalized Cauchy kernel for homogeneous materials,

$$-\frac{1}{(x_1 + t_1 + 2h_1)} + \frac{6(x_1 + h_1)}{(x_1 + t_1 + 2h_1)^2} - \frac{4(x_1 + h_1)^2}{(x_1 + t_1 + 2h_1)^3}. \quad (3.49)$$

$K_{12}(\alpha, x_1, t_2)$:

The expression for $K_{12}(\alpha, x_1, t_2)$ is given in Appendix A. For easy reference it has been reproduced here

$$K_{12}(\alpha, x_1) = 2 \int_0^\infty R_{21b}(\alpha, x_1, t_2) d\alpha \left(\frac{\kappa + 1}{4(\kappa - 1)} \right). \quad (3.50)$$

After performing some tedious asymptotic analysis on $R_{21b}(\alpha, x_1, t_2)$ we find that for $\alpha \rightarrow \infty$,

$$R_{21b}(\alpha, x_1, t_2) \sim \left(r_1^* \alpha + r_2^* + \frac{r_3^*}{\alpha} + \frac{r_4^*}{\alpha^2} \right) e^{(x_1 - t_2)\alpha}, \quad (3.51)$$

where expressions for the variables are given in Appendix B. Again here only the terms involving $O(\alpha)$ and $O(1)$ give rise to singularities in the kernel. Separating these singular terms from K_{12} we can write

$$K_{12}(\alpha, x_1, t_2) = K_{12}^c(\alpha, x_1, t_2) + K_{12}^b(\alpha, x_1, t_2) \quad (3.52)$$

where

$$K_{12}^c(\alpha, x_1, t_2) = \left(\frac{k+1}{2(\kappa-1)} \right) \int_0^\infty \left\{ (r_1^* \alpha + r_2^*) e^{(x_1-t_2)\alpha} \right\} d\alpha, \quad (3.53)$$

$$K_{12}^b(\alpha, x_1, t_2) = \left(\frac{k+1}{2(\kappa-1)} \right) \left\{ \left(R_{21a}(\alpha, x_1, t_2) - (r_1^* \alpha + r_2^*) e^{(x_1-t_2)\alpha} \right) d\alpha \right\}. \quad (3.54)$$

Upon integration $K_{12}^c(\alpha, x_1, t_2)$ can be simplified as

$$K_{12}^c(\alpha, x_1, t_2) = \left(\frac{k+1}{2(\kappa-1)} \right) \left\{ \frac{r_1^*}{(x_1-t_2)^2} - \frac{r_2^*}{(x_1-t_2)} \right\}. \quad (3.55)$$

$K_{21}(\alpha, x_2, t_1)$:

The expression for $K_{21}(\alpha, x_2, t_1)$ is given in Appendix A. For easy reference it has been reproduced here

$$K_{21}(\alpha, x_2, t_1) = 2 \int_0^\infty R_{22a}(\alpha, x_2, t_1) d\alpha \left(\frac{\kappa+1}{4} \right). \quad (3.56)$$

After performing some tedious asymptotic analysis on $R_{22a}(\alpha, x_2, t_1)$ we find that,

$$R_{22a}(\alpha, x_2, t_1) \sim \left(t_1^* \alpha + t_2^* + \frac{t_3^*}{\alpha} + \frac{t_4^*}{\alpha^2} + \frac{t_5^*}{\alpha^3} \right) e^{-(x_2-t_1)\alpha} \quad (3.57)$$

where expressions for the variables are given in Appendix B. In this case, too, only the terms involving $O(\alpha)$ and $O(1)$ terms give rise to singularities in the kernel. Separating these singular terms from K_{21} we can write,

$$K_{21}(\alpha, x_2, t_1) = K_{21}^c(\alpha, x_2, t_1) + K_{21}^b(\alpha, x_2, t_1) \quad (3.58)$$

where

$$K_{21}^c(\alpha, x_2, t_1) = \left(\frac{\kappa + 1}{2} \right) \int_0^\infty \left\{ \left(t_1^* \alpha + t_2^* \right) e^{-(x_2 - t_1) \alpha} \right\} d\alpha, \quad (3.59)$$

$$K_{21}^b(\alpha, x_2, t_1) = \left(\frac{\kappa + 1}{2} \right) \left\{ \left(R_{22a}(\alpha, x_2, t_1) - \left(t_1^* \alpha + t_2^* \right) e^{-(x_2 - t_1) \alpha} \right) d\alpha \right\}. \quad (3.60)$$

Upon integration $K_{21}^c(\alpha, x_2, t_1)$ can be simplified as

$$K_{21}^c(\alpha, x_2, t_1) = \left(\frac{\kappa + 1}{2} \right) \left\{ \frac{t_1^*}{(x_2 - t_1)^2} + \frac{t_2^*}{(x_2 - t_1)} \right\}. \quad (3.61)$$

$K_{22}(\alpha, x_2, t_2)$:

The expression for $K_{22}(\alpha, x_2, t_2)$ is given in Appendix A. For easy reference it has been reproduced here

$$K_{22}(\alpha, x_2, t_2) = 2 \int_0^\infty R_{22b}(\alpha, x_2, t_1) d\alpha \left(\frac{\kappa + 1}{4} \right). \quad (3.62)$$

After performing some tedious asymptotic analysis on $R_{22b}(\alpha, x_2, t_2)$ we find that

$$R_{22b}(\alpha, x_2, t_2) \sim \left(o_1^* \alpha + o_2^* + \frac{o_3^*}{\alpha} + \frac{o_4^*}{\alpha^2} + \frac{o_5^*}{\alpha^3} \right) e^{-(x_2 + t_2) \alpha} + \left(p_1^* \alpha^2 + p_2^* \alpha + p_3^* \right) e^{(x_2 + t_2 - 2h_2) \alpha} \quad (3.63)$$

where expressions for the variables are given in Appendix B. Again here only the $O(\alpha)$ and $O(1)$ terms give rise to singular terms. Separating these singular terms from K_{22} we can write,

$$K_{22}(\alpha, x_2, t_2) = K_{22}^c(\alpha, x_2, t_2) + K_{22}^b(\alpha, x_2, t_2) \quad (3.64)$$

where

$$K_{22}^c(\alpha, x_2, t_2) = \left(\frac{k+1}{2} \right) \int_0^\infty \left(o_1^* \alpha + o_2^* \right) e^{-(x_2+t_2)\alpha} \\ + \left(p_1^* \alpha^2 + p_2^* \alpha + p_3^* \right) e^{(x_2+t_2-2h_2)\alpha} \Big\} d\alpha, \quad (3.65)$$

$$K_{22}^b(\alpha, x_2, t_2) = \left(\frac{k+1}{2} \right) \left\{ \left(R_{22b}(\alpha, x_2, t_2) - \left(o_1^* \alpha + o_2^* \right) e^{-(x_2+t_2)\alpha} \right. \right. \\ \left. \left. + \left(p_1^* \alpha^2 + p_2^* \alpha + p_3^* \right) e^{(x_2+t_2-2h_2)\alpha} \right) d\alpha \right\}. \quad (3.66)$$

Upon integration $K_{22}^c(\alpha, x_2, t_2)$ can be simplified as

$$K_{22}^c(\alpha, x_2, t_2) = \left(\frac{\kappa+1}{2} \right) \\ \left\{ \frac{o_1^*}{(t_2+x_2)^2} + \frac{o_2^*}{(t_2+x_2)} \right. \\ \left. + \frac{2p_1^*}{(2h_2-t_2-x_2)^3} + \frac{p_2^*}{(2h_2-t_2-x_2)^2} + \frac{p_3^*}{(2h_2-t_2-x_2)} \right\}. \quad (3.67)$$

If we now substitute expressions for p_1^* , p_2^* , p_3^* we obtain the following generalized Cauchy kernel for a homogeneous medium with a stress-free boundary at $x_2 = h_2$.

$$\frac{4(h_2 - x_2)^2}{(2h_2 - t_2 - x_2)^3} - \frac{6(h_2 - x_2)}{(2h_2 - t_2 - x_2)^2} + \frac{1}{(2h_2 - t_2 - x_2)} \quad (3.68)$$

The kernel in (3.68) is identical to that found by Rizk[67] and Wu and Erdogan[46].

3.3 Evaluation of singularities and expressions for stress intensity factors

With the knowledge of the possible singular kernels obtained in the previous section, we can now evaluate the singularities of the unknown functions g_1 and g_2 at the crack tips for different crack configurations. Each crack configuration has been considered separately as the singularities may be different in each case.

3.3.1 Internal crack in the Nonhomogeneous material only

For this case, the relevant integral equation is (3.36) without the coupling term and can be written as

$$\frac{1}{\pi} \int_{-b_1}^{-a_1} \frac{g_1(t_1)}{(t_1 - x_1)} dt_1 + \frac{1}{\pi} \int_{-b_1}^{-a_1} g_1(t_1) K_{11}(x_1, t_1) dt_1 = p_1(x_1) \frac{\kappa + 1}{4\mu_0 e^{\beta x_1}}. \quad (3.69)$$

From (3.48) it can be seen that $K_{11}(x_1, t_1)$ may have singular terms only when x_1, t_1 either both go to zero or both go to $-h_1$. Hence in the case of an internal crack $K_{11}(x_1, t_1)$ is a bounded term and does not contribute to the singularity. The only singular term is the dominant term $\frac{1}{(t_1 - x_1)}$. The integral equation can now be written as

$$\frac{1}{\pi} \int_{-b_1}^{-a_1} \frac{g_1(t_1)}{(t_1 - x_1)} dt_1 = \Psi_1(x_1) \quad (3.70)$$

where $\Psi_1(x_1)$ represents all the bounded terms. To study the behavior of $g_1(t_1)$ near the endpoints $-a_1$ and $-b_1$, let us assume that

$$g_1(t_1) = \frac{g_1^*(t_1)}{(t_1 + b_1)^{\alpha_1} (-a_1 - t_1)^{\beta_1}} \quad (3.71)$$

where $g_1^*(t_1)$ satisfies the Hölder condition on $-b_1 \leq t_1 \leq -a_1$. Also, the singularities α_1 and β_1 should satisfy the condition $0 < \text{Re}(\alpha_1, \beta_1) < 1$. Defining a sectionally holomorphic function

$$F(z) = \frac{1}{\pi} \int_{-b_1}^{-a_1} \frac{g_1(t_1)}{(t_1 - z)} dt_1 \quad (3.72)$$

and substituting (3.71) into (3.72) we obtain,

$$F(z) = \frac{1}{\pi} \int_{-b_1}^{-a_1} \frac{g_1^*(t_1) e^{\pi i \beta_1}}{(t_1 + b_1)^{\alpha_1} (t_1 + a_1)^{\beta_1} (t_1 - z)} dt_1. \quad (3.73)$$

Following Muskhelishvili[55], the asymptotic behavior of (3.73) near the end points $-a_1$ and $-b_1$ can be expressed as

$$\begin{aligned} F(z) &= \frac{g_1^*(-b_1) e^{\pi i \alpha_1}}{(b_1 - a_1)^{\beta_1} (z + b_1)^{\alpha_1} \sin(\pi \alpha_1)} - \frac{g_1^*(-a_1)}{(b_1 - a_1)^{\alpha_1} (z + a_1)^{\beta_1} \sin(\pi \beta_1)} \\ &\quad + F_0(z) \end{aligned} \quad (3.74)$$

where $F_0(z)$ has singularity less than α_1, β_1 . Now using the Plemelj formula, we obtain,

$$\frac{1}{\pi} \int_{-b_1}^{-a_1} \frac{g_1(t_1)}{(t_1 - x_1)} dt_1 = \frac{1}{2} \left(F_1^+(x_1) + F_1^-(x_1) \right). \quad (3.75)$$

From (3.74) and (3.75) it then follows that

$$\begin{aligned} \frac{1}{\pi} \int_{-b_1}^{-a_1} \frac{g_1(t_1)}{(t_1 - x_1)} dt_1 &= \frac{g_1^*(-b_1) \cot(\pi \alpha_1)}{(b_1 - a_1)^{\beta_1} (x_1 + b_1)^{\alpha_1}} - \frac{g_1^*(-a_1) \cot(\pi \beta_1)}{(b_1 - a_1)^{\alpha_1} (-a_1 - x_1)^{\beta_1}} \\ &+ F_0(x_1). \end{aligned} \quad (3.76)$$

Substituting (3.76) into (3.70) we obtain,

$$\frac{g_1^*(-b_1) \cot(\pi \alpha_1)}{(b_1 - a_1)^{\beta_1} (x_1 + b_1)^{\alpha_1}} - \frac{g_1^*(-a_1) \cot(\pi \beta_1)}{(b_1 - a_1)^{\alpha_1} (-a_1 - x_1)^{\beta_1}} = \Psi_1(x_1) \quad (3.77)$$

Multiplying the entire equation by $(x_1 + b_1)^{\alpha_1}$ and taking limit as $x_1 \rightarrow -b_1$, we obtain,

$$\frac{g_1^*(-b_1) \cot(\pi \alpha_1)}{(b_1 - a_1)^{\beta_1}} = 0 \quad (3.78)$$

or

$$\cot(\pi \alpha_1) = 0. \quad (3.79)$$

Now multiplying the equation (3.77) by $(-a_1 - x_1)^{\beta_1}$ and taking limit as $x_1 \rightarrow -a_1$, we obtain,

$$\frac{g_1^*(-a_1) \cot(\pi \beta_1)}{(b_1 - a_1)^{\alpha_1}} = 0 \quad (3.80)$$

or

$$\cot(\pi \beta_1) = 0. \quad (3.81)$$

The only acceptable roots of (3.79) and (3.81) are $\alpha_1 = \beta_1 = \frac{1}{2}$. Thus we recover the square root singularity at the crack tips.

Stress intensity factor:

The stress intensity factor at irregular points $-b_1$ and $-a_1$ can be defined as,

$$k_1(-b_1) = \lim_{x_1 \rightarrow -b_1} \sqrt{2(-b_1 - x_1)} \sigma_{yy1}(x_1, 0), \quad (3.82)$$

$$k_1(-a_1) = \lim_{x_1 \rightarrow -a_1} \sqrt{2(x_1 + a_1)} \sigma_{yy1}(x_1, 0) \quad (3.83)$$

where x_1 lies outside the crack. It should be noted here that the left hand side of the singular integral equation in (3.36) is the expression for $\sigma_{yy1}(x_1, 0)$ inside as well as outside of the crack. Using that expression we can write (3.82) as,

$$\begin{aligned} k_1(-b_1) = \frac{4\mu_0}{\kappa + 1} \lim_{x_1 \rightarrow -b_1} e^{\beta x_1} \sqrt{2(-b_1 - x_1)} & \left\{ \frac{1}{\pi} \int_{-b_1}^{-a_1} \frac{g_1(t_1)}{(t_1 - x_1)} dt_1 \right. \\ & \left. + \frac{1}{\pi} \int_{-b_1}^{-a_1} g_1(t_1) K_{11}(x_1, t_1) dt_1 + \frac{1}{\pi} \int_{a_2}^{b_2} g_2(t_2) K_{12}(x_1, t_2) dt_2 \right\} \end{aligned} \quad (3.84)$$

Since $K_{11}(x_1, t_1)$ and $K_{12}(x_1, t_2)$ are bounded, we can rewrite (3.84) as

$$\begin{aligned} k_1(-b_1) = \frac{4\mu_0}{\kappa + 1} \lim_{x_1 \rightarrow -b_1} e^{\beta x_1} \sqrt{2(-b_1 - x_1)} \\ \left\{ \frac{1}{\pi} \int_{-b_1}^{-a_1} \frac{g_1(t_1)}{(t_1 - x_1)} dt_1 + \text{bounded terms} \right\} \end{aligned} \quad (3.85)$$

Defining a sectionally holomorphic function,

$$F(z) = \frac{1}{\pi} \int_{-b_1}^{-a_1} \frac{g_1(t_1)}{(t_1 - z)} dt_1 \quad (3.86)$$

and substituting the expression for $g_1(t_1)$ from (3.71) and noting that $\alpha_1 = \beta_1 = \frac{1}{2}$, we obtain,

$$F(z) = \frac{g_1^*(-b_1)e^{\frac{\pi i}{2}}}{(b_1 - a_1)^{\frac{1}{2}}(z + b_1)^{\frac{1}{2}}} - \frac{g_1^*(-a_1)}{(b_1 - a_1)^{\frac{1}{2}}(z + a_1)^{\frac{1}{2}}} + F_0(z). \quad (3.87)$$

Using Plemelj formulas, we can write

$$\frac{1}{\pi} \int_{-b_1}^{-a_1} \frac{g_1(t_1)}{(t_1 - x_1)} dt_1 = \frac{g_1^*(-b_1)}{(b_1 - a_1)^{\frac{1}{2}}(-b_1 - x_1)^{\frac{1}{2}}} - \frac{g_1^*(-a_1)}{(b_1 - a_1)^{\frac{1}{2}}(x_1 + a_1)^{\frac{1}{2}}} + F_0(z). \quad (3.88)$$

In (3.85) $x_1 < -b_1$ and $x_1 > -a_1$. Substituting back into (3.82), we obtain,

$$k_1(-b_1) = \frac{4\mu_0}{\kappa + 1} \lim_{x_1 \rightarrow -b_1} e^{\beta x_1} \sqrt{2(-b_1 - x_1)} \left\{ \frac{g_1^*(-b_1)}{(b_1 - a_1)^{\frac{1}{2}}(-b_1 - x_1)^{\frac{1}{2}}} - \frac{g_1^*(-a_1)}{(b_1 - a_1)^{\frac{1}{2}}(x_1 + a_1)^{\frac{1}{2}}} + \text{bounded terms} \right\} \quad (3.89)$$

which gives us,

$$k_1(-b_1) = \frac{4\mu_0 e^{-\beta b_1}}{\kappa + 1} \sqrt{\frac{2}{b_1 - a_1}} g_1^*(-b_1). \quad (3.90)$$

By similar analysis we obtain,

$$k_1(-a_1) = -\frac{4\mu_0 e^{-\beta a_1}}{\kappa + 1} \sqrt{\frac{2}{b_1 - a_1}} g_1^*(-a_1). \quad (3.91)$$

3.3.2 Internal crack in the homogeneous material only

For this case, the relevant integral equation is (3.42) without the coupling term and can be written as

$$\frac{1}{\pi} \int_{a_2}^{b_2} \frac{g_2(t_2)}{(t_2 - x_2)} dt_2 + \frac{1}{\pi} \int_{a_2}^{b_2} g_2(t_2) K_{22}(x_2, t_2) dt_2 = p_2(x_2) \frac{\kappa + 1}{4\mu_0}. \quad (3.92)$$

The analysis in this case is similar to that in Section 3.3.1 and we find singularities again

to be $\alpha_2 = \beta_2 = \frac{1}{2}$.

Stress intensity factor:

The analysis exactly similar to that in Section 3.3.1 and the resultant stress intensity factors are found as follows,

$$k_1(a_2) = \frac{4\mu_0}{\kappa + 1} \sqrt{\frac{2}{b_2 - a_2}} g_2^*(a_2), \quad (3.93)$$

$$k_1(b_2) = -\frac{4\mu_0}{\kappa + 1} \sqrt{\frac{2}{b_2 - a_2}} g_2^*(b_2). \quad (3.94)$$

3.3.3 Internal cracks in homogeneous and nonhomogeneous materials

In this case we obtain two coupled singular integral equations as follows:

$$\begin{aligned} \frac{1}{\pi} \int_{-b_1}^{-a_1} \frac{g_1(t_1)}{(t_1 - x_1)} dt_1 + \frac{1}{\pi} \int_{-b_1}^{-a_1} g_1(t_1) K_{11}(x_1, t_1) dt_1 \\ + \frac{1}{\pi} \int_{a_2}^{b_2} g_2(t_2) K_{12}(x_1, t_2) dt_2 = p_1(x_1) \frac{\kappa + 1}{4\mu_0 e^{\beta x_1}}, \end{aligned} \quad (3.95)$$

$$\begin{aligned} \frac{1}{\pi} \int_{a_2}^{b_2} \frac{g_2(t_2)}{(t_2 - x_2)} dt_2 + \frac{1}{\pi} \int_{-b_1}^{-a_1} g_1(t_1) K_{21}(x_2, t_1) dt_1 \\ + \frac{1}{\pi} \int_{a_2}^{b_2} g_2(t_2) K_{22}(x_2, t_2) dt_2 = p_2(x_2) \frac{\kappa + 1}{4\mu_0}. \end{aligned} \quad (3.96)$$

From (3.48), (3.55), (3.61) and (3.67), we see that K_{11} , K_{12} , K_{21} , K_{22} have no singular terms as long as the cracks are internal. Hence the only contribution to the singularity comes from the dominant terms $\frac{1}{(t_1 - x_1)}$ and $\frac{1}{(t_2 - x_2)}$. The analysis is then the same as

the previous cases considered in Sections 3.3.1 and 3.3.2 and we recover the expected square root singularities i.e. $\alpha_1 = \beta_1 = \alpha_2 = \beta_2 = \frac{1}{2}$.

Stress intensity factor:

Since the coupling kernels do not have any singular terms as long as the cracks are internal, this case is similar to cases considered previously. Hence the expressions for stress intensity factors would be identical to those found in Sections 3.3.1 and 3.3.2.

3.3.4 Edge crack in the nonhomogeneous material

For the case of an edge crack in the nonhomogeneous medium, the singular integral equation be written as,

$$\frac{1}{\pi} \int_{-h_1}^{-a_1} \frac{g_1(t_1)}{(t_1 - x_1)} dt_1 + \frac{1}{\pi} \int_{-h_1}^{-a_1} g_1(t_1) K_{11}(x_1, t_1) dt_1 = p_1(x_1) \frac{\kappa + 1}{4\mu_0 e^{\beta x_1}}. \quad (3.97)$$

In this case apart from the dominant term $\frac{1}{(t_1 - x_1)}$, we have contributions to the singular behavior of the solution from the Fredholm kernel. From (3.48), if we carry out a careful analysis, we find that the singular part of $K_{11}(x_1, t_1)$ can be written as,

$$K_{11}^s(x_1, t_1) = -\frac{1}{(x_1 + t_1 + 2h_1)} + \frac{6(x_1 + h_1)}{(x_1 + t_1 + 2h_1)^2} - \frac{4(x_1 + h_1)^2}{(x_1 + t_1 + 2h_1)^3}. \quad (3.98)$$

Putting all the bounded parts to the right hand side, we can write (3.97) as,

$$\frac{1}{\pi} \int_{-h_1}^{-a_1} \left(\frac{1}{(t_1 - x_1)} + K_{11}^s(x_1, t_1) \right) g_1(t_1) dt_1 = \Psi_1(x_1). \quad (3.99)$$

Again assume that,

$$g_1(t_1) = \frac{g_1^*(t_1)}{(t_1 - (-h_1))^{\alpha_1} ((-a_1) - t_1)^{\beta_1}} \quad (3.100)$$

Defining a sectionally holomorphic function

$$F(z) = \frac{1}{\pi} \int_{-h_1}^{-a_1} \frac{g_1(t_1)}{(t_1 - z)} dt_1 \quad (3.101)$$

and substituting (3.100) into (3.101) we obtain

$$F(z) = \frac{1}{\pi} \int_{-h_1}^{-a_1} \frac{g_1^*(t_1) e^{\pi i \beta_1}}{(t_1 - (-h_1))^{\alpha_1} (t_1 - (-a_1))^{\beta_1} (t_1 - z)} dt_1. \quad (3.102)$$

Following Muskhelishvili[55], the asymptotic behavior of $F(z)$ can be written as

$$F(z) = \frac{g_1^*(-h_1) e^{\pi i \alpha_1}}{(h_1 - a_1)^{\beta_1} (z - (-h_1))^{\alpha_1} \sin(\pi \alpha_1)} - \frac{g_1^*(-a_1)}{(h_1 - a_1)^{\alpha_1} (z - (-a_1))^{\beta_1} \sin(\pi \beta_1)} + F_0(z) \quad (3.103)$$

where $F_0(z)$ has singularity less than α_1, β_1 . Again following the same procedure as followed in Section 3.3.1, we can write,

$$\frac{1}{\pi} \int_{-h_1}^{-a_1} \frac{g_1(t_1)}{(t_1 - x_1)} dt_1 = \frac{g_1^*(-h_1) \cot(\pi \alpha_1)}{(h_1 - a_1)^{\beta_1} (x_1 + h_1)^{\alpha_1}} - \frac{g_1^*(-a_1) \cot(\pi \beta_1)}{(h_1 - a_1)^{\alpha_1} (-a_1 - x_1)^{\beta_1}} + F_0(x_1). \quad (3.104)$$

$$\frac{1}{\pi} \int_{-h_1}^{-a_1} \frac{g_1(t_1)}{(t_1 + x_1 + 2h_1)} dt_1 = \frac{g_1^*(-h_1)}{(h_1 - a_1)^{\beta_1} (x_1 + h_1)^{\alpha_1} \sin(\pi \alpha_1)} + F_0^*(x_1). \quad (3.105)$$

Differentiating (3.102) with respect to x_1 we obtain,

$$\frac{1}{\pi} \int_{-h_1}^{-a_1} \frac{g_1(t_1)}{(t_1 + x_1 + 2h_1)^2} dt_1 = \frac{\alpha_1 g_1^*(-h_1)}{(h_1 - a_1)^{\beta_1} (x_1 + h_1)^{\alpha_1 + 1} \sin(\pi \alpha_1)} + \frac{d}{dx_1} F_0^*(x_1). \quad (3.106)$$

Differentiating once again, we obtain

$$\frac{1}{\pi} \int_{-h_1}^{-a_1} \frac{g_1(t_1)}{(t_1 + x_1 + 2h_1)^3} dt_1 = \frac{\alpha_1(\alpha_1 + 1) g_1^*(-h_1)}{2(h_1 - a_1)^{\beta_1} (x_1 + h_1)^{\alpha_1 + 2} \sin(\pi \alpha_1)} + \frac{d^2}{dx_1^2} F_0^*(x_1). \quad (3.107)$$

Using (3.104 – 3.107) and (3.98), (3.99) may be expressed as,

$$\begin{aligned} & \frac{g_1^*(-h_1) \cot(\pi \alpha_1)}{(h_1 - a_1)^{\beta_1} (x_1 + h_1)^{\alpha_1}} - \frac{g_1^*(-a_1) \cot(\pi \beta_1)}{(h_1 - a_1)^{\alpha_1} (-a_1 - x_1)^{\beta_1}} - \frac{g_1^*(-h_1)}{(h_1 - a_1)^{\beta_1} (x_1 + h_1)^{\alpha_1} \sin(\pi \alpha_1)} \\ & + \frac{6\alpha_1 g_1^*(-h_1)}{(h_1 - a_1)^{\beta_1} (x_1 + h_1)^{\alpha_1} \sin(\pi \alpha_1)} - \frac{2\alpha_1(\alpha_1 + 1) g_1^*(-h_1)}{(h_1 - a_1)^{\beta_1} (x_1 + h_1)^{\alpha_1} \sin(\pi \alpha_1)} = \Psi_1^*(x_1). \end{aligned} \quad (3.108)$$

Multiplying (3.105) by $(-a_1 - x_1)^{\beta_1}$ and letting x_1 go to $-a_1$, we find the characteristic equation,

$$\cot(\pi \beta_1) = 0, \quad \Rightarrow \beta_1 = \frac{1}{2}. \quad (3.109)$$

On the other hand, multiplying (3.105) by $(x_1 + h_1)^{\alpha_1}$ and letting x_1 go to $-h_1$ we obtain the characteristic equation,

$$\cot(\pi \alpha_1) - 2\alpha_1(\alpha_1 + 1) + 6\alpha_1 - 1 = 0. \quad (3.110)$$

$\alpha_1 = 1$ is an unacceptable solution. Only acceptable solution is $\alpha_1 = 0$.

Stress intensity factor:

Observing that there is no singularity at $x_1 = -h_1$, the only point of interest is $x_1 = -a_1$. We can define the stress intensity factor at $x_1 = -a_1$ as

$$k_1(-a_1) = \lim_{x_1 \rightarrow -a_1} \sqrt{2(x_1 + a_1)} \sigma_{yy1}(x_1, 0). \quad (3.111)$$

Following a procedure similar to that in Section 3.3.1, we obtain,

$$k_1(-a_1) = -\frac{4\mu_0 e^{-\beta a_1}}{\kappa + 1} \sqrt{2} g_1^*(-a_1). \quad (3.112)$$

3.3.5 Crack in the nonhomogeneous material terminating at the interface

The relevant integral equation for this case can be written as,

$$\frac{1}{\pi} \int_{-b_1}^0 \frac{g_1(t_1)}{(t_1 - x_1)} dt_1 + \frac{1}{\pi} \int_{-b_1}^0 g_1(t_1) dt_1 K_{11}(x_1, t_1) = p_1(x_1) \frac{\kappa + 1}{4\mu_0 e^{\beta x_1}}. \quad (3.113)$$

In this case if we carry out a careful analysis of $K_{11}(x_1, t_1)$, we find that $K_{11}(x_1, t_1)$ contributes no singular terms to the integral equation. The only singular term is the dominant term $\frac{1}{(t_1 - x_1)}$. Hence this case becomes quite similar to that discussed in

Section 3.3.1 and if we follow the same procedure as in Section 3.3.1 we find,

$$\alpha_1 = \beta_1 = \frac{1}{2}. \quad (3.114)$$

Stress intensity factor:

The stress intensity factors are identical to Case I and are given as,

$$k_1(-b_1) = \frac{4\mu_0 e^{-\beta b_1}}{\kappa + 1} \sqrt{\frac{2}{b_1}} g_1^*(-b_1), \quad (3.115)$$

$$k_1(0) = -\frac{4\mu_0}{\kappa+1}\sqrt{\frac{2}{b_1}}g_1^*(0). \quad (3.116)$$

3.3.6 Crack in the homogeneous material terminating at the interface

The relevant integral equation for this problem can be written as,

$$\frac{1}{\pi}\int_0^{b_1}\frac{g_2(t_2)}{(t_2-x_2)}dt_2 + \frac{1}{\pi}\int_0^{b_1}g_2(t_2)dt_2K_{22}(x_2,t_2) = p_2(x_2)\frac{\kappa+1}{4\mu_0}. \quad (3.117)$$

In this case again we find that $K_{22}(x_2, t_2)$ contributes no singular terms to the integral equation. The only singular term is the dominant term $\frac{1}{(t_2-x_2)}$. Hence this case becomes exactly similar to that discussed in Section 3.3.2 and if we follow the same procedure we find,

$$\alpha_2 = \beta_2 = \frac{1}{2}. \quad (3.118)$$

This result was also obtained by Erdogan et.al.[42].

Stress intensity factor:

The stress intensity factors are identical to those of Section 3.3.2 and are given as,

$$k_1(0) = \frac{4\mu_0}{\kappa+1}\sqrt{\frac{2}{b_2}}g_2^*(0), \quad (3.119)$$

$$k_1(b_2) = -\frac{4\mu_0}{\kappa+1}\sqrt{\frac{2}{b_2}}g_2^*(b_2). \quad (3.120)$$

3.3.7 Crack passing through interface

For this case, we obtain two singular integral equations as follows:

$$\begin{aligned} \frac{1}{\pi} \int_{-b_1}^0 \frac{g_1(t_1)}{(t_1 - x_1)} dt_1 + \frac{1}{\pi} \int_{-b_1}^0 g_1(t_1) K_{11}(x_1, t_1) dt_1 \\ + \frac{1}{\pi} \int_0^{b_2} g_2(t_2) K_{12}(x_1, t_2) dt_2 = p_1(x_1) \frac{\kappa + 1}{4\mu_0 e^{\beta x_1}}, \end{aligned} \quad (3.121)$$

$$\begin{aligned} \frac{1}{\pi} \int_0^{b_2} \frac{g_2(t_2)}{(t_2 - x_2)} dt_2 + \frac{1}{\pi} \int_{-b_1}^0 g_1(t_1) K_{21}(x_2, t_1) dt_1 \\ + \frac{1}{\pi} \int_0^{b_2} g_2(t_2) K_{22}(x_2, t_2) dt_2 = p_2(x_2) \frac{\kappa + 1}{4\mu_0}. \end{aligned} \quad (3.122)$$

As was observed in Section 3.3.5 and Section 3.3.6, Fredholm kernels $K_{11}(x_1, t_1)$ and $K_{22}(x_2, t_2)$ do not contain any singular terms. Hence they do not contribute to the singularity. The coupling terms, however, do contain singular terms and after some analysis the singular terms are found as,

$$K_{12}^s(x_1, t_2) = \frac{1}{(t_2 - x_1)}, \quad -h_1 < x_1 < 0, 0 < t_2 < h_2, \quad (3.123)$$

$$K_{21}^s(x_2, t_1) = \frac{1}{(t_1 - x_2)}, \quad -h_1 < t_1 < 0, 0 < x_2 < h_2. \quad (3.124)$$

It should be noted here that t_1, x_1 are always negative while t_2, x_2 are always positive.

Hence $K_{12}^s(x_1, t_2)$ is singular only when both x_1 and t_2 go to zero. Similarly, $K_{21}^s(x_2, t_1)$ is singular only when both x_2 and t_1 go to zero. Putting all the bounded parts to the right hand side, (3.121) and (3.122) may be expressed as,

$$\frac{1}{\pi} \int_{-b_1}^0 \frac{g_1(t_1)}{(t_1 - x_1)} dt_1 + \frac{1}{\pi} \int_0^{b_2} \frac{g_2(t_2)}{(t_2 - x_1)} dt_2 = \Psi_1(x_1), \quad (3.125)$$

$$\frac{1}{\pi} \int_{-b_1}^0 \frac{g_1(t_1)}{(t_1 - x_2)} dt_1 + \frac{1}{\pi} \int_0^{b_2} \frac{g_2(t_2)}{(t_2 - x_2)} dt_2 = \Psi_2(x_2). \quad (3.126)$$

where $\Psi_1(x_1)$ and $\Psi_2(x_2)$ represent the bounded terms. Let us assume that

$$g_1(t_1) = \frac{g_1^*(t_1)}{(t_1 + b_1)^{\alpha_1} (-t_1)^{\beta_1}}, \quad (3.127)$$

$$g_2(t_2) = \frac{g_2^*(t_2)}{(t_2)^{\alpha_2} (b_2 - t_2)^{\beta_2}} \quad (3.128)$$

where $g_1^*(t_1)$ is Hölder continuous on $-b_1 < t_1 < 0$ and $g_2^*(t_2)$ is Hölder continuous on $0 < t_2 < b_2$. It should be noted that at zero there can be only one irregular point. Hence $\beta_1 = \alpha_2$. Defining sectionally holomorphic functions

$$F_1(z) = \frac{1}{\pi} \int_{-b_1}^0 \frac{g_1(t_1)}{(t_1 - z)} dt_1, \quad (3.129)$$

$$F_2(z) = \frac{1}{\pi} \int_0^{b_2} \frac{g_2(t_2)}{(t_2 - z)} dt_2 \quad (3.130)$$

and substituting (3.127) and (3.128) into (3.129) and (3.130) we obtain,

$$F_1(z) = \frac{1}{\pi} \int_{-b_1}^0 \frac{g_1^*(t_1) e^{\pi i \beta_1}}{(t_1 + b_1)^{\alpha_1} (t_1)^{\beta_1} (t_1 - z)} dt_1, \quad (3.131)$$

$$F_2(z) = \frac{1}{\pi} \int_0^{b_2} \frac{g_2^*(t_2)}{(t_2)^{\alpha_2} (b_2 - t_2)^{\beta_2} (t_2 - z)} dt_2. \quad (3.132)$$

Following Muskhelishvili[55], we can write,

$$F_1(z) = \frac{g_1^*(-b_1)e^{\pi i \alpha_1}}{(b_1)^{\beta_1}(z+b_1)^{\alpha_1}\sin(\pi \alpha_1)} - \frac{g_1^*(0)}{(b_1)^{\alpha_1}(z)^{\beta_1}\sin(\pi \beta_1)} + F_{10}(z) \quad (3.133)$$

and

$$F_2(z) = \frac{g_2^*(0)e^{\pi i \alpha_2}}{(b_2)^{\beta_2}(z)^{\alpha_2}\sin(\pi \alpha_2)} - \frac{g_2^*(b_2)}{(b_2)^{\alpha_2}(z-b_2)^{\beta_2}\sin(\pi \beta_2)} + F_{20}(z). \quad (3.134)$$

Using Plemelj formulas as before, we obtain,

$$\frac{1}{\pi} \int_{-b_1}^0 \frac{g_1(t_1)}{(t_1-x_1)} dt_1 = \frac{g_1^*(-b_1)\cot(\pi \alpha_1)}{(b_1)^{\beta_1}(x_1+b_1)^{\alpha_1}} - \frac{g_1^*(0)\cot(\pi \beta_1)}{(b_1)^{\alpha_1}(-x_1)^{\beta_1}} + F_{10}(x_1) \quad (3.135)$$

and

$$\frac{1}{\pi} \int_0^{b_2} \frac{g_2(t_2)}{(t_2-x_2)} dt_2 = \frac{g_2^*(0)\cot(\pi \alpha_2)}{(b_2)^{\beta_2}(x_2)^{\alpha_2}} - \frac{g_2^*(b_2)\cot(\pi \beta_2)}{(b_2)^{\alpha_2}(b_2-x_2)^{\beta_2}} + F_{20}(x_2). \quad (3.136)$$

Also,

$$\frac{1}{\pi} \int_{-b_1}^0 \frac{g_1(t_1)}{(t_1-x_2)} dt_1 = - \frac{g_1^*(0)}{(b_1)^{\alpha_1}(x_2)^{\beta_1}\sin(\pi \beta_1)} + F_{10}^*(x_2), \quad (3.137)$$

$$\frac{1}{\pi} \int_0^{b_2} \frac{g_2(t_2)}{(t_2-x_1)} dt_2 = \frac{g_2^*(0)}{(b_2)^{\beta_2}(-x_1)^{\alpha_2}\sin(\pi \alpha_2)} + F_{20}^*(x_1). \quad (3.138)$$

Substituting back into (3.125) and (3.126) we obtain,

$$\frac{g_1^*(-b_1)\cot(\pi \alpha_1)}{(b_1)^{\beta_1}(x_1+b_1)^{\alpha_1}} - \frac{g_1^*(0)\cot(\pi \beta_1)}{(b_1)^{\alpha_1}(-x_1)^{\beta_1}} + \frac{g_2^*(0)}{(b_2)^{\beta_2}(-x_1)^{\alpha_2}\sin(\pi \alpha_2)} = \Psi_1^*(x_1), \quad (3.139)$$

$$\frac{g_2^*(0)\cot(\pi \alpha_2)}{(b_2)^{\beta_2}(x_2)^{\alpha_2}} - \frac{g_2^*(b_2)\cot(\pi \beta_2)}{(b_2)^{\alpha_2}(b_2-x_2)^{\beta_2}} - \frac{g_1^*(0)}{(b_1)^{\alpha_1}(x_2)^{\beta_1}\sin(\pi \beta_1)} = \Psi_2^*(x_2). \quad (3.140)$$

Multiplying (3.139) by $(x_1 + b_1)^{\alpha_1}$ and letting x_1 go to $-b_1$ and multiplying (3.140) by $(b_2 - x_2)^{\beta_2}$ and letting x_2 go to b_2 , we obtain the characteristic equations,

$$\cot(\pi\alpha_1) = 0 \quad \Rightarrow \alpha_1 = \frac{1}{2} \quad (3.141)$$

and

$$\cot(\pi\beta_2) = 0 \quad \Rightarrow \beta_2 = \frac{1}{2}. \quad (3.142)$$

Now multiplying (3.140) by $(-x_1)^{\beta_1}$ and letting x_1 go to zero and multiplying (3.141) by $x_2^{\beta_1}$ and letting x_2 go to zero, keeping in mind that $\beta_1 = \alpha_2$, we obtain,

$$-\frac{g_1^*(0)\cot(\pi\beta_1)}{(b_1)^{\alpha_1}} + \frac{g_2^*(0)}{(b_2)^{\beta_2}\sin(\pi\beta_1)} = 0, \quad (3.143)$$

$$-\frac{g_1^*(0)}{(b_1)^{\alpha_1}\sin(\pi\beta_1)} + \frac{g_2^*(0)\cot(\pi\beta_1)}{(b_2)^{\beta_2}} = 0. \quad (3.144)$$

From equation (3.143), we obtain,

$$\frac{g_2^*(0)}{(b_2)^{\beta_2}\sin(\pi\beta_1)} = \frac{g_1^*(0)\cos(\pi\beta_1)}{(b_1)^{\alpha_1}\sin(\pi\beta_1)}. \quad (3.145)$$

Substituting (3.145) into (3.144) we obtain the following equation

$$-\frac{g_1^*(0)}{(b_1)^{\alpha_1}\sin(\pi\beta_1)} + \frac{g_1^*(0)\cos^2(\pi\beta_1)}{(b_1)^{\alpha_1}\sin(\pi\beta_1)} = 0. \quad (3.146)$$

Solving (3.146) we obtain,

$$\frac{g_1^*(0)\sin(\pi\beta_1)}{(b_1)^{\alpha_1}} = 0. \quad (3.147)$$

For non-trivial solution, we obtain,

$$\beta_1 = (0, \pm 1, \pm 2, \dots). \quad (3.148)$$

The only acceptable solution is

$$\beta_1 = 0. \quad (3.149)$$

We can now write the unknown functions as

$$g_1(t_1) = \frac{g_1^*(t_1)}{(t_1 + b_1)^{\frac{1}{2}}}, \quad (3.150)$$

$$g_2(t_2) = \frac{g_2^*(t_2)}{(b_2 - t_2)^{\frac{1}{2}}}. \quad (3.151)$$

From (3.143) and (3.144) it is clear that $g_1^*(0)$ and $g_2^*(0)$ are related and the relation can be expressed as

$$-\frac{g_1^*(0)\cos(\pi\beta_1)}{(b_1)^{\frac{1}{2}}\sin(\pi\beta_1)} + \frac{g_2^*(0)}{(b_2)^{\frac{1}{2}}\sin(\pi\beta_1)} = 0 \quad (3.152)$$

or

$$-\frac{g_1(0)\cos(\pi\beta_1)}{\sin(\pi\beta_1)} + \frac{g_2(0)}{\sin(\pi\beta_1)} = 0. \quad (3.153)$$

As $\beta_1 = 0$, (3.153) will be satisfied if

$$g_2(0) = g_1(0). \quad (3.154)$$

The result $\beta_1 = 0$ implies that there is no power singularity at the interface. There is a possibility of a weaker logarithmic singularity. We investigate it as follows. Defining sectionally holomorphic functions

$$F_1(z) = \frac{1}{\pi} \int_{-b_1}^0 \frac{g_1(t_1)}{(t_1 - z)} dt_1, \quad (3.155)$$

$$F_2(z) = \frac{1}{\pi} \int_0^{b_2} \frac{g_2(t_2)}{(t_2 - z)} dt_2 \quad (3.156)$$

and substituting (3.150) and (3.151) into (3.155) and (3.156) we obtain,

$$F_1(z) = \frac{1}{\pi} \int_{-b_1}^0 \frac{g_1^*(t_1)}{(t_1 + b_1)^{\frac{1}{2}}(t_1 - z)} dt_1, \quad (3.157)$$

$$F_2(z) = \frac{1}{\pi} \int_0^{b_2} \frac{g_2^*(t_2)}{(b_2 - t_2)^{\frac{1}{2}}(t_2 - z)} dt_2. \quad (3.158)$$

Investigating in the neighborhood of zero, we obtain,

$$F_1(z) \simeq \frac{g_1^*(0)}{b_1^{\frac{1}{2}}} \log(z) \quad (3.159)$$

$$F_2(z) \simeq -\frac{g_2^*(0)}{b_2^{\frac{1}{2}}} \log(z) \quad (3.160)$$

Using Plemelj formulas, in the neighborhood of zero, we can write

$$\frac{1}{\pi} \int_{-b_1}^0 \frac{g_1(t_1)}{(t_1 - x_1)} dt_1 \simeq \frac{g_1^*(0)}{b_1^{\frac{1}{2}}} \frac{1}{\pi} \log|x_1| \quad (3.161)$$

$$\frac{1}{\pi} \int_0^{b_2} \frac{g_2(t_2)}{(t_2 - x_1)} dt_2 \simeq -\frac{g_2^*(0)}{b_2^{\frac{1}{2}}} \frac{1}{\pi} \log|x_1| \quad (3.162)$$

$$\frac{1}{\pi} \int_{-b_1}^0 \frac{g_1(t_1)}{(t_1 - x_2)} dt_1 \simeq \frac{g_1^*(0)}{b_1^{\frac{1}{2}}} \frac{1}{\pi} \log|x_2| \quad (3.163)$$

$$\frac{1}{\pi} \int_0^{b_2} \frac{g_2(t_2)}{(t_2 - x_2)} dt_2 \simeq -\frac{g_2^*(0)}{b_2^{\frac{1}{2}}} \frac{1}{\pi} \log|x_2| \quad (3.164)$$

It should be noted that in (3.159 – 3.164), there are bounded terms that have not been

mentioned. Hence the \simeq sign has been used. Substituting (3.161 – 3.164) into (3.125) and (3.126), we obtain,

$$\frac{g_1^*(0)}{b_1^{\frac{1}{2}}} \frac{1}{\pi} \log |x_1| - \frac{g_2^*(0)}{b_2^{\frac{1}{2}}} \frac{1}{\pi} \log |x_1| = \Psi_1^*(x_1), \quad (3.165)$$

$$\frac{g_1^*(0)}{b_1^{\frac{1}{2}}} \frac{1}{\pi} \log |x_2| - \frac{g_2^*(0)}{b_2^{\frac{1}{2}}} \frac{1}{\pi} \log |x_2| = \Psi_2^*(x_2) \quad (3.166)$$

where $\Psi_1^*(x_1)$, $\Psi_2^*(x_2)$ are bounded functions. Using (3.150), (3.151), (3.154) it can now be clearly seen that the coefficient of the logarithmic term cancels out. Hence there is no singularity at the interface. This is an important conclusion. This should be compared with the case of bonded layers of dissimilar materials. It was shown by Ritz[67] and Lu, Erdogan[26, 27] that when a crack crosses the interface between two dissimilar materials there is an irregular point at the interface apart from the two irregular points at the crack tips. The strength of the singularity at the irregular point at the interface has to be determined from the asymptotic analysis at the interface. In our study of FGMs, it was found that there is no irregular point at the interface or, in other words, there is no singularity at the interface.

Since there is no singularity at the interface, we can pose (3.121) and (3.122) as one singular integral equation as

$$\frac{1}{\pi} \int_{-b_1}^{b_2} \frac{g(t)}{(t-x)} dt + \frac{1}{\pi} \int_{-b_1}^{b_2} g(t) dt K(x, t) = p(x) \frac{\kappa + 1}{4\mu_0} \quad (3.167)$$

where

$$g(t) = \begin{cases} g_1(t) & t < 0 \\ g_2(t) & t > 0 \end{cases} \quad (3.168)$$

$$K(x, t) = \begin{cases} K_{11}(x, t) & (x, t) < 0 \\ K_{12}(x, t) - \frac{1}{(t-x)} & x < 0, t > 0 \\ K_{21}(x, t) - \frac{1}{(t-x)} & x > 0, t < 0 \\ K_{22}(x, t) & (x, t) > 0 \end{cases} \quad (3.169)$$

$$p(x) = \begin{cases} \frac{p_1(x)}{e^{\beta x_1}} & x < 0 \\ p_2(x) & x > 0 \end{cases}. \quad (3.170)$$

It should be noted that the only irregular points are $x = -b_1$ and $x = b_2$. Hence, we can write,

$$g(t) = \frac{g^*(t)}{(t+b_1)^{\frac{1}{2}}(b_2-t)^{\frac{1}{2}}} \quad (3.171)$$

where $g^*(t)$ is a bounded function.

Stress intensity factors:

The analysis is similar to previous cases. Keeping in mind that irregular point $x = -b_1$ lies in the nonhomogeneous material while $x = b_2$ lies in homogeneous we can write the stress intensity factors as,

$$k_1(-b_1) = \frac{4\mu_0 e^{-\beta b_1}}{\kappa + 1} \sqrt{\frac{2}{b_1 + b_2}} g^*(-b_1), \quad (3.172)$$

$$k_1(b_2) = -\frac{4\mu_0}{\kappa + 1} \sqrt{\frac{2}{b_1 + b_2}} g^*(b_2). \quad (3.173)$$

3.3.8 Edge crack passing through interface

This case is covered by some of the previous cases. The analysis for the singularity at $x = -h_1$ is identical to that for an edge crack. The singularity at the interface can be

evaluated in a manner identical to that in Section 3.3.7. If we carry out the analysis, we find that,

$$\alpha_1 = \beta_1 = \alpha_2 = 0, \beta_2 = \frac{1}{2}. \quad (3.174)$$

Here again we can represent the problem by a single singular integral equation as follows:

$$\frac{1}{\pi} \int_{-h_1}^{b_2} \frac{g(t)}{(t-x)} dt + \frac{1}{\pi} \int_{-h_1}^{b_2} g(t) dt K(x, t) = p(x) \frac{\kappa + 1}{4\mu_0} \quad (3.175)$$

where

$$g(t) = \begin{cases} g_1(t) & t < 0 \\ g_2(t) & t > 0 \end{cases} \quad (3.176)$$

$$K(x, t) = \begin{cases} K_{11}(x, t) & x, t < 0 \\ K_{12}(x, t) - \frac{1}{(t-x)} & x < 0, t > 0 \\ K_{21}(x, t) - \frac{1}{(t-x)} & x > 0, t < 0 \\ K_{22}(x, t) & x, t > 0 \end{cases} \quad (3.177)$$

$$p(x) = \begin{cases} p_1(x) & x < 0 \\ p_2(x) & x > 0. \end{cases} \quad (3.178)$$

$g(t)$ can be represented as

$$g(t) = \frac{g^*(t)}{(b_2 - t)^{\frac{1}{2}}} \quad (3.179)$$

Stress intensity factor:

The stress intensity factor at $x = b_2$ can now be written as

$$k_1(b_2) = -\frac{4\mu_0}{\kappa + 1} \sqrt{2} g^*(b_2). \quad (3.180)$$

CHAPTER 4

NUMERICAL PROCEDURE

The singular integral equations derived in Chapter 3 can not be solved in closed form. Hence there is a need to use some kind of numerical procedure to solve these equations. In the literature various approaches have been studied. The two most common approaches are the quadrature method and the series expansion method. In this study, the expansion technique described in [57,58] is used. In this chapter the method will be explained in some detail. For different crack configurations, the numerical procedure has to be modified. These modifications will also be explained in this chapter.

4.1 Numerical procedure for a general case

For the most general crack configuration the singular integral equations are given by (3.36) and (3.42) and may be expressed as

$$\begin{aligned} \frac{1}{\pi} \int_{-b_1}^{-a_1} \left[\frac{1}{(t_1 - x_1)} + K_{11}(x_1, t_1) \right] g_1(t_1) dt_1 \\ + \frac{1}{\pi} \int_{a_2}^{b_2} K_{12}(x_1, t_2) g_2(t_2) dt_2 = p_1(x_1) \frac{\kappa + 1}{4\mu_0 e^{\beta x_1}}, \quad -b_1 < x_1 < -a_1, \end{aligned} \quad (4.1)$$

$$\begin{aligned} \frac{1}{\pi} \int_{-b_1}^{-a_1} K_{21}(x_2, t_1) g_1(t_1) dt_1 \\ + \frac{1}{\pi} \int_{a_2}^{b_2} \left[\frac{1}{(t_2 - x_2)} + K_{22}(x_2, t_2) \right] g_2(t_2) dt_2 = p_2(x_2) \frac{\kappa + 1}{4\mu_0}, \\ a_2 < x_2 < b_2. \end{aligned} \quad (4.2)$$

In equation (4.1), $-b_1 < x_1 < -a_1$ and in equation (4.2), $a_2 < x_2 < b_2$. Now normalizing the integral equations with respect to the crack lengths as follows,

$$t_1 = \frac{b_1 - a_1}{2} r_1 - \frac{b_1 + a_1}{2}, \quad (4.3)$$

$$x_1 = \frac{b_1 - a_1}{2} s_1 - \frac{b_1 + a_1}{2}, \quad (4.4)$$

$$t_2 = \frac{b_2 - a_2}{2} r_2 + \frac{b_2 + a_2}{2}, \quad (4.5)$$

$$x_2 = \frac{b_2 - a_2}{2} s_2 + \frac{b_2 + a_2}{2}, \quad (4.6)$$

we obtain

$$\begin{aligned} \frac{1}{\pi} \int_{-1}^1 \left[\frac{1}{(r_1 - s_1)} + \hat{K}_{11}(s_1, r_1) \right] \hat{g}_1(r_1) dr_1 + \frac{1}{\pi} \int_{-1}^1 \hat{K}_{12}(s_1, r_2) \hat{g}_2(r_2) dr_2 \\ = \hat{p}_1(s_1) \frac{\kappa + 1}{4\mu_0}, |s_1| < 1 \end{aligned} \quad (4.7)$$

$$\begin{aligned} \frac{1}{\pi} \int_{-1}^1 \hat{K}_{21}(s_2, r_1) \hat{g}_1(r_1) dr_1 + \frac{1}{\pi} \int_{-1}^1 \left[\frac{1}{(t_2 - x_2)} + \hat{K}_{22}(s_2, r_2) \right] \hat{g}_2(r_2) dr_2 \\ = \hat{p}_2(s_2) \frac{\kappa + 1}{4\mu_0}, |s_2| < 1 \end{aligned} \quad (4.8)$$

where

$$\hat{K}_{ij}(s_i, r_j) = \left(\frac{b_j - a_j}{2} \right) K_{ij}(x_i, t_j), \quad (4.9)$$

$$\hat{g}_j(r_j) = g_j(t_j), \quad (4.10)$$

$$\hat{p}_1(s_1) = \frac{p_1(x_1)}{e^{\beta x_1}}, \quad (4.11)$$

$$\hat{p}_2(s_2) = p_2(x_2). \quad (4.12)$$

From Chapter 3 it can be seen that the density function $\hat{g}_j(r_j)$ can generally be represented as a product of a bounded function and a weight function. Thus we can represent $\hat{g}_j(r_j)$ as

$$\hat{g}_1(r_1) = \frac{g_1^*(t_1)}{(t_1 + b_1)^{\alpha_1} (-a_1 - t_1)^{\beta_1}} \quad (4.13)$$

or

$$\hat{g}_1(r_1) = \frac{F_1(r_1)}{(1 + r_1)^{\alpha_1} (1 - r_1)^{\beta_1}} \quad (4.14)$$

where $F_1(r_1)$ is a bounded function and

$$\hat{g}_2(r_2) = \frac{g_2^*(t_2)}{(t_2 - a_2)^{\beta_2} (b_2 - t_2)^{\alpha_2}} \quad (4.15)$$

or

$$\hat{g}_2(r_2) = \frac{F_2(r_2)}{(1 + r_2)^{\alpha_2} (1 - r_2)^{\beta_2}} \quad (4.16)$$

where $F_2(r_2)$ is a bounded function. The values of the exponents $\alpha_1, \beta_1, \alpha_2, \beta_2$ depend on the crack configuration as shown in Chapter 3. As $F_1(r_1)$ and $F_2(r_2)$ are bounded functions we can expand them in terms of orthogonal polynomials as

$$F_1(r_1) = \sum_{n=0}^N A_n O_n(r_1) \text{ and} \quad (4.17)$$

$$F_2(r_2) = \sum_{n=0}^M B_n O_n(r_2). \quad (4.18)$$

The choice of the orthogonal polynomial $O_n(r)$ which is generally a special case of the Jacobi polynomials $P_n^{(\alpha, \beta)}(r)$ depends on the weight function. It can be seen that on substituting (4.17) and (4.18) into (4.11) and (4.12) we have $(N + 1)$ unknowns $A_0 \dots A_N$ and $(M + 1)$ unknowns $B_0 \dots B_M$. Hence we need to have $(N + M + 2)$

equations. This is usually done by choosing collocation points where the equations are satisfied exactly. Though there is no restriction on the choice of the collocation points, usually the roots of Chebyshev polynomials are chosen as collocation points. These seem to give better convergence in numerical results. The number of collocation points depends on the number of unknowns. Evaluating the equations at the collocation points we obtain a system of algebraic equations which can be solved by matrix inversion. It should be noted here that particular crack configurations may dictate some physical conditions for a unique solution. These conditions known as single valuedness conditions need to be incorporated into the system of linear equations. We will now analyze the different crack configurations separately.

4.2 Numerical procedure for specific crack configurations

4.2.1 Internal crack in the nonhomogeneous material only

From (3.69) we can see that the singular integral equation for this case is

$$\frac{1}{\pi} \int_{-b_1}^{-a_1} \frac{g_1(t_1)}{(t_1 - x_1)} dt_1 + \frac{1}{\pi} \int_{-b_1}^{-a_1} g_1(t_1) K_{11}(x_1, t_1) dt_1 = p_1(x_1) \frac{\kappa + 1}{4\mu_0 e^{\beta x_1}},$$

$$-b_1 < x_1 < -a_1. \quad (4.19)$$

Normalizing using (4.3) and (4.4) the singular integral equation can be written as

$$\frac{1}{\pi} \int_{-1}^1 \left[\frac{1}{(r_1 - s_1)} + \hat{K}_{11}(s_1, r_1) \right] \hat{g}_1(r_1) dr_1 = \hat{p}_1(s_1) \frac{\kappa + 1}{4\mu_0}, \quad |s_1| < 1 \quad (4.20)$$

where

$$\hat{K}_{11}(s_1, r_1) = \left(\frac{b_1 - a_1}{2} \right) K_{11} \left(\frac{b_1 - a_1}{2} s_1 - \frac{b_1 + a_1}{2}, \frac{b_1 - a_1}{2} r_1 - \frac{b_1 + a_1}{2} \right), \quad (4.21)$$

$$\hat{g}_1(r_1) = g_1\left(\frac{b_1 - a_1}{2}r_1 - \frac{b_1 + a_1}{2}\right), \quad (4.22)$$

$$\hat{p}_1(s_1) = \frac{p_1(x_1)}{e^{\beta x_1}}. \quad (4.23)$$

Observing from equations (3.79) and (3.81) that $\alpha_1 = \beta_1 = \frac{1}{2}$, we can write (4.14) as

$$\hat{g}_1(r_1) = \frac{F_1(r_1)}{\sqrt{1 - r_1^2}} \quad (4.24)$$

where

$$F_1(r_1) = g_1^*\left(\frac{b_1 - a_1}{2}r_1 - \frac{b_1 + a_1}{2}\right) \left(\frac{2}{b_1 - a_1}\right) \quad (4.25)$$

As $g_1^*(t_1)$ is a bounded function, $F_1(r_1)$ is a bounded function. Hence it can be expanded in series of polynomials. The orthogonal polynomials corresponding to the weight function $\frac{1}{\sqrt{1 - r_1^2}}$ are Chebyshev polynomials of the first kind. We now expand $F_1(r_1)$ as follows ,

$$F_1(r_1) = \sum_{n=0}^N A_n T_n(r_1). \quad (4.26)$$

Equation (4.20) can now be written as

$$\frac{1}{\pi} \int_{-1}^1 \left[\frac{1}{(r_1 - s_1)} + \hat{K}_{11}(s_1, r_1) \right] \frac{\sum_{n=0}^N A_n T_n(r_1)}{\sqrt{1 - r_1^2}} dr_1 = \hat{p}_1(s_1) \frac{\kappa + 1}{4\mu_0}. \quad (4.27)$$

Since the crack is closed the single valuedness condition dictates that

$$\int_{-b_1}^{-a_1} g_1(t_1) dt_1 = 0 \quad (4.28)$$

which can also be written as

$$\int_{-1}^1 \frac{\sum_{n=0}^N A_n T_n(r_1)}{\sqrt{1 - r_1^2}} dr_1 = 0. \quad (4.29)$$

Chebyshev polynomials satisfy the following orthogonality relations:

$$\int_{-1}^1 \frac{T_n(r_1)T_m(r_1)}{\sqrt{1-r_1^2}} dr_1 = \begin{cases} 0 & n \neq m \\ \pi & n = m = 0 \\ \frac{\pi}{2} & n = m > 0 \end{cases} \quad (4.30)$$

Using these orthogonality relations we clearly observe from (4.29) that $A_0 = 0$. The singular integral equation in (4.27) can thus be written as

$$\frac{1}{\pi} \int_{-1}^1 \left[\frac{1}{(r_1 - s_1)} + \hat{K}_{11}(s_1, r_1) \right] \frac{\sum_{n=1}^N A_n T_n(r_1)}{\sqrt{1-r_1^2}} dr_1 = \hat{p}_1(s_1) \frac{\kappa + 1}{4\mu_0}, |s_1| < 1. \quad (4.31)$$

By choosing collocation points we can convert this singular integral equation into a system of linear algebraic equations as

$$\frac{1}{\pi} \int_{-1}^1 \left[\frac{1}{(r_1 - s_k)} + \hat{K}_{11}(s_k, r_1) \right] \frac{\sum_{n=1}^N A_n T_n(r_1)}{\sqrt{1-r_1^2}} dr_1 = \hat{p}_1(s_k) \frac{\kappa + 1}{4\mu_0}. \quad (k = 1, \dots, N) \quad (4.32)$$

The collocation points can be arbitrarily chosen but good convergences are obtained if the points are symmetric about the center of the crack with dense distribution near the ends of the crack. The roots of Chebyshev polynomials are used as the collocation points. Thus,

$$s_k = \frac{(2k-1)\pi}{2N} \quad (k = 1, \dots, N). \quad (4.33)$$

The Cauchy part of this equation is evaluated in closed form while the Fredholm part is evaluated numerically. In the numerical evaluation of the Fredholm kernel Gauss Quadrature method is used. It should be noted that the Fredholm kernel contains a logarithmic singularity of the form

$$\frac{1}{\pi} \int_{-1}^1 [\log|r_1 - s_1|] \frac{\sum_{n=1}^N A_n T_n(r_1)}{\sqrt{1-r_1^2}} dr_1.$$

Considering the numerical difficulties involved in this integral (eg. Joseph [56]), it is evaluated in closed form. The closed form expressions for some of these integrals are given in Appendix D. Integrals of the type

$$\frac{1}{\pi} \int_{-1}^1 (r_1 - s_1)^m [\log|r_1 - s_1|] \frac{\sum_{n=1}^N A_n T_n(r_1)}{\sqrt{1-r_1^2}} dr_1$$

where m is a positive integer emerge from the Fredholm kernel too. But these can be easily evaluated numerically by splitting the integral from -1 to s_1 and s_1 to 1 [41]. Thus by evaluating the integrals, from (4.31) we obtain an $(N \times N)$ system of linear algebraic equations which can be solved by matrix inversion. The right hand sides depend on the specific loading conditions. The expressions for $\hat{p}_1(s_1)$ for different loading conditions are given in Appendix C. Thus the solution to the unknown coefficients is obtained. Some useful expressions used in evaluating these integrals are given in Appendix D.

Stress intensity factors:

Equations (3.90) and (3.91) give stress intensity factors as follows :

$$k_1(-b_1) = \frac{4\mu_0 e^{-\beta b_1}}{\kappa + 1} \sqrt{\frac{2}{b_1 - a_1}} g_1^*(-b_1) \quad (4.34)$$

and

$$k_1(-a_1) = -\frac{4\mu_0 e^{-\beta a_1}}{\kappa + 1} \sqrt{\frac{2}{b_1 - a_1}} g_1^*(-a_1). \quad (4.35)$$

Using (4.24) we can write,

$$k_1(-b_1) = \frac{4\mu_0 e^{-\beta b_1}}{\kappa + 1} \sqrt{\frac{b_1 - a_1}{2}} F_1(-1) \quad (4.36)$$

and

$$k_1(-a_1) = -\frac{4\mu_0 e^{-\beta a_1}}{\kappa + 1} \sqrt{\frac{b_1 - a_1}{2}} F_1(1) \quad (4.37)$$

where

$$F_1(-1) = \sum_{n=1}^N A_n T_n(-1) = \sum_{n=1}^N A_n (-1)^n \quad (4.38)$$

and

$$F_1(1) = \sum_{n=1}^N A_n T_n(1) = \sum_{n=1}^N A_n. \quad (4.39)$$

4.2.2 Internal crack in the homogeneous material only

The relevant singular integral equation can be written as

$$\frac{1}{\pi} \int_{a_2}^{b_2} \frac{g_2(t_2)}{(t_2 - x_2)} dt_2 + \frac{1}{\pi} \int_{a_2}^{b_2} g_2(t_2) K_{22}(x_2, t_2) dt_2 = p_2(x_2) \frac{\kappa + 1}{4\mu_0}, \quad a_2 < x_2 < b_2. \quad (4.40)$$

Normalizing (4.40) using (4.5) and (4.6), equation (4.40) can be written as

$$\frac{1}{\pi} \int_{-1}^1 \left[\frac{1}{(r_2 - s_2)} + \hat{K}_{22}(s_2, r_2) \right] \hat{g}_2(r_2) dr_2 = \hat{p}_2(s_2) \frac{\kappa + 1}{4\mu_0}, \quad |s_2| < 1, \quad (4.41)$$

where

$$\hat{K}_{22}(s_2, r_2) = \left(\frac{b_2 - a_2}{2} \right) K_{22} \left(\frac{b_2 - a_2}{2} s_2 - \frac{b_2 + a_2}{2}, \frac{b_2 - a_2}{2} r_2 - \frac{b_2 + a_2}{2} \right), \quad (4.42)$$

$$\hat{g}_2(r_2) = g_2 \left(\frac{b_2 - a_2}{2} r_2 - \frac{b_2 + a_2}{2} \right). \quad (4.43)$$

From Chapter 3 we find that $\alpha_2 = \beta_2 = \frac{1}{2}$. Hence (4.16) may be expressed as

$$\widehat{g}_2(r_2) = \frac{F_2(r_2)}{\sqrt{1-r_2^2}} \quad (4.44)$$

where $F_2(r_2)$ is a bounded function. The numerical procedure in this case is now identical to that in Section 4.2.1. By expanding $F_2(r_2)$ in terms of Chebyshev polynomials we can now write (4.41) as

$$\frac{1}{\pi} \int_{-1}^1 \left[\frac{1}{(r_2 - s_2)} + \widehat{K}_{22}(s_2, r_2) \right] \frac{\sum_{n=1}^M B_n T_n(r_2)}{\sqrt{1-r_2^2}} dr_2 = \widehat{p}_2(s_2) \frac{\kappa+1}{4\mu_0}, |s_2| < 1. \quad (4.45)$$

Here we have used the single valuedness condition to find that $B_0 = 0$. Choosing the collocation points as in (4.33), we obtain the following system of algebraic equations :

$$\frac{1}{\pi} \int_{-1}^1 \left[\frac{1}{(r_2 - s_k)} + \widehat{K}_{22}(s_k, r_2) \right] \frac{\sum_{n=1}^M B_n T_n(r_2)}{\sqrt{1-r_2^2}} dr_2 = \widehat{p}_2(s_k) \frac{\kappa+1}{4\mu_0}. \quad (k = 1..M) \quad (4.46)$$

After evaluating the integrals as in Section 4.2.1, this $(M \times M)$ system can now be solved by matrix inversion.

Stress intensity factors:

Using expressions for stress intensity factors (3.93), (3.94) from Chapter 3 and the normalization in (4.5), (4.6) we obtain the expressions for stress intensity factors as

$$k_1(a_2) = \frac{4\mu_0}{\kappa+1} \sqrt{\frac{b_2 - a_2}{2}} F_2(-1) \quad (4.47)$$

and

$$k_1(b_2) = -\frac{4\mu_0}{\kappa+1} \sqrt{\frac{b_2 - a_2}{2}} F_2(1). \quad (4.48)$$

where

$$F_2(-1) = \sum_{n=1}^N B_n T_n(-1) = \sum_{n=1}^N B_n (-1)^n \quad (4.49)$$

and

$$F_2(1) = \sum_{n=1}^N B_n T_n(1) = \sum_{n=1}^N B_n \quad (4.50)$$

4.2.3 Internal cracks in homogeneous and nonhomogeneous materials

Using (4.3 – 4.6), singular integral equations for this case can be written in normalized form as

$$\begin{aligned} \frac{1}{\pi} \int_{-1}^1 \left[\frac{1}{(r_1 - s_1)} + \hat{K}_{11}(s_1, r_1) \right] \hat{g}_1(r_1) dr_1 + \frac{1}{\pi} \int_{-1}^1 \hat{K}_{12}(s_1, r_2) \hat{g}_2(r_2) dr_2 \\ = \hat{p}_1(s_1) \frac{\kappa + 1}{4\mu_0}, |s_1| < 1, \end{aligned} \quad (4.51)$$

$$\begin{aligned} \frac{1}{\pi} \int_{-1}^1 \hat{K}_{21}(s_2, r_1) \hat{g}_1(r_1) dr_1 + \frac{1}{\pi} \int_{-1}^1 \left[\frac{1}{(r_2 - s_2)} + \hat{K}_{22}(s_2, r_2) \right] \hat{g}_2(r_2) dr_2 \\ = \hat{p}_2(s_2) \frac{\kappa + 1}{4\mu_0}, |s_2| < 1, \end{aligned} \quad (4.52)$$

where

$$\hat{K}_{ij}(s_i, r_j) = \left(\frac{b_j - a_j}{2} \right) K_{ij}(x_i, t_j) \quad (i, j = 1, 2), \quad (4.53)$$

$$\hat{g}_j(r_j) = g_j(t_j) \quad (j = 1, 2), \quad (4.54)$$

$$\hat{p}_1(s_1) = \frac{p_1(x_1)}{e^{\beta x_1}}, \quad (4.55)$$

$$\hat{p}_2(s_2) = p_2(x_2). \quad (4.56)$$

Since the singularities in this case are identical to those in Section 4.2.1 and Section 4.2.2, the numerical procedure is identical. We find that we obtain a system of $(N \times M)$ algebraic equations as follows ,

$$\begin{aligned} & \frac{1}{\pi} \int_{-1}^1 \left[\frac{1}{(r_1 - s_k)} + \hat{K}_{11}(s_k, r_1) \right] \frac{\sum_{n=1}^N A_n T_n(r_1)}{\sqrt{1 - r_1^2}} dr_1 \\ & + \frac{1}{\pi} \int_{-1}^1 \hat{K}_{12}(s_k, r_2) \frac{\sum_{n=1}^M B_n T_n(r_2)}{\sqrt{1 - r_2^2}} dr_2 = \hat{p}_1(s_k) \frac{\kappa + 1}{4\mu_0}, \quad (k = 1, \dots, N) \end{aligned} \quad (4.57)$$

$$\begin{aligned} & \frac{1}{\pi} \int_{-1}^1 \hat{K}_{21}(s_k, r_1) \frac{\sum_{n=1}^N A_n T_n(r_1)}{\sqrt{1 - r_1^2}} dr_1 \\ & + \frac{1}{\pi} \int_{-1}^1 \left[\frac{1}{(r_2 - s_k)} + \hat{K}_{22}(s_k, r_2) \right] \frac{\sum_{n=1}^M B_n T_n(r_2)}{\sqrt{1 - r_2^2}} = \hat{p}_2(s_k) \frac{\kappa + 1}{4\mu_0} \quad (k = 1, \dots, M). \end{aligned} \quad (4.58)$$

The collocation points are again chosen as roots of Chebyshev polynomials as in (4.33).

The resulting system of equations can be solved by matrix inversion.

Stress intensity factors:

The expressions for the stress intensity factors at the 4 irregular points can be derived in an identical manner to Section 4.2.1 and Section 4.2.2 and are found to be

$$k_1(-b_1) = \frac{4\mu_0 e^{-\beta b_1}}{\kappa + 1} \sqrt{\frac{b_1 - a_1}{2}} \sum_{n=1}^N A_n (-1)^n, \quad (4.59)$$

$$k_1(-a_1) = -\frac{4\mu_0 e^{-\beta a_1}}{\kappa + 1} \sqrt{\frac{b_1 - a_1}{2}} \sum_{n=1}^N A_n, \quad (4.60)$$

$$k_1(a_2) = \frac{4\mu_0}{\kappa + 1} \sqrt{\frac{b_2 - a_2}{2}} \sum_{n=1}^N B_n (-1)^n, \quad (4.61)$$

$$k_1(b_2) = -\frac{4\mu_0}{\kappa + 1} \sqrt{\frac{b_2 - a_2}{2}} \sum_{n=1}^N B_n. \quad (4.62)$$

4.2.4 Edge crack in the nonhomogeneous material

From (3.97) the singular integral equation for this case is as follows:

$$\begin{aligned} \frac{1}{\pi} \int_{-h_1}^{-a_1} \frac{g_1(t_1)}{(t_1 - x_1)} dt_1 + \frac{1}{\pi} \int_{-h_1}^{-a_1} g_1(t_1) K_{11}(x_1, t_1) dt_1 \\ = p_1(x_1) \frac{\kappa + 1}{4\mu_0 e^{\beta x_1}}, \quad -h_1 < x_1 < -a_1, \end{aligned} \quad (4.63)$$

Normalizing the interval $(-h_1, -a_1)$ by using,

$$t_1 = \frac{h_1 - a_1}{2} r_1 - \frac{h_1 + a_1}{2}, \quad (4.64)$$

$$x_1 = \frac{h_1 - a_1}{2} s_1 - \frac{h_1 + a_1}{2} \quad (4.65)$$

the integral equation can be written as

$$\frac{1}{\pi} \int_{-1}^1 \left[\frac{1}{(r_1 - s_1)} + \widehat{K}_{11}(s_1, r_1) \right] \widehat{g}_1(r_1) dr_1 = \widehat{p}_1(s_1) \frac{\kappa + 1}{4\mu_0}, \quad |s_1| < 1, \quad (4.66)$$

From (3.109) and (3.110) we see that, $\alpha_1 = 0, \beta_1 = \frac{1}{2}$. The density function can then be written as

$$\widehat{g}_1(r_1) = \frac{F_1(r_1)}{\sqrt{1 - r_1}} \quad (4.67)$$

where $F_1(r_1)$ is a bounded function. The corresponding orthogonal polynomial for the weight function $\frac{1}{\sqrt{1 - r_1}}$ is the Jacobi polynomial $P_n^{(0, -\frac{1}{2})}(r_1)$. The use of Jacobi

polynomials is quite cumbersome, though. Even the closed form solutions involving Jacobi polynomials contain serieses that have to be summed up accurately. To avoid this inconvenience, the orthogonal polynomial used here is again the Chebyshev polynomial of the first kind. Thus,

$$\hat{g}_1(r_1) = \frac{\sum_{n=0}^N A_n T_n(r_1)}{\sqrt{1-r_1}}. \quad (4.68)$$

Substituting into (4.66) we obtain,

$$\frac{1}{\pi} \int_{-1}^1 \left[\frac{1}{(r_1 - s_1)} + \hat{K}_{11}(s_1, r_1) \right] \frac{\sum_{n=0}^N A_n T_n(r_1)}{\sqrt{1-r_1}} dr_1 = \hat{p}_1(s_1) \frac{\kappa + 1}{4\mu_0}, |s_1| < 1, \quad (4.69)$$

In case of the edge crack there is no single valuedness condition. Hence there are $N + 1$ unknowns $A_0 \dots A_N$. We need to choose $N + 1$ collocation points as follows:

$$s_k = \frac{(2k-1)\pi}{2(N+1)} \quad (k = 1, \dots, N+1). \quad (4.70)$$

We then obtain an $(N+1) \times (N+1)$ system of algebraic equations as follows:

$$\frac{1}{\pi} \int_{-1}^1 \left[\frac{1}{(r_1 - s_k)} + \hat{K}_{11}(s_k, r_1) \right] \frac{\sum_{n=0}^N A_n T_n(r_1)}{\sqrt{1-r_1}} dr_1 = \hat{p}_1(s_k) \frac{\kappa + 1}{4\mu_0} \quad (k = 1, \dots, N+1). \quad (4.71)$$

It should be noted here that because of choosing $T_n(r_1)$ as the orthogonal polynomial we encounter integrals of the type,

$$\frac{1}{\pi} \int_{-1}^1 \frac{1}{(r_1 - s_k)} \frac{T_n(r_1)}{\sqrt{1-r_1}} dr_1$$

We do not have closed form expressions for these integrals. In this case we use some algebraic manipulations to get around this problem as follows,

$$\begin{aligned} \frac{1}{\pi} \int_{-1}^1 \frac{1}{(r_1 - s_k)} \frac{T_n(r_1)}{\sqrt{1 - r_1}} dr_1 &= \frac{1}{\pi} \int_{-1}^1 \frac{1}{(r_1 - s_k)} \frac{T_n(r_1) - T_n(s_k)}{\sqrt{1 - r_1}} dr_1 \\ &+ \frac{T_n(s_k)}{\pi} \int_{-1}^1 \frac{1}{(r_1 - s_k)} \frac{1}{\sqrt{1 - r_1}} dr_1. \end{aligned} \quad (4.72)$$

The second integral on the right hand side has a closed form solution and is given in Appendix D. The first integral on the right hand side is a smooth integral and can be evaluated numerically. The logarithmic singularity coming out of the Fredholm kernel can also be similarly handled.

Stress intensity factor:

The only irregular point is $x = -a_1$. The expression for the stress intensity factor is found in (3.112) as

$$k_1(-a_1) = -\frac{4\mu_0 e^{-\beta a_1}}{\kappa + 1} \sqrt{2} g_1^*(-a_1) \quad (4.73)$$

which can be written as

$$k_1(-a_1) = -\frac{4\mu_0 e^{-\beta a_1}}{\kappa + 1} \sqrt{h_1 - a_1} \sum_{n=0}^N A_n. \quad (4.74)$$

4.2.5 Crack in the nonhomogeneous material terminating at interface

The singular integral equation for this case is as follows:

$$\begin{aligned} \frac{1}{\pi} \int_{-b_1}^0 \frac{g_1(t_1)}{(t_1 - x_1)} dt_1 + \frac{1}{\pi} \int_{-b_1}^0 g_1(t_1) K_{11}(x_1, t_1) dt_1 &= p_1(x_1) \frac{\kappa + 1}{4\mu_0 e^{\beta x_1}}. \\ -b_1 < x_1 < 0 \end{aligned} \quad (4.75)$$

Normalizing the interval $(-b_1, 0)$ by using

$$t_1 = \frac{b_1}{2}(r_1 - 1), \quad x_1 = \frac{b_1}{2}(s_1 - 1) \quad (4.76)$$

we obtain,

$$\frac{1}{\pi} \int_{-1}^1 \left[\frac{1}{(r_1 - s_1)} + \hat{K}_{11}(s_1, r_1) \right] \hat{g}_1(r_1) dr_1 = \hat{p}_1(s_1) \frac{\kappa + 1}{4\mu_0}, |s_1| < 1. \quad (4.77)$$

From (3.114) we find that $\alpha_1 = \beta_1 = \frac{1}{2}$. This case is identical to that treated in Section 4.2.1. The same numerical analysis is followed where a_1 is now replaced by 0. The resulting system of algebraic equations is as follows

$$\frac{1}{\pi} \int_{-1}^1 \left[\frac{1}{(r_1 - s_k)} + \hat{K}_{11}(s_k, r_1) \right] \frac{\sum_{n=1}^N A_n T_n(r_1)}{\sqrt{1 - r_1^2}} dr_1 = \hat{p}_1(s_k) \frac{\kappa + 1}{4\mu_0} \quad (k = 1, \dots, N). \quad (4.78)$$

Stress intensity factors:

By an analysis similar to that in Section 4.2.1 we find the stress intensity factors as

$$k_1(-b_1) = \frac{4\mu_0 e^{-\beta b_1}}{\kappa + 1} \sqrt{\frac{2}{b_1}} \sum_{n=1}^N A_n (-1)^n, \quad (4.79)$$

$$k_1(0) = -\frac{4\mu_0}{\kappa + 1} \sqrt{\frac{2}{b_1}} \sum_{n=1}^N A_n. \quad (4.80)$$

4.2.6 Crack in the homogeneous material terminating at interface

The singular integral equation for this case is as follows:

$$\frac{1}{\pi} \int_0^{b_1} \frac{g_2(t_2)}{(t_2 - x_2)} dt_2 + \frac{1}{\pi} \int_0^{b_1} g_2(t_2) K_{22}(x_2, t_2) dt_2 = p_2(x_2) \frac{\kappa + 1}{4\mu_0},$$

$$a_2 < x_2 < b_2. \quad (4.81)$$

Normalizing the interval $(0, b_2)$ by using

$$t_2 = \frac{b_2}{2}(1 + r_2), \quad x_2 = \frac{b_2}{2}(1 + s_2) \quad (4.82)$$

we obtain

$$\frac{1}{\pi} \int_{-1}^1 \left[\frac{1}{(r_2 - s_2)} + \hat{K}_{22}(s_2, r_2) \right] \hat{g}_2(r_2) dr_2 = \hat{p}_2(s_2) \frac{\kappa + 1}{4\mu_0}, \quad |s_2| < 1. \quad (4.83)$$

From (3.115), we obtain $\alpha_2 = \beta_2 = \frac{1}{2}$. Hence this case is the same as that treated in Section 4.2.2 where a_2 is replaced by 0. The system of algebraic equations we obtain can be expressed as

$$\frac{1}{\pi} \int_{-1}^1 \left[\frac{1}{(r_2 - s_k)} + \hat{K}_{22}(s_k, r_1) \right] \frac{\sum_{n=1}^M B_n T_n(r_2)}{\sqrt{1 - r_2^2}} dr_2 = \hat{p}_2(s_k) \frac{\kappa + 1}{4\mu_0} \quad (k = 1, \dots, M). \quad (4.84)$$

Stress intensity factors:

By an analysis similar to the analysis in Section 4.2.2 we find the stress intensity factors as

$$k_1(0) = \frac{4\mu_0}{\kappa + 1} \sqrt{\frac{2}{b_2}} \sum_{n=1}^N B_n (-1)^n, \quad (4.85)$$

$$k_1(b_2) = -\frac{4\mu_0}{\kappa + 1} \sqrt{\frac{2}{b_2}} \sum_{n=1}^N B_n. \quad (4.86)$$

4.2.7 Crack passing through interface

As discussed in Chapter 3 there is no singularity at the interface. Hence we can write one singular integral equation for the entire crack as,

$$\frac{1}{\pi} \int_{-b_1}^{b_2} \frac{g(t)}{(t-x)} dt + \frac{1}{\pi} \int_{-b_1}^{b_2} g(t) K(x, t) dt = p(x) \frac{\kappa + 1}{4\mu_0}, \quad -b_1 < x < b_2. \quad (4.87)$$

Normalizing the interval $(-b_1, b_2)$ by defining,

$$t = \frac{b_2 + b_1}{2} r + \frac{b_2 - b_1}{2}, \quad (4.88)$$

$$x = \frac{b_2 + b_1}{2} s + \frac{b_2 - b_1}{2} \quad (4.89)$$

we can write (4.87) as

$$\frac{1}{\pi} \int_{-1}^1 \left[\frac{1}{(r-s)} + \hat{K}(s, r) \right] \hat{g}(r) dr = \hat{p}(s) \frac{\kappa + 1}{4\mu_0}, \quad |s| < 1. \quad (4.90)$$

where

$$\hat{K}(s, r) = \left(\frac{b_2 + b_1}{2} \right) K(x, t), \quad (4.91)$$

$$\hat{g}(r) = g(t), \quad (4.92)$$

$$\hat{p}(s) = \begin{cases} \frac{p(x)}{e^{\beta x}} & x < 0 \\ p(x) & x > 0 \end{cases}. \quad (4.93)$$

From Chapter 3 it can be seen that $\hat{g}(r)$ can be represented as,

$$\hat{g}(r) = \frac{g^*(t)}{(t + b_1)^{\frac{1}{2}} (b_2 - t)^{\frac{1}{2}}} \quad (4.94)$$

or

$$\hat{g}(r) = \frac{F(r)}{\sqrt{1-r^2}} \quad (4.95)$$

where $F(r)$ is a bounded function which can be expanded in terms of Chebyshev polynomials of the first kind as follows

$$F(r) = \sum_{n=1}^N A_n T_n(r). \quad (4.96)$$

Using the single valuedness condition and the orthogonality properties of Chebyshev polynomials we find that $A_0 = 0$. We can now write (4.90) as,

$$\frac{1}{\pi} \int_{-1}^1 \left[\frac{1}{(r-s)} + \hat{K}(s, r) \right] \frac{\sum_{n=1}^N A_n T_n(r)}{\sqrt{1-r^2}} dr = \hat{p}(s) \frac{\kappa+1}{4\mu_0}, |s| < 1. \quad (4.97)$$

This equation is identical in form to (4.27). It is solved in an identical manner. Care has to be taken while evaluating the Fredholm kernel. The Fredholm kernel is defined by (4.45) and (3.167). Hence the integral has to be split into two integrals with intervals

$$\left(-1, \frac{b_1 - b_2}{b_1 + b_2}\right) \text{ and } \left(\frac{b_1 - b_2}{b_1 + b_2}, 1\right).$$

Stress intensity factors:

The stress intensity factors in this case are expressed as

$$k_1(-b_1) = \frac{4\mu_0 e^{-\beta b_1}}{\kappa+1} \sqrt{\frac{2}{b_1+b_2}} g^*(-b_1), \quad (4.98)$$

$$k_1(b_2) = -\frac{4\mu_0}{\kappa+1} \sqrt{\frac{2}{b_1+b_2}} g^*(b_2). \quad (4.99)$$

Using the normalization in (4.76 – 4.77) we can write these expressions as

$$k_1(-b_1) = \frac{4\mu_0 e^{-\beta b_1}}{\kappa+1} \sqrt{\frac{b_1+b_2}{2}} \sum_{n=1}^N A_n (-1)^n, \quad (4.100)$$

$$k_1(b_2) = -\frac{4\mu_0}{\kappa+1} \sqrt{\frac{b_1+b_2}{2}} \sum_{n=1}^N A_n. \quad (4.101)$$

4.2.8 Edge crack passing through interface

As in Section 4.2.7, we see from Chapter 3 that we can write a single integral equation as,

$$\frac{1}{\pi} \int_{-h_1}^{b_2} \frac{g(t)}{(t-x)} dt + \frac{1}{\pi} \int_{-h_1}^{b_2} g(t) K(x, t) dt = p(x) \frac{\kappa+1}{4\mu_0}, \quad -h_1 < x < b_2. \quad (4.102)$$

Normalizing the interval $(-h_1, b_2)$ by defining,

$$t = \frac{b_2 + h_1}{2} r + \frac{b_2 - h_1}{2}, \quad (4.103)$$

$$x = \frac{b_2 + h_1}{2} s + \frac{b_2 - h_1}{2} \quad (4.104)$$

we can write (4.50) as

$$\frac{1}{\pi} \int_{-1}^1 \left[\frac{1}{(r-s)} + \hat{K}(s, r) \right] \hat{g}(r) dr = \hat{p}(s) \frac{\kappa+1}{4\mu_0}, \quad |s| < 1 \quad (4.105)$$

where

$$\hat{K}(s, r) = \left(\frac{b_2 + h_1}{2} \right) K(x, t), \quad (4.106)$$

$$\hat{g}(r) = g(t), \quad (4.107)$$

$$\hat{p}(s) = \begin{cases} \frac{p(x)}{e^{\beta x}} & x < 0 \\ p(x) & x > 0 \end{cases}. \quad (4.108)$$

From Chapter 3 we find that, we can write $\hat{g}(r)$ as,

$$\widehat{g}(r) = \frac{g^*(t)}{(b_2 - t)^{\frac{1}{2}}} \quad (4.109)$$

or

$$\widehat{g}(r) = \frac{F(r)}{\sqrt{1-r}} \quad (4.110)$$

where $F(r)$ is a bounded function which can be expanded in terms of an orthogonal polynomial. As in Section 4.2.4, we choose Chebyshev polynomial of the first kind as the orthogonal polynomial. Thus,

$$\widehat{g}(r) = \frac{\sum_{n=0}^N A_n T_n(r)}{\sqrt{1-r}}. \quad (4.111)$$

Equation (4.105) can now be written as

$$\frac{1}{\pi} \int_{-1}^1 \left[\frac{1}{(r-s)} + \widehat{K}(s, r) \right] \frac{\sum_{n=0}^N A_n T_n(r)}{\sqrt{1-r}} dr = \widehat{p}(s) \frac{\kappa+1}{4\mu_0}, |s| < 1 \quad (4.112)$$

Equation (4.112) is identical in form to (4.69) and is solved in an identical manner. It should be noted here that there is no single valuedness condition in this case. Hence we have $N + 1$ unknowns. Thus we need to choose $N + 1$ collocation points. The points are chosen according to (4.70). We then obtain an $(N + 1) \times (N + 1)$ system of linear algebraic equations which can be solved for A_n 's by matrix inversion.

Stress intensity factor:

The stress intensity factor at $x = b_2$ can be written as

$$k_1(b_2) = - \frac{4\mu_0}{\kappa+1} \sqrt{2} g^*(b_2). \quad (4.113)$$

By using the normalization in (4.103 – 4.104) we can write the stress intensity factor as

$$k_1(b_2) = -\frac{4\mu_0}{\kappa+1}\sqrt{b_1+b_2}\sum_{n=0}^N A_n . \quad (4.114)$$

CHAPTER 5

RESULTS AND DISCUSSIONS

In Chapter 4, the numerical procedure for solving the integral equations has been explained. This chapter provides numerical solutions for various crack configurations and loading conditions.

The loading conditions can be divided into two main classes :

1. Mechanical loading,
2. Thermal loading.

In mechanical loadings, three different types of loadings are considered. First loading is a fixed grip loading. In this, the strain $\epsilon_{yy} = \epsilon_0$ is constant throughout the section. Second loading, is the membrane loading. It is assumed that a tensile load is applied at the midplane of the specimen. Third loading is a 4-point bending giving a uniform moment at the midsection of the specimen. In thermal loadings, there are mainly two cases. In the first case, the specimen is uniformly heated or cooled. In the second case, one surface of the specimen is kept at a constant temperature while the other is heated or cooled. The second case corresponds to the condition, for example, on a turbine blade where one surface is exposed to high temperatures while the substrate is kept at a lower temperature by some cooling mechanism.

The results of interest are the stress intensity factors at the crack tips and the crack opening displacements. The stress intensity factors show the propensity for a crack to grow. Higher stress intensity factors show a propensity for the crack to grow in that direction whereas lower stress intensity factors show a tendency for crack arrest. The crack opening displacements show the shape of the crack. These provide information on whether the crack is closing or not.

In this study, two real material combinations are used. They are :

1. Partially Stabilized Zirconia (PSZ) on René-41 ($\frac{\mu_0}{\mu_1} = 1.45, \beta h_1 = 0.375$)
2. Partially Stabilized Zirconia (PSZ) on Ti-6Al-4V ($\frac{\mu_0}{\mu_1} = 0.77, \beta h_1 = -0.2576$).

The thermomechanical properties for these materials are given in Appendix E. Apart from these material combinations, some hypothetical material combinations are used for comparison purposes. These combinations are :

1. $\frac{\mu_0}{\mu_1} = 5.0, \beta h_1 = 1.6094,$
2. $\frac{\mu_0}{\mu_1} = 0.5, \beta h_1 = -0.6931.$

$\beta h_1 = 0.0001$ represents the homogeneous case extremely closely. It is not possible to put βh_1 identically equal to zero in this model due to numerical difficulties.

The results in this study are for plane strain case unless otherwise mentioned. In most cases results for generalized plane stress case differ from those in plane strain case only in the second or third significant digit. Also, in this analysis the Poisson's ratio is assumed to be constant for all materials ($\nu = 0.3$).

5.1 Mechanical loading

5.1.1 Stresses in uncracked specimens

Before the stress intensity factors and the crack opening displacements of cracked specimens are studied, it is important to investigate the stresses in uncracked specimens. As mentioned before, the specimens were subjected to fixed grip loading, membrane loading and 4-point bending. The stress profiles for each of these loadings are shown in Figures 5.1 – 5.3 respectively for a thickness ratio of $\frac{h_2}{h_1} = 1$. Equal and opposite stresses are applied on the crack surfaces when studying the crack problems. Figure 5.1 shows that in the fixed grip case, the stress profile in the FGM layer follows the stiffness profile. In the pure bending case, the area under the stress curve is equal to zero (Fig. 5.3). Also, the point where the normal stress is zero denotes the location of the neutral axis. It can be

seen that for a softer coating, the neutral axis lies in the substrate whereas for a stiffer coating, it lies in the coating. Figure 5.4 and 5.5 show the normal stress in the uncracked specimen for membrane loading and pure bending respectively when the substrate to coating thickness ratio is 5.

5.1.2 Internal crack in homogeneous substrate only

This is the case where an existing flaw in the substrate is put under various loading conditions. We are interested in finding out the direction in which the crack will propagate if at all it propagates. The problem of a crack in a homogeneous half plane bonded to an FGM half plane was solved by Erdogan et. al. [43]. The results obtained in [43] and those obtained in this work for the special case of $h_1 = h_2 = \infty$ are tabulated in Table 5.1. It can be seen that there is an excellent match in the results of these two independent works.

Figures 5.6 – 5.8 show the stress intensity factors for internal cracks in the substrate. The normalized stress intensity factors (see Appendix C for details on the normalization process) are plotted against the normalized crack lengths. The crack is allowed to grow symmetrically in the substrate. It should be noted here that as $c \rightarrow 0$, the stress intensity factor goes to some definite limit. In fact, the value of the normalized stress intensity factor approaches the normalized stress in the uncracked specimen at that point as $c \rightarrow 0$. In other words, $k_1(c \rightarrow 0) = \sigma_{yy}(\frac{h_2}{2}, 0)\sqrt{c}$. These limits determined analytically for fixed grip loading for $\beta h_1 = 1.6094, 0.375, 0.0001, -0.2576$ and -0.6931 are identically equal to 1.0. In Figure 5.6, we can see that the numerically calculated values approach these analytically determined limit. It is also seen from Fig. 5.6 that as the crack tip b_2 approaches the free surface of the homogeneous strip, the stress intensity factors increase very fast. This indicates that the crack will grow towards the free surface. In fact, when $b_2 \rightarrow h_2$, the stress intensity factor $k_1(b_2) \rightarrow \infty$. The other crack tip a_2 growing towards the interface also shows an increasing stress intensity factor. But it

is much lower than that at b_2 . In fact, as $b_2 \rightarrow h_2$ and $a_2 \rightarrow 0$, $k_1(a_2)$ would approach a finite limit corresponding to the edge crack in homogeneous material. That problem has not been solved in this work as usually it is the coating which undergoes surface cracking. It can also be seen that stress intensity factors are higher when the coating is weaker and vice versa. This is because the overall stiffness of the material combination is lower. Also, when the crack is very small the effect of the coating is negligible and the stress intensity factors for all different material combinations is the same as that in case of homogeneous materials. The increase in the stress intensity factor for the end a_2 can again be attributed to overall weakening of the specimen.

In Fig. 5.7 the stress intensity factors for membrane loading are plotted. Analytically, we find that the limits for $c \rightarrow 0$ for $\beta h_1 = 1.6094, 0.375, 0.0001, -0.2576$ and -0.6931 are 0.5041, 0.5001, 0.5, 0.49998, 0.49966 respectively. In Figure 5.7, we can see all the curves approaching 0.5 as $c \rightarrow 0$. It is peculiar that for end b_2 , weaker the coating, lower is the stress intensity factor whereas for end a_2 , the trend is exactly opposite. But it should be expected from the stress distribution for an uncracked specimen under membrane loading shown in Fig. 5.2. The stress distribution is such that for end a_2 the stress is higher than end b_2 . Also, weaker the coating, more pronounced is the difference. Hence for $\beta h_1 = 1.6094$, the stress felt by end b_2 is much lower than the stress felt by b_2 when $\beta h_1 = -0.6931$. Similar argument holds for the end a_2 . Under bending loading (Fig. 5.8), the limits as $c \rightarrow 0$ for $\beta h_1 = 1.6094, 0.375, 0.0001, -0.2576$ and -0.6931 are 0.7778, 0.7607, 0.75, 0.7415 and 0.7253 respectively. The end b_2 experiences a much higher load than the end a_2 . As a result the stress intensity factors for b_2 are much higher. Another factor is that the end b_2 is getting closer to the edge. That pushes the stress intensity factors even higher. End a_2 experiences lower stress (Fig. 5.3). Hence the lower stress intensity factors at a_2 . The slight increase at the end is the effect of overall weakening of the material. It should be noted that the results are shown only up to

$\frac{c}{h_1} = 0.45$ because the accuracy of the results was highly diminished as the crack approached the boundary. The numerical values of the stress intensity factors have been tabulated for $\beta h_1 = 0.375$ (PSZ-René 41) and $\beta h_1 = -0.2576$ (PSZ-Ti-6Al-4V) in Tables 5.2 and 5.3 respectively.

Figures 5.9 – 5.11 show the crack opening displacements for the three different types of mechanical loadings. The crack runs from $0.25 h_1$ to $0.75 h_1$. In the fixed grip case (Fig. 5.9), there is hardly any change in the crack opening displacement though it can be seen that weaker the coating, higher is the crack opening displacement. In the membrane loading (Fig. 5.10) the difference is more pronounced. It can also be seen that the crack surface is pulled towards the loading axis which is in this case at the interface. The loading intensity is higher on the left part of the crack than the right. This effect can be seen again in the bending case. Figure 5.11 shows the crack surface displacement is now higher away from the interface. This is because a bending moment causes higher stresses farther from the interface than closer to the interface.

Figures 5.12 – 5.14 show the effect of thickness of the substrate on the stress intensity factors. The thickness ratios are varied from $\frac{h_2}{h_1} = 1.0$ to $\frac{h_2}{h_1} = 10.0$. The case where $\frac{h_2}{h_1} = 10.0$ roughly matches the semi-infinite substrate case. Also, higher thicknesses for substrates is closer to practical situations. From the plots it can be seen that the thickness of substrate reduces the stress intensity factors. In fact, for $\frac{h_2}{h_1} = 10.0$, there is hardly any change in the stress intensity factors as the crack grows. This result is important as it provides us with an effective technique to suppress crack growth. If the substrate is sufficiently large, the inherent flaws in it will be suppressed. The same effect can be seen in membrane loading and in pure bending. Figures 5.15 and 5.16 show the effect of thickness on crack opening displacement under fixed grip and membrane loading.

In each case, the crack opening displacement is lower when the substrate thickness is higher.

5.1.3 Internal crack in nonhomogeneous coating only

Now we assume that there is a crack in the coating. Figures 5.17 and 5.19 show the effect of the material nonhomogeneity on the stress intensity factors of such a crack. In Fig. 5.17, the specimen is put under fixed grip loading. It should be noted here that for a positive nonhomogeneity value, the material stiffens towards the interface whereas for a negative nonhomogeneity value, the material softens towards the interface. Again it is seen that as $c \rightarrow 0$, the stress intensity factor goes to some definite limit. In fact, the value of the normalized stress intensity factor approaches the normalized stress in the uncracked specimen at that point as $c \rightarrow 0$. In other words, $k_1(c \rightarrow 0) = \sigma_{yy}(\frac{-h_1}{2}, 0)\sqrt{c}$. For fixed grip loading, the limits for $\beta h_1 = 1.6094, 0.375, 0.0001, -0.2576$ and -0.6931 are 0.4472, 0.8290, 1.0, 1.1375 and 1.4142 respectively. The numerical results match closely with these analytical limits. In general, it is seen that a crack tip moving into a stiffening region has an increasing stress intensity factor. In Fig. 5.17, $\beta h_1 = 1.6094$ is represented by the lowermost curves. The stress intensity factor at tip a_1 denoted by the solid line increases steadily as the crack grows. On the other hand, for $\beta h_1 = -0.6931$, represented by the topmost curves, the stress intensity factor at tip a_1 decreases as the crack grows. As the crack grows very large, there is a slight increase which is attributed to the overall weakening of the specimen. These results are consistent with previously published results [43].

For the crack tip b_1 , there are two factors to be considered. One is the material stiffness and other is the proximity to the edge. For $\beta h_1 = 1.6094$, the stress intensity factor initially drops as the crack tip is entering softer material. But as the crack tip comes closer to the edge, the ligament becomes very small and the stress intensity factor starts

increasing. For $\beta h_1 = -0.6931$, both these factors tend to increase the stress intensity factor and as a result the stress intensity factor rises very fast. This would suggest that there is a high propensity for crack growth in that direction.

As $c \rightarrow \frac{h_1}{2}$, the internal crack approaches an edge crack. Then it should be expected that $k_1(b_1) \rightarrow \infty$ and $k_1(a_1)$ should approach a finite value obtained in the edge crack problem. The results for edge crack are given in Section 5.1.6. The limiting values obtained for $k_1(a_1)$ for $\beta h_1 = 1.6094, 0.375, 0.0001, -0.2576$ and -0.6931 are 1.89337, 3.29216, 3.9943, 4.5893 and 5.8545 respectively. It is seen that these values are approached asymptotically and the slope of the curve is infinite as the crack approaches the interface. This phenomenon can be explained from the fact that during the transition from an internal crack to an edge crack there is a jump when the ligament breaks. This causes the unbounded slope. The limiting value is still bounded.

Figure 5.19 shows the effect of material stiffness under bending. It should be noted here that the bending is reversed as compared to that shown in Fig. 5.3. Hence the plot in Fig. 5.3 should be reflected about the x-axis to get the proper stress distribution. This has been plotted in Fig. 5.18. Again, as $c \rightarrow 0$, the stress intensity factor goes to some definite limit. These limits are obtained for $\beta h_1 = 1.6094, 0.375, 0.0001, -0.2576$ and -0.6931 as 0.8544, 0.8009, 0.75, 0.7062 and 0.6169 respectively. Numerical results match with these analytical limits. The trends in Fig. 5.19 are in agreement with the observations made in the fixed grip case. Only difference is seen in the plot for $\beta h_1 = 1.6094$. The tip a_1 grows into a stiffer region and hence should have an increasing stress intensity factor. From Figure 5.19, though, it can be seen that for $\frac{c}{h_1} = 0.45$, the stress intensity factor actually decreases. This can be explained on the basis of Fig. 5.18 where there is a decrease in the stress around that region. Hence the stress intensity factor decreases inspite of increasing stiffness. The numerical values of the stress intensity

factors have been tabulated for $\beta h_1 = 0.375$ (PSZ-René 41) and $\beta h_1 = -0.2576$ (PSZ-Ti-6Al-4V) in Tables 5.4 and 5.5, respectively.

A very practical situation is where a homogeneous coating is laid on an FGM substrate. Under fixed grip loading it was observed that crack propagated beneath the interface. To analyze this situation, a crack was introduced starting at the interface and growing into the FGM substrate. If the FGM substrate is softer, it was observed that the stress intensity factor reduces (Fig. 5.20) whereas if the FGM substrate is stiffer, the stress intensity factor tends to increase (Fig. 5.21).

The crack opening displacements for an internal crack in the FGM coating show some interesting features. In Fig. 5.22, the specimen is put under fixed grip loading. It is observed that the crack opening displacements are lower when the nonhomogeneity parameter is positive i.e. for coatings that stiffen toward the interface. This is due to the fact that under fixed grip loading, the load is distributed in such a way that the softer part of the coating bears lesser load (Fig. 5.1). If, on the other hand, the nonhomogeneity parameter is negative, the coating softens towards the interface and the load under fixed grip loading is higher for the coating. As a result, the crack opening displacements are higher. For all different nonhomogeneity parameters, the crack opening displacements are skewed towards or away from the interface depending on the sign of βh_1 . Figures 5.23 and 5.24 show the crack opening displacements for membrane loading and pure bending respectively. Here again the curves are skewed depending on the sign of βh_1 . Also, it is observed that the crack opening displacements are higher for a softer coating than for a stiffer coating.

The effect of thickness ratio on the stress intensity factors and the crack opening displacements is shown in Fig. 5.25 and Fig. 5.26 respectively. It is seen that the stress intensity factors as well as the crack opening displacements are lower with increasing thickness of the substrate. The difference is even more pronounced for the pure bending

case (Figures 5.27, 5.28). Note that the stress intensity factors and the crack opening displacements for $\frac{h_2}{h_1} = 10.0$ seem to be almost negligible. This is due to the fact that the stress intensity factors are normalized with respect to the square of the thickness.

5.1.4 Internal cracks in nonhomogeneous coating and in homogeneous substrate

In this section the interaction effects of a crack present in the homogeneous substrate on the stress intensity factors and crack opening displacements for crack in the FGM coating are studied. First a crack ranging from $0.4h_1$ to $0.6h_1$ is placed in the homogeneous substrate. Then a longer crack ranging from $0.2h_1$ to $0.8h_1$ is placed. The effect of these cracks on a crack located symmetrically in the FGM coating is studied by comparing the stress intensity factors in these two cases with those obtained from Section 5.1.3 where there was no crack in the substrate. The results are tabulated in Table 5.6.

It can be seen from Table 5.6 that the presence of a crack in the homogeneous substrate enhances the stress intensity factors at tip a_1 . As the ligament between the crack shortens in length, the effect is more pronounced. The stress intensity factor at tip b_1 on the other hand is relatively unchanged. A complete table of stress intensity factors for the crack in the FGM coating in the presence of a crack in the homogeneous substrate for different mechanical loadings is given in Table 5.7. It should be noted that the bending is reversed so that the crack in the FGM coating is open.

Fig. 5.29 shows the effect of the substrate thickness on the stress intensity factors. The stress intensity factors are lower for higher substrate thickness. In Fig. 5.30, the stress intensity factors are plotted when both the cracks are growing symmetrically. It is seen that the stress intensity factors at ends a_1 and a_2 are rapidly increasing. This is because of the close interaction of the two tips. Tips b_1 and b_2 show high stress intensities when they are very close to the edges. The crack opening displacements for the pure bending case are

shown in Fig. 5.31. At higher thicknesses of the substrate the crack opening displacements are negligible.

5.1.5 Internal crack crossing the interface

In Section 5.1.4, it was observed that the stress intensity factors at tip a_1 and a_2 tend to increase as the ligament size in between them decreases. This leads to the possibility of the cracks fusing together at the interface forming one single closed crack crossing the interface. The stress intensity factors for such an internal crack are discussed in this section.

Figure 5.32 shows the stress intensity factors for a crack running from $-b_1$ to b_2 subjected to fixed grip loading. First, it should be noted that as $c \rightarrow 0$, $k_1(b_1)$ and $k_1(b_2)$ both tend identically $\sigma_0 \sqrt{c}$ for all different material combinations. The crack is then allowed to grow symmetrically. When the coating has lower stiffness than the substrate (eg. $\beta h_1 = 1.6094$), end b_1 grows into a softer region. In this case, it is observed that the stress intensity factors reduce. On the other hand, when the coating is stiffer than the substrate (eg. $\beta h_1 = -0.6931$), end b_1 grows into a stiffer region and the stress intensity factor increases. The numerical values for the stress intensity factors for a practical material (PSZ-René 41, $\beta h_1 = 0.375$) are tabulated in Table 5.8.

It should be noted here that the negative stress intensity factors under bending indicate that the crack tip is closing under the loading. The surfaces will be interpenetrating. A correct analysis of the problem should be performed by considering a crack-contact problem. But the negative stress intensity factors are still useful in the case of multiple loading, where under other applied loadings in conjunction with the bending, the crack is completely open. The negative stress intensity factors are valid only in such a situation where there is no closure of the crack.

Figure 5.33 shows the effect of thickness ratio on the stress intensity factors under reversed bending so that the crack is completely open. The results are in accordance with those obtained in previous cases. The crack opening displacements in case of membrane loading are shown in Figure 5.34. These curves are skewed depending upon the value of βh_1 .

5.1.6 Edge crack in FGM coating and passing through the interface

An edge crack in the nonhomogeneous coating is the most important practical crack configuration. The stress intensity factors and the crack opening displacements for this crack configuration will be discussed in detail in this section. Also, the crack will be allowed to pass through the interface and enter the homogeneous substrate.

The stress intensity factors for an edge crack in a homogeneous strip have been tabulated by Joseph [63]. By assuming a very small value for the nonhomogeneity parameter ($\beta h_1 = 0.0001$), those results have been reproduced in this work. The comparison of results is given in Table 5.9 and 5.10 for fixed grip loading and pure bending respectively. It can be seen from the comparison that the results in this work match very well with published results. In fact, in this work the convergence is much better for very small ligament lengths than that in previously published results.

Figure 5.35 shows the stress intensity factors for an edge crack in the nonhomogeneous coating under fixed grip loading. It should be noted that as $c \rightarrow 0$, the stress intensity factors approach a definite limit which is analytically found to be 1.121522 times $\sigma_{yy}(-h_1, 0)\sqrt{c}$ obtained from Koiter's integral. The numerical limits approach extremely closely to this analytical limit as seen in Figure 5.35. The crack is then allowed to reach up to the interface. The effect of the nonhomogeneity parameter is studied. It can be seen that an edge crack growing into a stiffer region ($\beta h_1 > 0$), shows increasing stress intensity factors. For $\beta h_1 = 1.6094$, the increase is very rapid. On the other hand,

an edge crack growing into a softer region ($\beta h_1 < 0$), shows a slight decrease before increasing very slowly. For a homogeneous medium ($\beta h_1 = 0.0001$), the slope of the curve for $\frac{c}{h_1} \rightarrow 0$, is zero. For a nonhomogeneous material, whether it is stiffening or softening, the same should hold true. As the crack is allowed to grow into the homogeneous substrate, the trends in the stress intensity factors continue. These are shown in Figure 5.36. The rapid increase in the stress intensity for $\beta h_1 = 1.6094$ may lead to catastrophic failure. It should be noted that the stress intensity factor curves are continuous at the interface. This is because there is no singularity at the interface as shown in Chapter 3. A table of stress intensity factors for different loadings for practical materials is given in Table 5.11 – 5.14.

Figure 5.37 – 5.40 show the variation of stress intensity factors for edge cracks under membrane loading and pure bending. Again it is seen analytically that as $c \rightarrow 0$, $k_1(a_1) \rightarrow 0.3037, 0.5042, 0.5608, 0.5942$ and 0.6344 for $\beta h_1 = 1.6094, 0.375, 0.0001, -0.2576$ and -0.6931 respectively for membrane loading. Also, $k_1(a_1) \rightarrow 0.7301, 1.41, 1.6823, 1.8893$ and 2.2809 respectively for pure bending. The numerical results match with these analytical limits very well. It can be seen from Fig. 5.38 and Fig. 5.40 that once the crack enters the homogeneous substrate, the variation in the stress intensity factors with the nonhomogeneity parameter is almost negligible. This suggests that under these loadings the influence of the nonhomogeneity of the coating is minimal especially if the crack grows into the substrate.

Figure 5.41 – 5.44 show the effect of thickness ratio on the stress intensity factor. In Fig. 5.41, it can be seen that the stress intensity factors are much lower for higher substrate thicknesses. From Fig. 5.42, it can be seen that as the crack tip reaches the edge, the stress intensity factors rise very rapidly. The numerical values for the stress intensity factors for PSZ-René41 for $\frac{h_2}{h_1} = 10.0$ are tabulated in Table 5.15 – 5.16.

Fig. 5.43 and Fig 5.44 show the effect of thickness for bending loading. It can be seen that for smaller thicknesses ($\frac{h_2}{h_1} = 0.1$), the stress intensity factors are very high but for higher thicknesses ($\frac{h_2}{h_1} = 10.0$), the stress intensity factors are very low. Again this is due to the normalization used for bending loading. As the crack passes through the interface, the stress intensity factors are still very low for higher thicknesses.

The crack opening displacements for varying nonhomogeneity parameters are plotted in Fig. 5.45 – 5.47. In Figure 5.45, an edge crack in the nonhomogeneous coating is considered. The crack opening displacement for softer coating (eg. $\beta h_1 = 1.6094$) is lowest because under fixed grip loading the stresses in uncracked specimen are lower for softer coatings (Fig. 5.1). The same trend is seen for a crack crossing the interface (Fig. 5.46). In membrane loading (Fig. 5.47), however, the stresses are higher for softer coatings (Fig. 5.2) and we see the expected result that the crack opening displacements are higher for softer coatings. The effect of stiffness is studied in Fig. 5.48 – 5.49. As the thickness of the substrate increases, the crack opening displacements are reduced.

5.2 Thermal loading

5.2.1 Stresses in uncracked specimens

The uncracked thermal stress problem needs to be solved for the specimen geometry. Because this is a one-dimensional heat conduction problem the thermal analysis is very straightforward and the temperature distribution and resulting thermal stresses can be obtained directly. If on the other hand, if the problem was two-dimensional, the crack will introduce partial insulation. In that case the diffusion problem as well as the stress problem will be analytically intractable. The problem of insulation due to the crack has been solved by Finite Element Analysis [69].

In the current problem, we assume that the thermal and mechanical problems are uncoupled. Hence it is only necessary to solve the diffusion problem and the thermal stress problem for an uncracked specimen. The thermal stresses thus obtained are then applied to the crack geometry to solve the elasticity problem. It should be noted that the thermo-mechanical properties of the FGM coating are functions of the space coordinate in the thickness direction.

Temperature distribution

The diffusion equation for the geometry shown in Figure 5.50 is

$$\frac{\partial}{\partial x} \left(k(x) \frac{\partial T}{\partial x} \right) = \rho(x) c(x) \frac{\partial T}{\partial t} \quad (5.1)$$

where $T(x, t)$ is the temperature, $k(x)$ is the coefficient of heat conduction, $\rho(x)$ is the density and $c(x)$ is the specific heat. For a steady state heat conduction problem (5.1) can be written as

$$k(x) \frac{\partial T}{\partial x} = \text{constant}. \quad (5.2)$$

The form of $k(x)$ can be arbitrary. But the elasticity problem can be solved analytically only for some specific forms of variations of the elasticity modulus. In this work, the exponential variation of the elasticity modulus is considered. Hence to be consistent, the coefficient of heat conduction is assumed to be of the form

$$k(x) = k_0 e^{\gamma x} \quad (5.3)$$

where k_0 is the coefficient of heat conduction of the homogeneous substrate and γ is the nonhomogeneity parameter for heat conduction defined as

$$\gamma = \frac{1}{h_1} \log \left(\frac{k_c}{k_0} \right) \quad (5.4)$$

where k_c is the coefficient of heat conduction of the coating and k_0 is the coefficient of heat conduction of the substrate. If the temperatures are specified as T_1 and T_2 at the boundaries as shown in Figure 5.50, the temperature distributions can be expressed as

$$T_{nh} = \frac{T_1 - T_i}{e^{\gamma h_1} - 1} (e^{-\gamma x} - 1) + T_i, \quad (5.5)$$

$$T_h = (T_2 - T_i) \frac{x}{h_2} + T_i \quad (5.6)$$

where T_i is the temperature at the interface given as

$$T_i = \left(\frac{T_1 \gamma}{e^{\gamma h_1} - 1} + \frac{T_2}{h_2} \right) / \left(\frac{\gamma}{e^{\gamma h_1} - 1} + \frac{1}{h_2} \right) \quad (5.7)$$

It should be noted that for uniform temperature change from some reference temperature T_0 to T , $T_{nh} = T_h = T_i = T$. It is more convenient to deal with temperature change rather than absolute temperatures. In this case $\Delta T = T - T_0 = \text{constant}$ throughout the specimen. If, on the other hand, we choose to hold the temperature $T_2 = T_0$ and vary T_1 , the driving force is the potential $\Delta T_1 = T_1 - T_0$. We can normalize the temperature distribution with respect to this potential ΔT_1 as

$$\Delta T_{nh} = \frac{(1 - \Delta T_i) e^{-\gamma x} - 1 + \Delta T_i e^{\gamma h_1}}{e^{\gamma h_1} - 1}, \quad (5.8)$$

$$\Delta T_h = \Delta T_i \left(\frac{h_2 - x}{h_2} \right). \quad (5.9)$$

where

$$\Delta T_i = \left(\frac{\gamma}{e^{\gamma h_1} - 1} \right) / \left(\frac{\gamma}{e^{\gamma h_1} - 1} + \frac{1}{h_2} \right). \quad (5.10)$$

The temperature distributions thus obtained can now be used to find the thermal stresses in the uncracked specimen.

Thermal stress distribution

For an unconstrained beam, the strain can be written as[68]

$$\epsilon_{yy} = -\hat{\alpha}(x)\Delta T(x) + Ax + B \quad (5.11)$$

where $\hat{\alpha}(x)$ is the coefficient of thermal expansion of the FGM coating assumed to be of the form of

$$\hat{\alpha}(x) = \alpha_0 e^{\alpha x} \quad (5.12)$$

where α_0 is the coefficient of linear expansion of the homogeneous substrate and α is the nonhomogeneity parameter defined as

$$\alpha = \frac{1}{h_1} \log\left(\frac{\alpha_1}{\alpha_0}\right) \quad (5.13)$$

where α_1 is the coefficient of linear expansion of the ceramic. The stress can then be written as

$$\sigma_{yy} = \frac{8\mu(x)}{1+\kappa} \left(-\hat{\alpha}(x)\Delta T(x) + Ax + B \right) \quad (5.14)$$

where $\kappa = (3 - \nu)/(1 + \nu)$ for generalized plane stress. For plane strain $\kappa = 3 - 4\nu$ and $\hat{\alpha}$ should be replaced by $\hat{\alpha}(1 + \nu)$. A and B in (5.14) are evaluated from equilibrium conditions

$$\int_{-h_1}^{h_2} \sigma_{yy}(x) dx = 0, \quad (5.15)$$

$$\int_{-h_1}^{h_2} x \sigma_{yy}(x) dx = 0. \quad (5.16)$$

A and B are obtained as

$$A = \frac{R_1 c_4 - R_2 c_2}{c_1 c_4 - c_3 c_4}, \quad (5.17)$$

$$B = \frac{R_2 c_1 - R_1 c_3}{c_1 c_4 - c_3 c_4} \quad (5.18)$$

where c_i ($i = 1..4$) and R_1, R_2 are given in Appendix C. The thermal stress in uncracked specimens under uniform temperature change and under steady state heat conduction is

shown in Figures 5.51 to 5.56. It should be noted that the plots are for positive ΔT . If ΔT is negative, the plots should be just reversed about the zero stress axis (i.e. stresses are exactly equal and opposite). This is important when determining if a surface crack will open or close under a given loading.

It can be seen from Figures 5.51-5.56 that the stress profiles are such that the area under the curve is zero. This is indeed expected as pure thermal loading is self-equilibrating since there is no external load acting on the specimen. The consequence is that the loading changes from compression to tension and vice-versa. This represents a peculiar situation. The loading maybe compressive on part of the crack while it could be tensile on the rest of the crack. This could lead to smooth crack closing. For example, for an edge crack, if the loading is tensile on the surface, the crack tends to grow until it reaches the compressive zone where it gets arrested. On the other hand, if the loading is compressive on the surface, it closes the crack at its mouth. A long crack, however, might open up in the interior region under tensile loading. This leads to the crack-contact problem which needs to be looked into carefully.

5.2.2 Crack-Contact problem

A possible crack-contact problem is shown in Figure 5.56. We can see here that the crack is closed from $x = -h_1$ to $x = -a$. It is open, however from $x = -a$ to $x = -a_1$. At $x = -a$, the crack will form a cusp i.e. there is smooth closure of the crack. The stress intensity factor at $x = -a$ will be zero. At $x = -a_1$, though, the crack is open and the stress intensity factor is positive.

This problem is again solved by a superposition technique. The thermal problem is first solved as described in Section 5.2.1. Equal and opposite stresses are applied on the crack face. If the stresses are compressive along the entire length of the crack, the stress intensity factor at the crack tip will be negative. This indicates a complete closing of the

crack. If the crack is deep enough so that the crack tip is in the tensile zone, the stress intensity factor at the crack tip will be positive but there will be interpenetrating crack opening displacements indicating that the crack is closing at some point. This is the case shown in Figure 5.57. The point where the crack closes ($x = -a$) is unknown but can be found out by satisfying the condition

$$k_1(-a) = 0, \quad (5.19)$$

where k_1 is the Mode I stress intensity factor. Equation (5.17) is highly nonlinear in a . We employ a simple iterative procedure to determine a . We first introduce an internal crack instead of an edge crack. Reader is referred to Chapter 4 for details of the internal crack problem. The crack tip a is varied to determine the exact location where (5.17) is satisfied. Usually a good four significant digit accuracy is obtained within five iterations.

5.2.3 Surface cracks and cracks passing through the interface

The important results in this fracture characterization are the stress intensity factors under given loadings. Two different kinds of loadings are considered. In one loading, the temperature of the entire specimen is raised (or lowered) uniformly. In this case, there is no conduction. In another type of loading, the temperature of the substrate is maintained at a fixed temperature, whereas the surface of the coating is raised (or lowered) to a higher temperature. The latter case in which the surface of the coating is heated while the substrate is maintained at a lower temperature is observed in thermal barrier coatings. The stress intensity factors are evaluated under each of these loadings for two different practical material combinations :

- I. Partially Stabilized Zirconia (PSZ) on René-41 ($\frac{\mu_0}{\mu_1} = 1.45, \beta h_1 = 0.375$)
- II. Partially Stabilized Zirconia (PSZ) on Ti-6Al-4V ($\frac{\mu_0}{\mu_1} = 0.77, \beta h_1 = -0.2576$).

First we consider Material combination I. Figure 5.58 shows the stress intensity factors under uniform temperature rise. It can be seen from Figure 5.51 that the thermal stresses are tensile near the surface. At $x = -0.4073$, the stresses become compressive. The crack initially grows under the tensile loading which can be seen by the positive stress intensity factors. As the loading becomes compressive, the stress intensity factors drop and almost go to zero as the crack approaches the interface. It can clearly be seen that the crack will soon be arrested. In fact, we can see in Figure 5.59, that the stresses do in fact go to zero when the crack passes through the interface. The numerical values of these stress intensity factors are tabulated in Table 5.17. Next, the same edge crack has been subjected to heat conduction (Figure 5.52). Here the stresses are compressive at the surface and tensile within. Hence we have a crack-contact problem. It can be seen from Figure 5.52 that the stresses change from compressive to tensile at $x = -0.6873$. Hence it is expected that cracks within the compressive zone will tend to remain closed. This is seen in Figure 5.60 which shows the point of closure of the crack as the crack tip $x = -a_1$ grows towards the interface. If the normalized crack tip distance from the surface $(\frac{h_1 - a_1}{h_1})$ is smaller than 0.3127, both the crack tips coincide. In other words, the crack is completely closed. If, on the other hand, it is larger than 0.3127, the tip where the crack closes (crack tip b_1 in this case) moves towards the surface. From the plot it can be seen that crack tip b_1 moves closer and closer to the surface and is expected to reach the surface when the open crack tip cuts completely through the entire thickness of the specimen. This can be seen in Figure 5.61. As the open crack tip reaches the surface $x = h_2$, b_1 reaches the surface $x = -h_1$. Figures 5.62 and 5.63 show the stress intensity factors for the conduction case for a surface crack in the coating and crack crossing the interface respectively. When the normalized crack tip distance is less than 0.3127, the stress intensity factors are zero as the crack is completely closed. For a longer crack, the stress intensity factors increase initially but as the loading drops, the stress intensity factors

drop. In fact, the stress intensity factors eventually go to zero as seen in Figure 5.63. As the loading is self-equilibrating, this is an expected result. It should be noted here that as the open crack tip reaches $x = h_2$, the numerical accuracy drops rapidly due to convergence problems. Best values were obtained when the open crack tip was at least $0.1 h_1$ distance away from the free surface.

When the loadings considered in the two previous cases are reversed, we see that the compressive loadings become tensile and vice versa. Consider the case of uniform cooling (Figures 5.64 – 5.65). Because the loading is a mirror image of that in Figure 5.51, the stresses are compressive near the surface and tensile within. Hence there will be crack-contact. The critical point where the stresses become tensile is $x = -0.4073$. In Figure 5.64, we can see that the two crack tips coincide before this point. After that point, the crack tips separate, the crack tip b_1 slowly moving toward the surface. Figure 5.65 shows the stress intensity factors for this case. The open crack tip in this case is only allowed to reach the interface in this case but it can be easily let to cross the interface following the same procedure as in the conduction case discussed before. If we now hold $T_2 = T_0$, and let T_1 decrease, the stress intensity factors are tensile near the surface. The crack grows initially but as it grows into the compressive zone, it gets arrested (Figure 5.66).

The same kind of analysis is done for Material combination II. Figures 5.53 – 5.54 show the uncracked stresses. Consider the uniform heating case. The stresses from Figure 5.53 show that this indeed will be a crack-contact problem. Figure 5.67 shows the location of the closed crack tip. The critical point is $x = -0.532$. The stress intensity factors in Figure 5.68 show correspondingly that stress intensity factors are zero when normalized crack tip distance is less than 0.468. In the case of uniform cooling, the crack is open at the surface. It will grow under the tensile loading but will be arrested in the compressive zone (Figure 5.69). Figures 5.70 – 5.71, show the crack-closure lengths and stress

intensity factors respectively for surface heating. Figure 5.72 shows the stress intensity factor for surface cooling case. The results in Figure 5.72 can now be compared with those obtained in Figure 5.66 as the loading conditions are identical. That comparison is showed in Figure 5.73.

In all the cases considered above, the thickness ratio was $\frac{h_2}{h_1} = 1.0$. In practical situations, the substrate is usually very large as compared to the coating. Hence a thickness ratio of $\frac{h_2}{h_1} = 10.0$ is considered. Figures 5.55 – 5.56 show the thermal stresses under uniform temperature change and under conduction respectively. Under uniform temperature rise, the coating is under very high tensile stress whereas the thick substrate is under somewhat uniform stress. The stress intensity factors under this tensile stress are positive (Figure 5.74) but as the crack approaches the interface, the loading changes sign and the stress intensity factor drops. This crack is arrested by the compressive zone (Figure 5.75). For uniform cooling the problem becomes one of crack-contact type. The crack-tip locations and the stress intensity factors are shown in Figures 5.76 and 5.77 respectively. For surface heating we observe the arrest of an open crack as it enters compressive zone (Figure 5.78).

Some general comments can be made from these results. It is observed that thermal loading either tends to arrest the crack growth or create a crack-contact. If the crack lies completely in the compressive zone, the crack will remain closed. This means that every particular loading is associated with a critical length. If the surface flaw is smaller than this critical length the flaw will not propagate. If the surface flaw does propagate, it will be arrested by the compressive zone under pure thermal loading. If other kinds of loadings are superposed along with the thermal loading, the stress intensity factors of the different loadings can be added up to obtain the resultant stress intensity factor. Care should however be taken to determine if the crack is open or closed under the

combination of loadings. If the resultant stress intensity factor is positive, the crack is open and the analysis is straightforward. If, on the other hand, the loadings tend to close the crack, the procedure described in Section 5.2.2 should be followed to find the point of crack closure and the correct stress intensity factors.

βc	$\frac{k_1(a_1)}{\sigma_0\sqrt{c}}$		$\frac{k_1(b_1)}{\sigma_0\sqrt{c}}$	
	<i>Present work</i>	<i>Ref [43]</i>	<i>Present work</i>	<i>Ref [43]</i>
0.1	1.0172	1.0172	1.0087	1.0087
0.5	1.0820	1.0820	1.0377	1.0377
1.0	1.1546	1.1546	1.0654	1.0653
2.0	1.27913	1.2791	1.1042	1.1042
5.0	1.5595	1.5586	1.1669	1.1665
10.0	1.8823	1.8785	1.2157	1.2138
20.0	2.3283	2.3105	1.2641	1.2562
50.0	3.248	3.103	1.3521	1.3029

Table 5.1 Comparison of normalized stress intensity factors for internal crack in homogeneous half plane bonded to nonhomogeneous half plane subjected to fixed grip loading. Published results are from Erdogan et. al.[43].

$$a_1 = 0.0, c = \frac{(b_1 - a_1)}{2}, h_1 = h_2 = 1000.0, \sigma_0 = \frac{8\mu_0\epsilon_0}{(1 + \kappa)}.$$

	Fixed grip		Membrane loading		Pure bending	
$\frac{c}{h_1}$	$\frac{k_1(a_2)}{\sigma_0\sqrt{c}}$	$\frac{k_1(b_2)}{\sigma_0\sqrt{c}}$	$\frac{k_1(a_2)}{\sigma_t\sqrt{c}}$	$\frac{k_1(b_2)}{\sigma_t\sqrt{c}}$	$\frac{k_1(a_2)}{\sigma_b\sqrt{c}}$	$\frac{k_1(b_2)}{\sigma_b\sqrt{c}}$
0.0001	1.0000	1.0000	0.5001	0.5000	0.7606	0.7608
0.05	1.0043	1.0047	0.5048	0.4998	0.7208	0.8074
0.1	1.0167	1.0199	0.5136	0.5049	0.6871	0.8623
0.15	1.0370	1.0483	0.5263	0.5165	0.6596	0.9274
0.2	1.0656	1.0938	0.5431	0.5366	0.6387	1.0065
0.25	1.1037	1.1633	0.5646	0.5686	0.6256	1.1059
0.3	1.1538	1.2692	0.5921	0.6185	0.6227	1.2376
0.35	1.2213	1.4365	0.6282	0.6985	0.6349	1.4262
0.4	1.3184	1.7284	0.6788	0.8393	0.6736	1.7344
0.45	1.483	2.383	0.763	1.157	0.775	2.402

Table 5.2 Normalized stress intensity factors for an internal crack located in the

homogeneous layer. $c = \frac{(b_2 - a_2)}{2}$, $\frac{(b_2 + a_2)}{2} = \frac{h_1}{2}$, $\frac{h_2}{h_1} = 1.0$,
 $\beta h_1 = 0.375$ (PSZ-Rene41), $\sigma_0 = \frac{8\mu_0}{1 + \kappa} \epsilon_0$, $\sigma_t = \frac{N}{h_1}$, $\sigma_b = \frac{M}{h_1^2}$.

	Fixed grip		Membrane loading		Pure bending	
$\frac{c}{h_1}$	$\frac{k_1(a_2)}{\sigma_0\sqrt{c}}$	$\frac{k_1(b_2)}{\sigma_0\sqrt{c}}$	$\frac{k_1(a_2)}{\sigma_t\sqrt{c}}$	$\frac{k_1(b_2)}{\sigma_t\sqrt{c}}$	$\frac{k_1(a_2)}{\sigma_b\sqrt{c}}$	$\frac{k_1(b_2)}{\sigma_b\sqrt{c}}$
0.0001	1.0000	1.0000	0.5000	0.5000	0.7414	0.7416
0.05	1.0042	1.0046	0.5006	0.5038	0.7106	0.7790
0.1	1.0163	1.0194	0.5051	0.5127	0.6855	0.8241
0.15	1.0360	1.0471	0.5135	0.5281	0.6662	0.8790
0.2	1.0636	1.0915	0.5258	0.5518	0.6531	0.9470
0.25	1.1001	1.1593	0.5426	0.5873	0.6471	1.0338
0.3	1.1480	1.2621	0.5651	0.6405	0.6504	1.1502
0.35	1.2121	1.4242	0.5958	0.7237	0.6674	1.3181
0.4	1.3036	1.7052	0.6403	0.8671	0.7081	1.5933
0.45	1.4573	2.3304	0.7164	1.1855	0.8045	2.1866

Table 5.3 Normalized stress intensity factors for an internal crack located in the

homogeneous layer. $c = \frac{(b_2 - a_2)}{2}$, $\frac{(b_2 + a_2)}{2} = \frac{h_1}{2}$, $\frac{h_2}{h_1} = 1.0$,

$$\beta h_1 = -0.2576 \text{ (PSZ-Ti-6Al-4V)}, \sigma_0 = \frac{8\mu_0}{1+\kappa}\epsilon_0, \sigma_t = \frac{N}{h_1}, \sigma_b = \frac{M}{h_1^2}.$$

	Fixed grip		Membrane loading		Pure bending	
$\frac{c}{h_1}$	$\frac{k_1(b_1)}{\sigma_0\sqrt{c}}$	$\frac{k_1(a_1)}{\sigma_0\sqrt{c}}$	$\frac{k_1(b_1)}{\sigma_t\sqrt{c}}$	$\frac{k_1(a_1)}{\sigma_t\sqrt{c}}$	$\frac{k_1(b_1)}{\sigma_b\sqrt{c}}$	$\frac{k_1(a_1)}{\sigma_b\sqrt{c}}$
0.0001	0.8290	0.8290	0.4997	0.4997	0.8009	0.8009
0.05	0.8203	0.8420	0.4965	0.5053	0.8275	0.7768
0.1	0.8202	0.8621	0.4985	0.5152	0.8612	0.7581
0.15	0.8302	0.8893	0.5064	0.5292	0.9034	0.7447
0.2	0.8530	0.9239	0.5220	0.5476	0.9570	0.7369
0.25	0.8929	0.9672	0.5479	0.5712	1.0270	0.7360
0.3	0.9579	1.0212	0.5890	0.6011	1.1223	0.7440
0.35	1.064	1.090	0.6552	0.6399	1.262	0.765
0.4	1.251	1.182	0.771	0.693	1.49	0.81
0.45	1.66	1.32	1.03	0.78	1.98	0.90

Table 5.4 Normalized stress intensity factors for an internal crack located symmetrically

in the nonhomogeneous layer. $c = \frac{(b_1 - a_1)}{2}, \frac{(b_1 + a_1)}{2} = \frac{h_1}{2}, \frac{h_2}{h_1} = 1.0,$
 $\beta h_1 = 0.375$ (PSZ-Rene41), $\sigma_0 = \frac{8\mu_0}{1 + \kappa} \epsilon_0, \sigma_t = \frac{N}{h_1}, \sigma_b = \frac{M}{h_1^2}.$

	Fixed grip		Membrane loading		Pure bending	
$\frac{c}{h_1}$	$\frac{k_1(b_1)}{\sigma_0\sqrt{c}}$	$\frac{k_1(a_1)}{\sigma_0\sqrt{c}}$	$\frac{k_1(b_1)}{\sigma_t\sqrt{c}}$	$\frac{k_1(a_1)}{\sigma_t\sqrt{c}}$	$\frac{k_1(b_1)}{\sigma_b\sqrt{c}}$	$\frac{k_1(a_1)}{\sigma_b\sqrt{c}}$
0.0001	1.1375	1.1374	0.5001	0.5001	0.7063	0.7061
0.05	1.1546	1.1334	0.5059	0.5000	0.7562	0.6655
0.1	1.1840	1.1380	0.5170	0.5037	0.8148	0.6314
0.15	1.2288	1.1510	0.5349	0.5110	0.8846	0.6038
0.2	1.2944	1.1726	0.5618	0.5220	0.9693	0.5829
0.25	1.3894	1.2038	0.6014	0.5371	1.0757	0.5698
0.3	1.5295	1.2473	0.6607	0.5576	1.2165	0.5665
0.35	1.747	1.309	0.7532	0.5858	1.418	0.578
0.4	2.12	1.40	0.914	0.627	1.746	0.614
0.45	2.96	1.57	1.28	0.70	2.46	0.71

Table 5.5 Normalized stress intensity factors for an internal crack located symmetrically

in the nonhomogeneous layer. $c = \frac{(b_1 - a_1)}{2}$, $\frac{(b_1 + a_1)}{2} = \frac{h_1}{2}$, $\frac{h_2}{h_1} = 1.0$,

$\beta h_1 = -0.2576$ (PSZ-Ti-6Al-4V), $\sigma_0 = \frac{8\mu_0}{1+\kappa}\epsilon_0$, $\sigma_t = \frac{N}{h_1}$, $\sigma_b = \frac{M}{h_1^2}$.

	$\frac{k_1(a_1)}{\sigma_0\sqrt{c}}$		
$\frac{c}{h_1}$	<i>Case I</i>	<i>Case II</i>	<i>Case III</i>
0.01	0.8290	0.8333	0.8552
0.05	0.8420	0.8448	0.8721
0.10	0.8621	0.8656	0.9004
0.15	0.8893	0.8936	0.9371
0.20	0.9239	0.9291	0.9829
0.25	0.9672	0.9735	1.0393
0.30	1.0212	1.0287	1.1093
0.35	1.090	1.0991	1.1985
0.40	1.182	1.194	1.318
0.45	1.32	1.34	1.50

Table 5.6 Normalized stress intensity factors for an internal crack located symmetrically in the nonhomogeneous layer subjected to fixed grip loading. $c = \frac{(b_1 - a_1)}{2}$,

$$\frac{(b_1 + a_1)}{2} = \frac{h_1}{2}, \frac{h_2}{h_1} = 1.0, \beta h_1 = 0.375 \text{ (PSZ-Rene41)}, \sigma_0 = \frac{8\mu_0}{1 + \kappa} \epsilon_0.$$

Case I : Crack only in nonhomogeneous layer

Case II : Crack in presence of another crack in homogeneous substrate,

$$a_2 = 0.4h_1, b_2 = 0.6h_1$$

Case III : Crack in presence of another crack in homogeneous substrate,

$$a_2 = 0.2h_1, b_2 = 0.8h_1$$

	Fixed grip		Membrane loading		Pure bending	
$\frac{c}{h_1}$	$\frac{k_1(b_1)}{\sigma_0\sqrt{c}}$	$\frac{k_1(a_1)}{\sigma_0\sqrt{c}}$	$\frac{k_1(b_1)}{\sigma_t\sqrt{c}}$	$\frac{k_1(a_1)}{\sigma_t\sqrt{c}}$	$\frac{k_1(b_1)}{\sigma_b\sqrt{c}}$	$\frac{k_1(a_1)}{\sigma_b\sqrt{c}}$
0.01	0.8286	0.8333	0.4997	0.5016	0.8043	0.7940
0.05	0.8218	0.8448	0.4973	0.5067	0.8265	0.7748
0.10	0.8212	0.8656	0.4990	0.5169	0.8605	0.7556
0.15	0.8307	0.8936	0.5067	0.5313	0.9031	0.7415
0.20	0.8530	0.9291	0.5221	0.5502	0.9571	0.7331
0.25	0.8925	0.9735	0.5478	0.5743	1.0273	0.7314
0.30	0.9571	1.0287	0.5887	0.6049	1.1229	0.7387
0.35	1.0629	1.0991	0.6547	0.6445	1.2624	0.7592
0.40	1.250	1.194	0.770	0.698	1.492	0.802
0.45	1.66	1.34	1.02	0.78	1.98	0.89

Table 5.7 The normalized stress intensity factors for the internal crack located

symmetrically in the nonhomogeneous material in presence of a crack in the

homogeneous material. $c = \frac{(b_1 - a_1)}{2}$, $\frac{(b_1 + a_1)}{2} = \frac{h_1}{2}$, $\frac{h_2}{h_1} = 1.0$, $a_2 = 0.4h_1$,

$b_2 = 0.6h_1$, $\beta h_1 = 0.375$ (PSZ-Rene41), $\sigma_0 = \frac{8\mu_0}{1 + \kappa}\epsilon_0$, $\sigma_t = \frac{N}{h_1}$, $\sigma_b = \frac{M}{h_1^2}$.

	Fixed grip		Membrane loading		Pure bending	
$\frac{c}{h_1}$	$\frac{k_1(b_1)}{\sigma_0\sqrt{c}}$	$\frac{k_1(b_2)}{\sigma_0\sqrt{c}}$	$\frac{k_1(b_1)}{\sigma_t\sqrt{c}}$	$\frac{k_1(b_2)}{\sigma_t\sqrt{c}}$	$\frac{k_1(b_1)}{\sigma_b\sqrt{c}}$	$\frac{k_1(b_2)}{\sigma_b\sqrt{c}}$
0.0001	0.9998	1.0001	0.5513	0.5514	-0.1035	-0.1018
0.1	0.9836	1.0115	0.5473	0.5526	-0.1843	-0.0174
0.2	0.9799	1.0351	0.5499	0.5604	-0.2615	0.0672
0.3	0.9903	1.0724	0.5599	0.5758	-0.3352	0.1514
0.4	1.0178	1.1272	0.5792	0.6006	-0.4074	0.2366
0.5	1.0682	1.2060	0.6111	0.6383	-0.4816	0.3258
0.6	1.1528	1.3222	0.6622	0.6957	-0.5647	0.4253
0.7	1.2958	1.5034	0.7465	0.7872	-0.6708	0.5488
0.8	1.5606	1.8216	0.9007	0.9497	-0.8364	0.7333
0.9	2.1983	2.5595	1.2705	1.3286	-1.2073	1.1269
0.95	3.1251	3.6099	1.8077	1.8686	-1.7429	1.6789

Table 5.8 The normalized stress intensity factors for a crack symmetrically located with

respect to the interface. $\frac{h_2}{h_1} = 1.0$, $c = \frac{(b_1 + b_2)}{2}$, $\beta h_1 = 0.375$ (PSZ-Rene41),

$$\sigma_0 = \frac{8\mu_0}{1+\kappa}\epsilon_0, \sigma_t = \frac{N}{h_1}, \sigma_b = \frac{M}{h_1^2}.$$

	$\frac{k_1}{\sigma_0 \sqrt{b}}$	
b/h	<i>Present</i>	<i>Ref 63</i>
0.001	1.12152	1.121531
0.05	1.1399	
0.1	1.1892	1.1892
0.15	1.2652	
0.2	1.3673	1.3673
0.25	1.4975	
0.3	1.6599	1.6599
0.35	1.8612	
0.4	2.1115	2.1114
0.45	2.4254	
0.5	2.8247	2.8246
0.55	3.3430	
0.6	4.0333	4.0332
0.65	4.9846	
0.7	6.3552	6.3549
0.75	8.4536	
0.8	11.9559	11.955
0.85	18.6285	18.628
0.9	34.6336	34.632
0.95	99.121	99.128
0.98	394.3	

Table 5.9 Comparison of results for stress intensity factors for edge crack in homogeneous strip under fixed grip loading. In solution in this work, nonhomogeneity parameter $\frac{\beta h}{2} = 0.0001$, $\sigma_0 = \frac{8\mu_0}{(1 + \kappa)} \epsilon_0$.

b/h	$\frac{k_1}{\sigma_b \sqrt{b}}$	
	<i>Present</i>	<i>Ref 63</i>
0.001	1.12161	1.1202
0.05	1.0710	
0.1	1.0473	1.0472
0.15	1.0433	
0.2	1.0554	1.0553
0.25	1.0824	
0.3	1.1243	1.1241
0.35	1.1828	
0.4	1.2609	1.2606
0.45	1.3633	
0.5	1.4975	1.4972
0.55	1.6749	
0.6	1.9143	1.9140
0.65	2.2463	
0.7	2.7257	2.7252
0.75	3.4588	
0.8	4.6772	4.6764
0.85	6.9829	6.9817
0.9	12.464	12.462
0.95	34.307	34.306

Table 5.10 Comparison of results for stress intensity factors for edge crack in

homogeneous strip under pure bending. In solution in this work, nonhomogeneity

parameter $\frac{\beta h}{2} = 0.0001$, $\sigma_b = \frac{6M}{h^2}$.

	Fixed grip	Membrane	Bending
$\frac{c}{h_1}$	$\frac{k_1(a_1)}{\sigma_0\sqrt{c}}$	$\frac{k_1(a_1)}{\sigma_t\sqrt{c}}$	$\frac{k_1(a_1)}{\sigma_b\sqrt{c}}$
0.0001	1.1215	0.5042	1.4100
0.1	1.1503	0.5121	1.3627
0.2	1.2142	0.5354	1.3512
0.3	1.3091	0.5718	1.3658
0.4	1.4356	0.6214	1.4024
0.5	1.5974	0.6855	1.4605
0.6	1.8016	0.7669	1.5416
0.7	2.0591	0.8698	1.6496
0.8	2.3868	1.0010	1.7919
0.9	2.8116	1.1715	1.9805
1.0	3.3871	1.4027	2.2418

Table 5.11 The normalized stress intensity factors for an edge crack located in the

nonhomogeneous layer. $c = (b_1 - a_1)$, $b_1 = h_1$, $\frac{h_2}{h_1} = 1.0$,

$$\beta h_1 = 0.375 \text{ (PSZ-Rene41)}, \sigma_0 = \frac{8\mu_1}{1+\kappa}\epsilon_0, \sigma_t = \frac{N}{h_1}, \sigma_b = \frac{M}{h_1^2}.$$

	Fixed grip	Membrane	Bending
$\frac{c}{h_1}$	$\frac{k_1(b_2)}{\sigma_0\sqrt{c}}$	$\frac{k_1(b_2)}{\sigma_t\sqrt{c}}$	$\frac{k_1(b_2)}{\sigma_b\sqrt{c}}$
1.1	4.0518	1.6674	2.5047
1.2	4.9205	2.0146	2.8675
1.3	6.1133	2.491	3.368
1.4	7.8292	3.177	4.088
1.5	10.4546	4.227	5.187
1.6	14.8381	5.978	7.016
1.7	23.191	9.314	10.473
1.8	43.241	17.317	18.695
1.9	124.063	49.554	51.444

Table 5.12 The normalized stress intensity factors for an edge crack crossing the

interface. $c = (b_1 + b_2)$, $b_1 = h_1$, $\frac{h_2}{h_1} = 1.0$,

$$\beta h_1 = 0.375 \text{ (PSZ-Rene41)}, \sigma_0 = \frac{8\mu_1}{1+\kappa}\epsilon_0, \sigma_t = \frac{N}{h_1}, \sigma_b = \frac{M}{h_1^2}.$$

	Fixed grip	Membrane	Bending
$\frac{c}{h_1}$	$\frac{k_1(a_1)}{\sigma_0\sqrt{c}}$	$\frac{k_1(a_1)}{\sigma_t\sqrt{c}}$	$\frac{k_1(a_1)}{\sigma_b\sqrt{c}}$
0.0001	1.1215	0.5942	1.8892
0.1	1.1337	0.6060	1.7897
0.2	1.1744	0.6330	1.7346
0.3	1.2392	0.6732	1.7117
0.4	1.3269	0.7261	1.7146
0.5	1.4384	0.7924	1.7404
0.6	1.5765	0.8736	1.7886
0.7	1.7456	0.9727	1.8600
0.8	1.9522	1.0932	1.9574
0.9	2.2044	1.2401	2.0842
1.0	2.5082	1.4168	2.2413

Table 5.13 The normalized stress intensity factors for an edge crack located in the

nonhomogeneous layer. $c = (b_1 - a_1)$, $b_1 = h_1$, $\frac{h_2}{h_1} = 1.0$,

$$\beta h_1 = -0.2576 \text{ (PSZ-Ti-6Al-4V)}, \sigma_0 = \frac{8\mu_1}{1+\kappa}\epsilon_0, \sigma_t = \frac{N}{h_1}, \sigma_b = \frac{M}{h_1^2}.$$

	Fixed grip	Membrane	Bending
$\frac{c}{h_1}$	$\frac{k_1(b_2)}{\sigma_0\sqrt{c}}$	$\frac{k_1(b_2)}{\sigma_t\sqrt{c}}$	$\frac{k_1(b_2)}{\sigma_b\sqrt{c}}$
1.1	2.9538	1.6740	2.5166
1.2	3.5489	2.0178	2.8731
1.3	4.3709	2.493	3.369
1.4	5.5566	3.178	4.088
1.5	7.3730	4.227	5.187
1.6	10.4032	5.977	7.014
1.7	16.176	9.314	10.472
1.8	30.018	17.316	18.692
1.9	85.783	49.570	51.468

Table 5.14 The normalized stress intensity factors for an edge crack crossing the

interface. $c = (b_1 + b_2)$, $b_1 = h_1$, $\frac{h_2}{h_1} = 1.0$, $\beta h_1 = -0.2576$ (PSZ-Ti-6Al-4V),
 $\sigma_0 = \frac{8\mu_1}{1+\kappa}\epsilon_0$, $\sigma_t = \frac{N}{h_1}$, $\sigma_b = \frac{M}{h_1^2}$.

	Fixed grip	Membrane	Bending
$\frac{c}{h_1}$	$\frac{k_1(a_1)}{\sigma_0\sqrt{c}}$	$\frac{k_1(a_1)}{\sigma_t\sqrt{c}}$	$\frac{k_1(a_1)}{\sigma_b\sqrt{c}}$
0.0001	1.1215	0.07434	0.04040
0.1	1.1344	0.07516	0.04042
0.2	1.1551	0.07649	0.04069
0.3	1.1816	0.07821	0.04114
0.4	1.2132	0.08026	0.04175
0.5	1.2495	0.08263	0.04249
0.6	1.2905	0.08530	0.04336
0.7	1.3365	0.08829	0.04436
0.8	1.3879	0.09165	0.04550
0.9	1.4462	0.09545	0.04682
1.0	1.5170	0.1001	0.04850

Table 5.15 The normalized stress intensity factors for an edge crack located in the

nonhomogeneous layer. $c = (b_1 - a_1)$, $b_1 = h_1$, $\frac{h_2}{h_1} = 10.0$,

$$\beta h_1 = 0.375 \text{ (PSZ-René41)}, \sigma_0 = \frac{8\mu_0}{1+\kappa}\epsilon_1, \sigma_t = \frac{N}{h_1}, \sigma_b = \frac{M}{h_1^2}.$$

	Fixed grip	Membrane	Bending
$\frac{c}{h_1}$	$\frac{k_1(b_2)}{\sigma_0\sqrt{c}}$	$\frac{k_1(b_2)}{\sigma_t\sqrt{c}}$	$\frac{k_1(b_2)}{\sigma_b\sqrt{c}}$
2.0	1.8149	0.1192	0.05122
3.0	2.1694	0.1419	0.05420
4.0	2.6796	0.1747	0.05946
5.0	3.4357	0.2233	0.06807
6.0	4.6113	0.2990	0.08211
7.0	6.5909	0.4265	0.1063
8.0	10.3839	0.6708	0.1529
9.0	19.5218	1.2593	0.2645
10.0	56.381	3.6327	0.7078

Table 5.16 The normalized stress intensity factors for an edge crack crossing the

interface. $c = (b_1 + b_2)$, $b_1 = h_1$, $\frac{h_2}{h_1} = 10.0$, $\beta h_1 = 0.375$ (PSZ-René41),

$$\sigma_0 = \frac{8\mu_1}{1+\kappa}\epsilon_0, \sigma_t = \frac{N}{h_1}, \sigma_b = \frac{M}{h_1^2}.$$

$\frac{c}{h_1}$	$\frac{k_1}{\sigma_T \sqrt{c}}$
0.0	0.0708
0.1	0.0673
0.2	0.0649
0.3	0.0628
0.4	0.0607
0.5	0.0580
0.6	0.0545
0.7	0.0497
0.8	0.0430
0.9	0.0336
1.0	0.0203
1.1	0.0097
1.2	0.0049
1.3	0.0026
1.4	0.0008
1.5	- 0.0003
1.6	- 0.0005
1.7	- 0.0009
1.8	- 0.0001

Table 5.17 Normalized stress intensity factors for an edge crack passing through the interface under uniform temperature rise.

$$c = \text{crack length, } b_1 = h_1, \frac{h_2}{h_1} = 1.0, \sigma_T = \frac{8\mu_0\alpha_0(T - T_0)(1 + \nu)}{(1 + \kappa)},$$

$$\frac{\mu_0}{\mu_1} = e^{\beta h_1}, \frac{\alpha_0}{\alpha_1} = e^{\alpha h_1}, \frac{k_0}{k_1} = e^{\gamma h_1}, T_1 = T_2 = T > T_0,$$

$$\beta h_1 = 0.375, \alpha h_1 = 0.513, \gamma h_1 = 2.5 \text{ (PSZ-René41).}$$

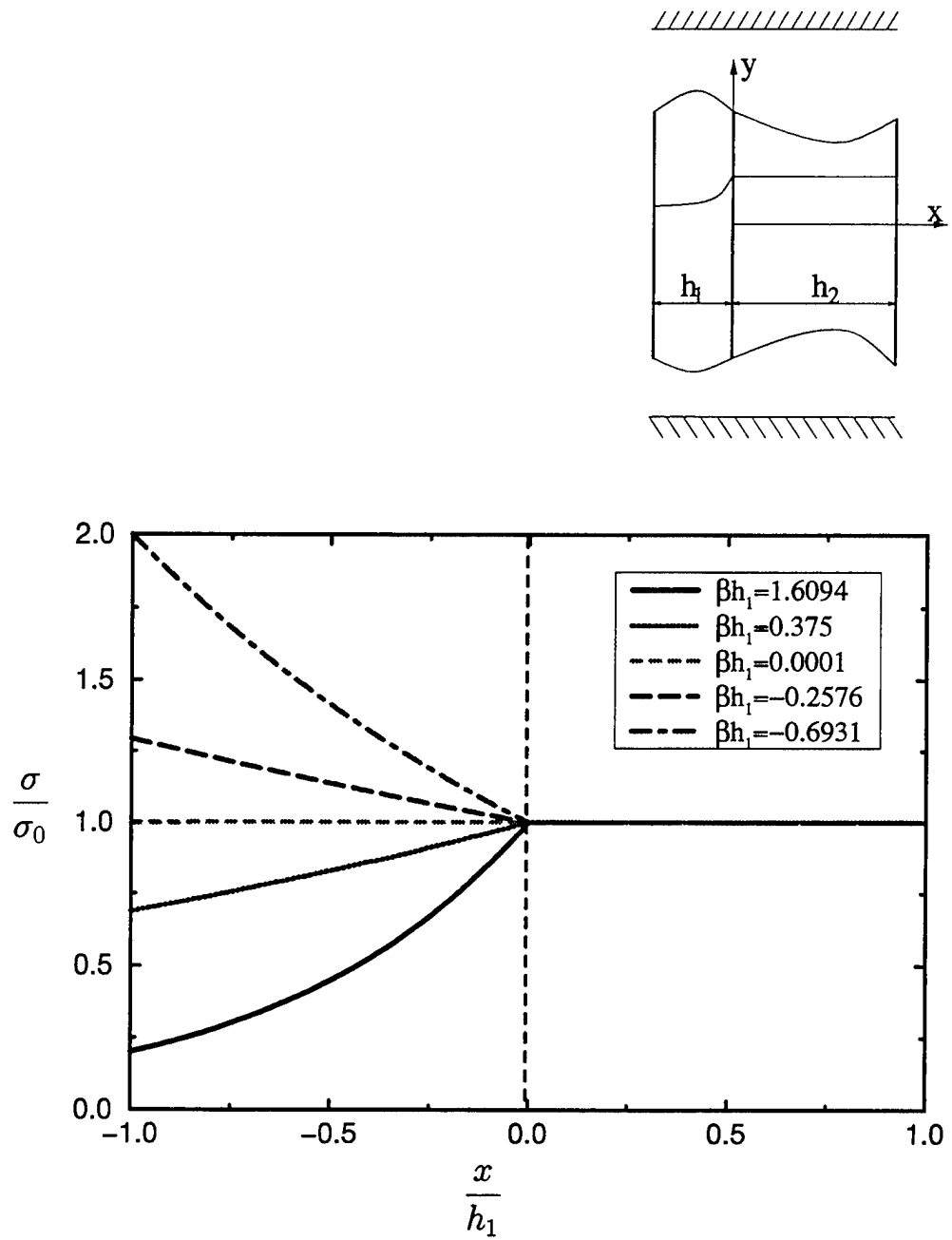


Figure 5.1 Stress distribution for an uncracked specimen under fixed grip loading.

$$\frac{h_2}{h_1} = 1.0, \sigma_0 = \frac{8\mu_0}{(1+\kappa)}\epsilon_0.$$

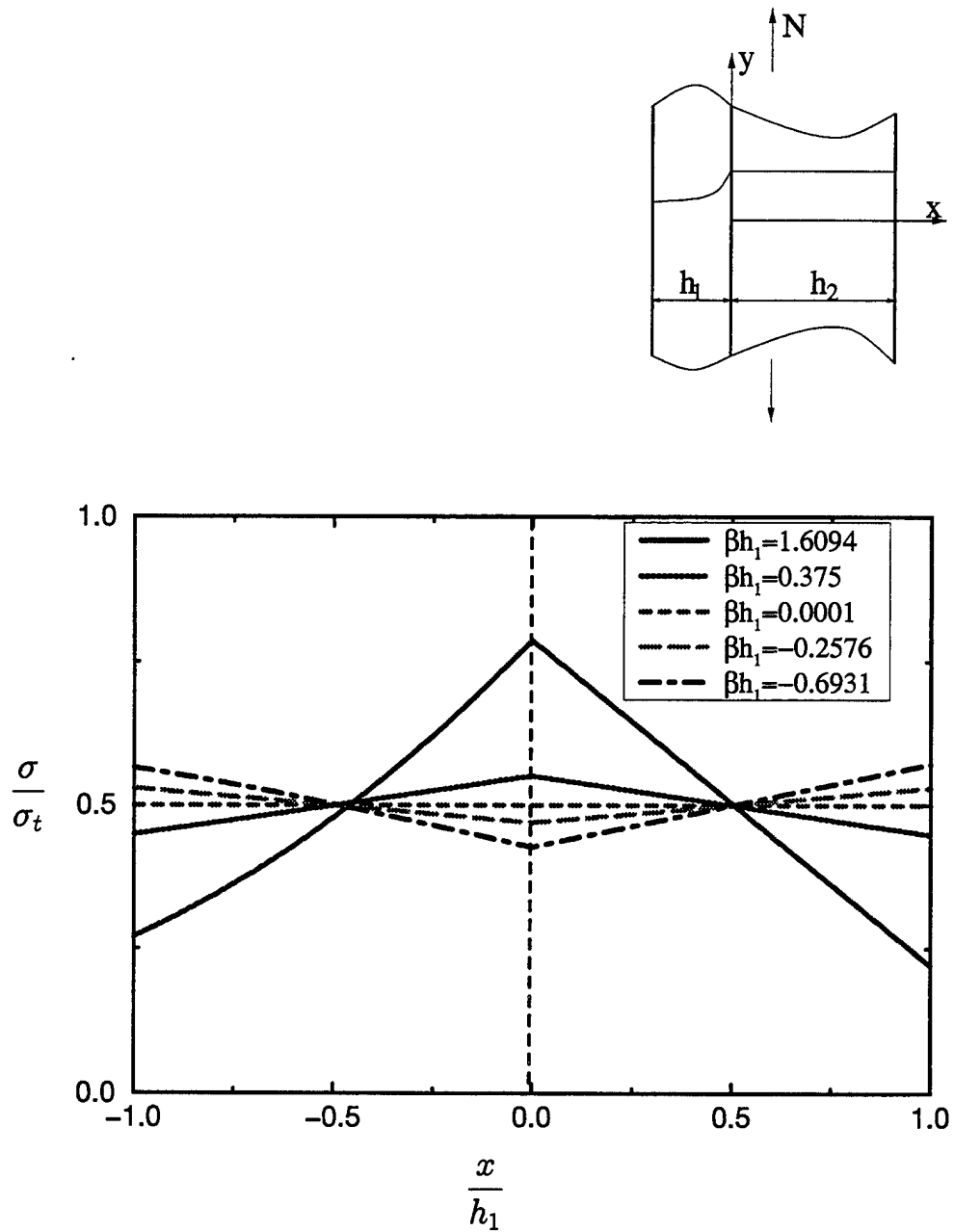


Figure 5.2 Stress distribution for an uncracked specimen under membrane

loading. $\frac{h_2}{h_1} = 1.0$, $\sigma_t = \frac{N}{h_1}$.

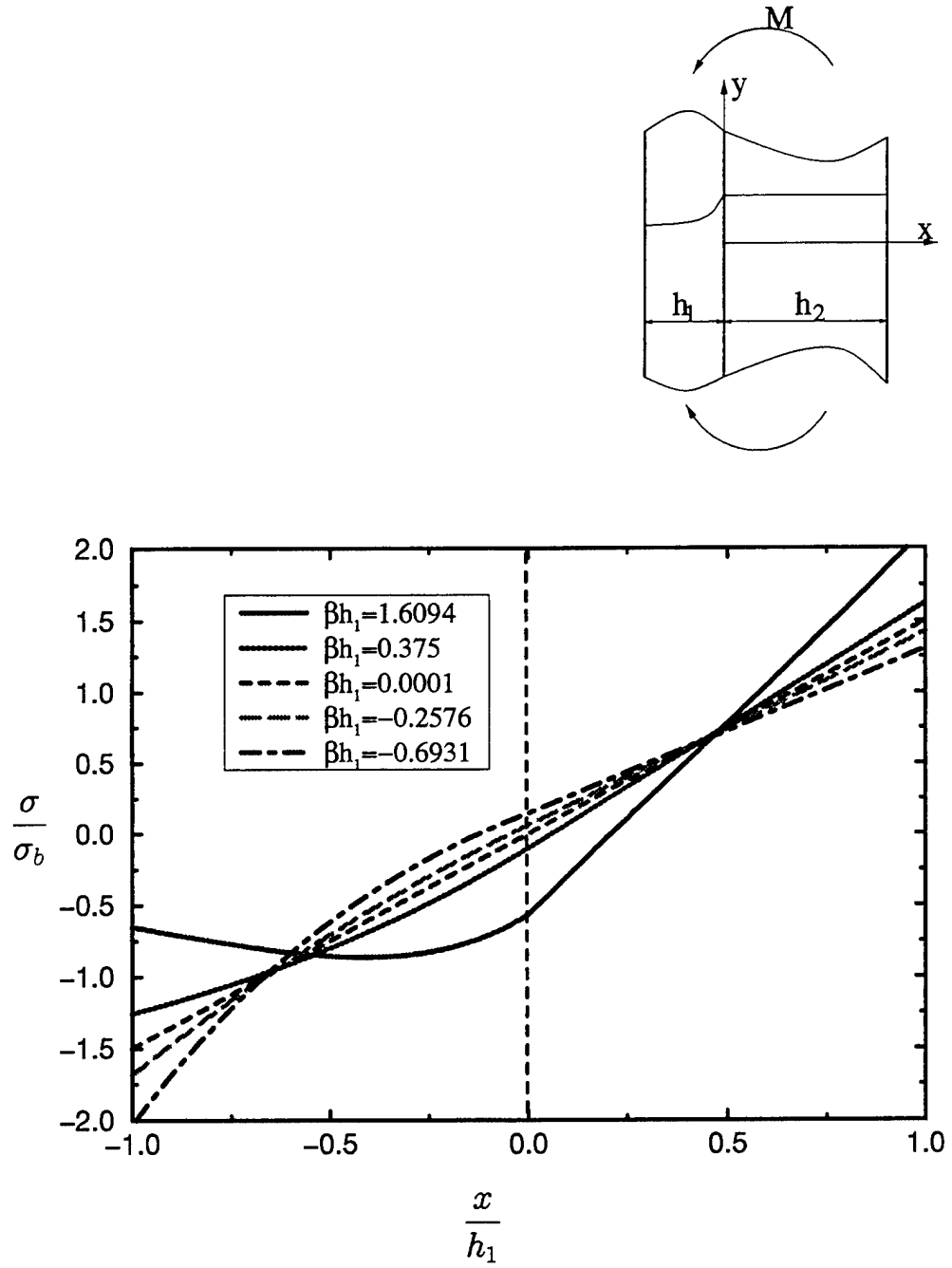


Figure 5.3 Stress distribution for an uncracked specimen under pure bending.

$$\frac{h_2}{h_1} = 1.0, \sigma_b = \frac{M}{h_1^2}.$$

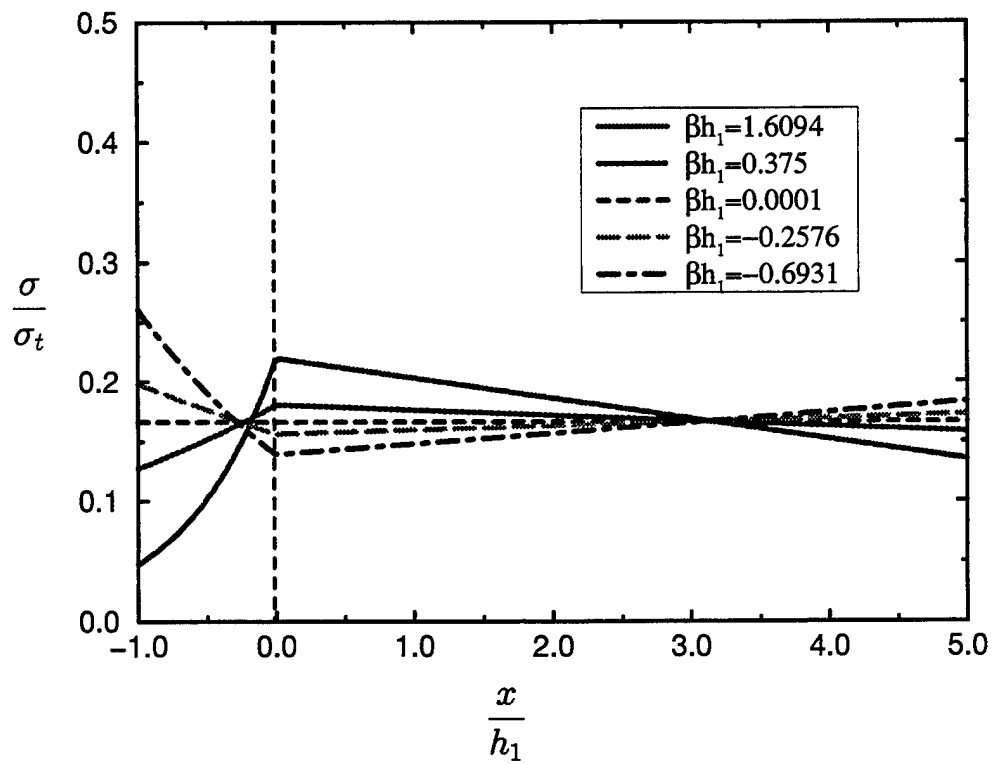
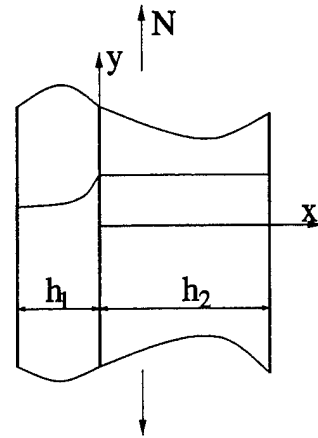


Figure 5.4 Stress distribution for an uncracked specimen under membrane

loading. $\frac{h_2}{h_1} = 5.0$, $\sigma_t = \frac{N}{h_1}$.

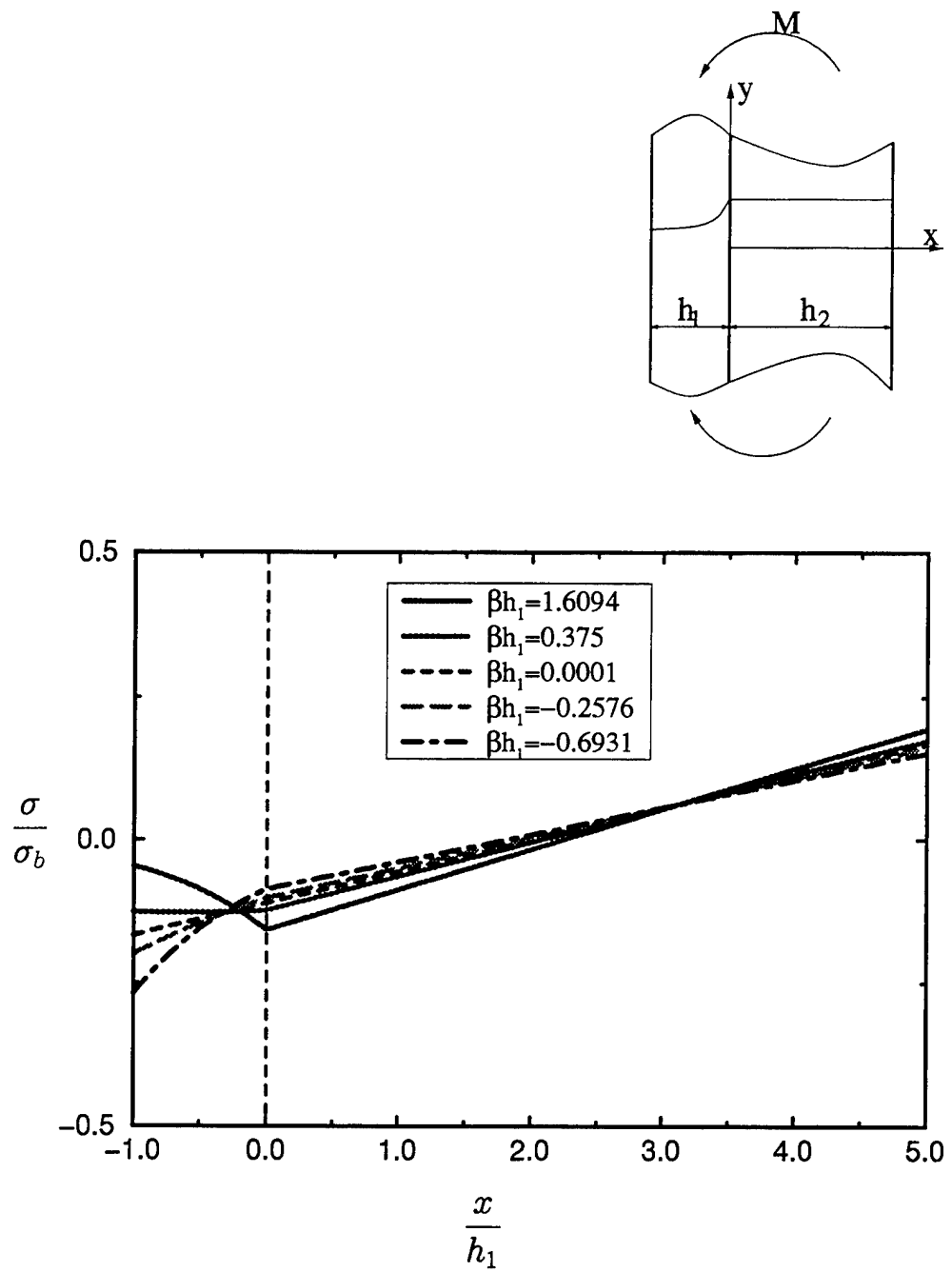


Figure 5.5 Stress distribution for an uncracked specimen under pure bending.

$$\frac{h_2}{h_1} = 5.0, \sigma_b = \frac{M}{h_1^2}.$$

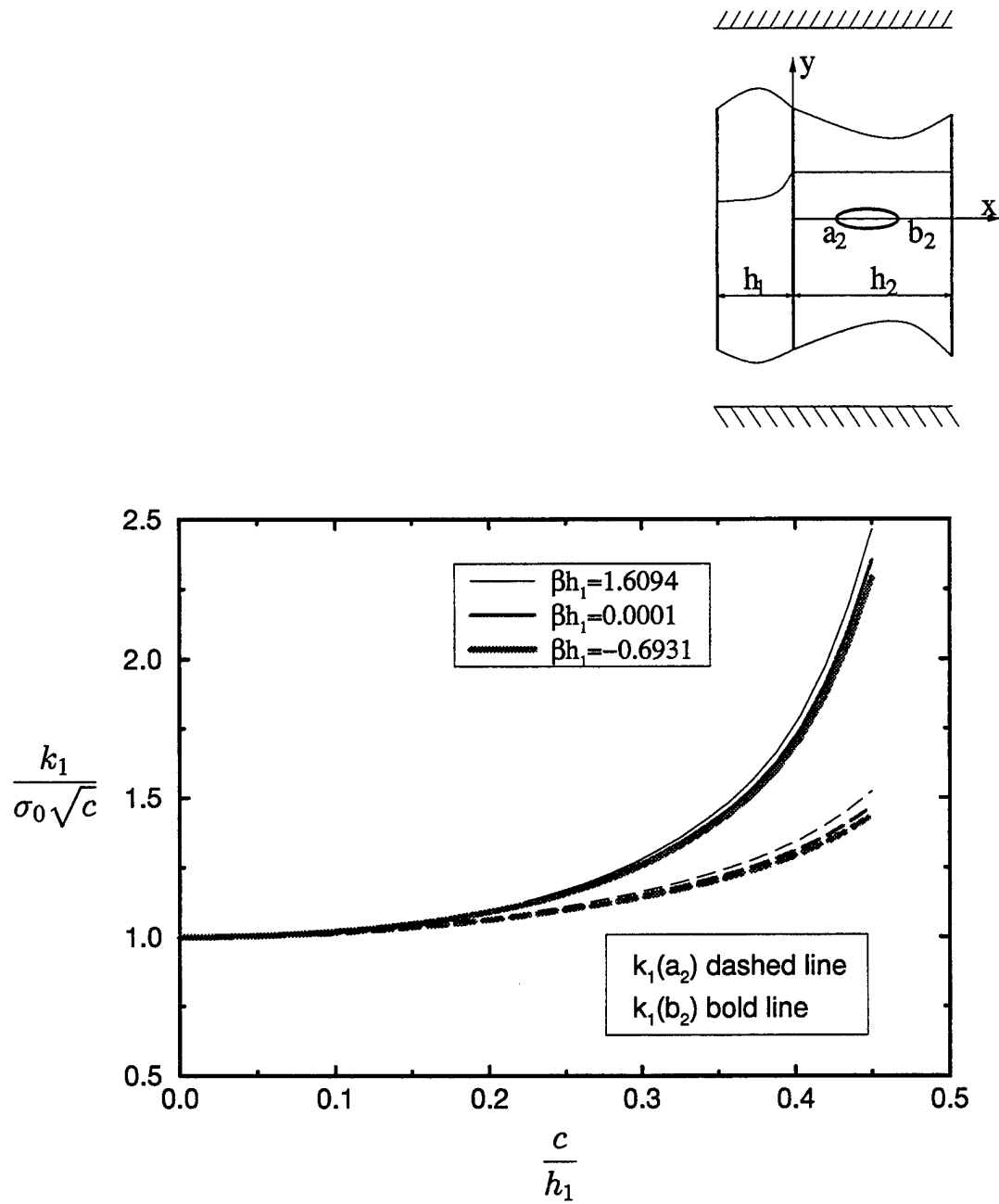


Figure 5.6 The effect of nonhomogeneity parameter on normalized stress intensity factors for an internal crack symmetrically located in the homogeneous layer subjected to fixed grip loading.

$$c = \frac{(b_2 - a_2)}{2}, \frac{(b_2 + a_2)}{2} = \frac{h_1}{2}, \frac{h_2}{h_1} = 1.0, \sigma_0 = \frac{8\mu_0}{(1 + \kappa)} \epsilon_0.$$

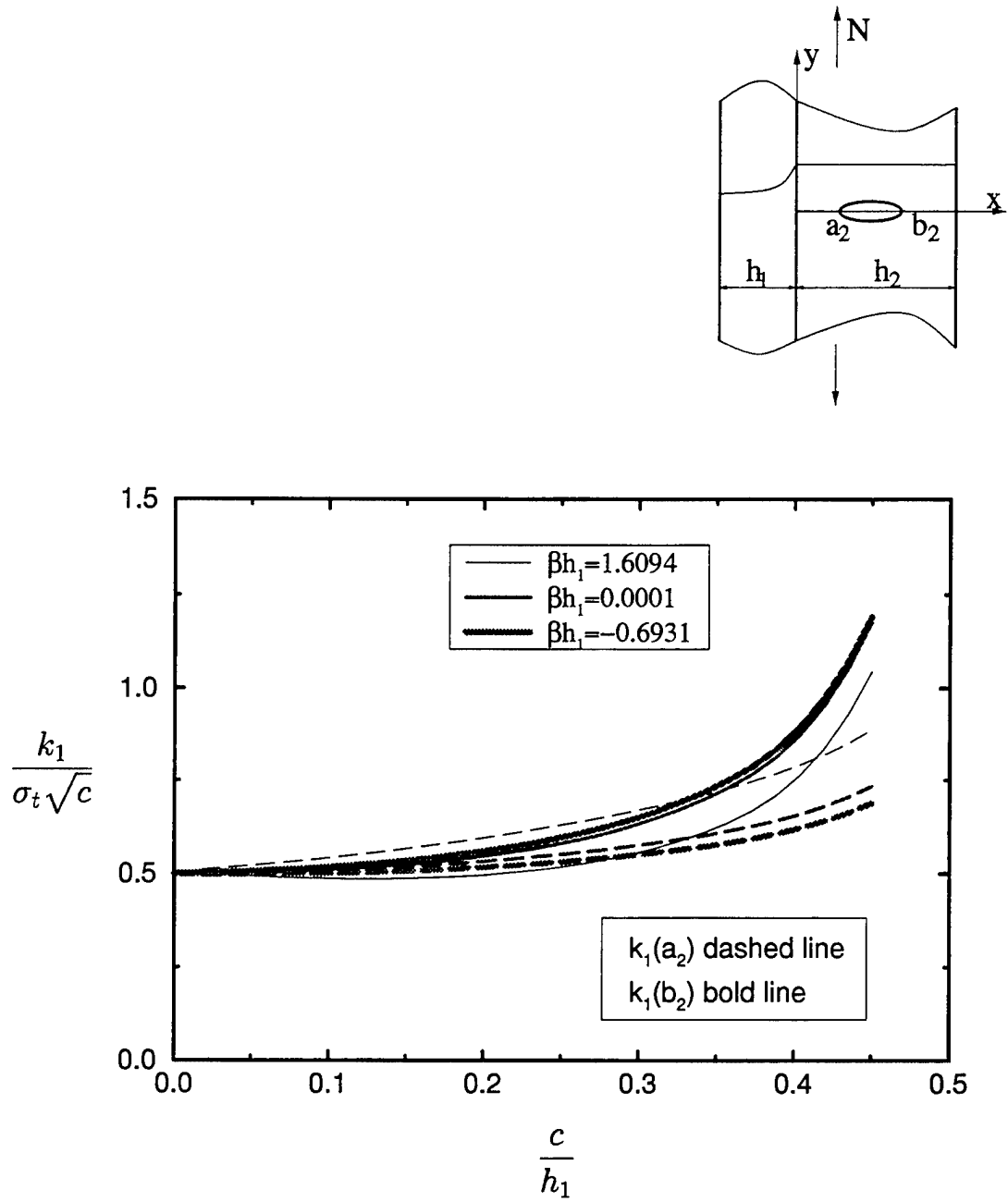


Figure 5.7 The effect of nonhomogeneity parameter on normalized stress intensity factors for an internal crack symmetrically located in the homogeneous layer subjected to membrane loading.

$$c = \frac{(b_2 - a_2)}{2}, \frac{(b_2 + a_2)}{2} = \frac{h_1}{2}, \frac{h_2}{h_1} = 1.0, \sigma_t = \frac{N}{h_1}.$$

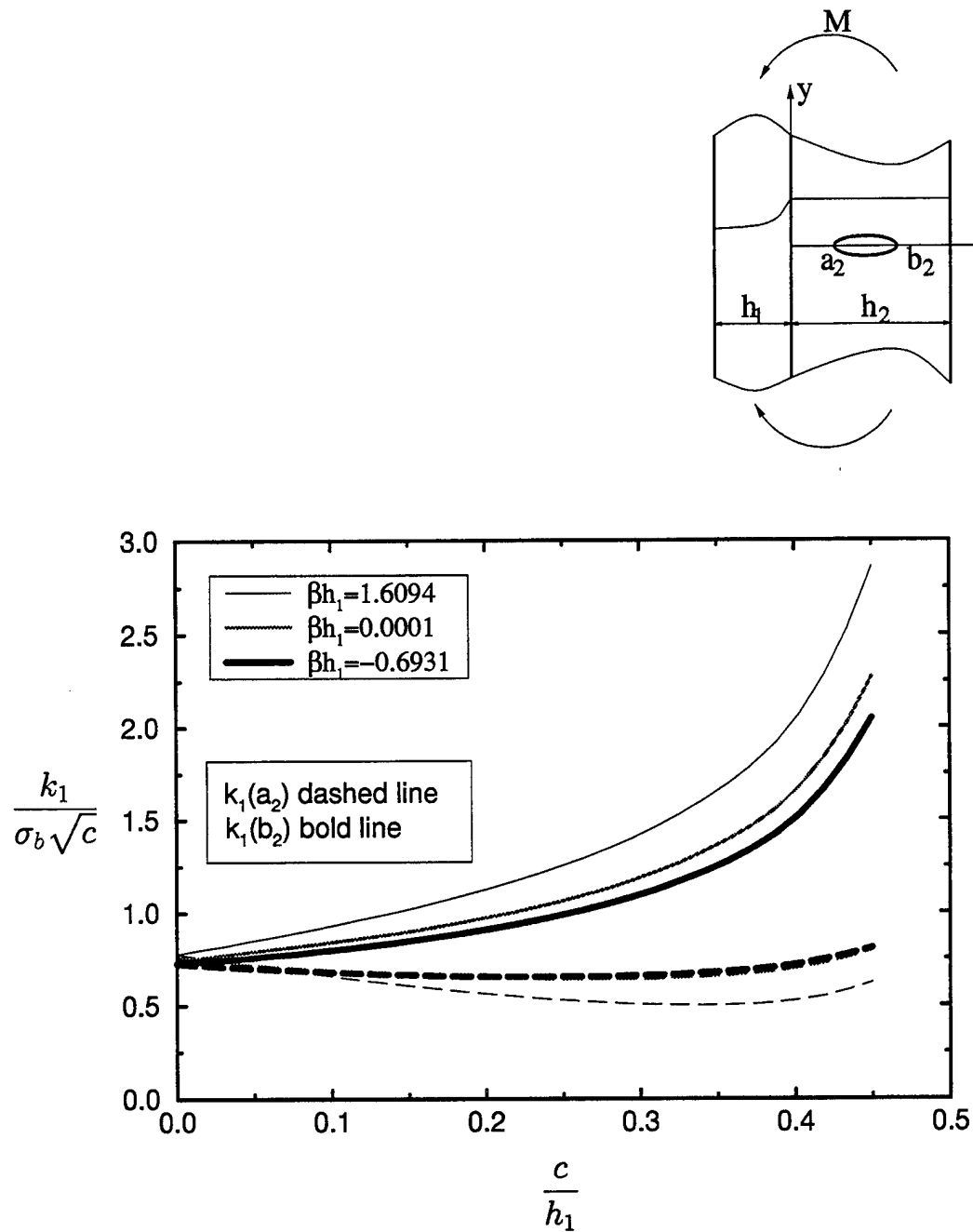


Figure 5.8 The effect of nonhomogeneity parameter on normalized stress intensity factors for an internal crack symmetrically located in the homogeneous layer subjected to pure bending.

$$c = \frac{(b_2 - a_2)}{2}, \frac{(b_2 + a_2)}{2} = \frac{h_1}{2}, \frac{h_2}{h_1} = 1.0, \sigma_b = \frac{M}{h_1^2}.$$

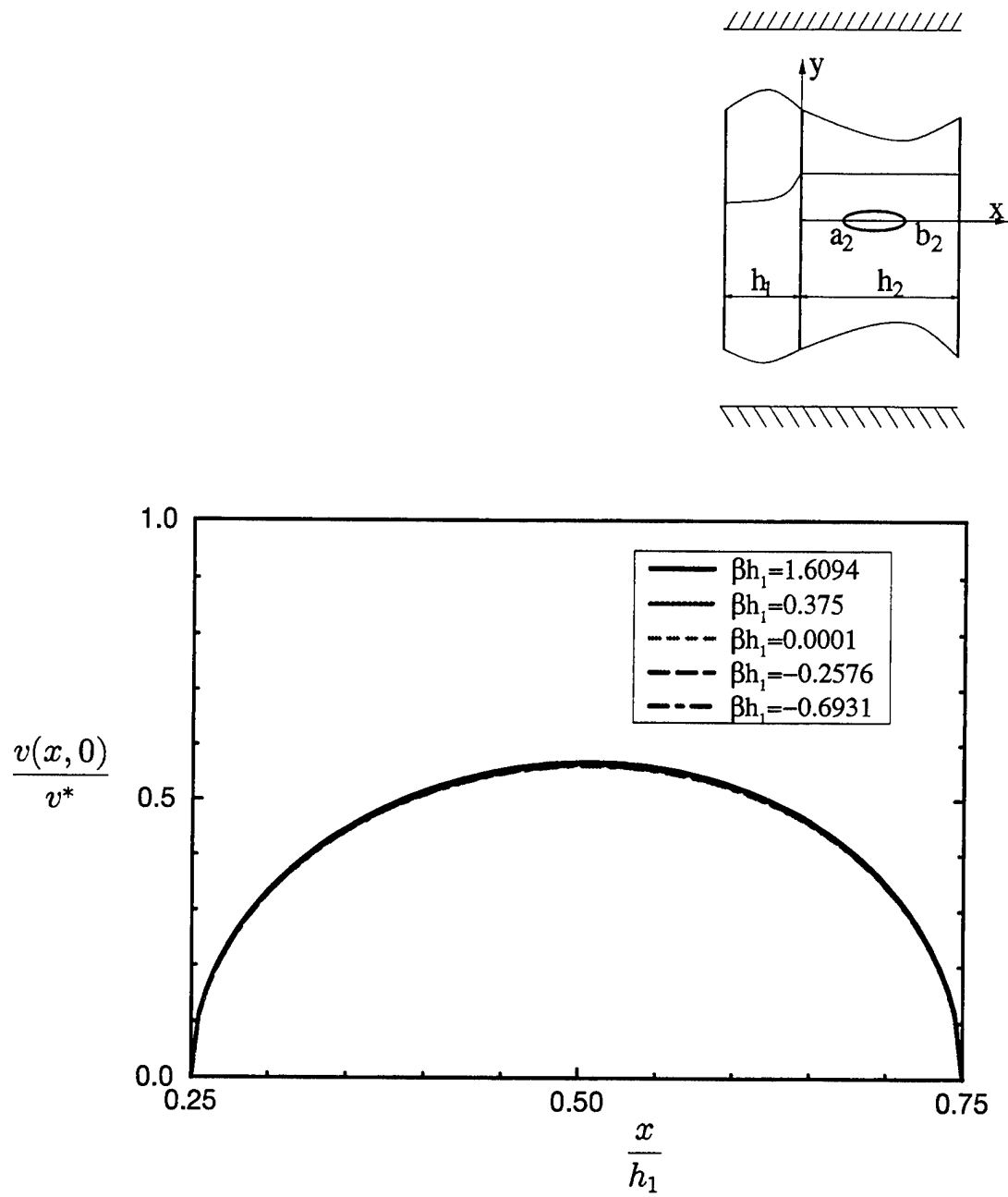


Figure 5.9 Effect of nonhomogeneity parameter on normalized crack opening displacement for an internal crack in the homogeneous material subjected to fixed grip loading. $v^* = 2h_1\epsilon_0$, $\frac{h_2}{h_1} = 1.0$, $a_2 = 0.25h_1$, $b_2 = 0.75h_1$.

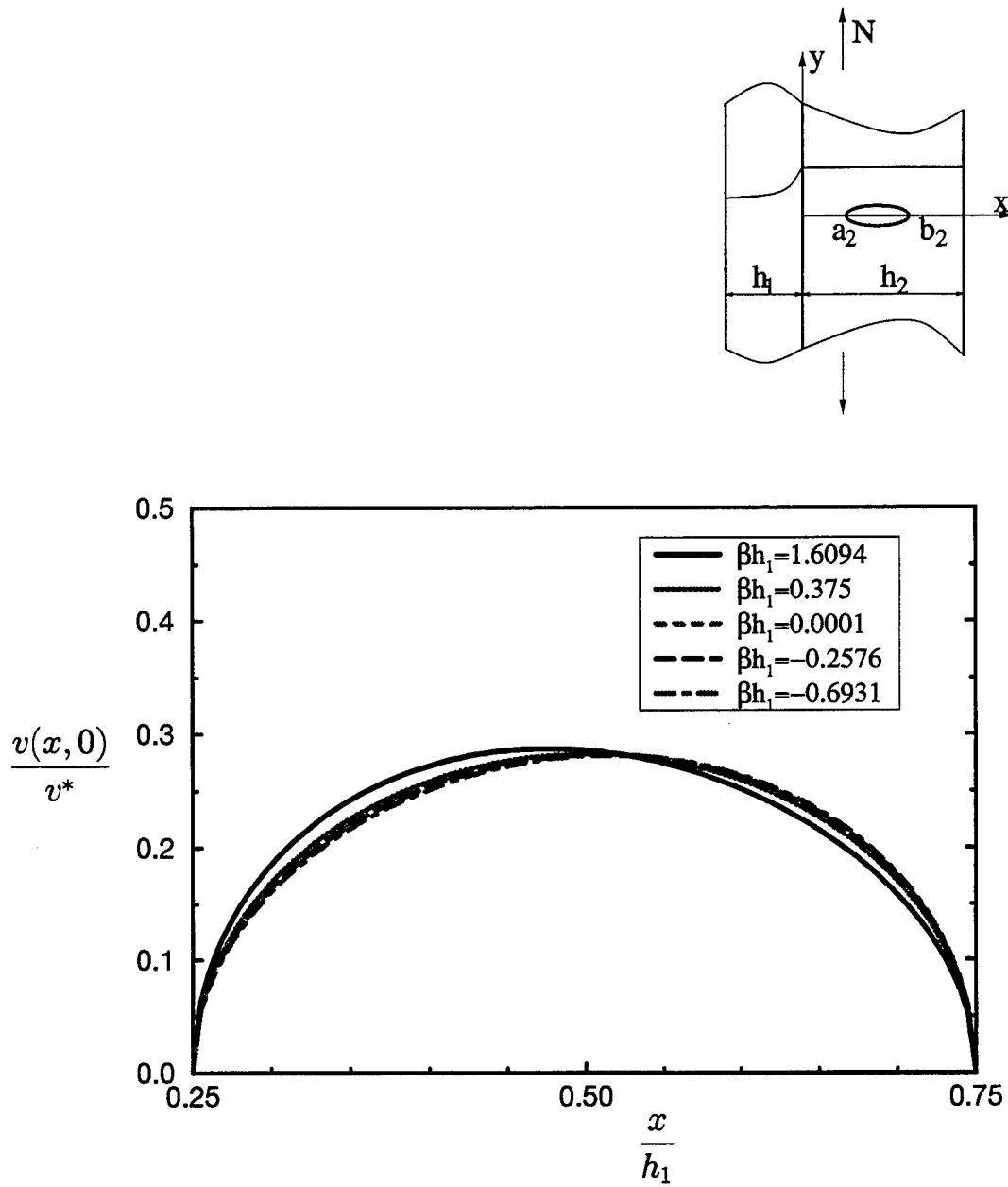


Figure 5.10 Effect of nonhomogeneity parameter on normalized crack opening

displacement for an internal crack in the homogeneous material subjected to membrane loading. $v^* = 2N \frac{(1 + \kappa)}{8\mu_0}$, $\frac{h_2}{h_1} = 1.0$, $a_2 = 0.25h_1$, $b_2 = 0.75h_1$.

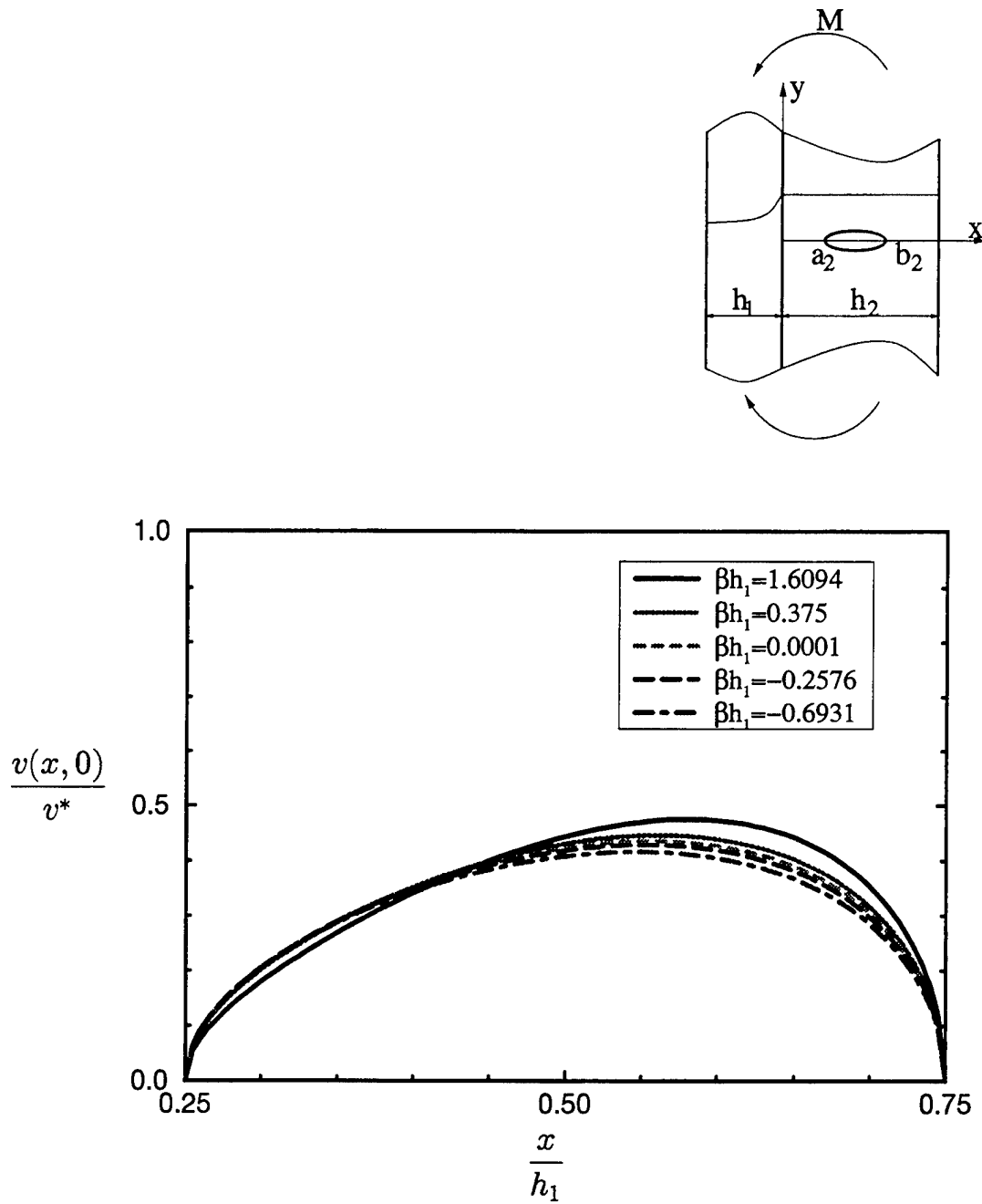


Figure 5.11 Effect of nonhomogeneity parameter on normalized crack opening displacement for an internal crack in the homogeneous material subjected to pure bending. $v^* = 2 \frac{M}{h_1} \frac{(1 + \kappa)}{8\mu_0}$, $\frac{h_2}{h_1} = 1.0$, $a_2 = 0.25h_1$, $b_2 = 0.75h_1$.

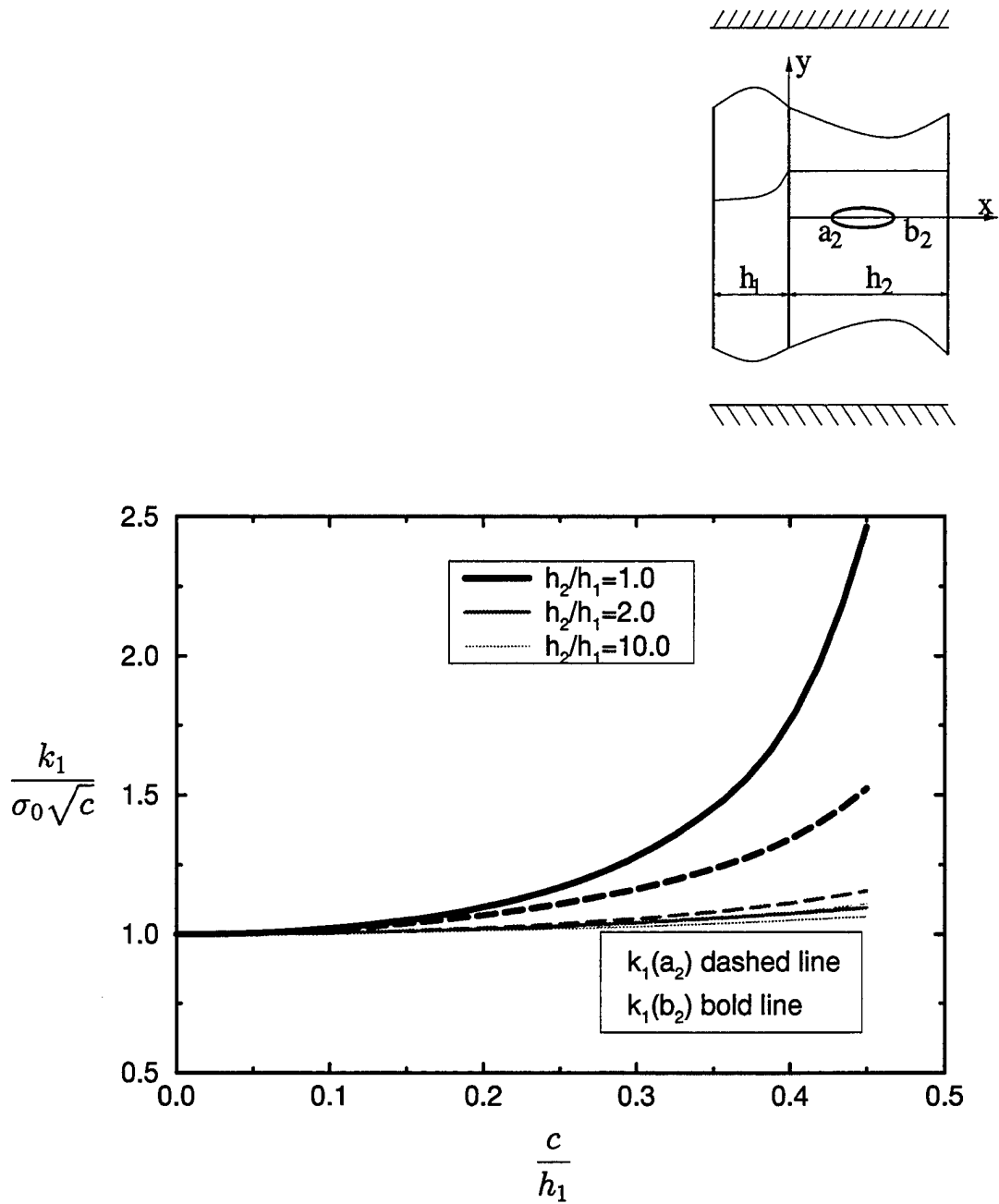


Figure 5.12 The effect of thickness ratio on normalized stress intensity factors for an internal crack located in the homogeneous layer subjected to fixed grip loading.

$$c = \frac{(b_2 - a_2)}{2}, \frac{(b_2 + a_2)}{2} = \frac{h_1}{2}, \beta h_1 = 1.6094, \sigma_0 = \frac{8\mu_0}{(1 + \kappa)} \epsilon_0.$$

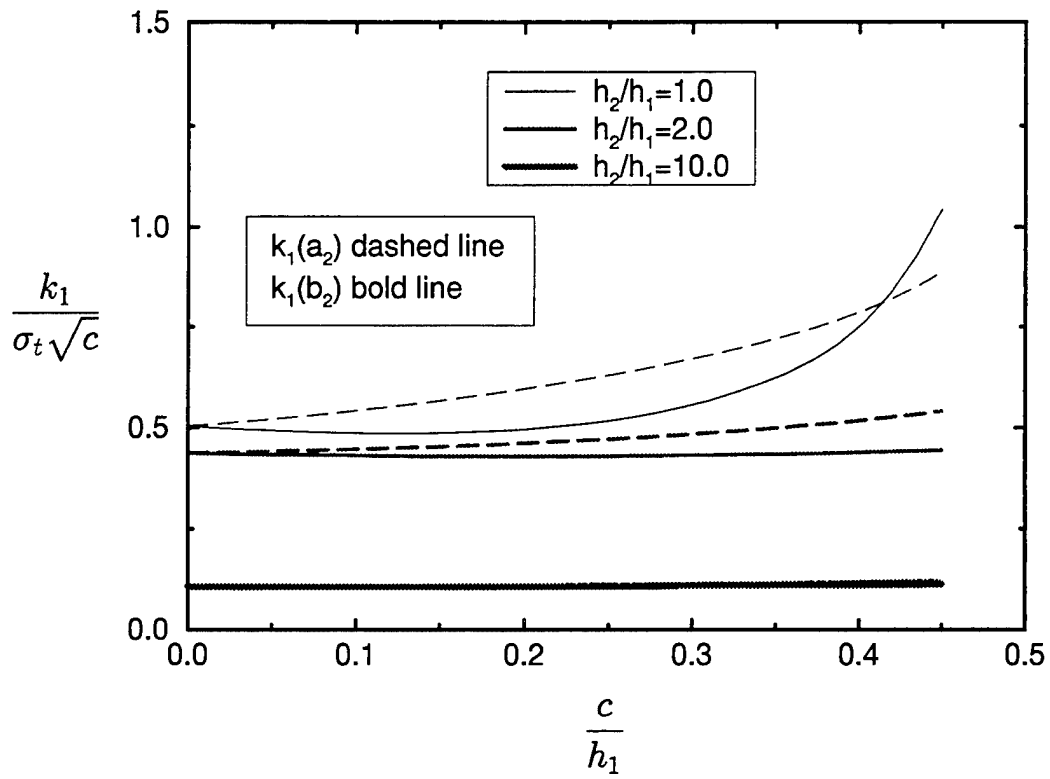
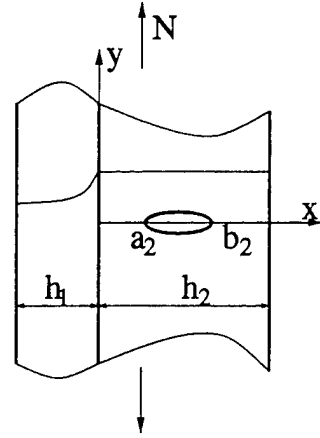


Figure 5.13 The effect of thickness ratio on normalized stress intensity factors for an internal crack located in the homogeneous layer subjected to membrane loading.

$$c = \frac{(b_2 - a_2)}{2}, \frac{(b_2 + a_2)}{2} = \frac{h_1}{2}, \beta h_1 = 1.6094, \sigma_t = \frac{N}{h_1}.$$

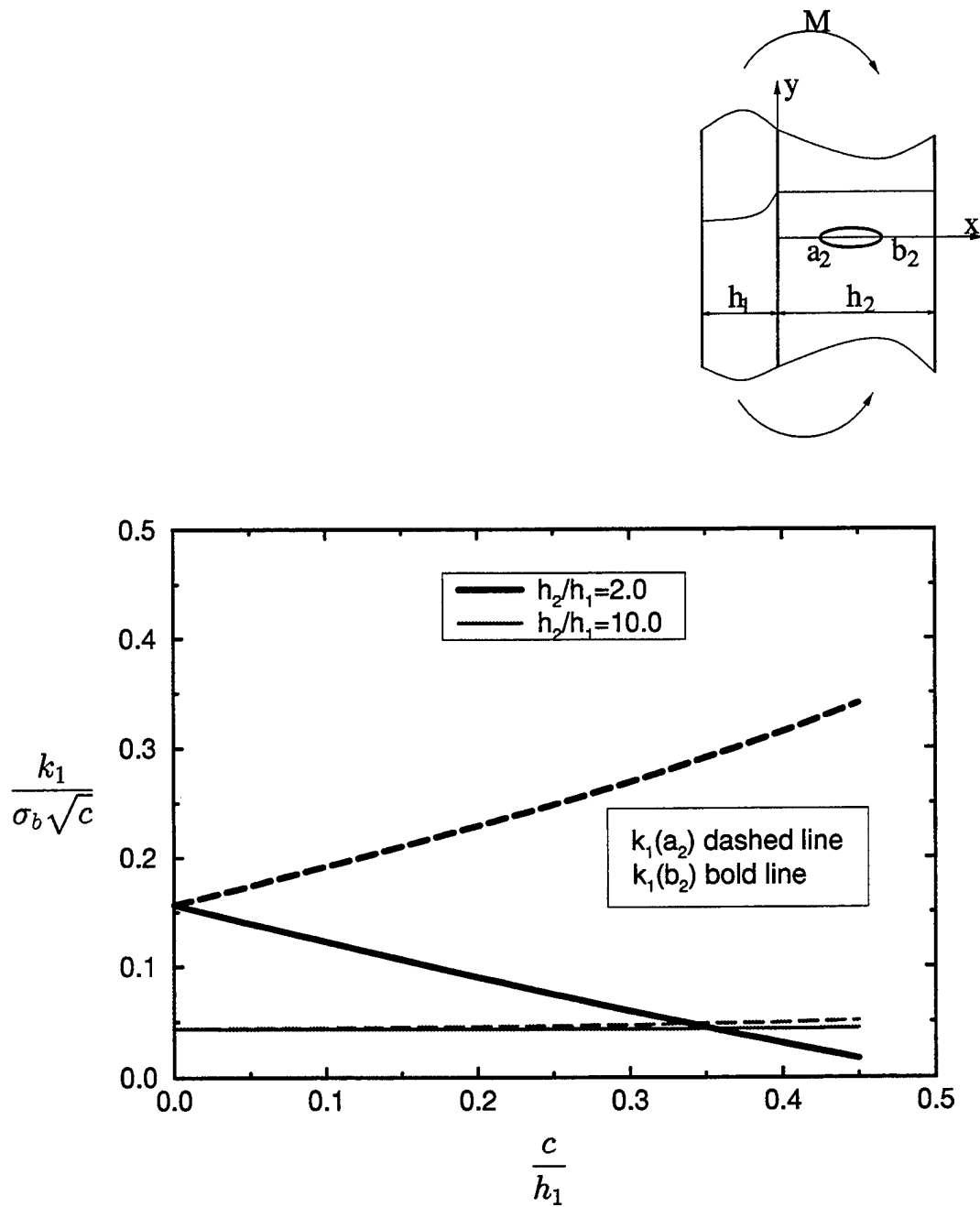


Figure 5.14 The effect of thickness ratio on normalized stress intensity factors for an internal crack located in the homogeneous layer subjected to pure bending.

$$c = \frac{(b_2 - a_2)}{2}, \frac{(b_2 + a_2)}{2} = \frac{h_1}{2}, \beta h_1 = 1.6094, \sigma_b = \frac{M}{h_1^2}.$$

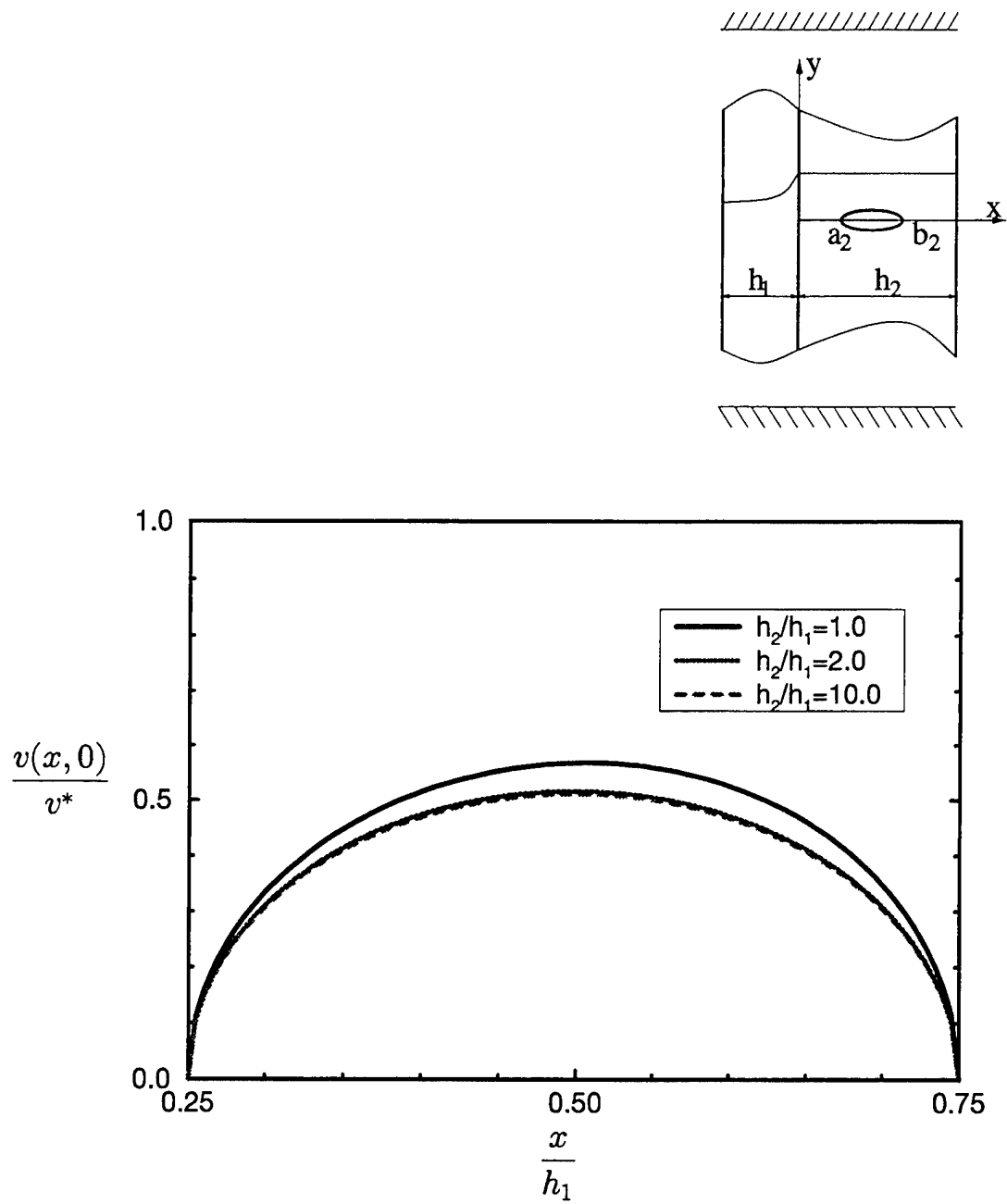


Figure 5.15 Effect of thickness ratio on normalized crack opening displacement for an internal crack in the homogeneous material subjected to fixed grip loading.

$$v^* = 2h_1\epsilon_0, \beta h_1 = 1.6094, a_2 = 0.25h_1, b_2 = 0.75h_1.$$

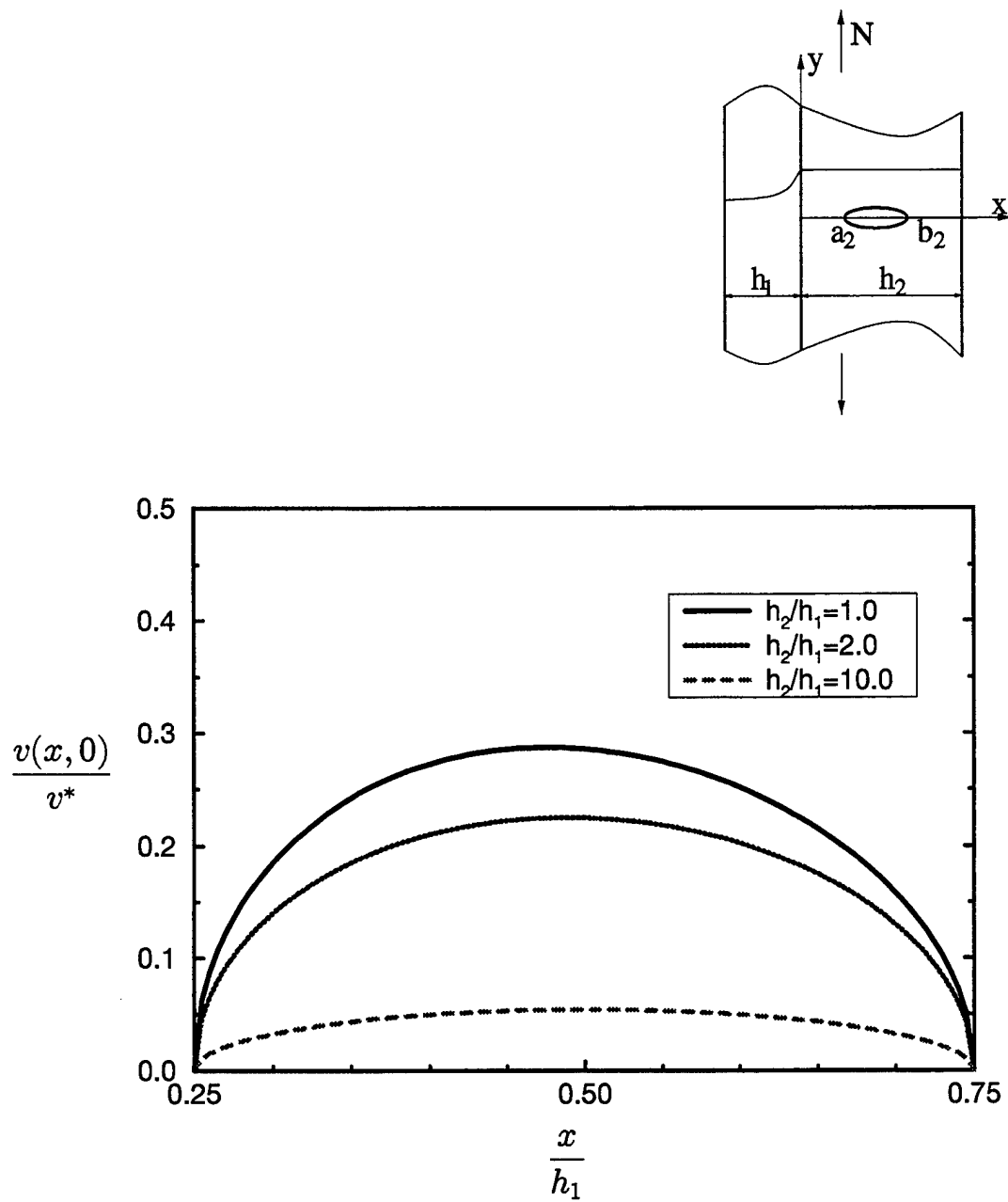


Figure 5.16 Effect of thickness ratio on normalized crack opening displacement for an internal crack in the homogeneous material subjected to membrane loading.

$$v^* = 2N \frac{(1 + \kappa)}{8\mu_0}, \beta h_1 = 1.6094, a_2 = 0.25h_1, b_2 = 0.75h_1.$$

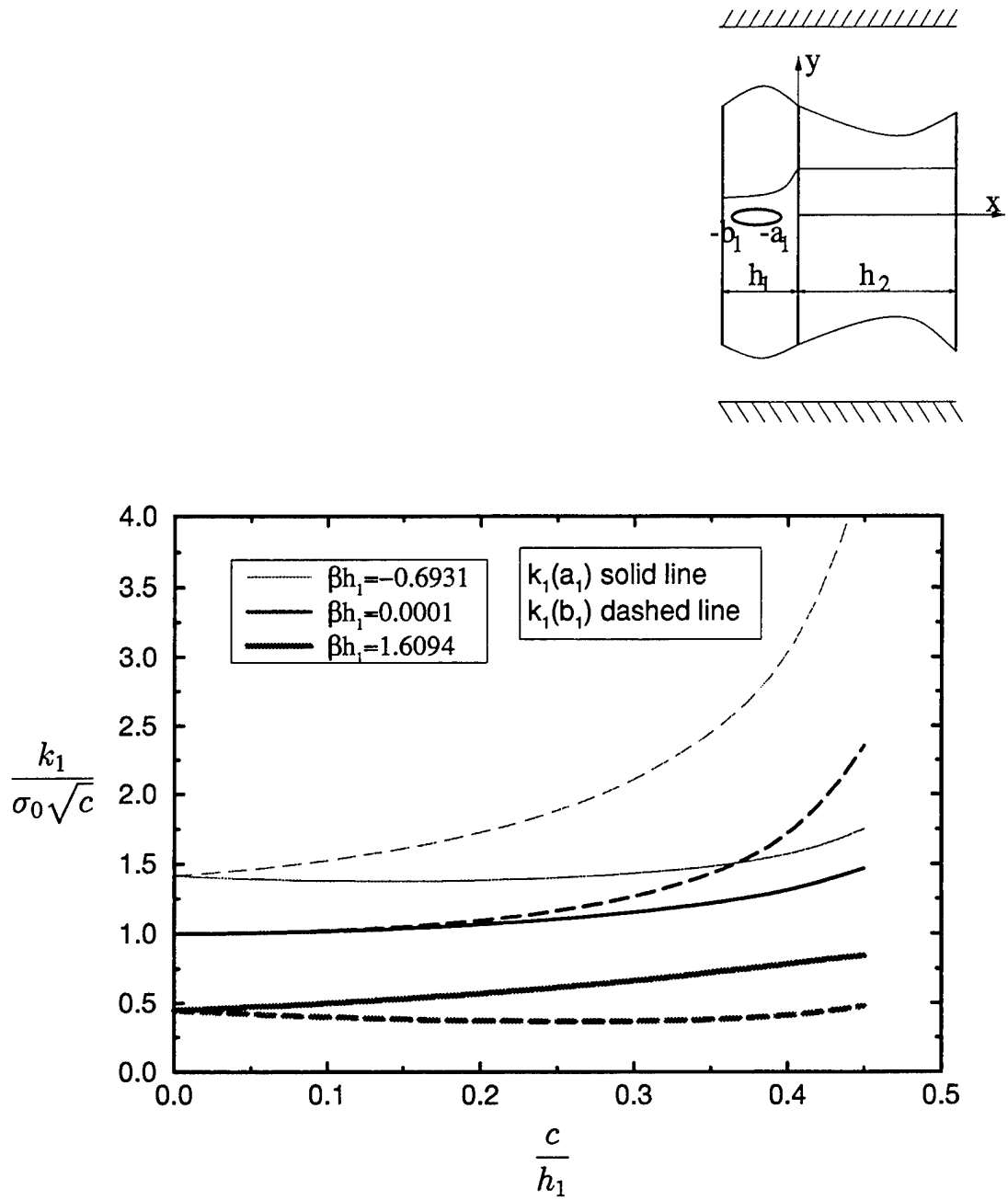


Figure 5.17 The effect of nonhomogeneity parameter on normalized stress intensity

factors for an internal crack symmetrically located in the nonhomogeneous

layer subjected to fixed grip loading. $c = \frac{(b_1 - a_1)}{2}$, $\frac{(b_1 + a_1)}{2} = \frac{h_1}{2}$,

$\frac{h_2}{h_1} = 1.0$, $\sigma_0 = \frac{8\mu_0}{(1 + \kappa)}\epsilon_0$.

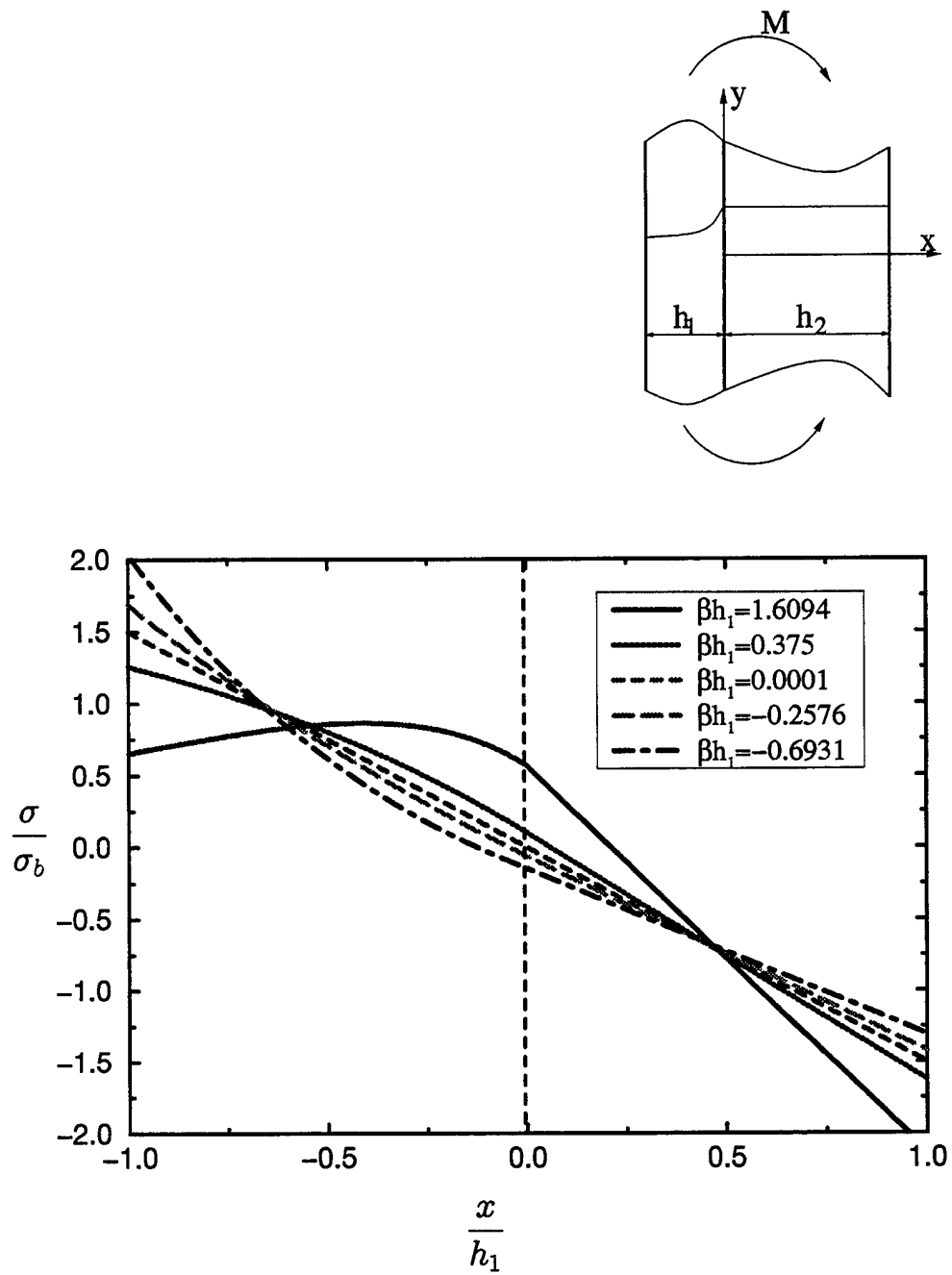


Figure 5.18 Stress distribution for an uncracked specimen under reversed bending.

$$\frac{h_2}{h_1} = 1.0, \sigma_b = \frac{M}{h_1^2}.$$

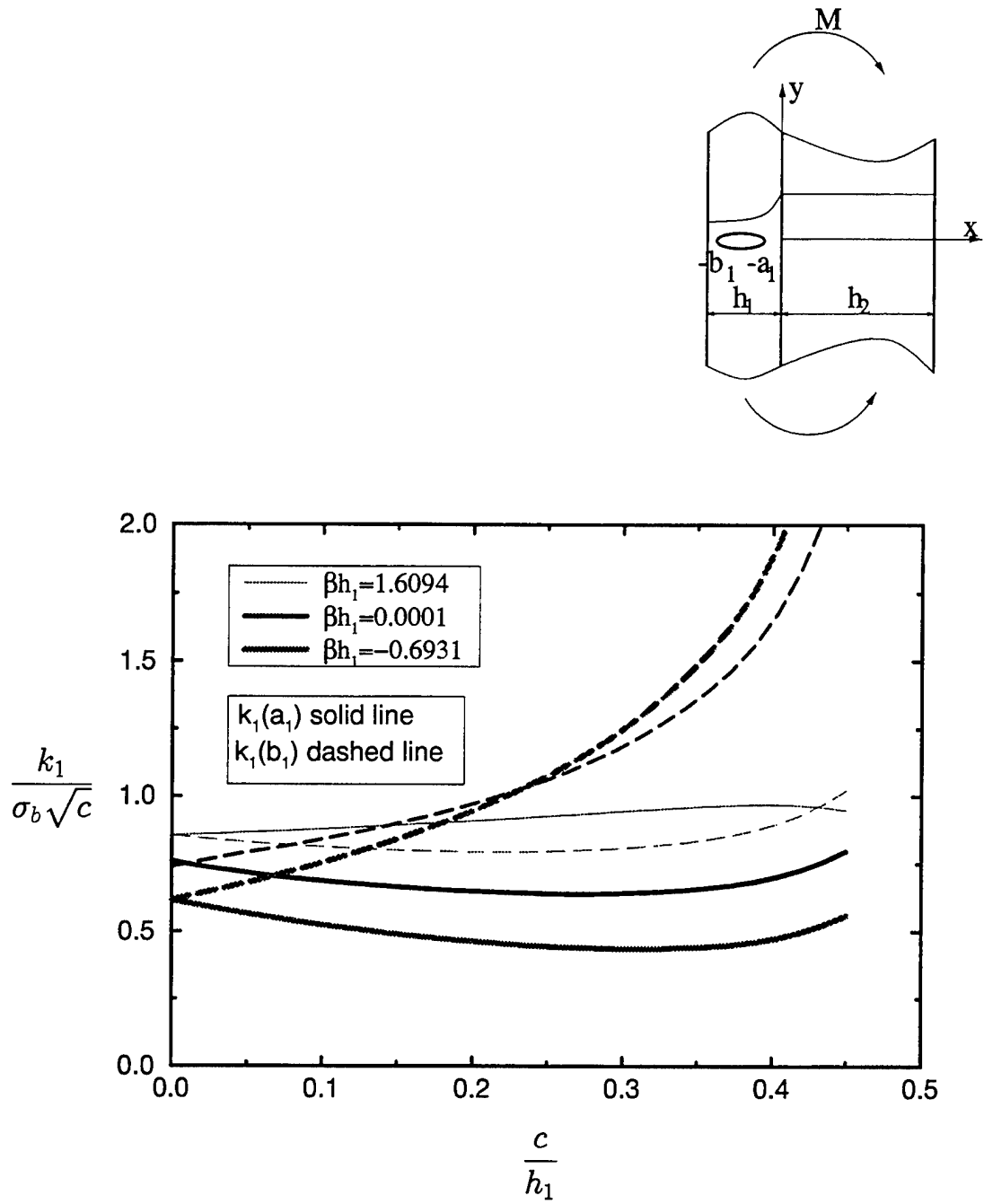


Figure 5.19 The effect of nonhomogeneity parameter on normalized stress intensity

factors for an internal crack symmetrically located in the nonhomogeneous

layer subjected to pure bending. $c = \frac{(b_1 - a_1)}{2}$, $\frac{(b_1 + a_1)}{2} = \frac{h_1}{2}$,

$\frac{h_2}{h_1} = 1.0$, $\sigma_b = \frac{M}{h_1^2}$.

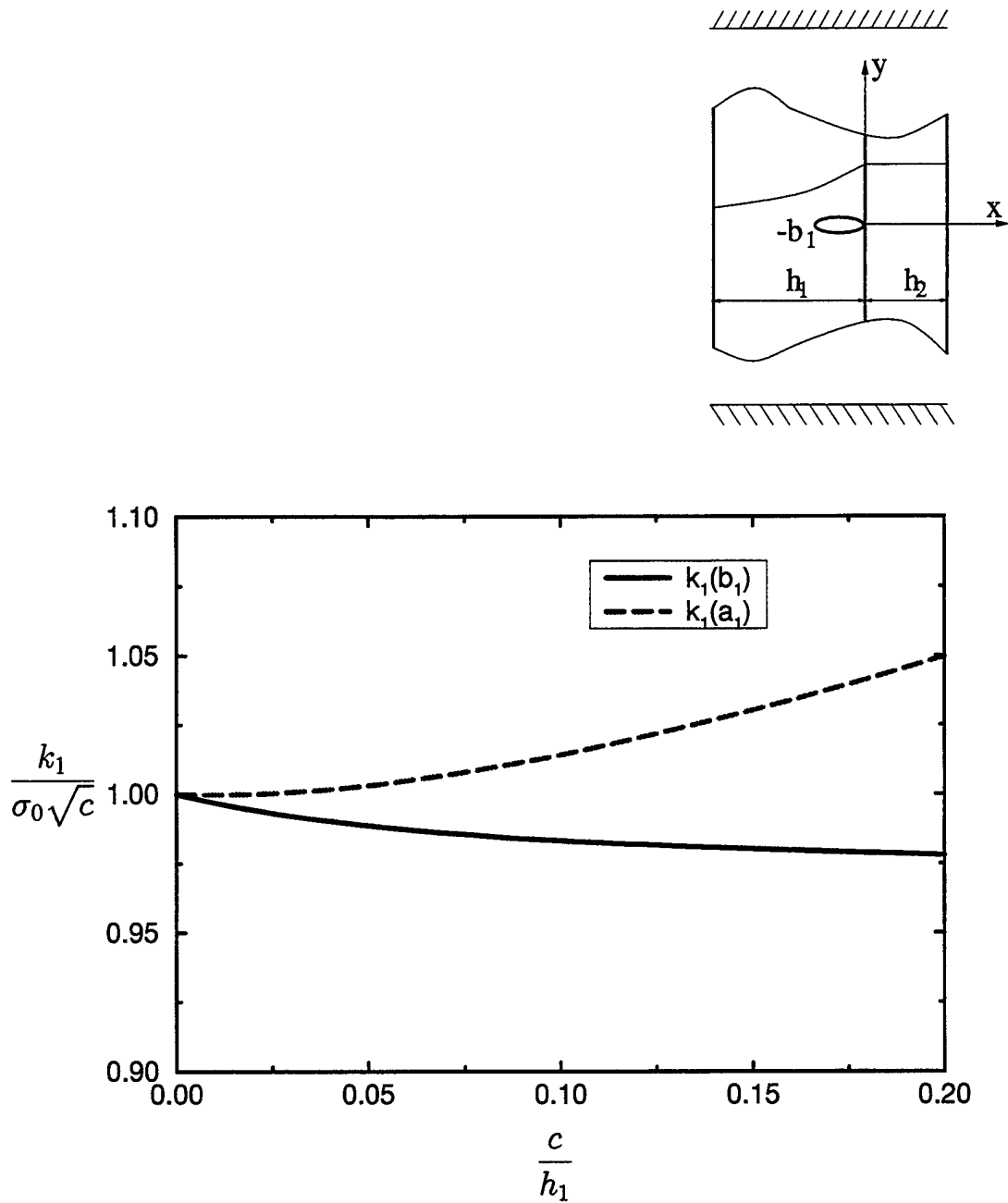


Figure 5.20 Normalized stress intensity factors for an internal crack located in the nonhomogeneous layer touching the interface and subjected to fixed grip loading. $c = \frac{(b_1 - a_1)}{2}$, $a_1 = 0.0$, $\frac{h_2}{h_1} = 0.2$, $\sigma_0 = \frac{8\mu_0}{(1 + \kappa)}\epsilon_0$, $\beta h_1 = 0.375$.

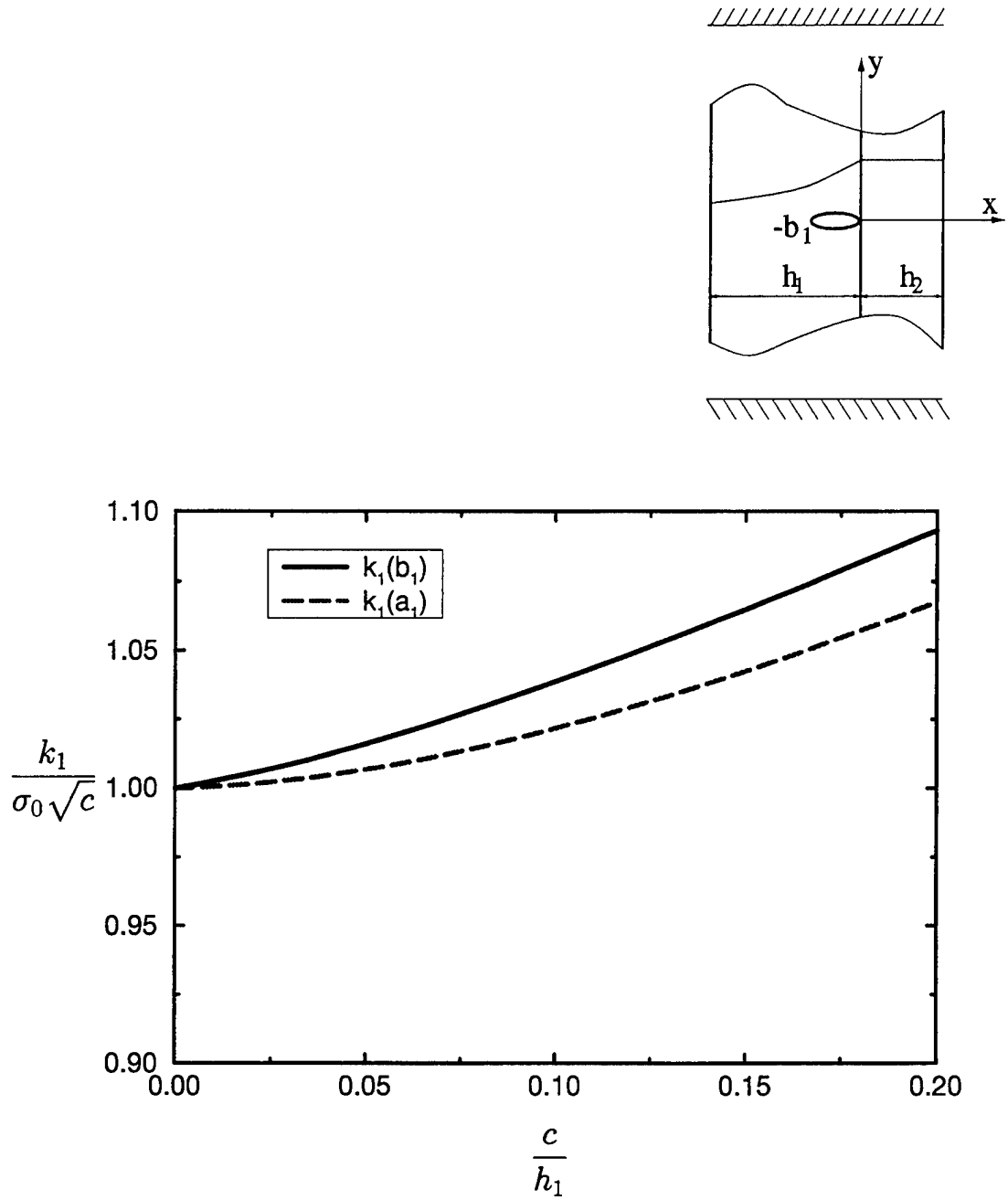


Figure 5.21 Normalized stress intensity factors for an internal crack located in the nonhomogeneous layer touching the interface and subjected to fixed grip loading.

$$c = \frac{(b_1 - a_1)}{2}, a_1 = 0.0, \frac{h_2}{h_1} = 0.2, \sigma_0 = \frac{8\mu_0}{(1 + \kappa)}\epsilon_0, \beta h_1 = -0.2576.$$

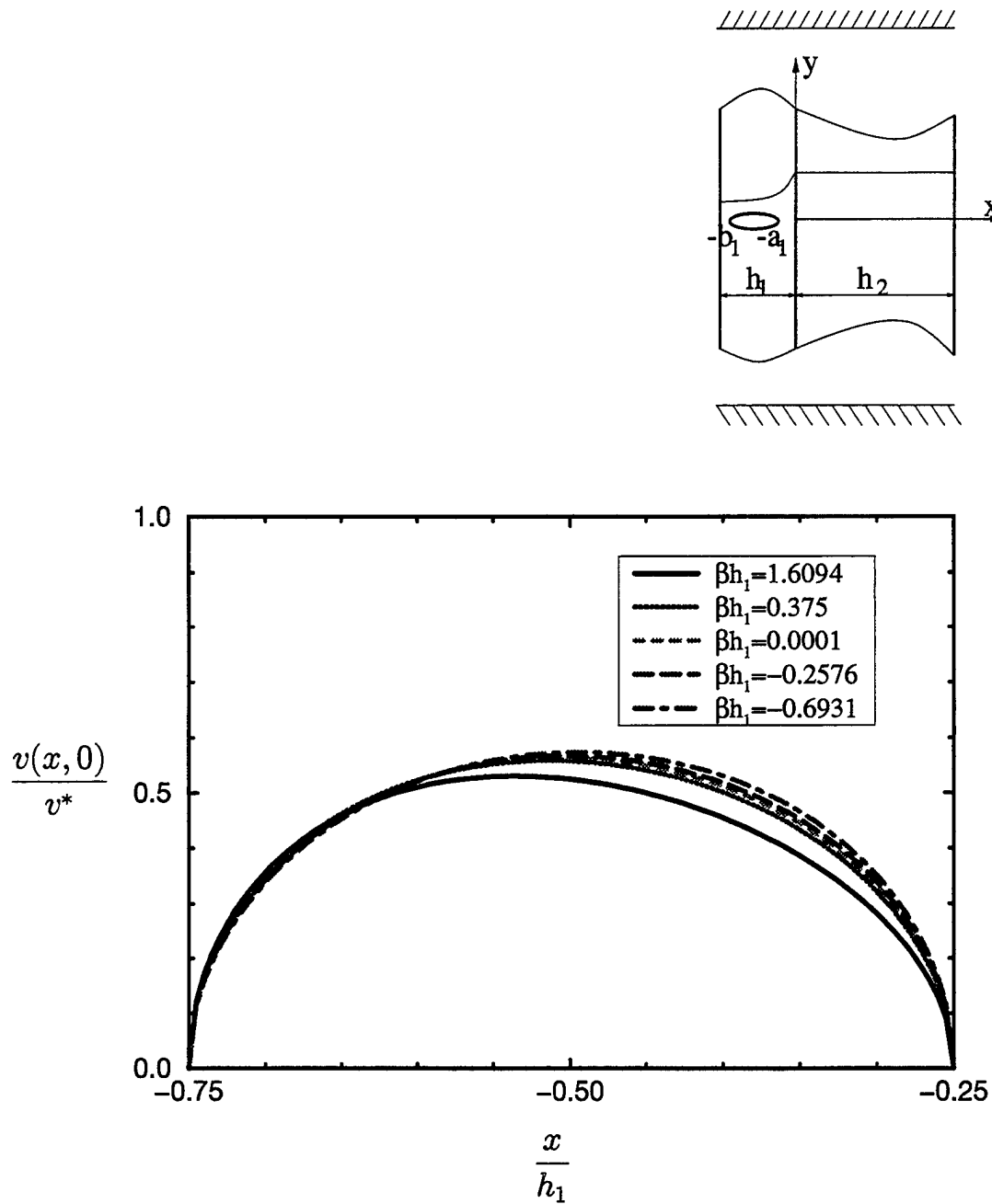


Figure 5.22 Effect of nonhomogeneity parameter on normalized crack opening displacement for an internal crack in the nonhomogeneous material subjected to fixed grip loading. $v^* = 2h_1\epsilon_0$, $\frac{h_2}{h_1} = 1.0$, $b_1 = 0.75h_1$, $a_1 = 0.25h_1$.

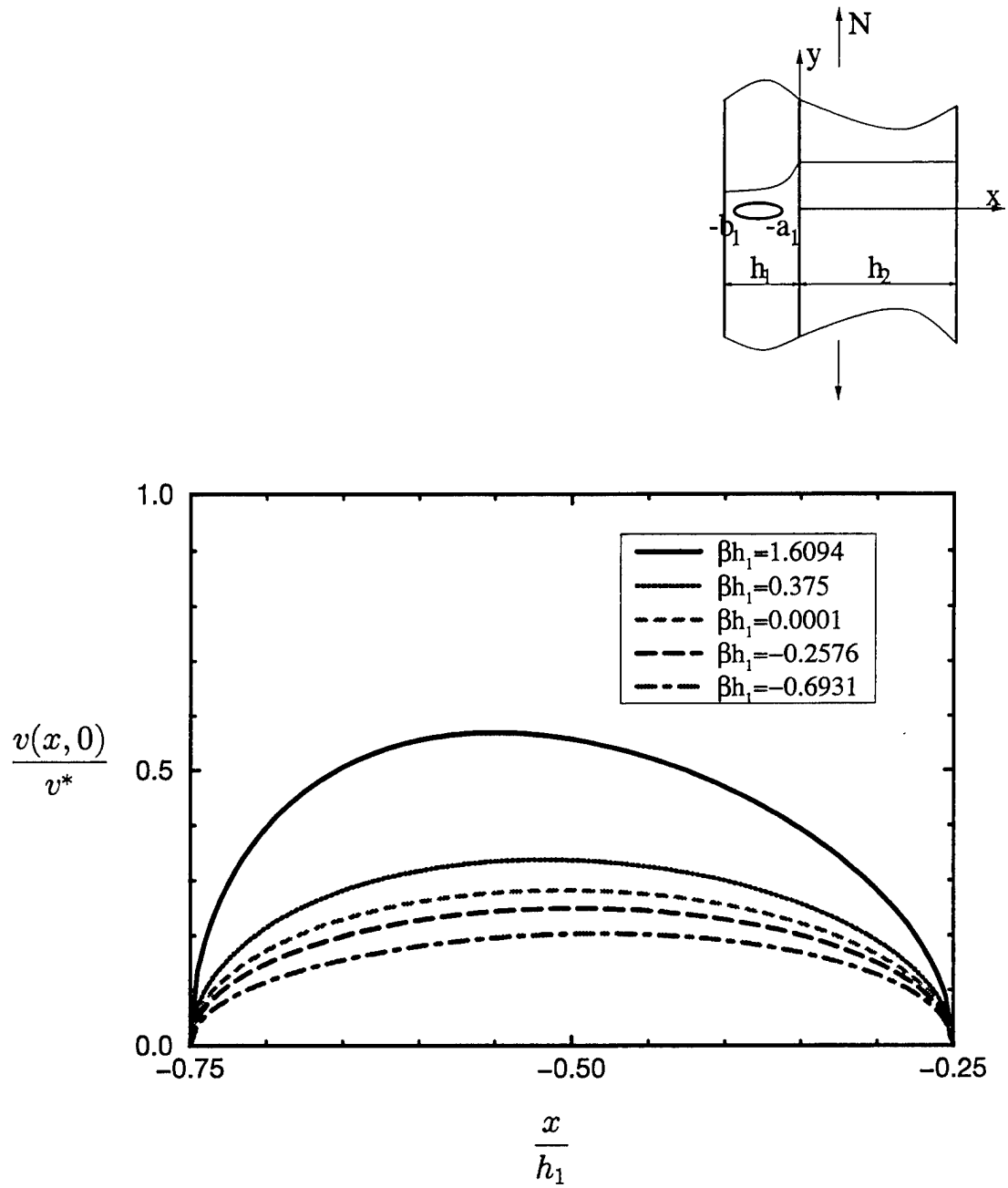


Figure 5.23 Effect of nonhomogeneity parameter on normalized crack opening

displacement for an internal crack in the nonhomogeneous material subjected to membrane loading. $v^* = 2N \frac{(1 + \kappa)}{8\mu_0}$, $\frac{h_2}{h_1} = 1.0$, $b_1 = 0.75h_1$, $a_1 = 0.25h_1$.

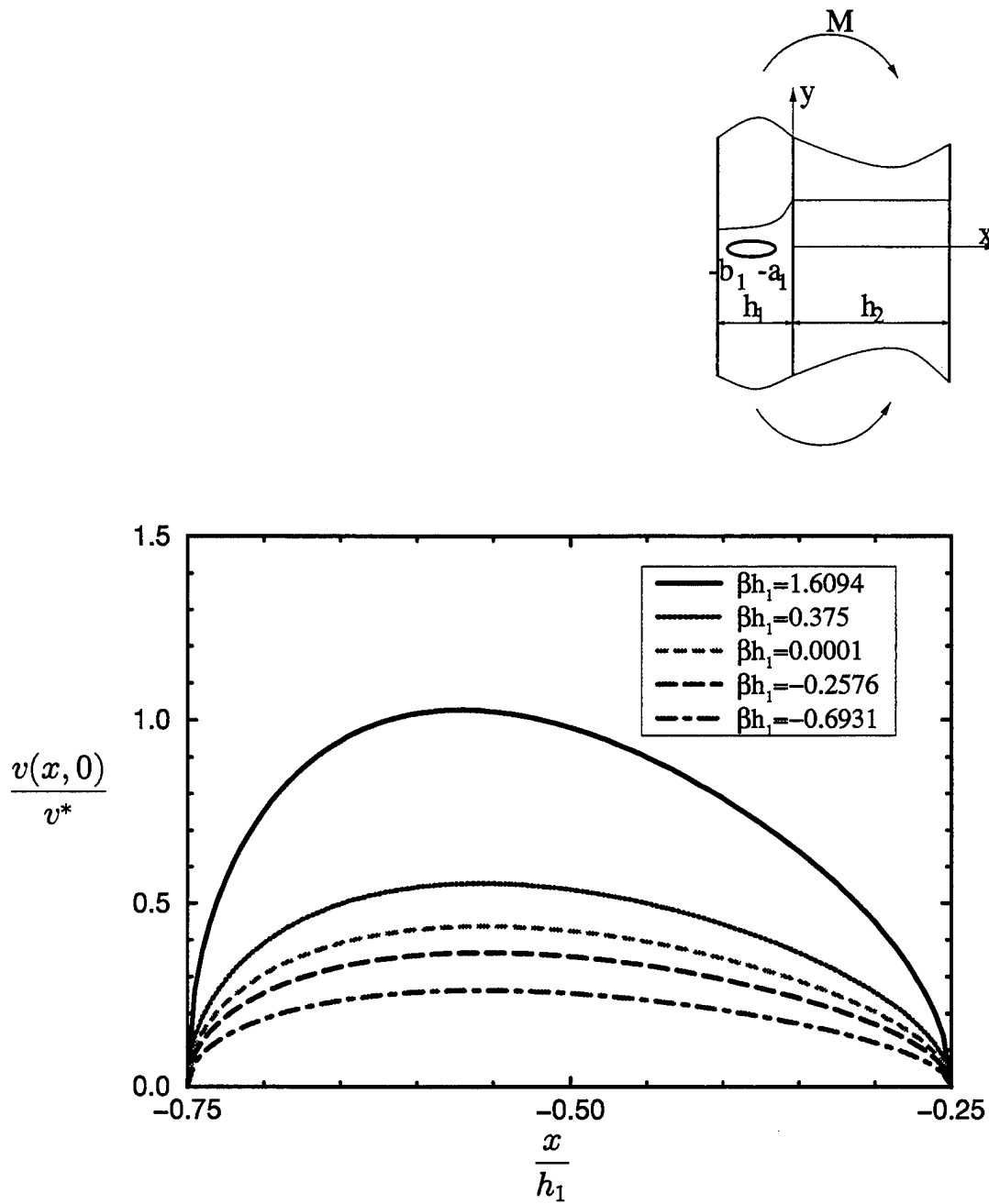


Figure 5.24 Effect of nonhomogeneity parameter on normalized crack opening displacement for an internal crack in the nonhomogeneous material subjected to pure bending. $v^* = 2 \frac{M}{h_1} \frac{(1 + \kappa)}{8\mu_0}$, $\frac{h_2}{h_1} = 1.0$, $b_1 = 0.75h_1$, $a_1 = 0.25h_1$.

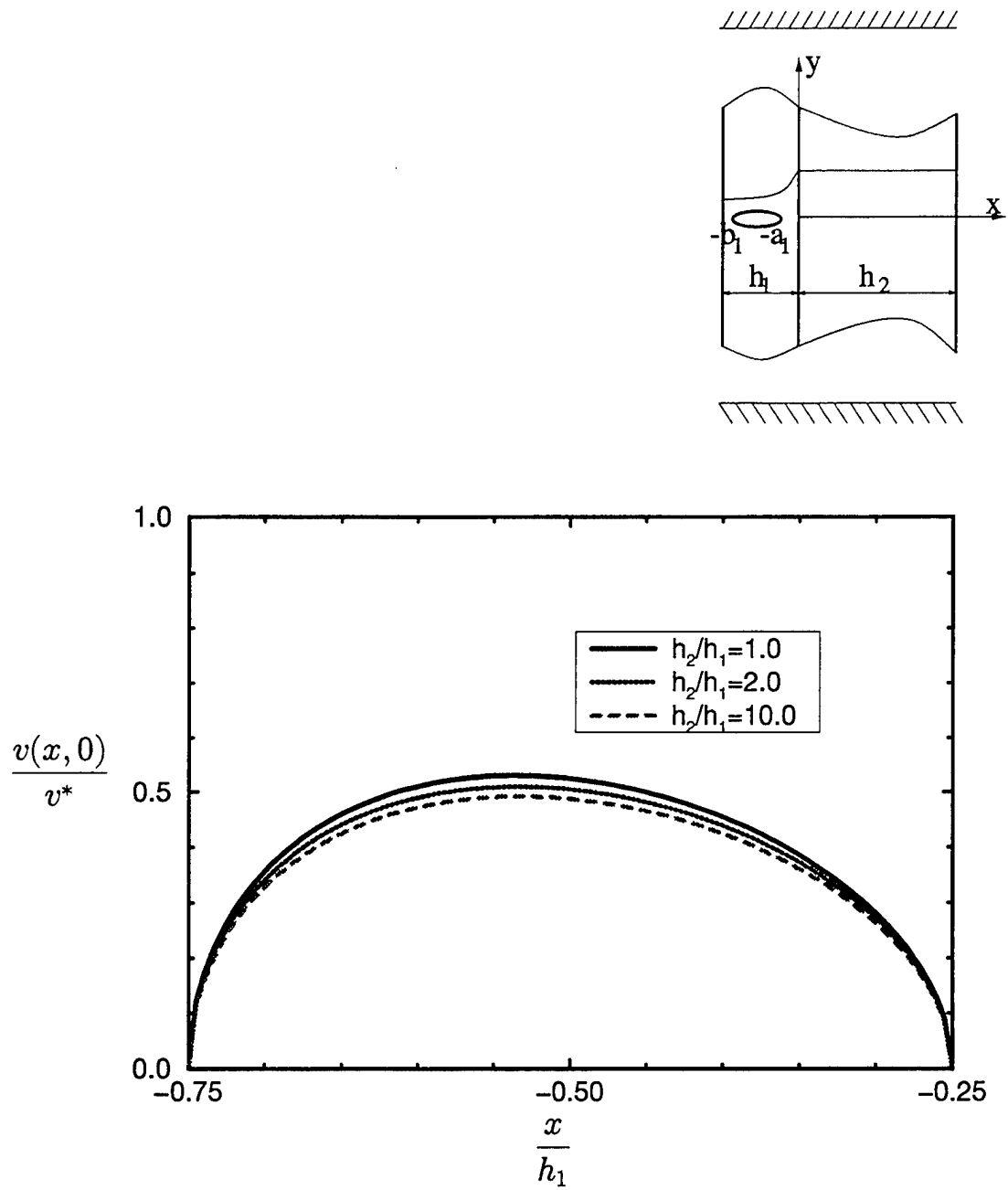


Figure 5.26 Effect of thickness ratio on normalized crack opening displacement for an internal crack in the nonhomogeneous material subjected to fixed grip loading.

$$v^* = 2h_1\epsilon_0, \beta h_1 = 1.6094, b_1 = 0.75h_1, a_1 = 0.25h_1.$$

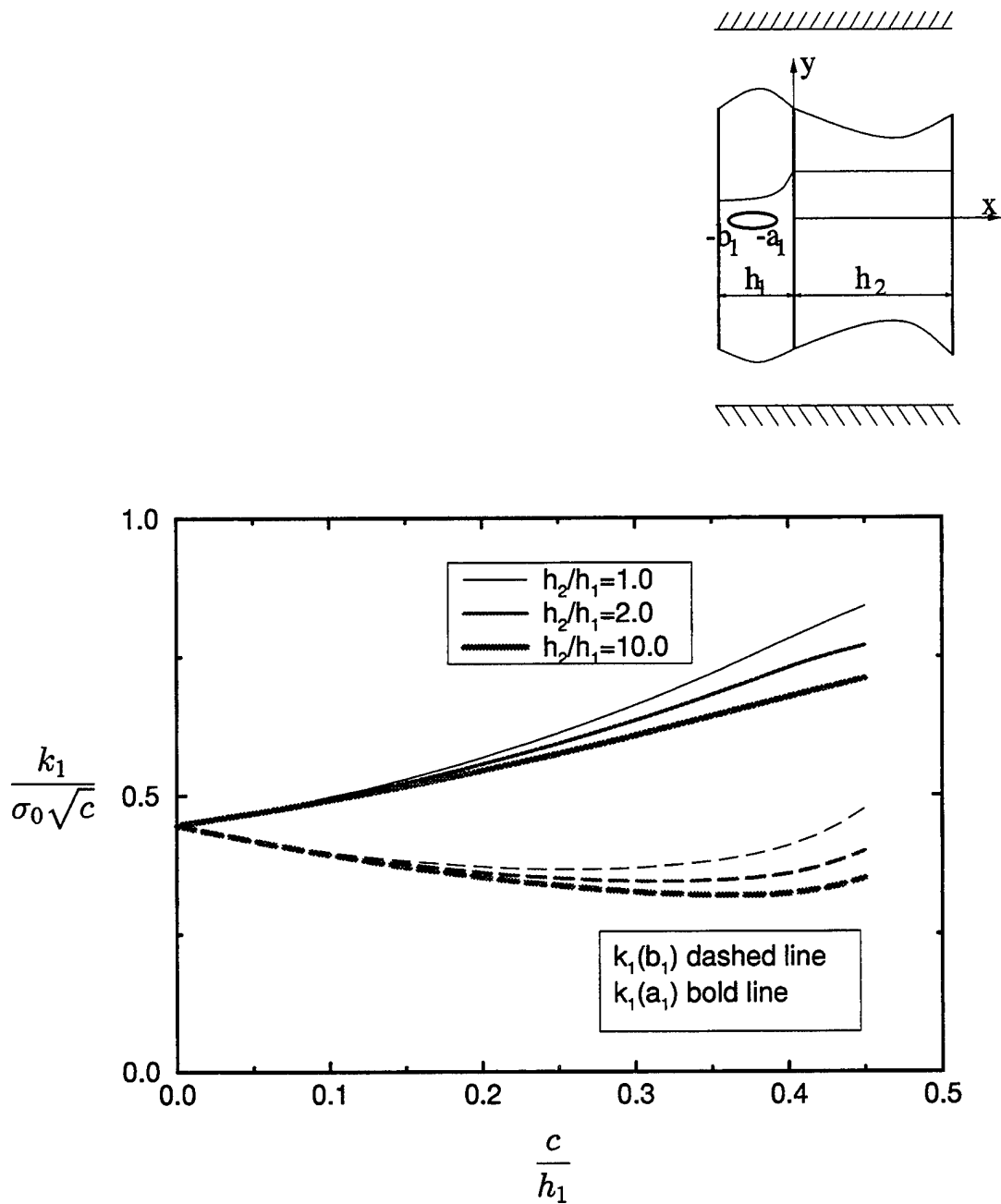


Figure 5.25 The effect of thickness ratio on normalized stress intensity factors for an internal crack located symmetrically in the nonhomogeneous layer subjected to fixed grip loading. $c = \frac{(b_1 - a_1)}{2}$, $\frac{(b_1 + a_1)}{2} = \frac{h_1}{2}$, $\beta h_1 = 1.6094$, $\sigma_0 = \frac{8\mu_0}{(1 + \kappa)} \epsilon_0$.

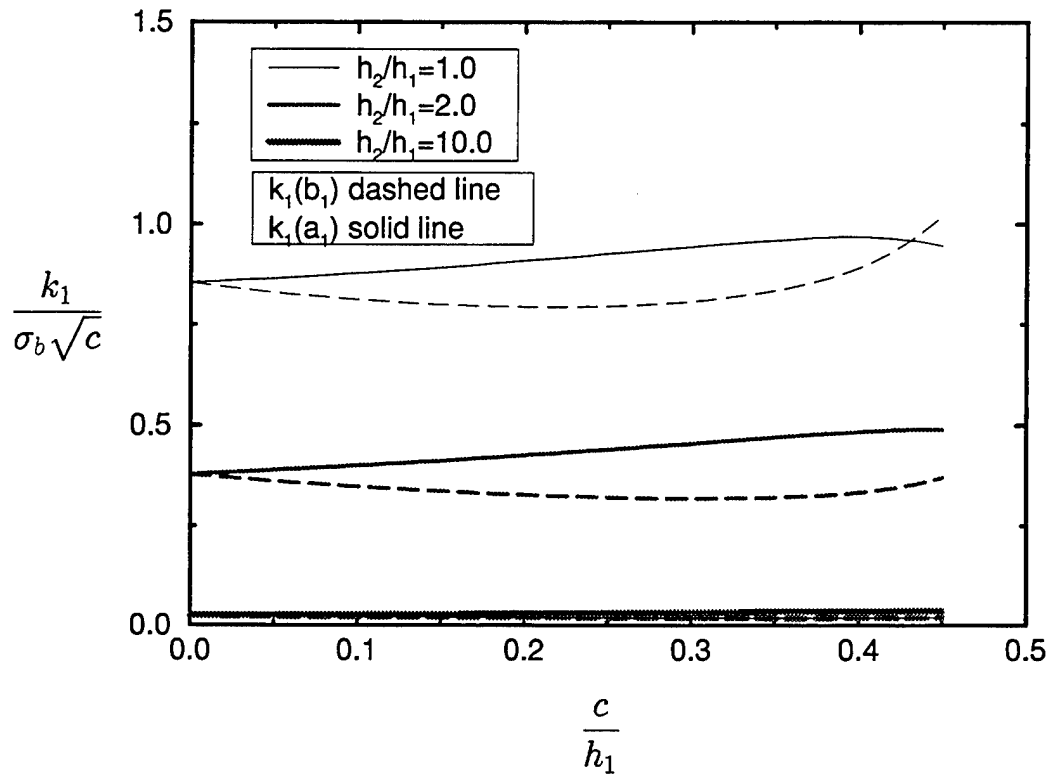
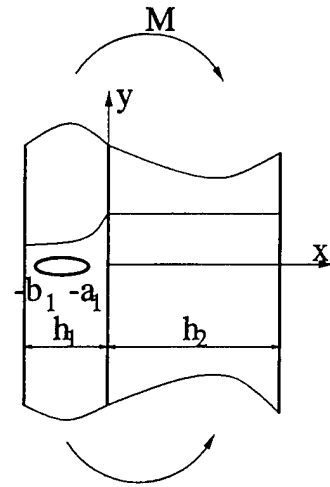


Figure 5.27 The effect of thickness ratio on normalized stress intensity factors for an internal crack located symmetrically in the nonhomogeneous layer subjected to pure bending. $c = \frac{(b_1 - a_1)}{2}$, $\frac{(b_1 + a_1)}{2} = \frac{h_1}{2}$, $\beta h_1 = 1.6094$, $\sigma_b = \frac{M}{h_1^2}$.

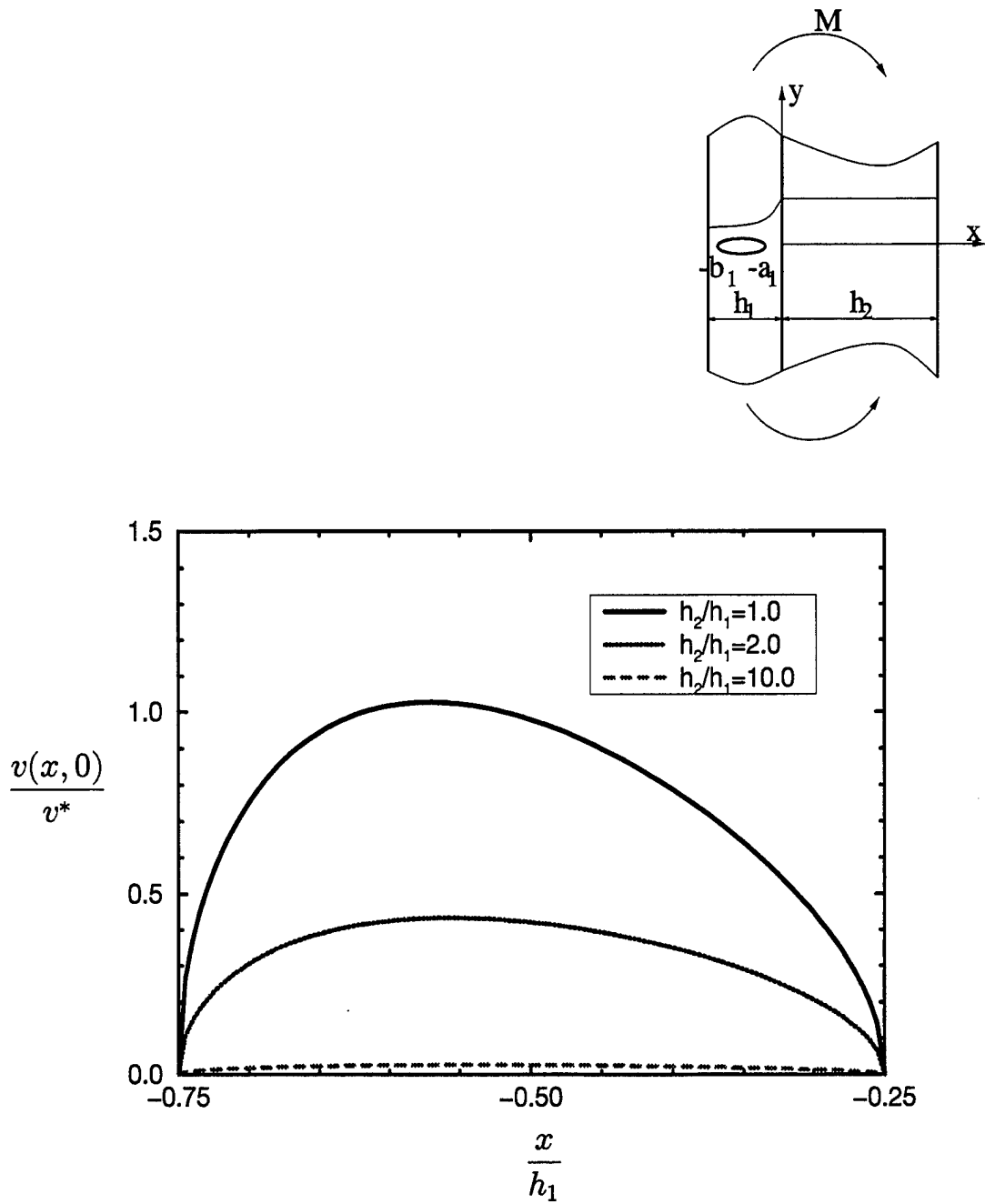


Figure 5.28 Effect of thickness ratio on normalized crack opening displacement for an internal crack in the nonhomogeneous material subjected to pure bending.

$$v^* = 2 \frac{M}{h_1} \frac{(1 + \kappa)}{8\mu_0}, \quad \beta h_1 = 1.6094, \quad b_1 = 0.75h_1, \quad a_1 = 0.25h_1.$$

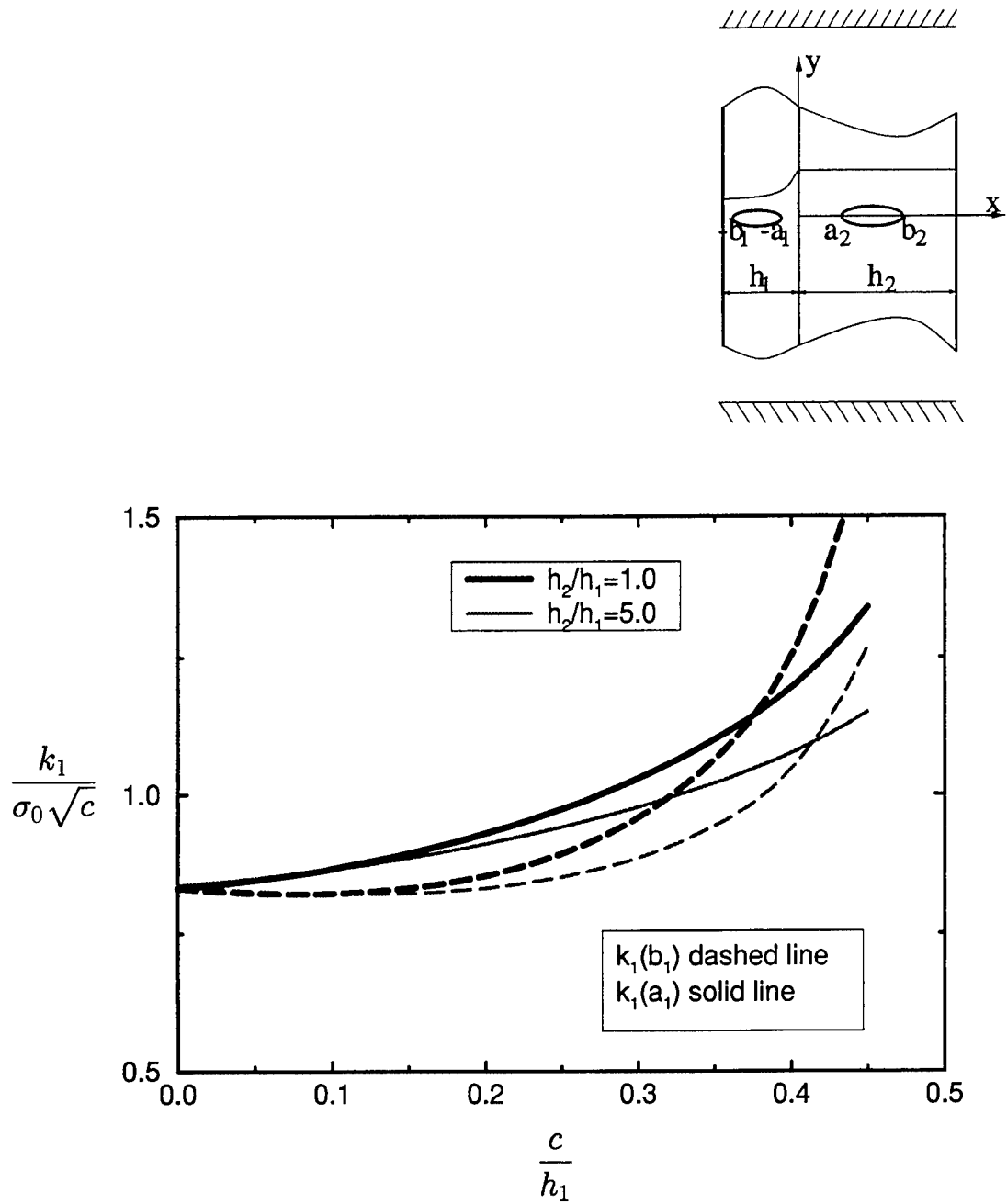


Figure 5.29 The effect of thickness ratio on normalized stress intensity factors for an internal crack symmetrically located in the nonhomogeneous layer subjected to fixed grip loading. $c = \frac{(b_1 - a_1)}{2}$, $\frac{(b_1 + a_1)}{2} = \frac{h_1}{2}$, $\beta h_1 = 0.375$, $\sigma_0 = \frac{8\mu_0}{(1 + \kappa)} \epsilon_0$, $a_2 = 0.4h_1$, $b_2 = 0.6h_1$.

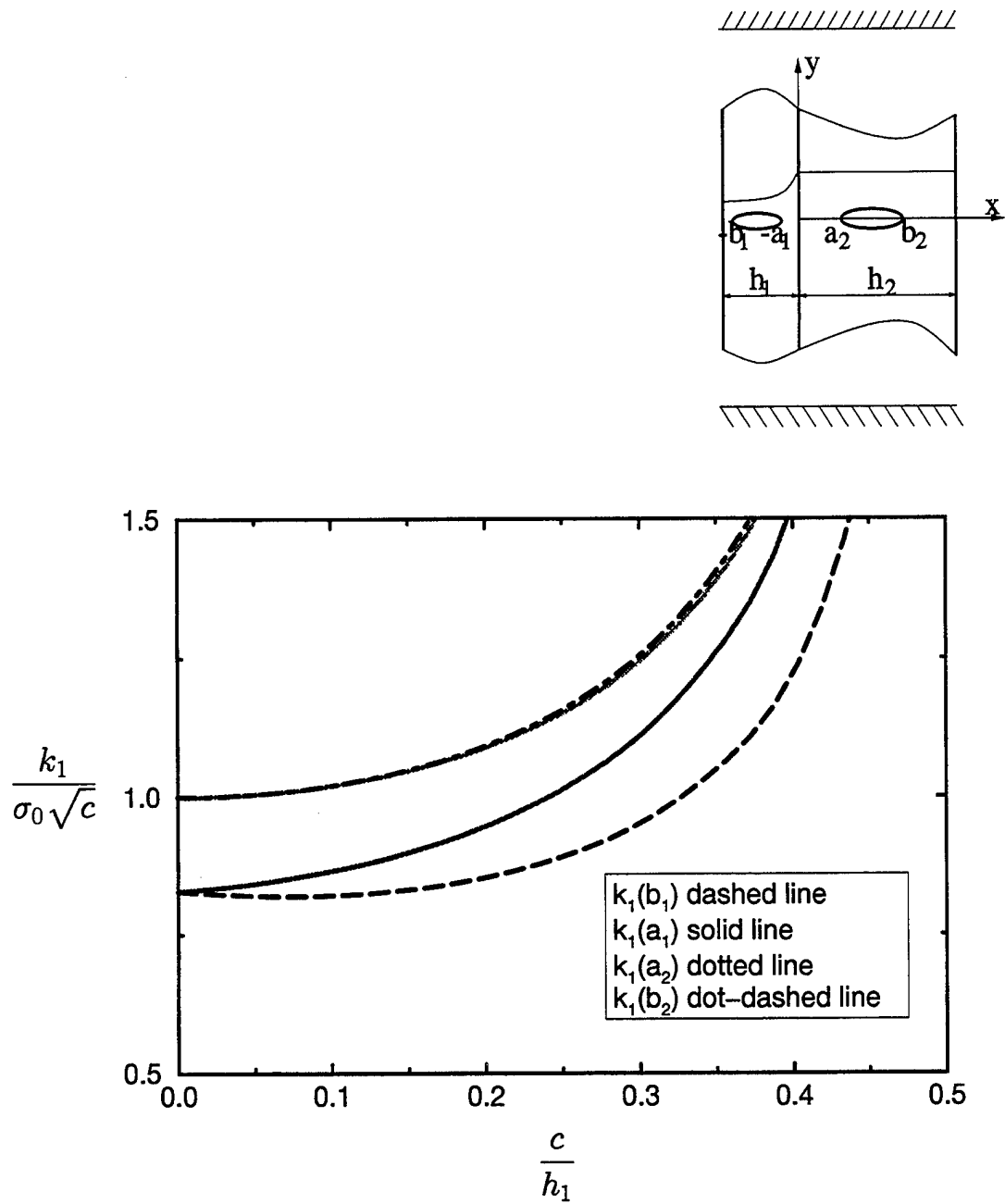


Figure 5.30 Comparative normalized stress intensity factors for two internal cracks symmetrically located in the nonhomogeneous and homogeneous layers

respectively subjected to fixed grip loading, c = crack length,

$$\sigma_0 = \frac{8\mu_0}{(1+\kappa)}\epsilon_0, \frac{h_2}{h_1} = 1.0, \beta h_1 = 0.375, \frac{(b_1 + a_1)}{2} = \frac{h_1}{2}, \frac{(b_2 + a_2)}{2} = \frac{h_1}{2}.$$

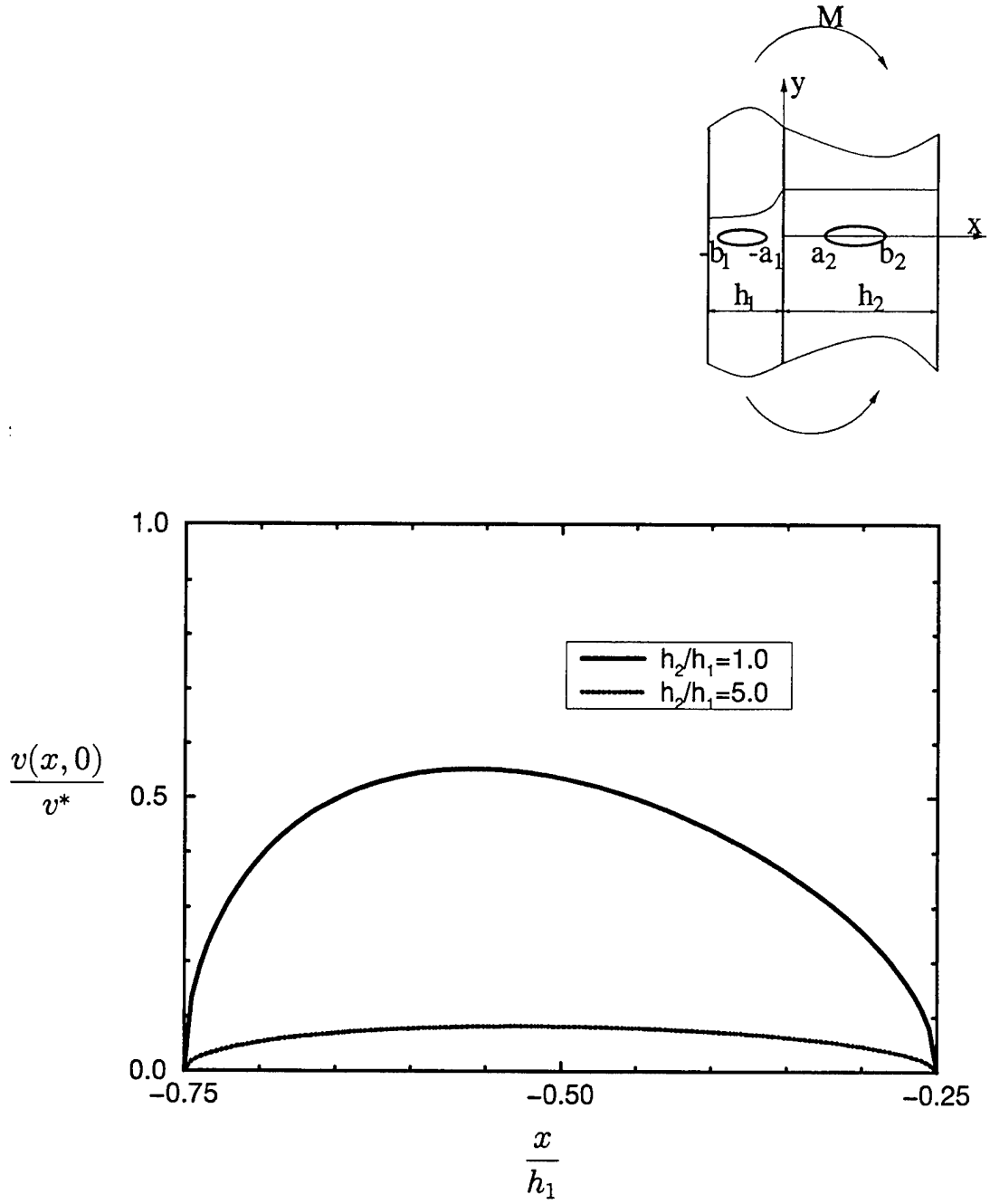


Figure 5.31 Effect of thickness ratio on normalized crack opening displacement for the internal crack in the nonhomogeneous material subjected to pure bending.

$$v^* = 2 \frac{M}{h_1} \frac{(1 + \kappa)}{8\mu_0}, \quad \beta h_1 = 0.375, \quad b_1 = 0.75h_1, \quad a_1 = 0.25h_1, \quad a_2 = 0.4h_1, \\ b_2 = 0.6h_1.$$

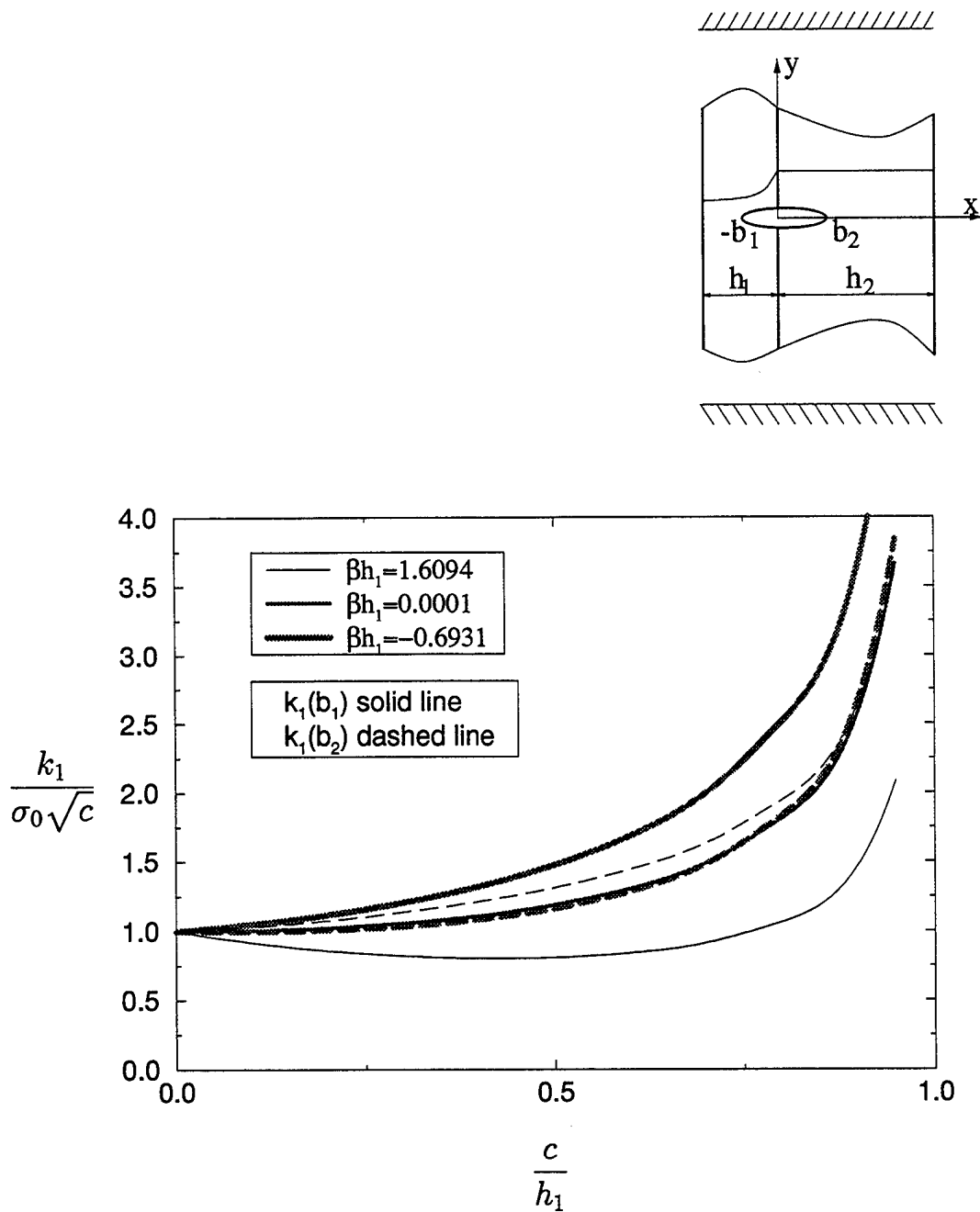


Figure 5.32 The effect of nonhomogeneity parameter on normalized stress intensity factors for a crack symmetrically located with respect to the interface and subjected to fixed grip loading. $\frac{h_2}{h_1} = 1.0$, $\sigma_0 = \frac{8\mu_0}{(1+\kappa)}\epsilon_0$.

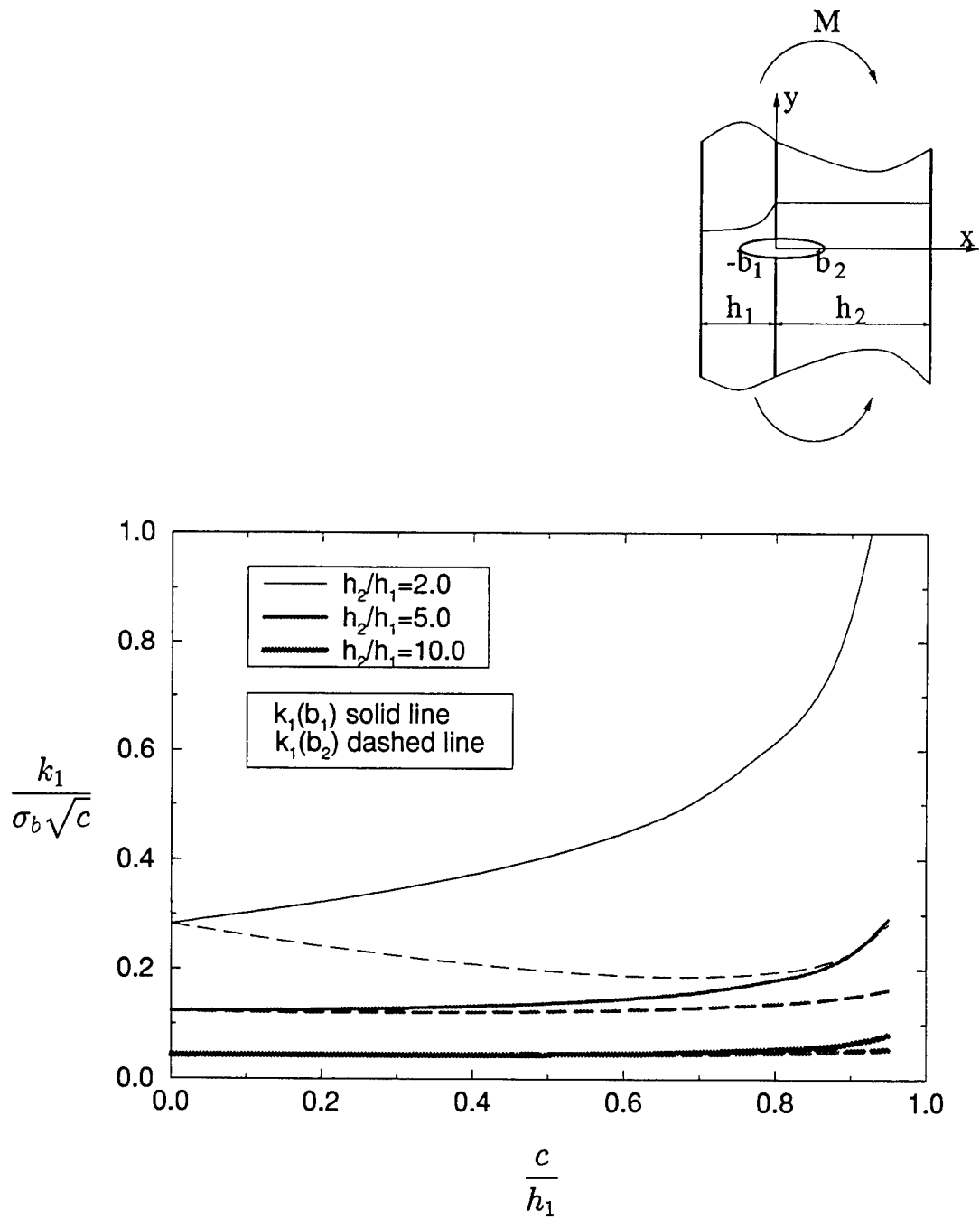


Figure 5.33 The effect of thickness ratio on normalized stress intensity factors for a crack symmetrically located with respect to the interface and subjected to pure bending.

$$\beta h_1 = 0.375, \sigma_b = \frac{M}{h_1^2}.$$

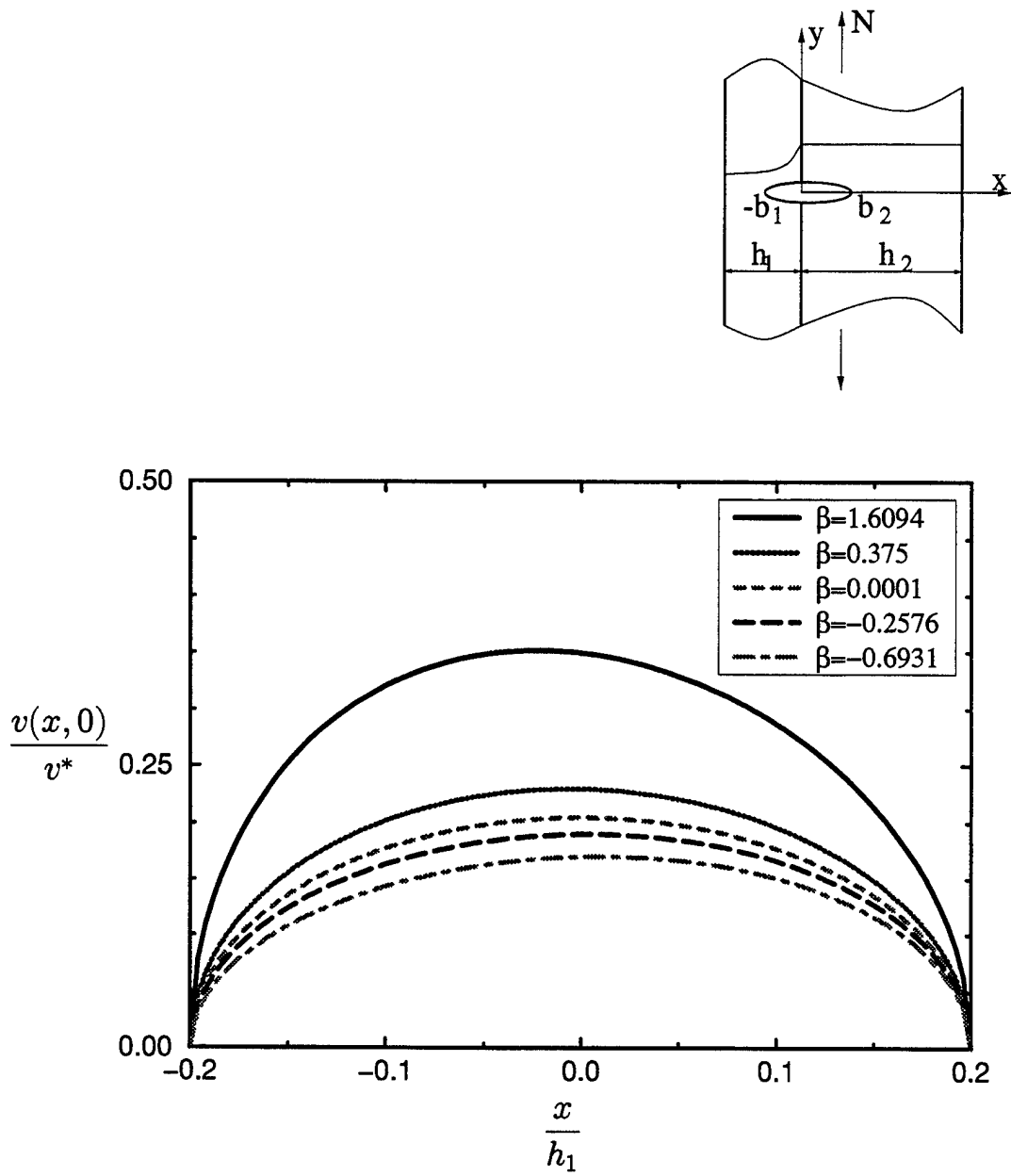


Figure 5.34 Effect of nonhomogeneity parameter on normalized crack opening displacement for a crack crossing the interface and subjected to membrane loading. $v^* = 2N \frac{(1 + \kappa)}{8\mu_0}$, $\frac{h_2}{h_1} = 1.0$, $b_1 = 0.2h_1$, $b_2 = 0.2h_1$.

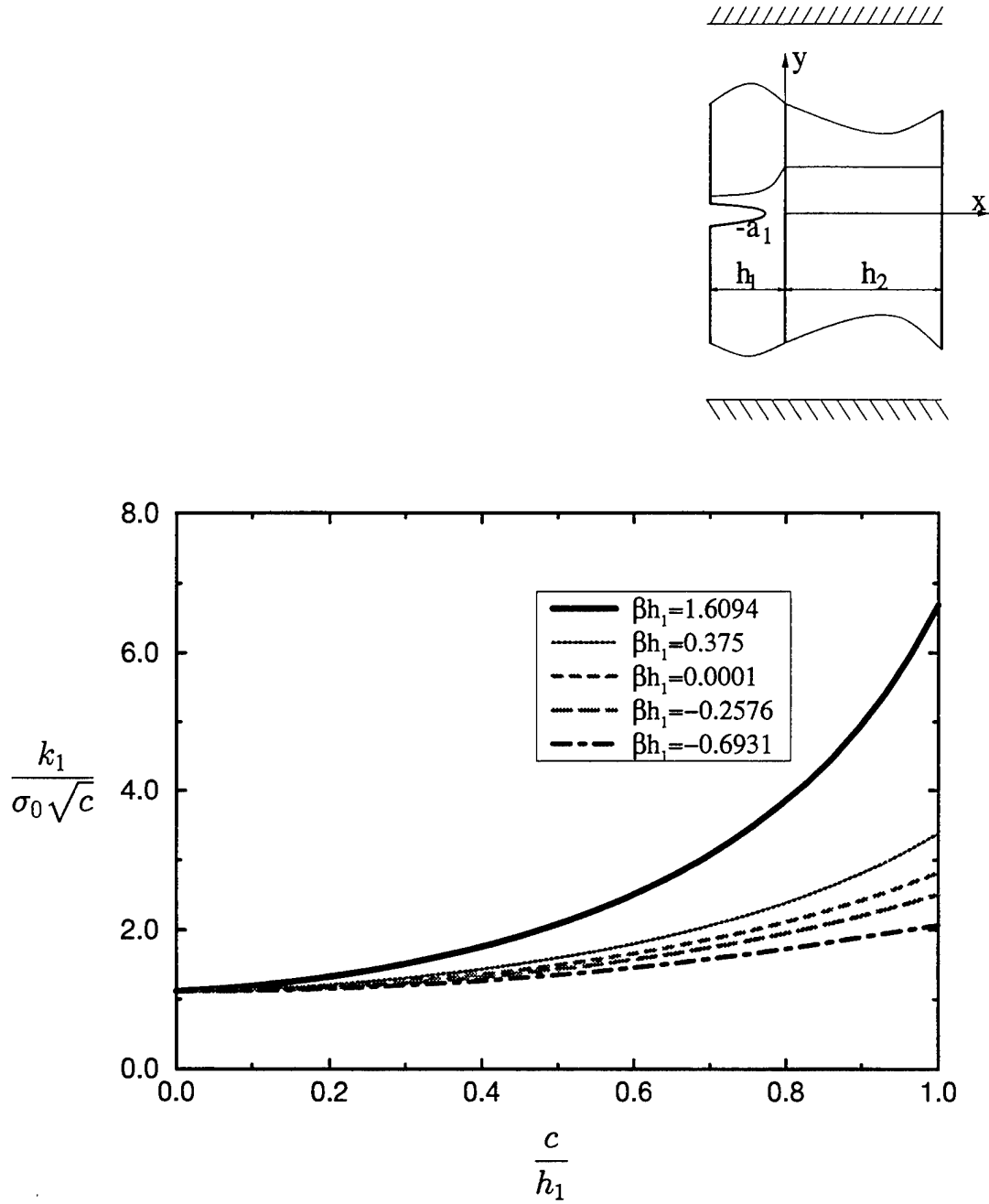


Figure 5.35 The effect of nonhomogeneity parameter on normalized stress intensity

factor for an edge crack located in the nonhomogeneous layer subjected to fixed

grip loading. $c = (b_1 - a_1)$, $b_1 = h_1$, $\frac{h_2}{h_1} = 1.0$, $\sigma_0 = \frac{8\mu_1}{(1 + \kappa)}\epsilon_0$.

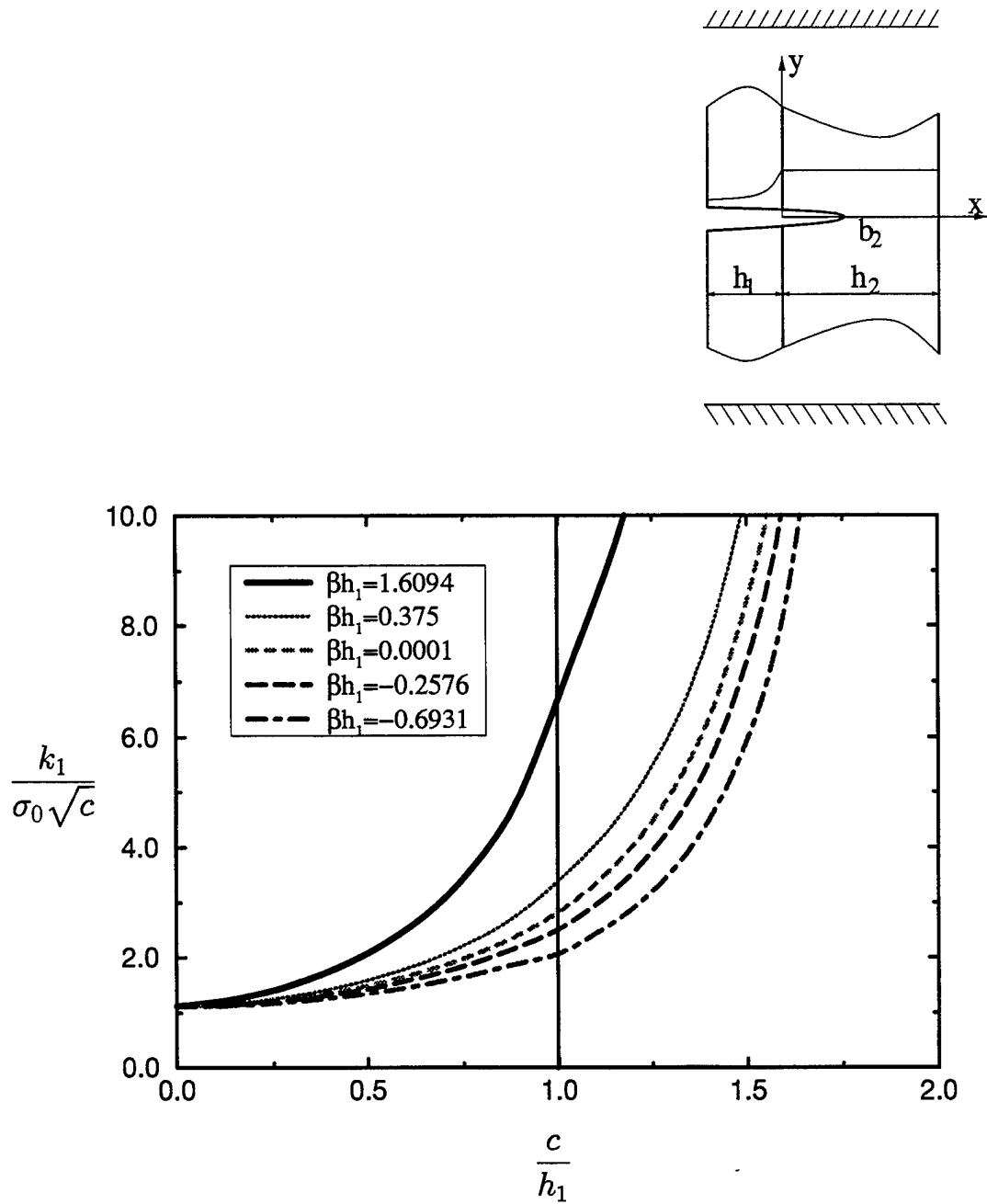


Figure 5.36 The effect of nonhomogeneity parameter on normalized stress intensity factor for an edge crack crossing the interface subjected to fixed grip loading.
 c = crack length, $b_1 = h_1$, $\frac{h_2}{h_1} = 1.0$, $\sigma_0 = \frac{8\mu_1}{(1+\kappa)}\epsilon_0$.

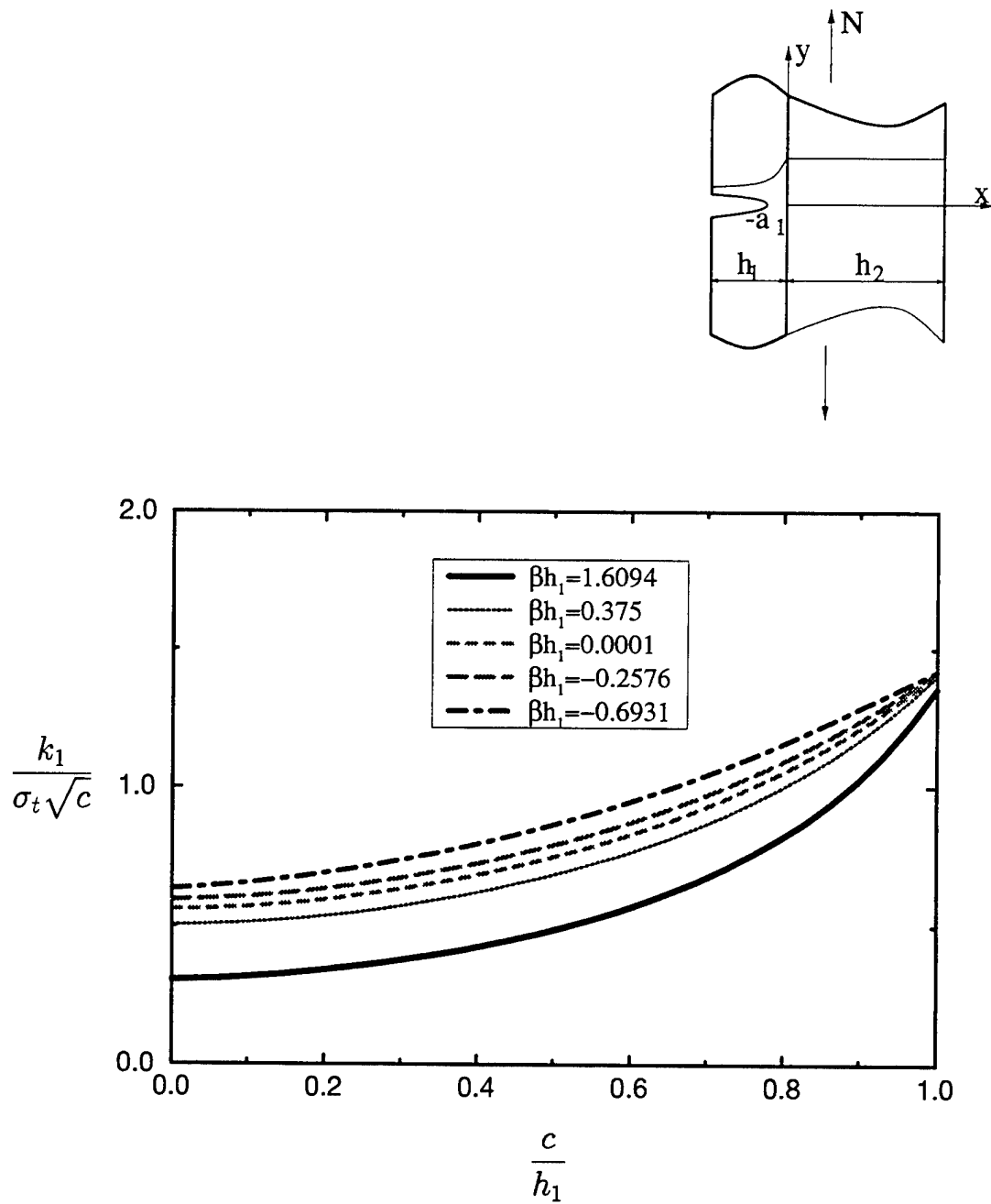


Figure 5.37 The effect of nonhomogeneity parameter on normalized stress intensity factor for an edge crack located in the nonhomogeneous layer subjected to membrane loading. $c = (b_1 - a_1)$, $b_1 = h_1$, $\frac{h_2}{h_1} = 1.0$, $\sigma_t = \frac{N}{h_1}$.

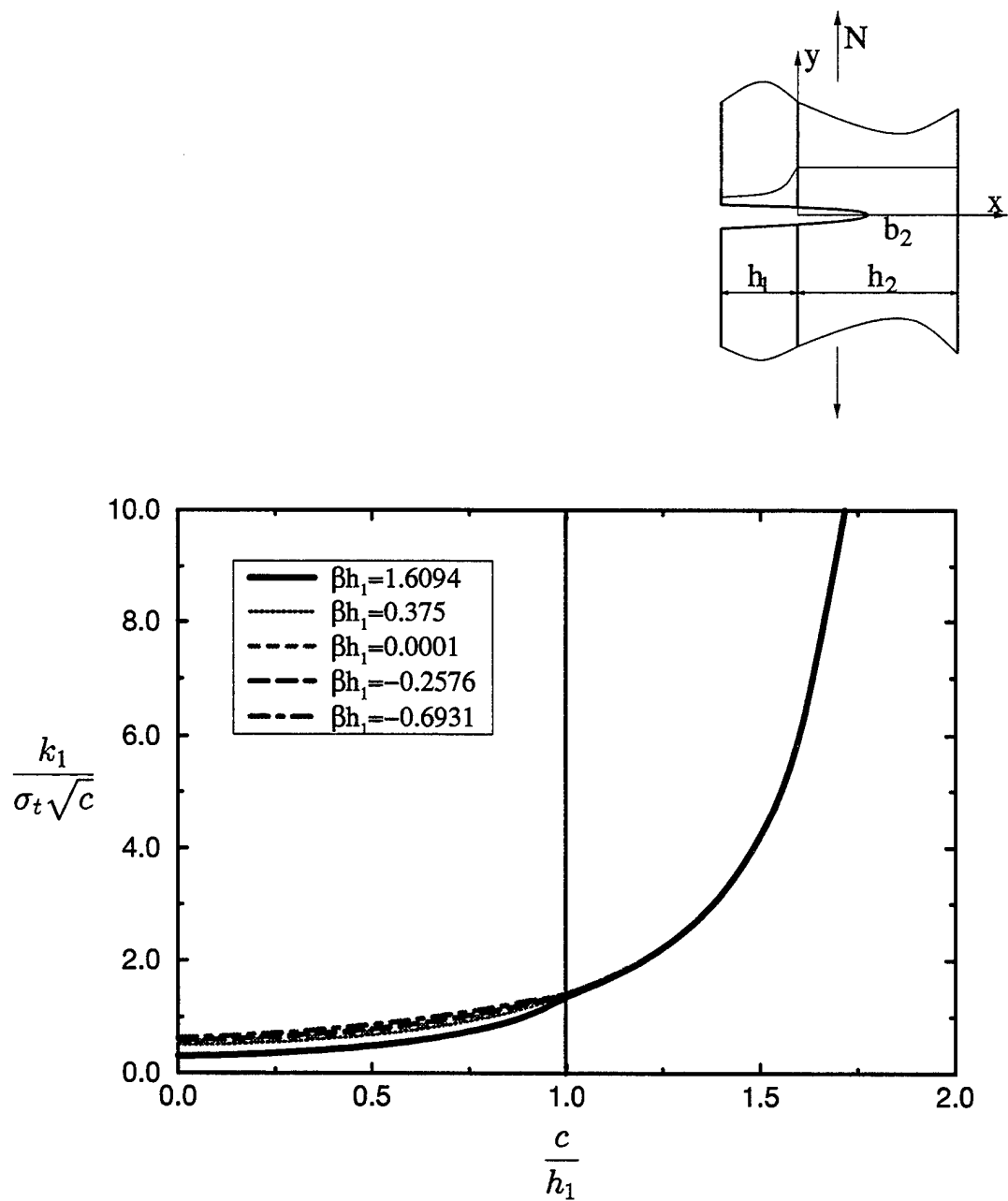


Figure 5.38 The effect of nonhomogeneity parameter on normalized stress intensity factor for an edge crack crossing the interface subjected to membrane loading.
 c = crack length, $b_1 = h_1$, $\frac{h_2}{h_1} = 1.0$, $\sigma_t = \frac{N}{h_1}$.

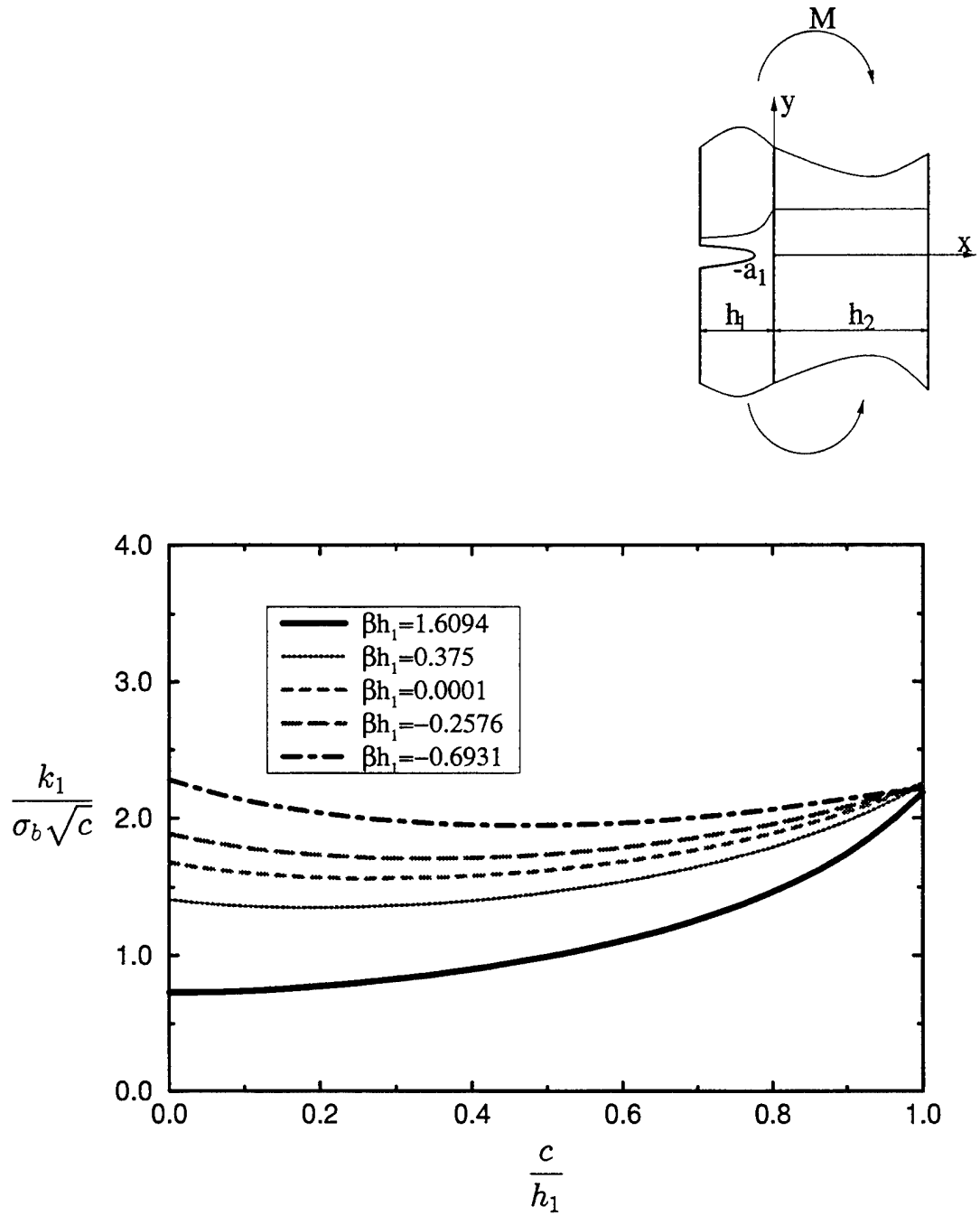


Figure 5.39 The effect of nonhomogeneity parameter on normalized stress intensity factor for an edge crack located in the nonhomogeneous layer subjected to pure bending. $c = (b_1 - a_1)$, $b_1 = h_1$, $\frac{h_2}{h_1} = 1.0$, $\sigma_b = \frac{M}{h_1^2}$.

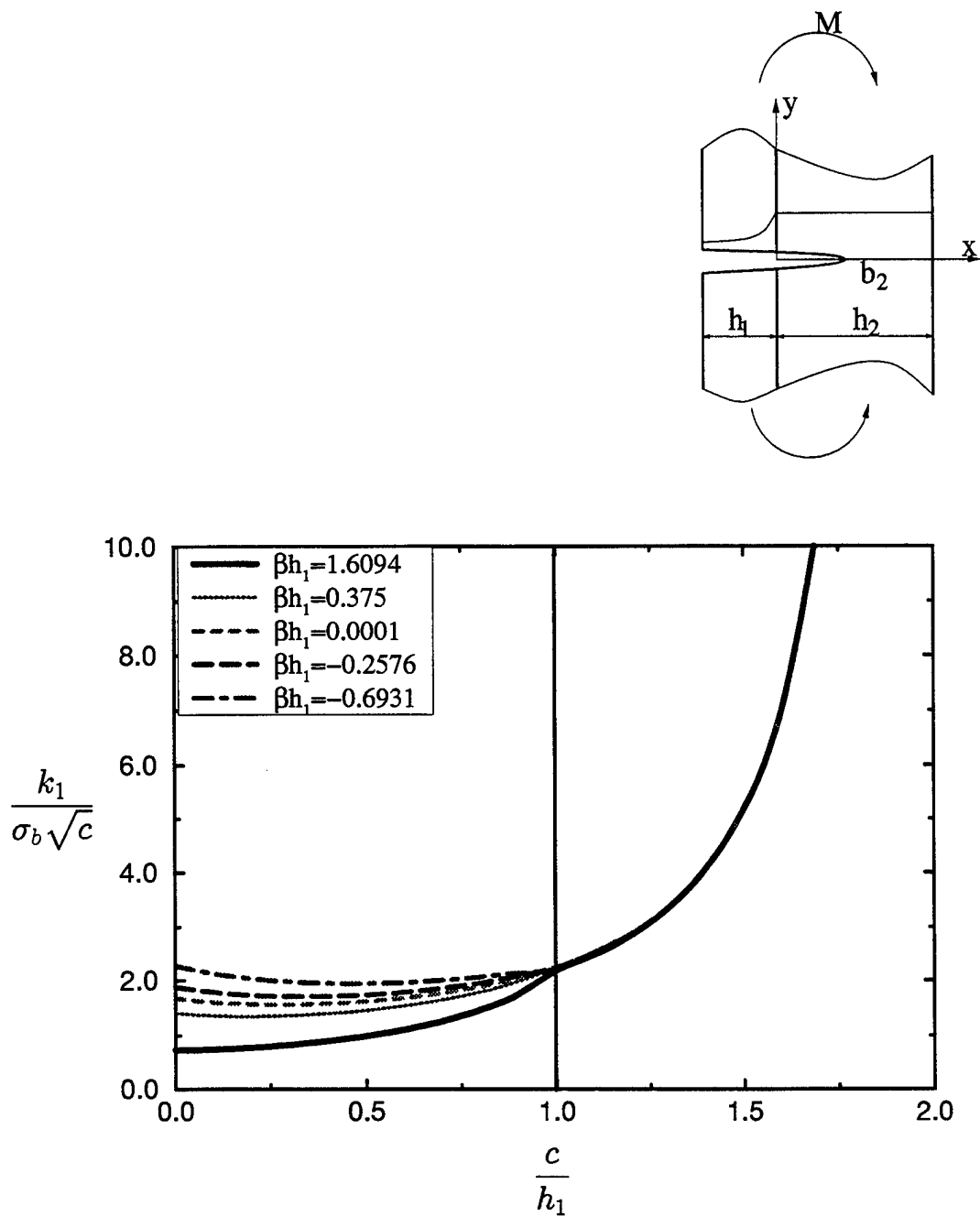


Figure 5.40 The effect of nonhomogeneity parameter on normalized stress intensity factor for an edge crack crossing the interface subjected to pure bending.

$$c = \text{crack length}, b_1 = h_1, \frac{h_2}{h_1} = 1.0, \sigma_b = \frac{M}{h_1^2}.$$

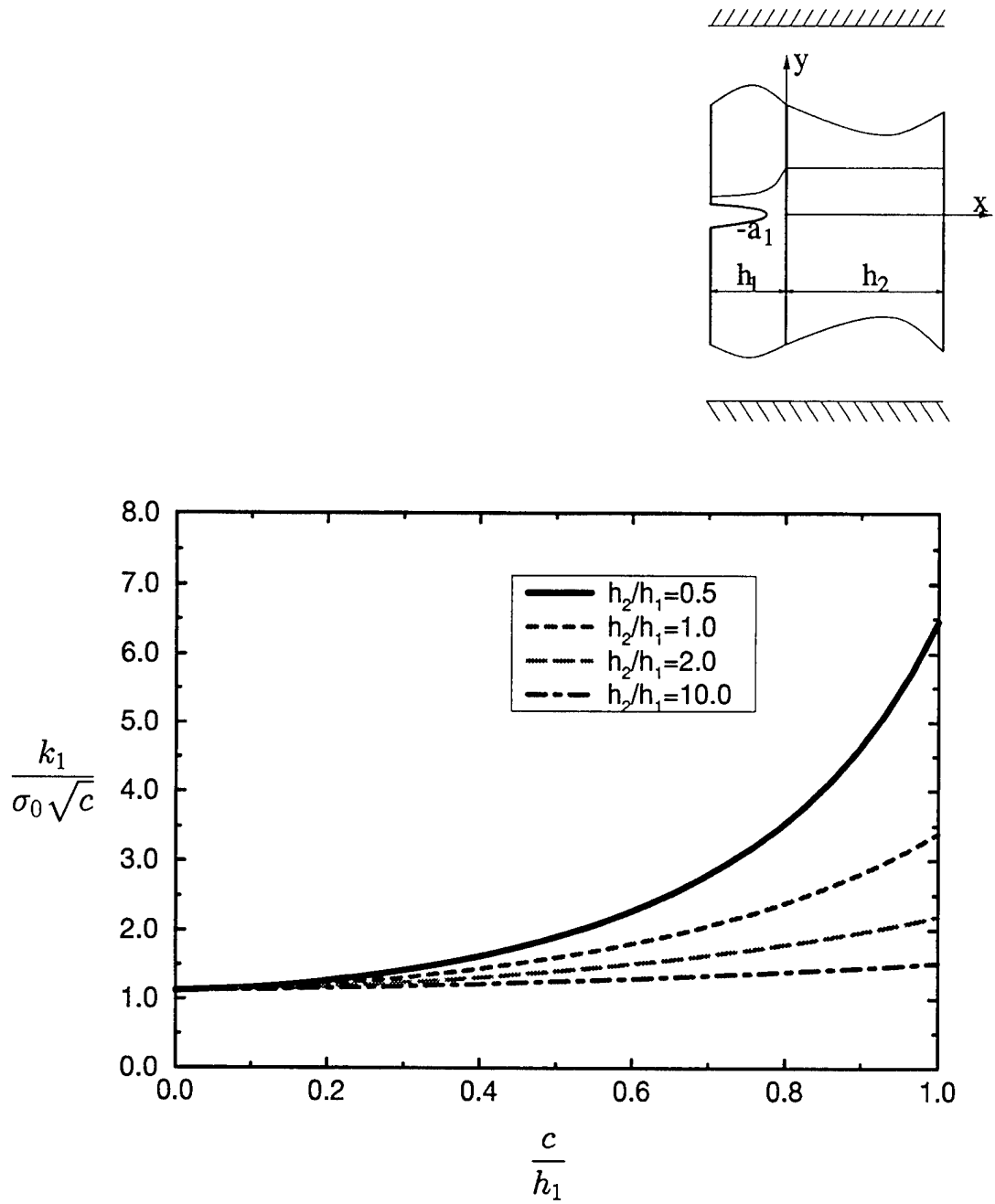


Figure 5.41 The effect of thickness ratio on normalized stress intensity factor for an edge crack located in the nonhomogeneous layer subjected to fixed grip loading.

$$c = (b_1 - a_1), b_1 = h_1, \beta h_1 = 0.375, \sigma_0 = \frac{8\mu_1}{(1 + \kappa)} \epsilon_0.$$

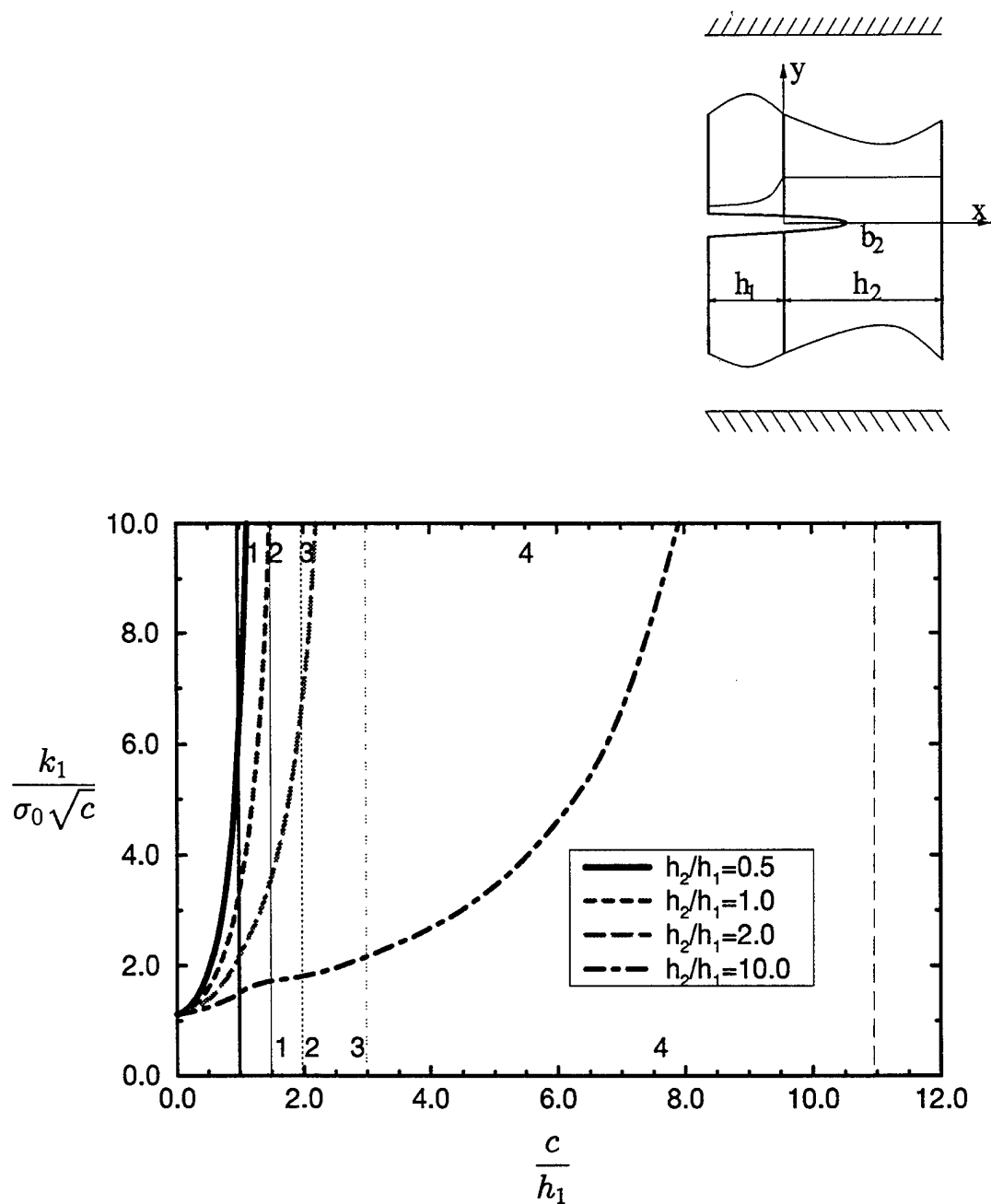


Figure 5.42 The effect of thickness ratio on normalized stress intensity factor for an edge crack crossing the interface subjected to fixed grip loading. c = crack length, $b_1 = h_1, \beta h_1 = 0.375, \sigma_0 = \frac{8\mu_1}{(1+\kappa)}\epsilon_0$.

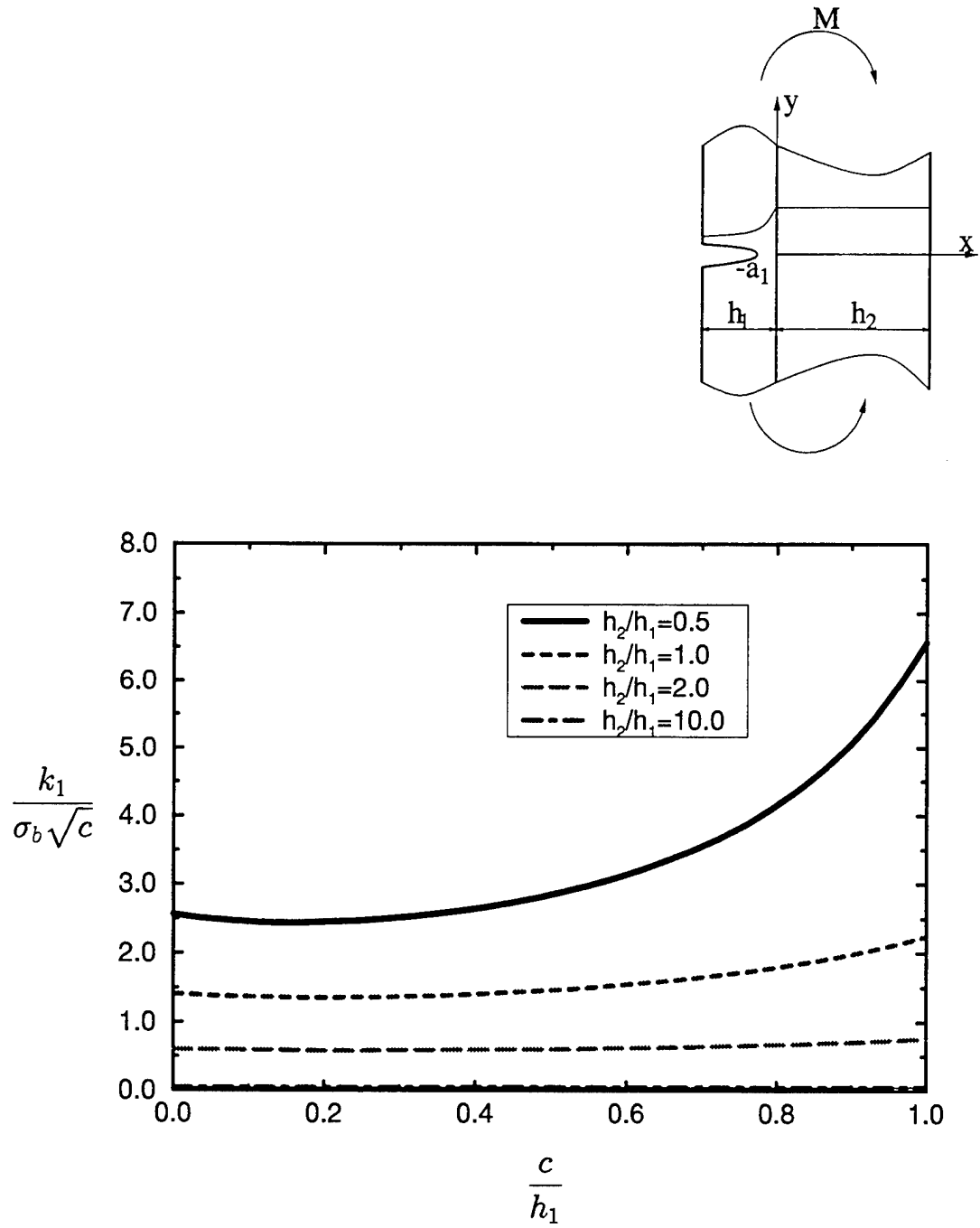


Figure 5.43 The effect of thickness ratio on normalized stress intensity factor for an edge crack located in the nonhomogeneous layer subjected to pure bending.

$$c = (b_1 - a_1), b_1 = h_1, \beta h_1 = 0.375, \sigma_b = \frac{M}{h_1^2}.$$

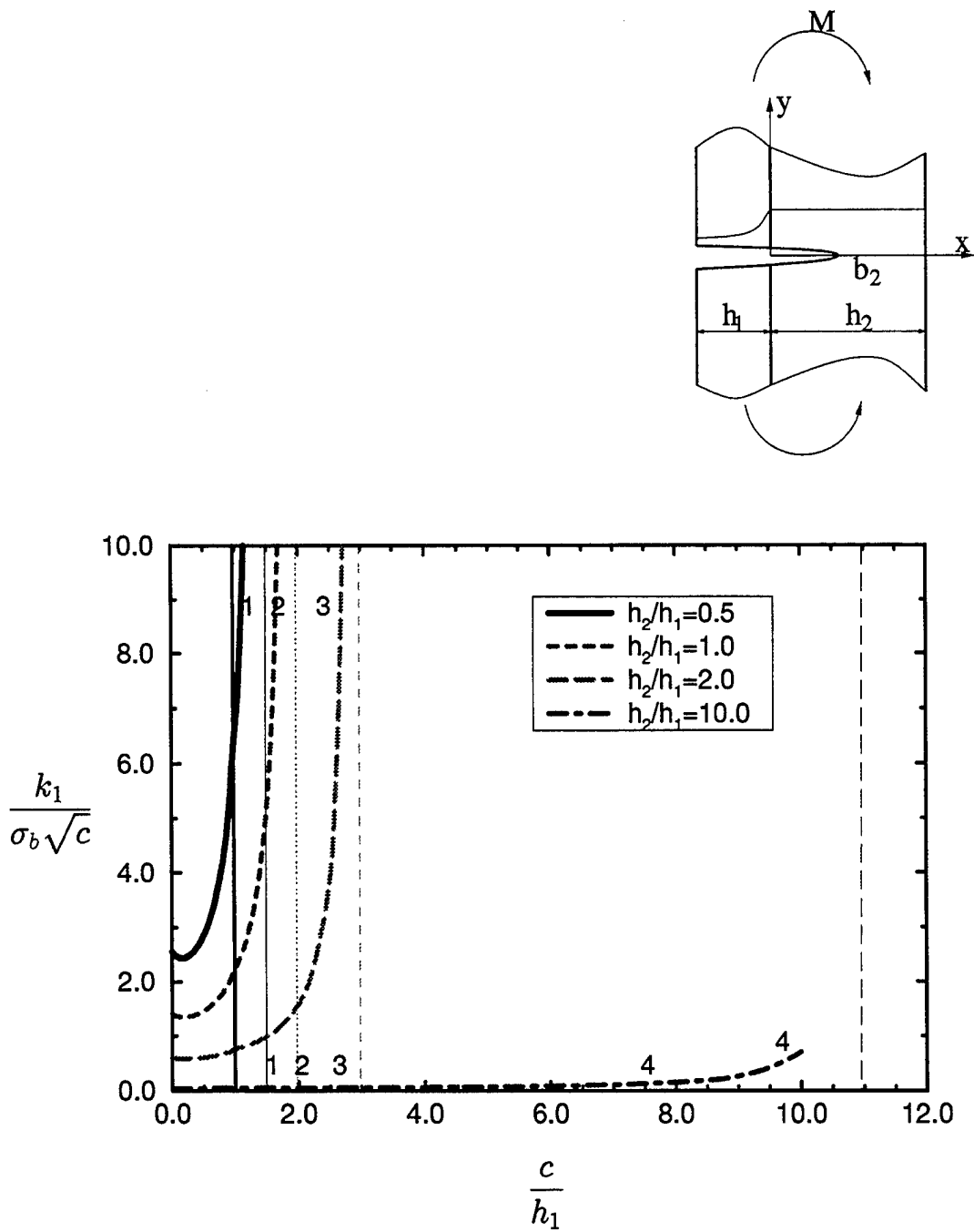


Figure 5.44 The effect of thickness ratio on normalized stress intensity factor for an edge crack crossing the interface subjected to pure bending. c = crack length, $b_1 = h_1, \beta h_1 = 0.375, \sigma_b = \frac{M}{h_1^2}$.

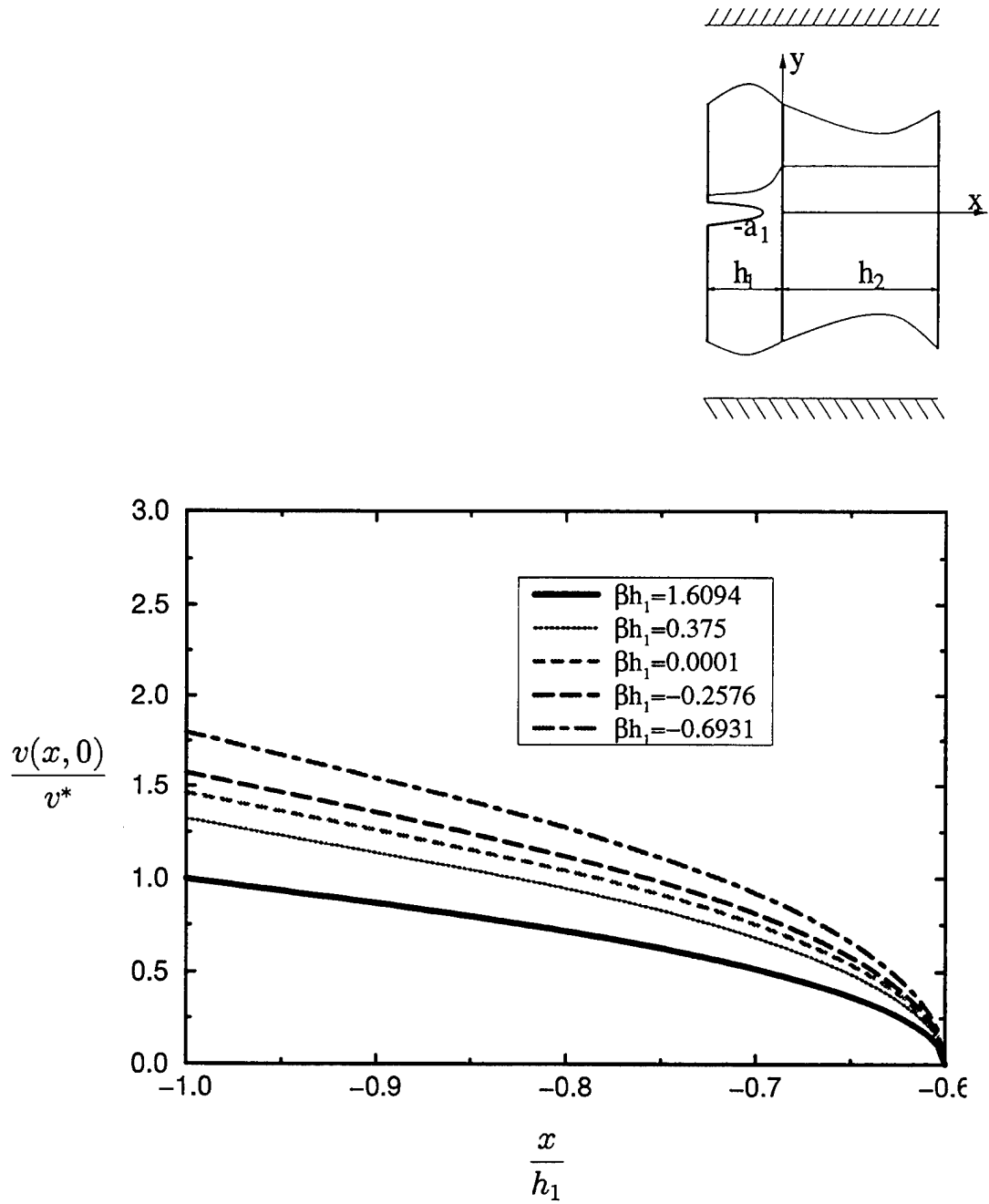


Figure 5.45 Effect of nonhomogeneity parameter on normalized crack opening displacement for an edge crack in the nonhomogeneous material subjected to fixed grip loading. $v^* = 2h_1\epsilon_0$, $\frac{h_2}{h_1} = 1.0$, $b_1 = h_1$, $a_1 = 0.6h_1$.

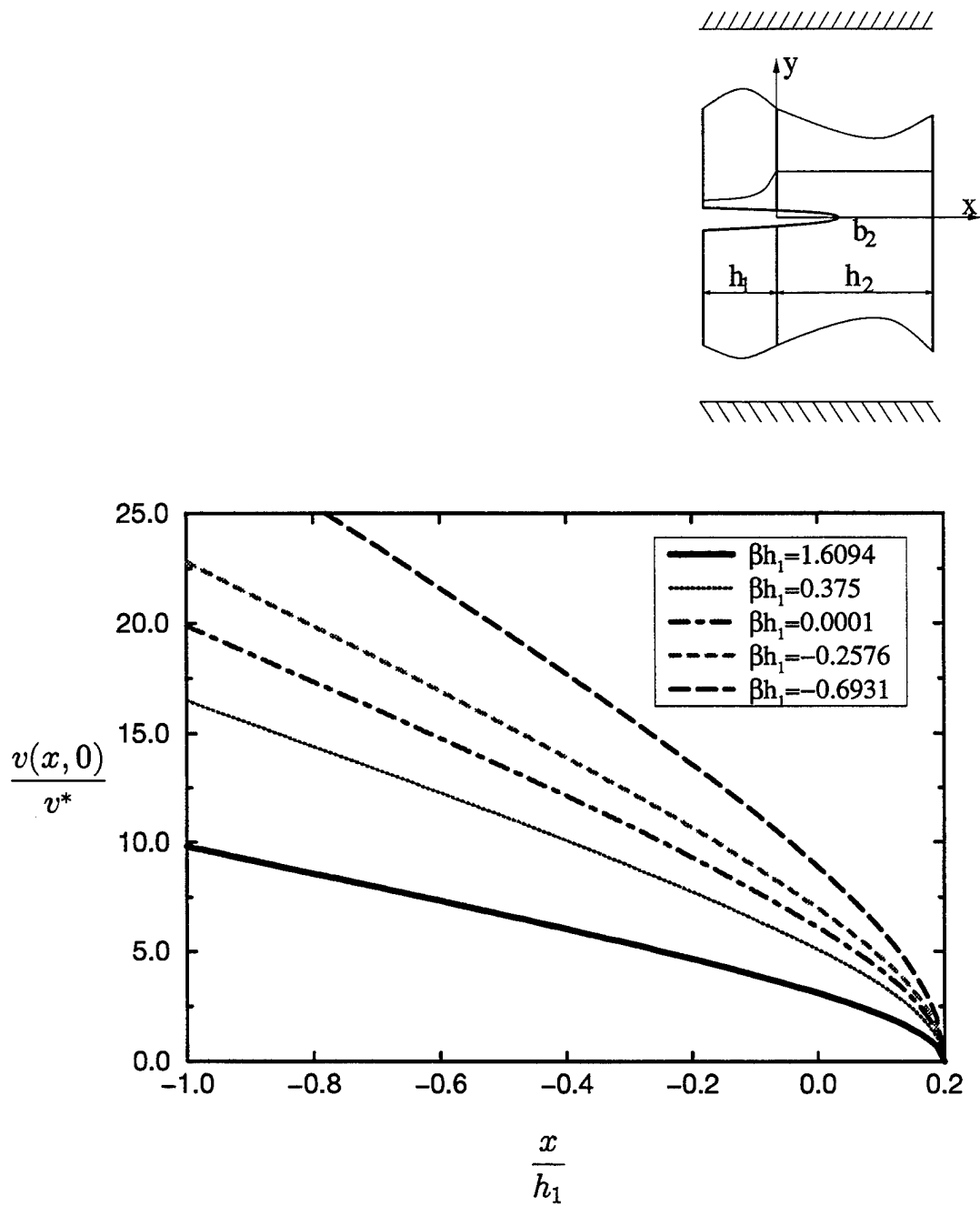


Figure 5.46 Effect of nonhomogeneity parameter on normalized crack opening displacement for an edge crack crossing the interface subjected to fixed grip loading. $v^* = 2h_1\epsilon_0$, $\frac{h_2}{h_1} = 1.0$, $b_1 = h_1$, $b_2 = 0.2h_1$.

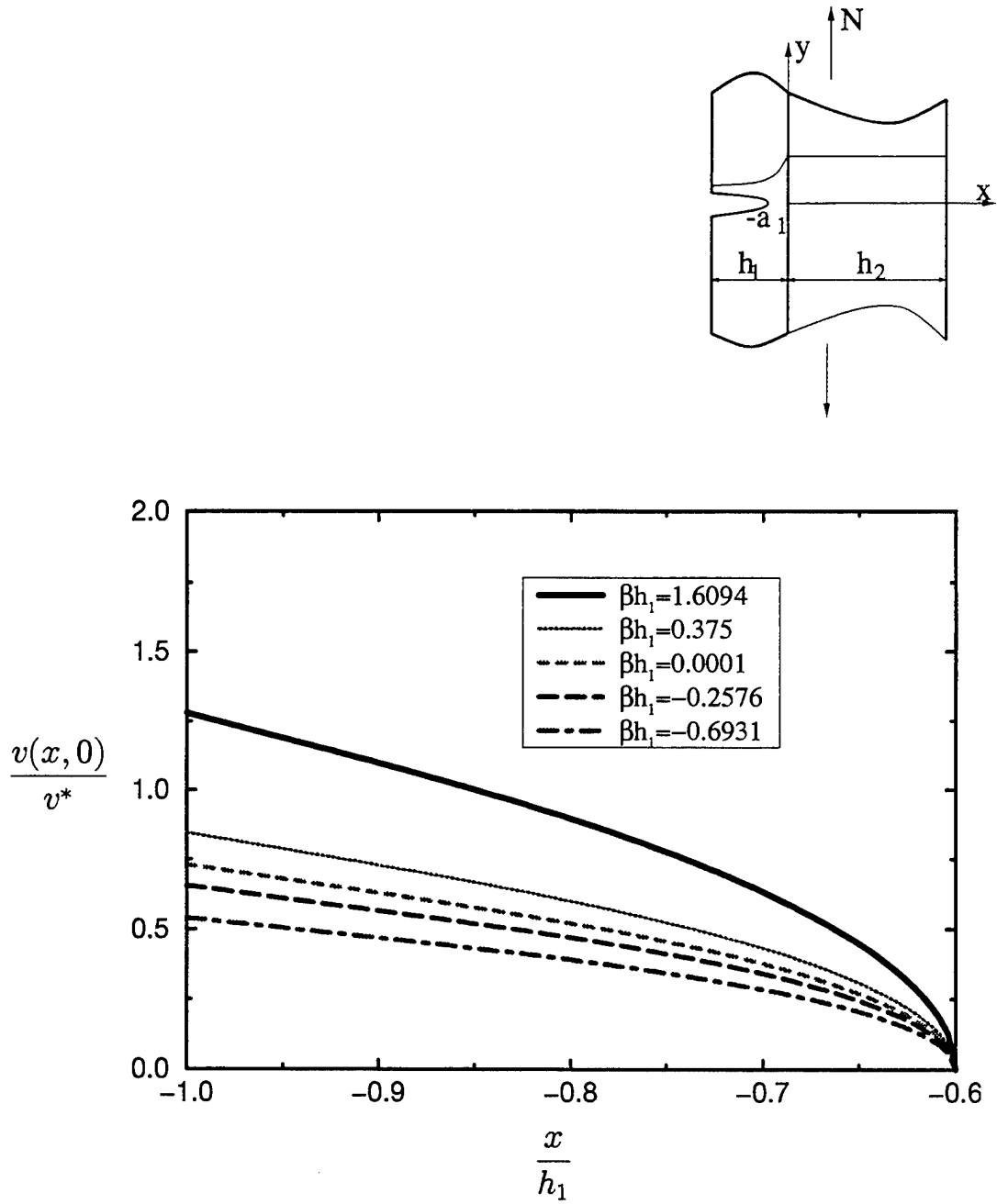


Figure 5.47 Effect of nonhomogeneity parameter on normalized crack opening displacement for an edge crack in the nonhomogeneous material subjected to membrane loading. $v^* = 2N \frac{(1 + \kappa)}{8\mu_0}$, $\frac{h_2}{h_1} = 1.0$, $b_1 = h_1$, $a_1 = 0.6h_1$.

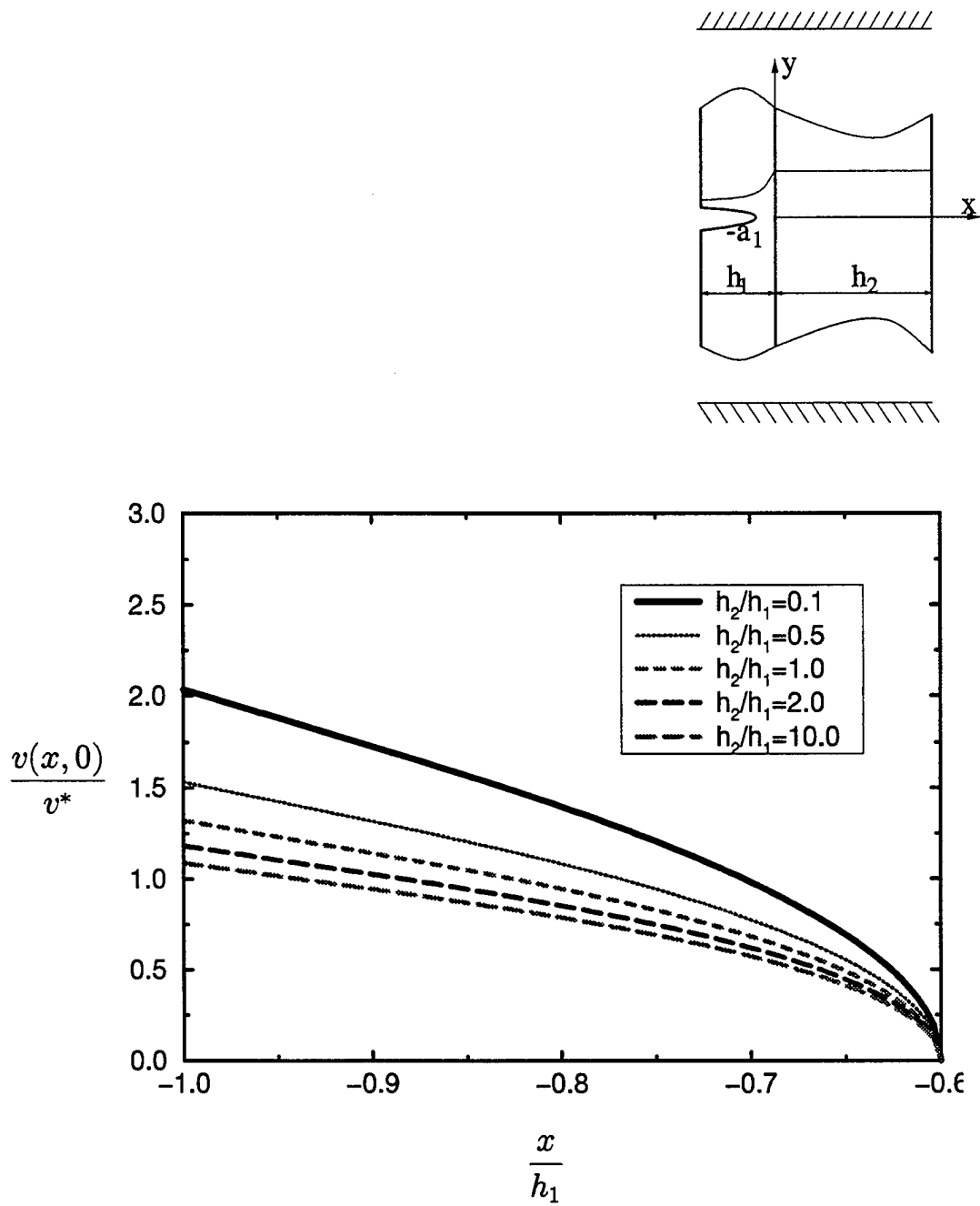


Figure 5.48 Effect of thickness ratio on normalized crack opening displacement for an edge crack in the nonhomogeneous material subjected to fixed grip loading.

$$v^* = 2h_1\epsilon_0, \beta h_1 = 0.375, b_1 = h_1, a_1 = 0.6h_1.$$

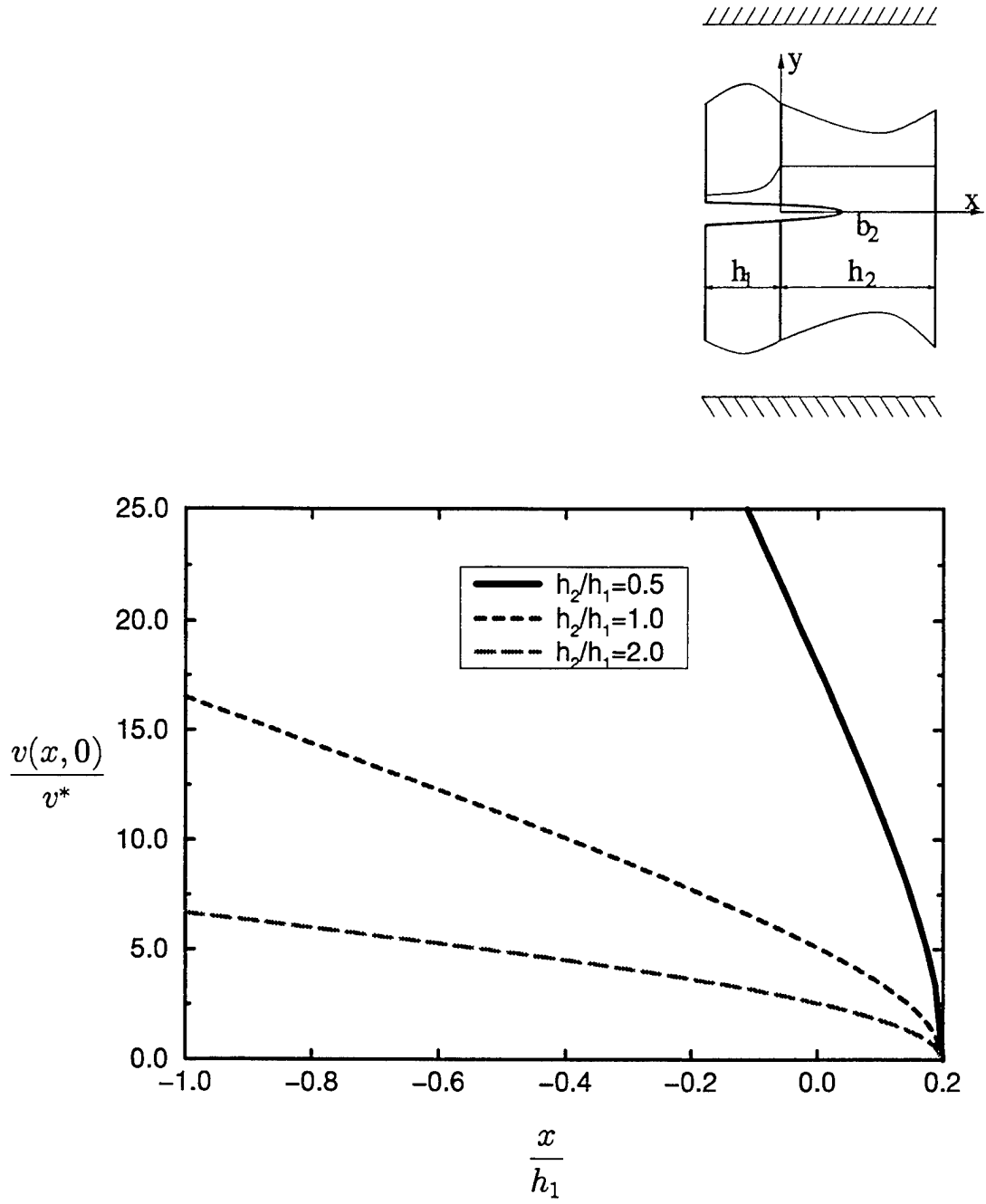


Figure 5.49 Effect of thickness ratio on normalized crack opening displacement for an edge crack crossing the interface subjected to fixed grip loading.

$$v^* = 2h_1\epsilon_0, \beta h_1 = 0.375, b_1 = h_1, b_2 = 0.2h_1.$$

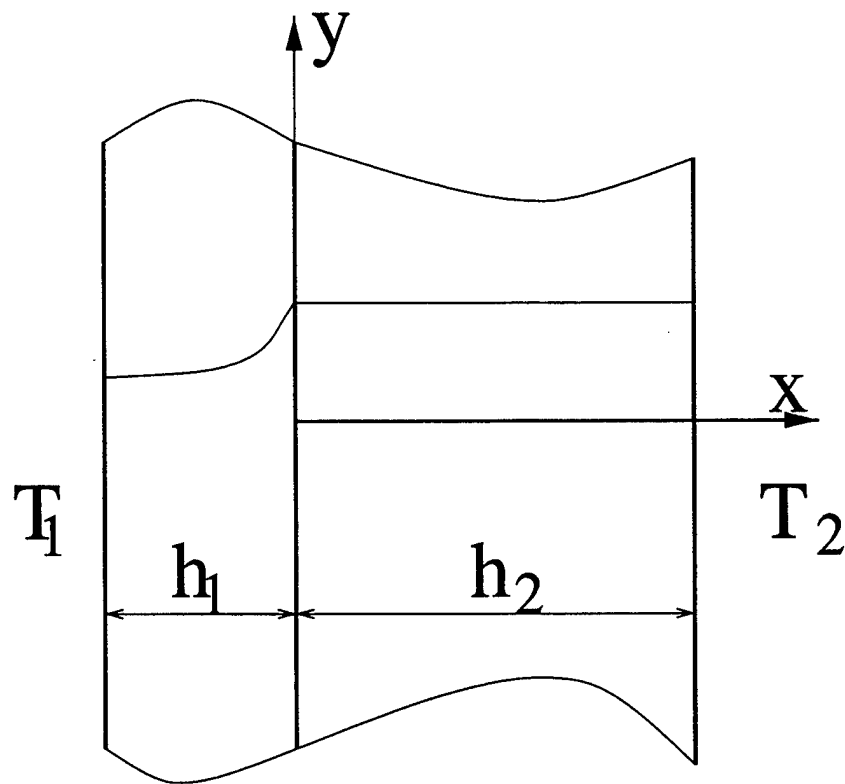


Figure 5.50 Geometry for the thermal loading problem for an uncracked specimen

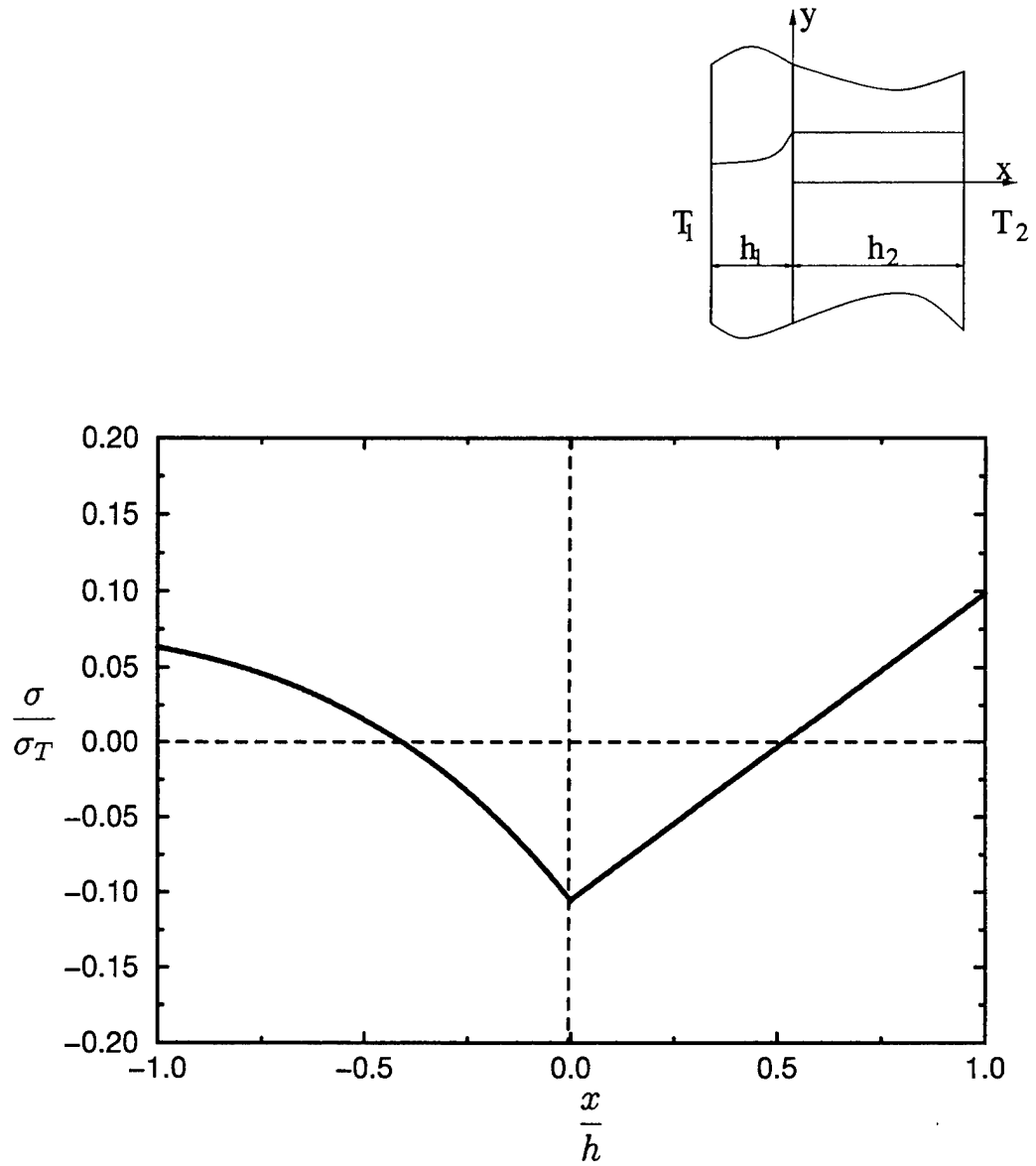


Figure 5.51 Thermal stress distribution for an uncracked specimen under uniform

temperature change. $\sigma_T = \frac{8\mu_0\alpha_0\Delta T(1+\nu)}{(1+\kappa)}$, $\frac{\mu_0}{\mu_1} = e^{\beta h_1}$,

$$\frac{\alpha_0}{\alpha_1} = e^{\alpha h_1}, \frac{k_0}{k_c} = e^{\gamma h_1},$$

$$\beta h_1 = 0.375, \alpha h_1 = 0.513, \gamma h_1 = 2.5, \frac{h_2}{h_1} = 1.0.$$

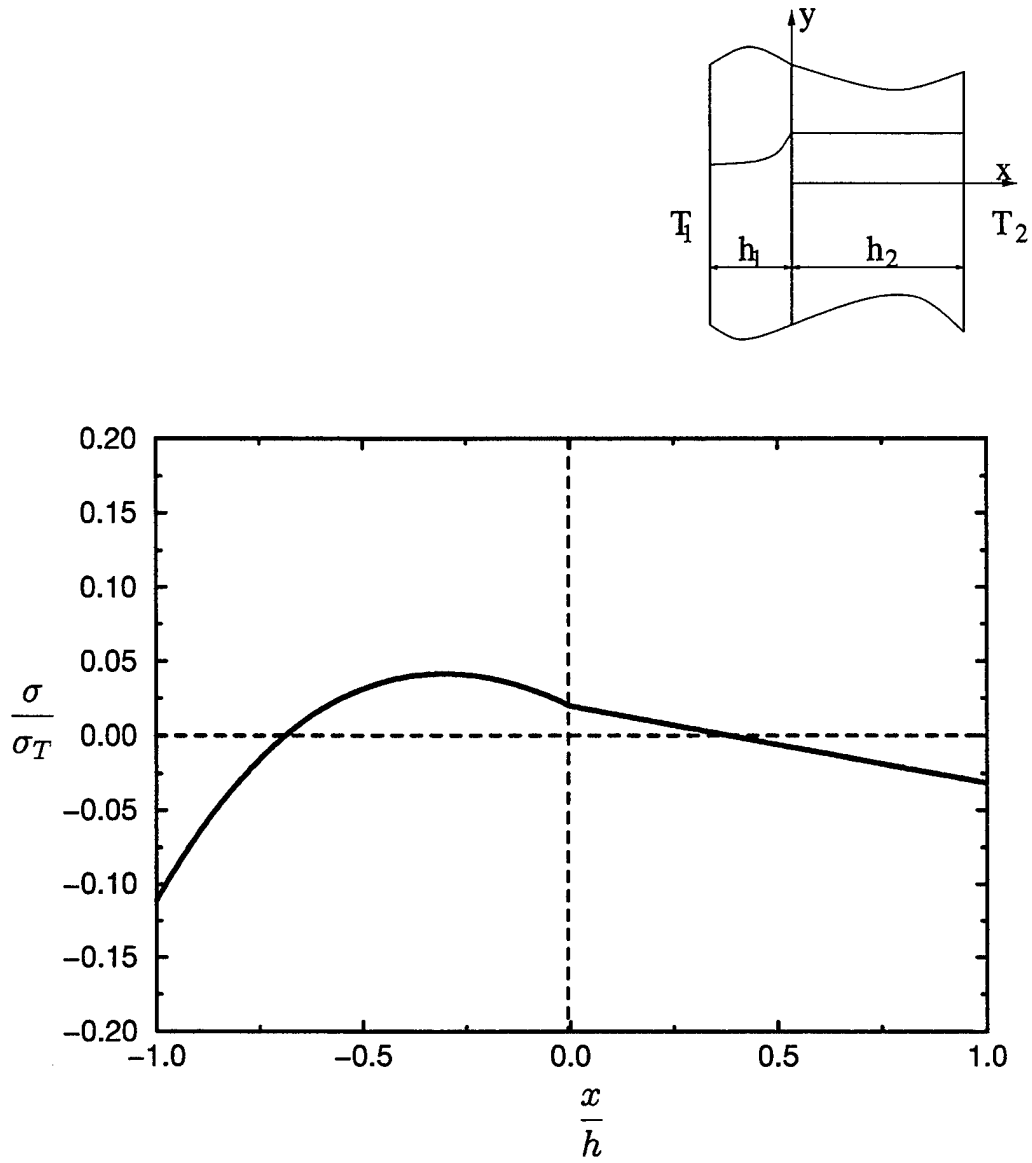


Figure 5.52 Thermal stress distribution for an uncracked specimen under

steady state heat conduction. T_1 =variable, $T_2 = T_0$,

$$\sigma_T = \frac{8\mu_0\alpha_0\Delta T(1+\nu)}{(1+\kappa)}, \frac{\mu_0}{\mu_1} = e^{\beta h_1}, \frac{\alpha_0}{\alpha_1} = e^{\alpha h_1}, \frac{k_0}{k_c} = e^{\gamma h_1},$$

$$\beta h_1 = 0.375, \alpha h_1 = 0.513, \gamma h_1 = 2.5, \frac{h_2}{h_1} = 1.0.$$

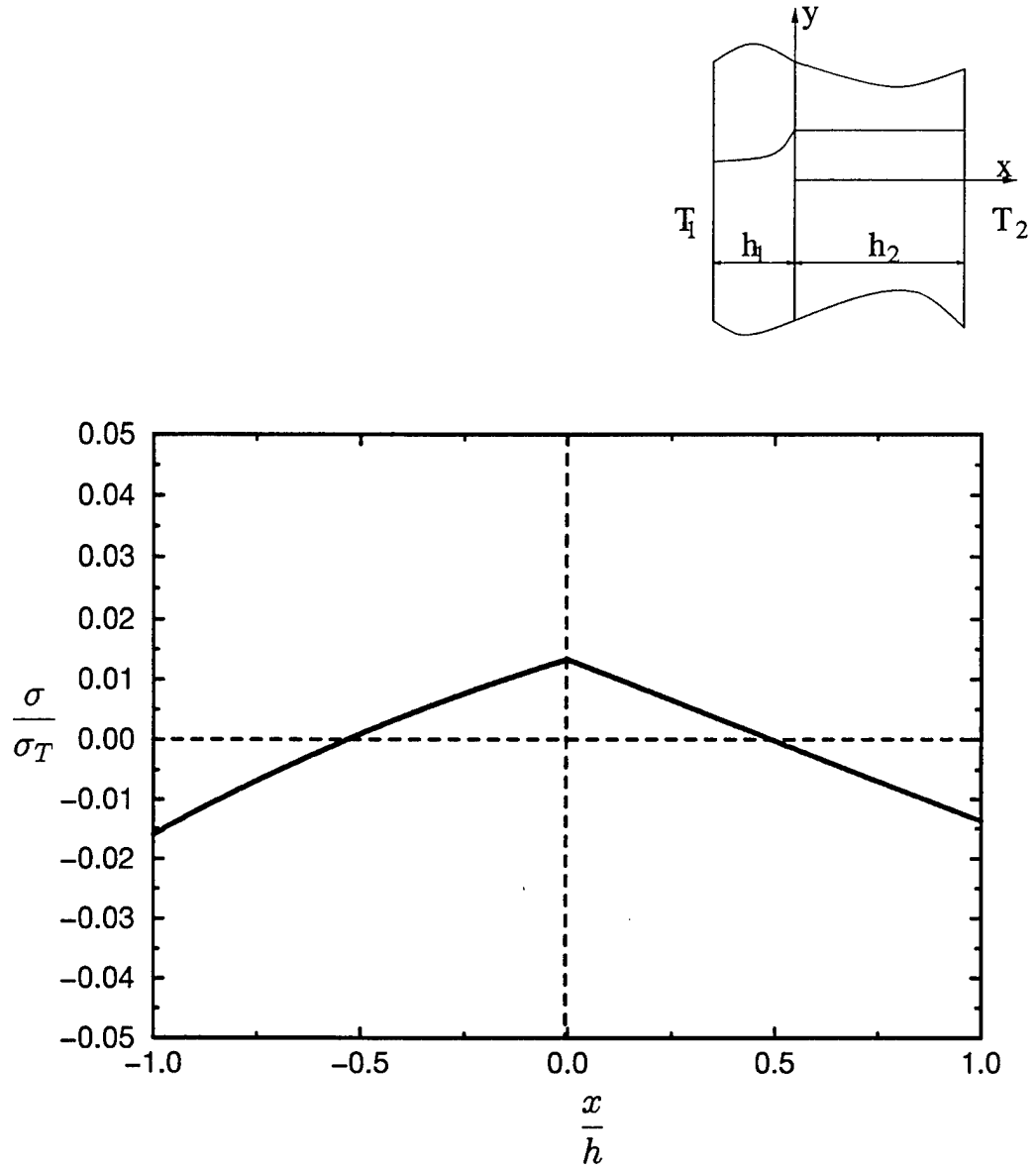


Figure 5.53 Thermal stress distribution for an uncracked specimen under uniform

temperature change. $\sigma_T = \frac{8\mu_0\alpha_0\Delta T(1+\nu)}{(1+\kappa)}$,

$$\frac{\mu_0}{\mu_1} = e^{\beta h_1}, \frac{\alpha_0}{\alpha_1} = e^{\alpha h_1}, \frac{k_0}{k_c} = e^{\gamma h_1},$$

$$\beta h_1 = -0.2576, \alpha h_1 = -0.0513, \gamma h_1 = 1.2777, \frac{h_2}{h_1} = 1.0.$$

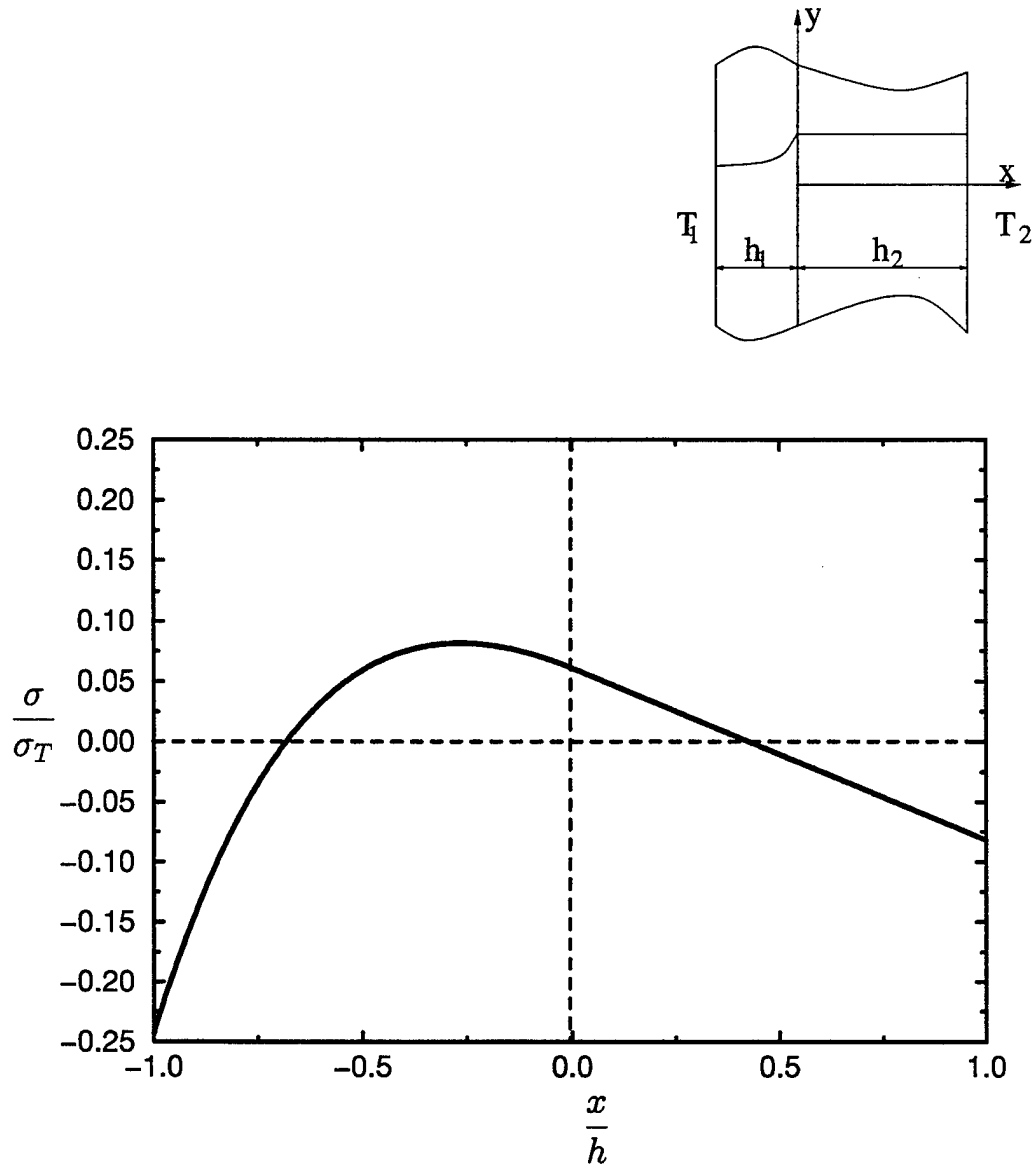


Figure 5.54 Thermal stress distribution for an uncracked specimen under

steady state heat conduction. $T_1 = \text{variable}$, $T_2 = T_0$,

$$\sigma_T = \frac{8\mu_0\alpha_0\Delta T(1+\nu)}{(1+\kappa)}, \frac{\mu_0}{\mu_1} = e^{\beta h_1}, \frac{\alpha_0}{\alpha_1} = e^{\alpha h_1}, \frac{k_0}{k_c} = e^{\gamma h_1},$$

$$\beta h_1 = -0.2576, \alpha h_1 = -0.0513, \gamma h_1 = 1.2777, \frac{h_2}{h_1} = 1.0.$$

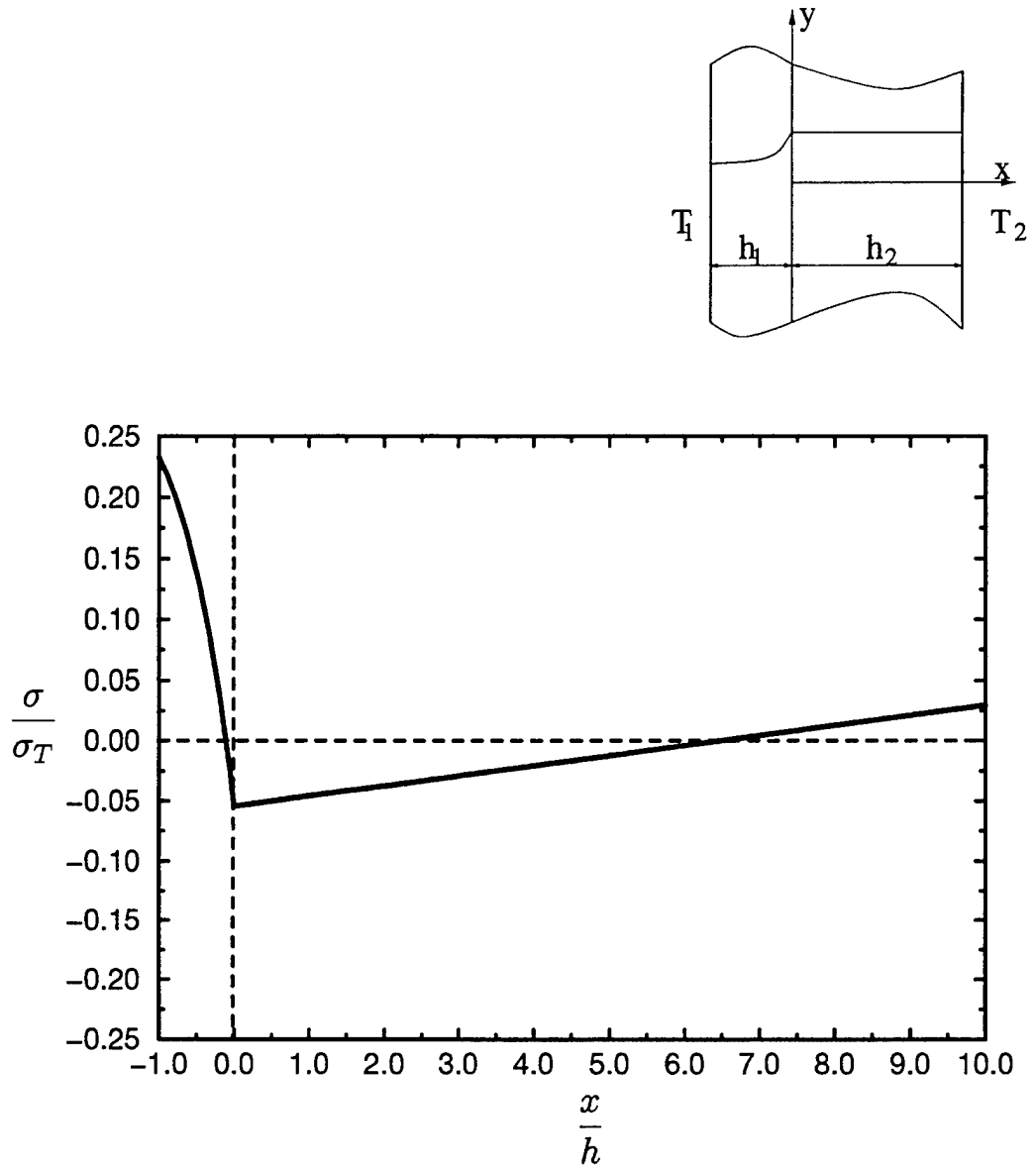


Figure 5.55 Thermal stress distribution for an uncracked specimen under uniform

temperature change. $\sigma_T = \frac{8\mu_0\alpha_0\Delta T(1+\nu)}{(1+\kappa)}$, $\frac{\mu_0}{\mu_1} = e^{\beta h_1}$,

$\frac{\alpha_0}{\alpha_1} = e^{\alpha h_1}$, $\frac{k_0}{k_c} = e^{\gamma h_1}$, $\beta h_1 = 0.375$, $\alpha h_1 = 0.513$, $\gamma h_1 = 2.5$,

$\frac{h_2}{h_1} = 10.0$.

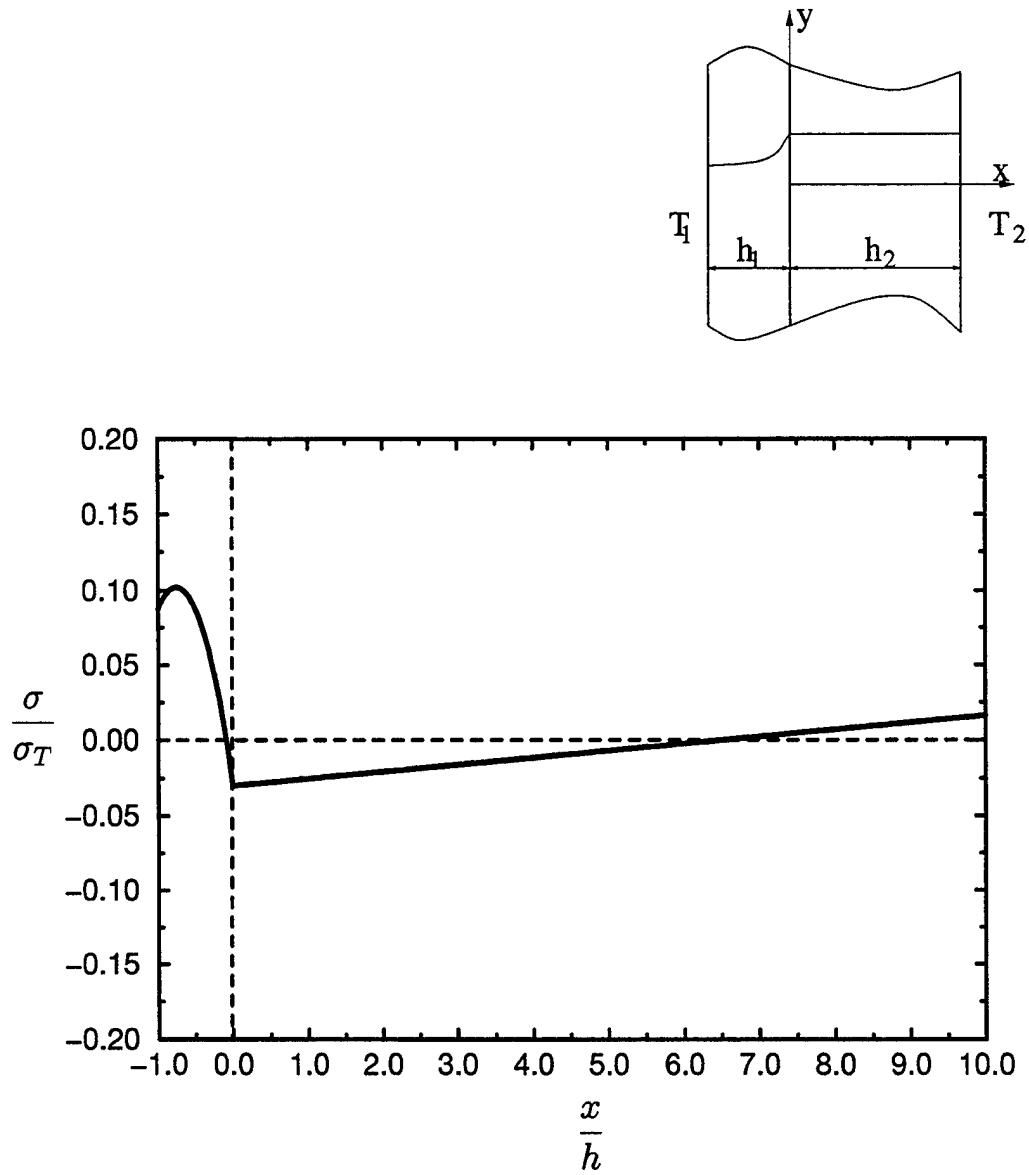


Figure 5.56 Thermal stress distribution for an uncracked specimen under

steady state heat conduction. $T_1 = \text{variable}$, $T_2 = T_0$,

$$\sigma_T = \frac{8\mu_0\alpha_0\Delta T(1+\nu)}{(1+\kappa)}, \frac{\mu_0}{\mu_1} = e^{\beta h_1}, \frac{\alpha_0}{\alpha_1} = e^{\alpha h_1}, \frac{k_0}{k_c} = e^{\gamma h_1},$$

$$\beta h_1 = 0.375, \alpha h_1 = 0.513, \gamma h_1 = 2.5, \frac{h_2}{h_1} = 10.0.$$

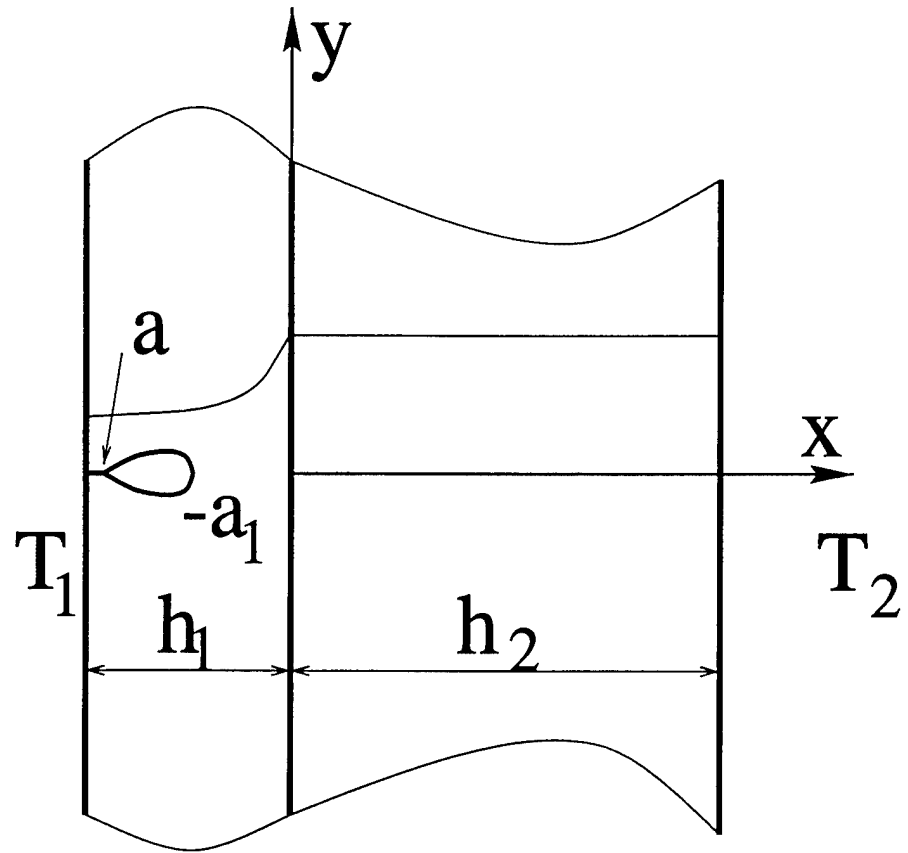


Figure 5.57 Crack-contact problem

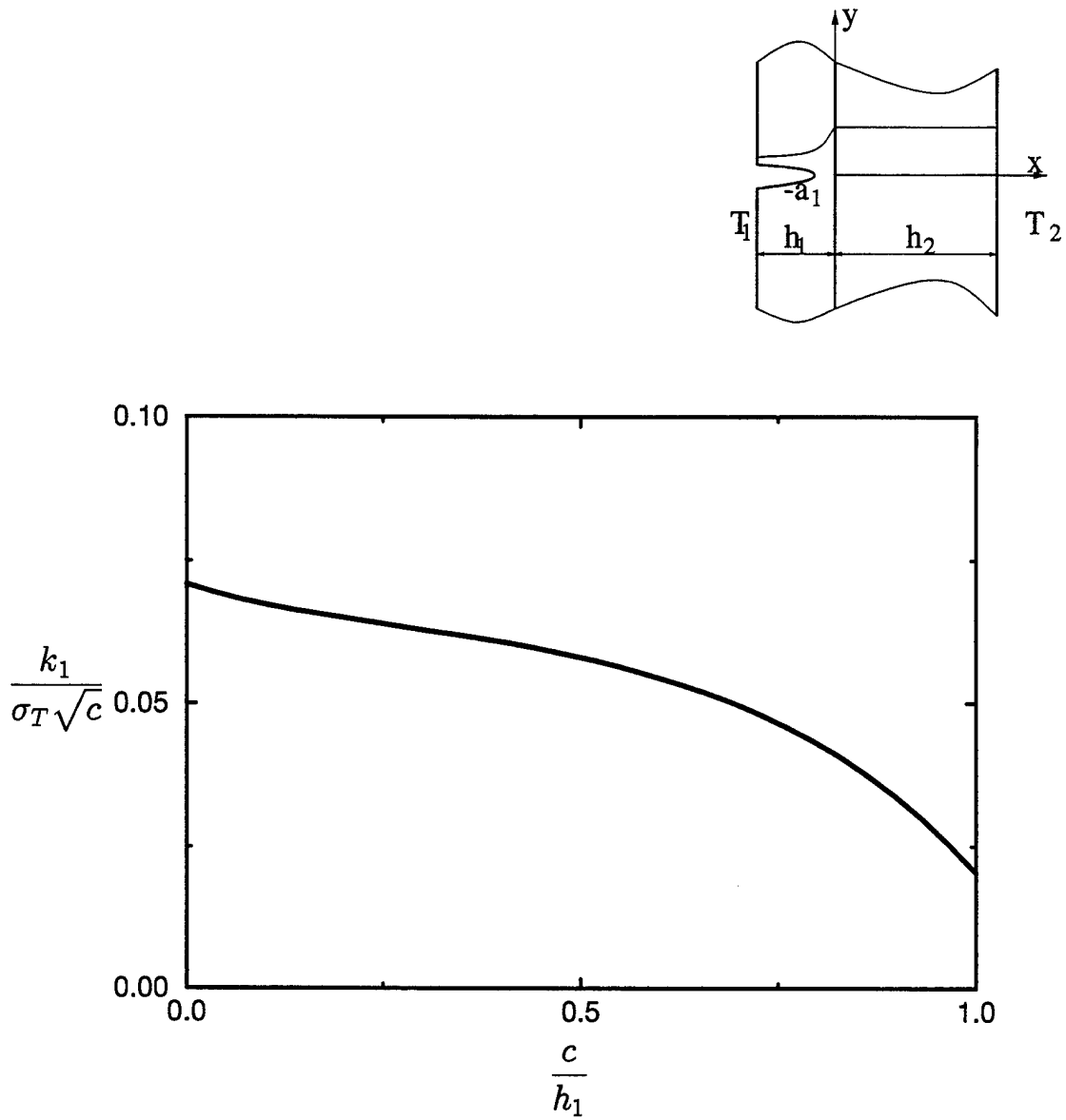


Figure 5.58 The effect of uniform temperature rise on normalized stress intensity

factor for an edge crack located in the nonhomogeneous layer.

$$c = (b_1 - a_1), b_1 = h_1, \frac{h_2}{h_1} = 1.0, \sigma_T = \frac{8\mu_0\alpha_0(T - T_0)(1 + \nu)}{(1 + \kappa)},$$

$$\frac{\mu_0}{\mu_1} = e^{\beta h_1}, \frac{\alpha_0}{\alpha_1} = e^{\alpha h_1}, \frac{k_0}{k_c} = e^{\gamma h_1}, T_1 = T_2 = T > T_0,$$

$$\beta h_1 = 0.375, \alpha h_1 = 0.513, \gamma h_1 = 2.5 \text{ (PSZ-René41).}$$

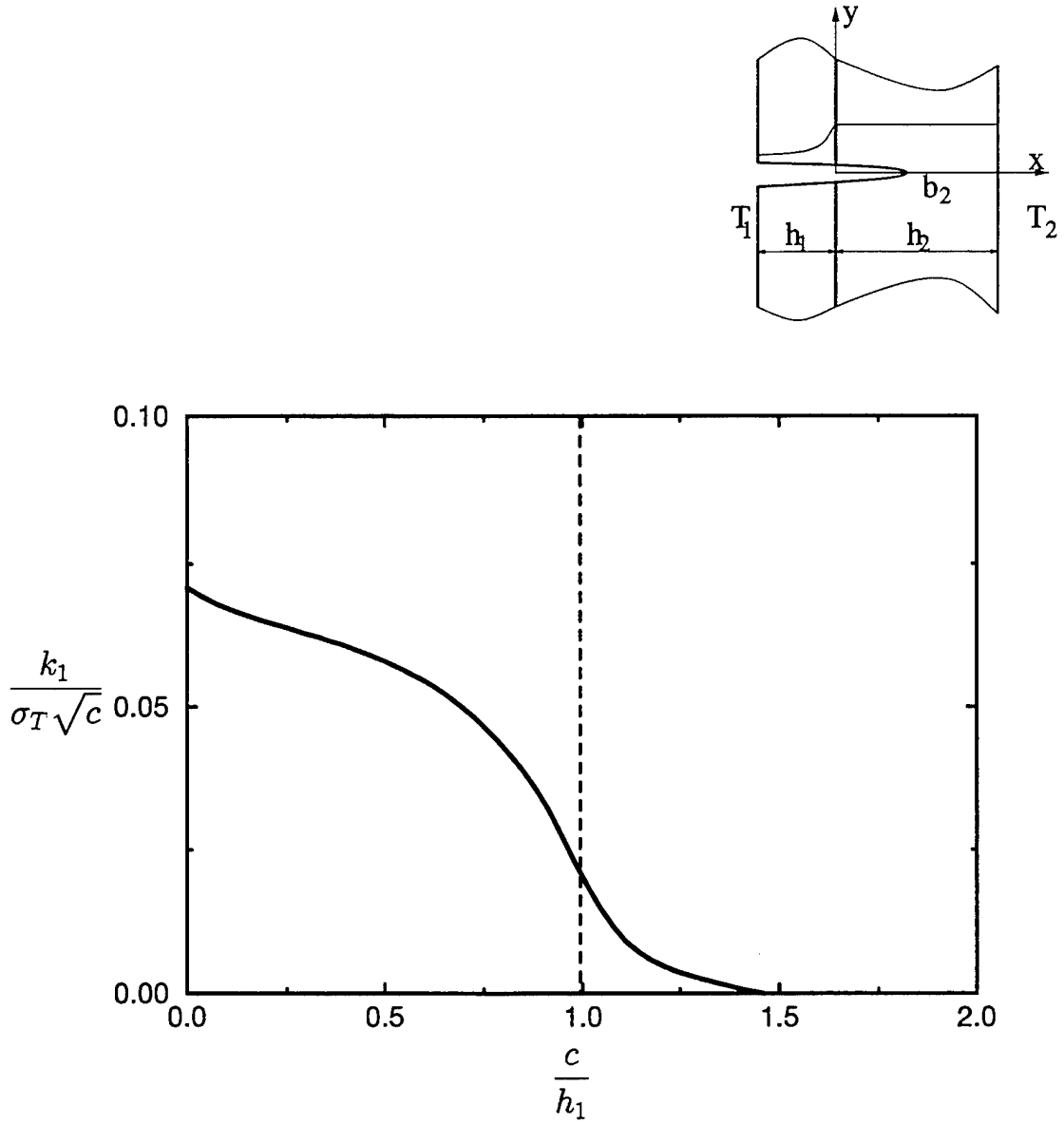


Figure 5.59 The effect of uniform temperature rise on normalized stress intensity

factor for an edge crack passing through the interface.

$$c = \text{crack length}, b_1 = h_1, \frac{h_2}{h_1} = 1.0, \sigma_T = \frac{8\mu_0\alpha_0(T - T_0)(1 + \nu)}{(1 + \kappa)},$$

$$\frac{\mu_0}{\mu_1} = e^{\beta h_1}, \frac{\alpha_0}{\alpha_1} = e^{\alpha h_1}, \frac{k_0}{k_c} = e^{\gamma h_1}, T_1 = T_2 = T > T_0,$$

$$\beta h_1 = 0.375, \alpha h_1 = 0.513, \gamma h_1 = 2.5 \text{ (PSZ-René41).}$$

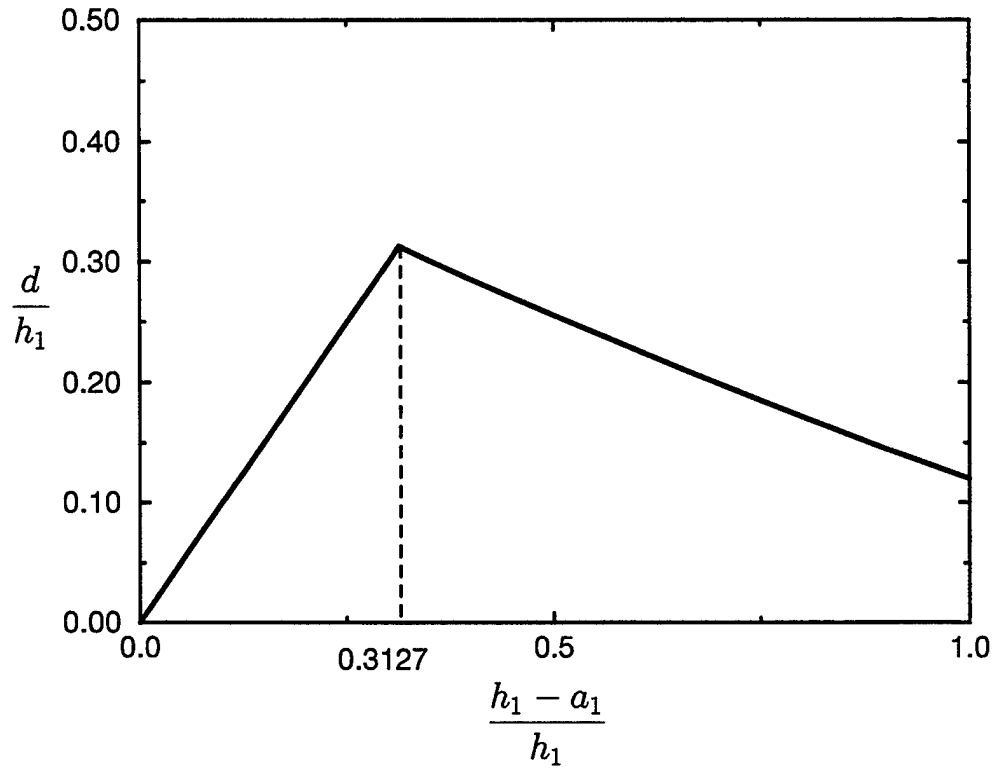
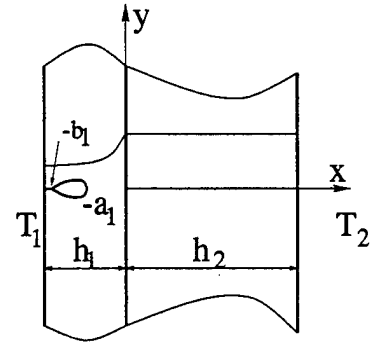


Figure 5.60 Crack closure length as a function of the location of the open crack

tip for an edge crack loaded thermally. $T_2 = T_0, T_1 > T_0$,

$$d = \frac{h_1 - b_1}{h_1}, \frac{h_2}{h_1} = 1.0, \frac{\mu_0}{\mu_1} = e^{\beta h_1}, \frac{\alpha_0}{\alpha_1} = e^{\alpha h_1}, \frac{k_0}{k_c} = e^{\gamma h_1},$$

$$\beta h_1 = 0.375, \alpha h_1 = 0.513, \gamma h_1 = 2.5 \text{ (PSZ-Ren 41).}$$

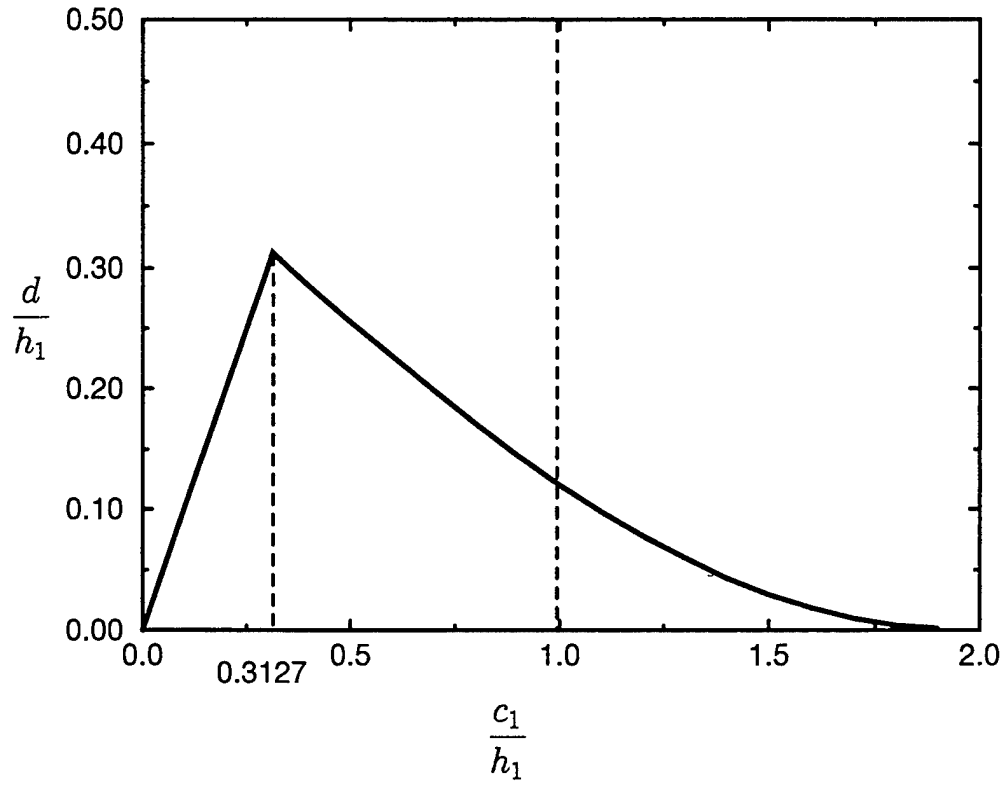
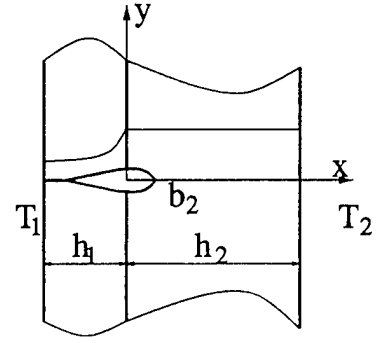


Figure 5.61 Crack closure length as a function of the location of the open crack tip

for an edge crack passing through the interface loaded thermally.

$$T_2 = T_0, T_1 > T_0, d = \frac{h_1 - b_1}{h_1}, \frac{h_2}{h_1} = 1.0, \frac{\mu_0}{\mu_1} = e^{\beta h_1}, \frac{\alpha_0}{\alpha_1} = e^{\alpha h_1},$$

$$\frac{k_0}{k_c} = e^{\gamma h_1}, \beta h_1 = 0.375, \alpha h_1 = 0.513, \gamma h_1 = 2.5 \text{ (PSZ-René41).}$$

$$c_1 = h_1 - a_1 \text{ for crack in coating, } c_1 = h_1 + b_2 \text{ for through crack}$$

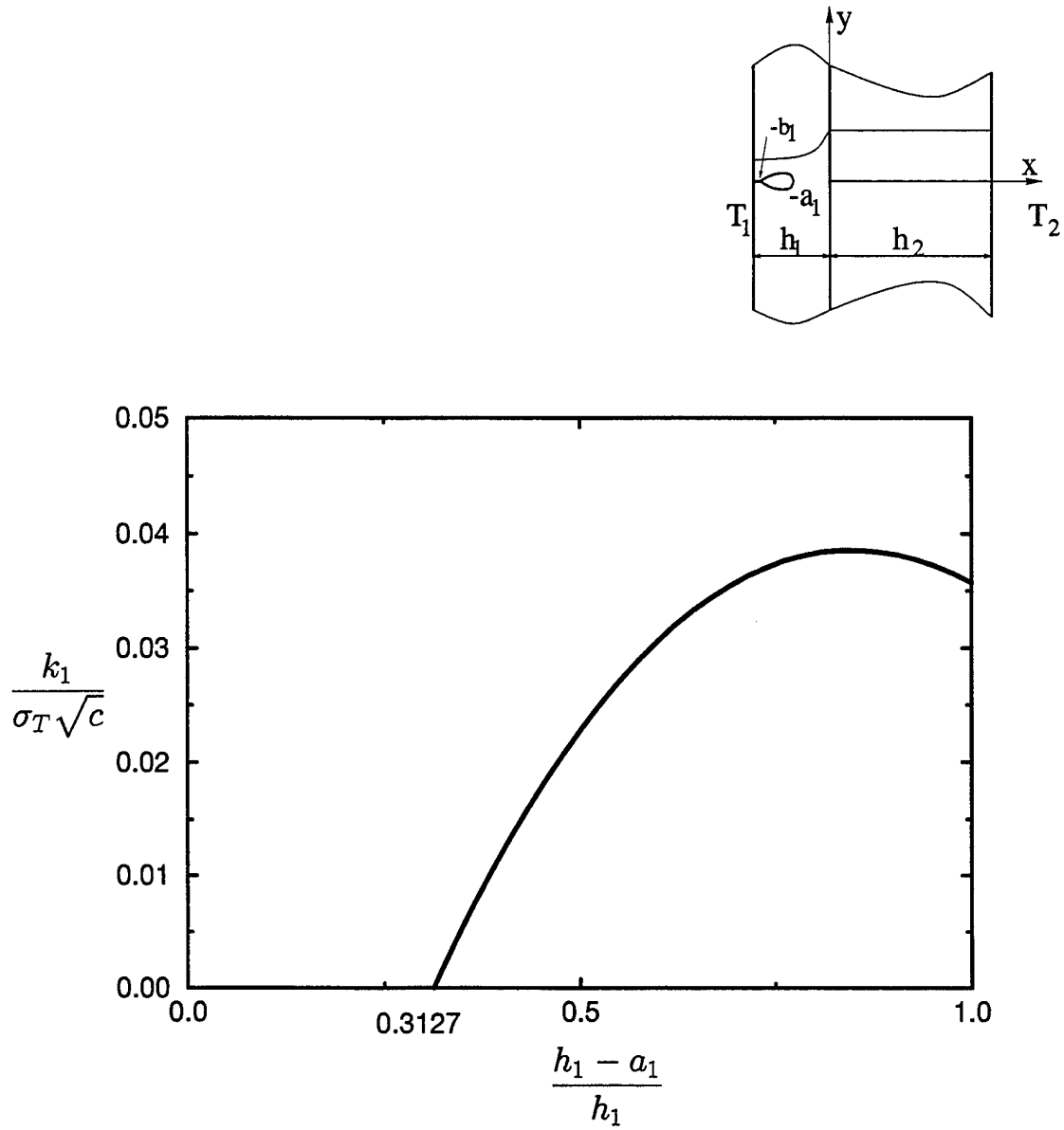


Figure 5.62 The effect of temperature rise at one boundary on normalized stress intensity factor for an edge crack located in the nonhomogeneous layer.

$$c = \frac{(b_1 - a_1)}{2}, b_1 \text{ determined from Fig. 5.60, } \frac{h_2}{h_1} = 1.0,$$

$$\sigma_T = \frac{8\mu_0\alpha_0(T_1 - T_0)(1 + \nu)}{(1 + \kappa)}, T_2 = T_0, T_1 > T_0, \frac{\mu_0}{\mu_1} = e^{\beta h_1}, \frac{\alpha_0}{\alpha_1} = e^{\alpha h_1},$$

$$\frac{k_0}{k_c} = e^{\gamma h_1}, \beta h_1 = 0.375, \alpha h_1 = 0.513, \gamma h_1 = 2.5 \text{ (PSZ-René41).}$$

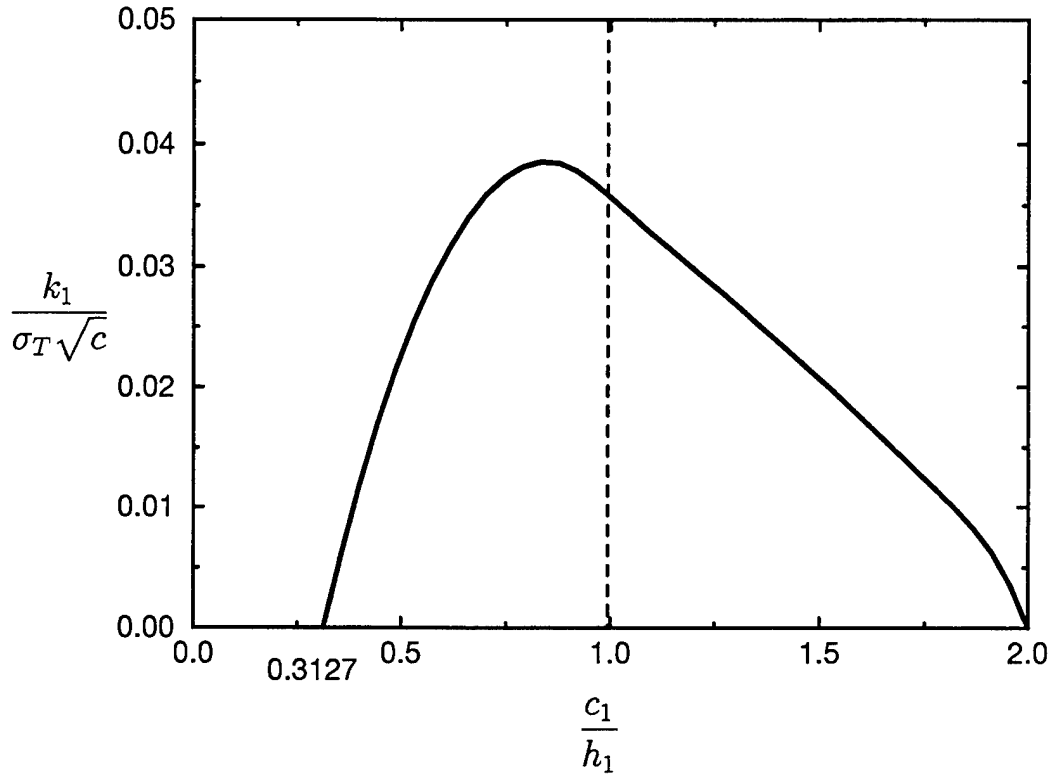
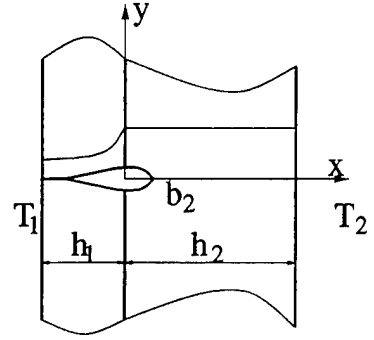


Figure 5.63 The effect of temperature rise at one boundary on normalized stress

intensity factor for an edge crack passing through the interface.

c = half crack length, b_1 determined from Fig. 5.61, $\frac{h_2}{h_1} = 1.0$,

$$\sigma_T = \frac{8\mu_0\alpha_0(T_1 - T_0)(1 + \nu)}{(1 + \kappa)}, T_2 = T_0, T_1 > T_0, \frac{\mu_0}{\mu_1} = e^{\beta h_1}, \frac{\alpha_0}{\alpha_1} = e^{\alpha h_1},$$

$$\frac{k_0}{k_c} = e^{\gamma h_1}, \beta h_1 = 0.375, \alpha h_1 = 0.513, \gamma h_1 = 2.5 \text{ (PSZ-René41).}$$

$c_1 = h_1 - a_1$ for crack in coating, $c_1 = h_1 + b_2$ for through crack

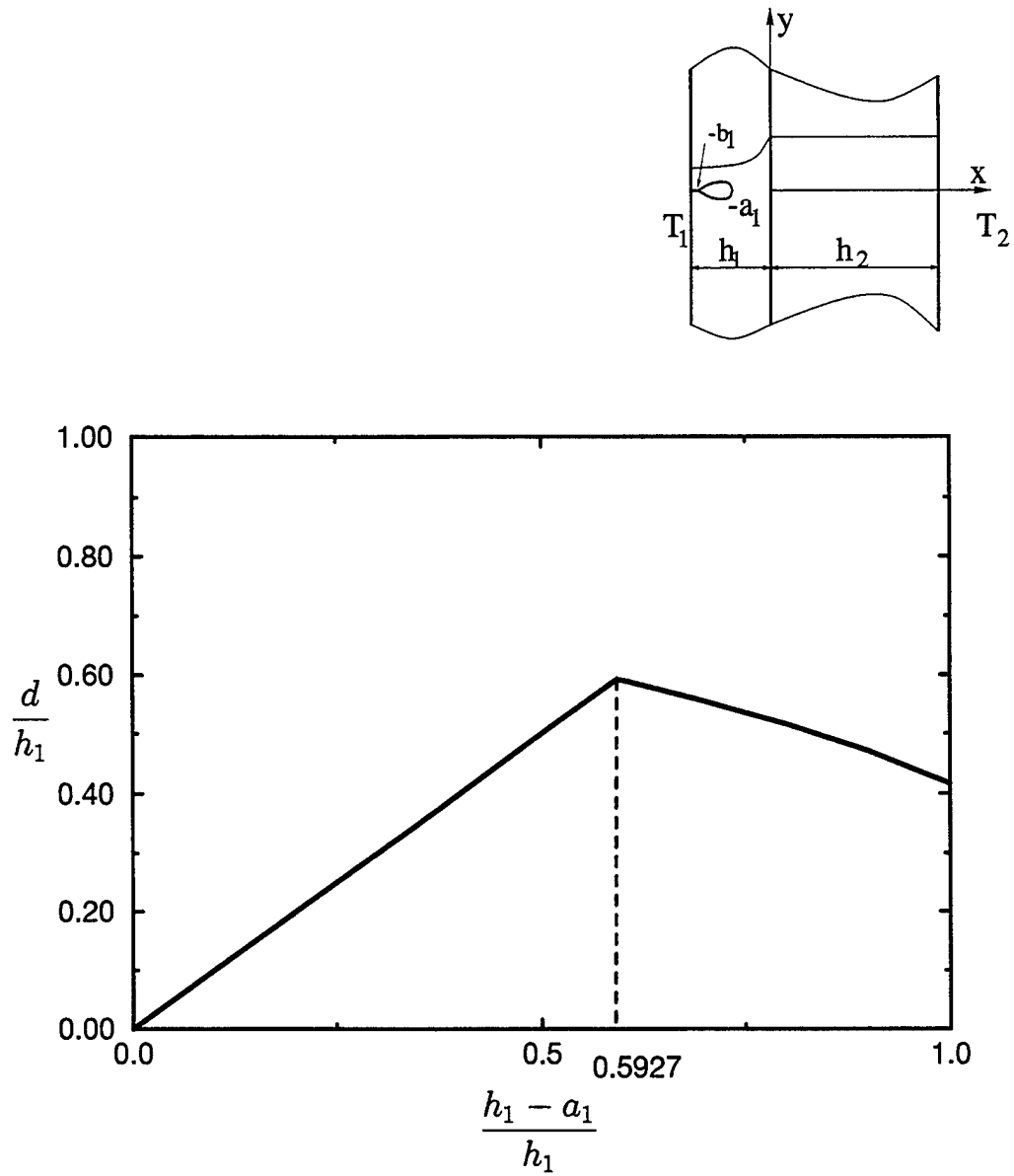


Figure 5.64 Crack closure length as a function of the location of the open crack tip

for an edge crack under uniform temperature fall. $d = \frac{h_1 - b_1}{h_1}$,

$$\frac{h_2}{h_1} = 1.0, \frac{\mu_0}{\mu_1} = e^{\beta h_1}, \frac{\alpha_0}{\alpha_1} = e^{\alpha h_1}, \frac{k_0}{k_c} = e^{\gamma h_1}, T_1 = T_2 = T < T_0,$$

$$\beta h_1 = 0.375, \alpha h_1 = 0.513, \gamma h_1 = 2.5 \text{ (PSZ-René41).}$$

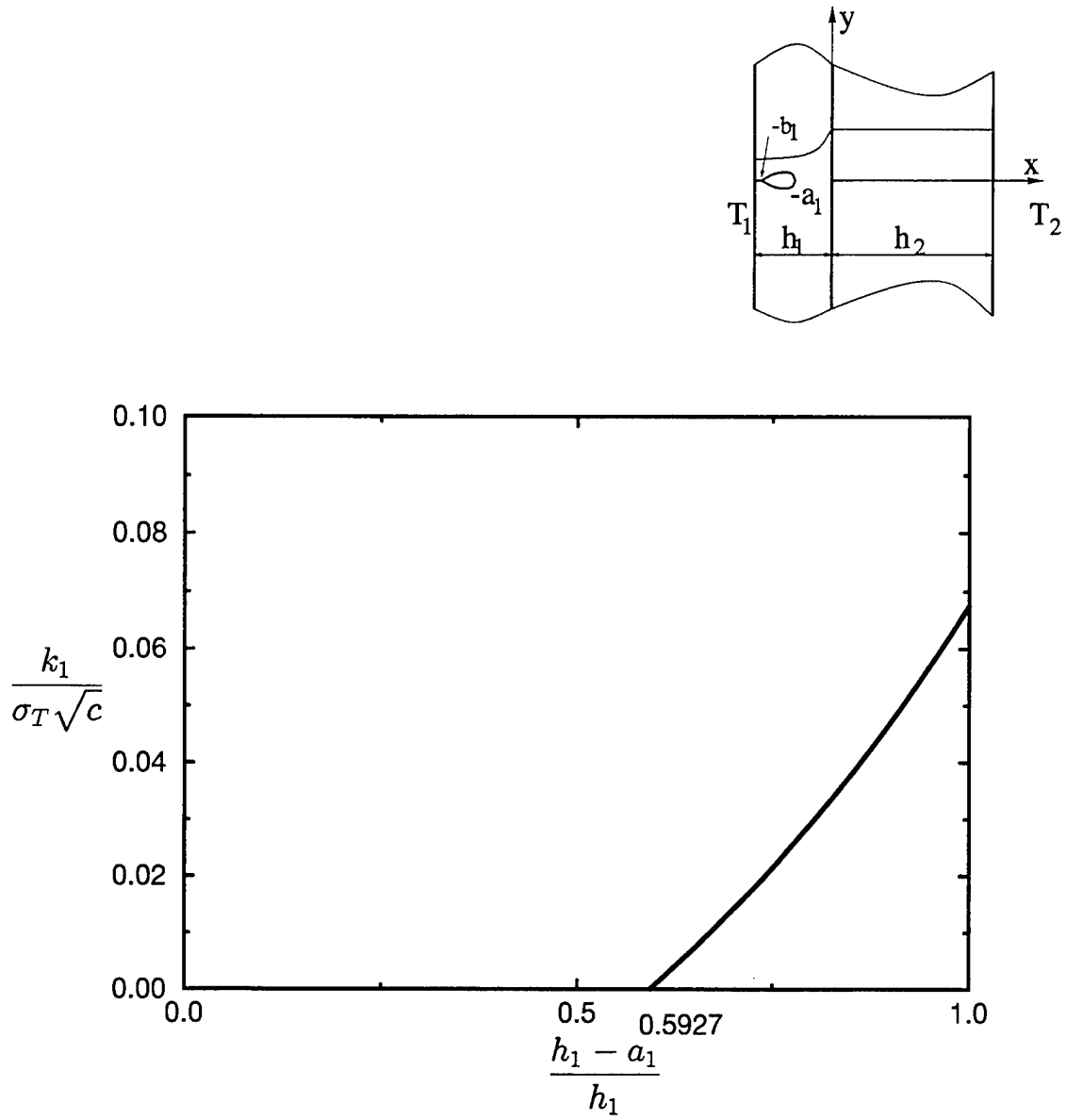


Figure 5.65 The effect of uniform temperature fall on normalized stress intensity

factor for an edge crack located in the nonhomogeneous layer.

$$c = \frac{(b_1 - a_1)}{2}, b_1 \text{ determined from Fig. 5.64, } \frac{h_2}{h_1} = 1.0,$$

$$\sigma_T = \frac{8\mu_0\alpha_0(T_0 - T)(1 + \nu)}{(1 + \kappa)}, \frac{\mu_0}{\mu_1} = e^{\beta h_1}, \frac{\alpha_0}{\alpha_1} = e^{\alpha h_1}, \frac{k_0}{k_c} = e^{\gamma h_1},$$

$$T_1 = T_2 = T < T_0, \beta h_1 = 0.375, \alpha h_1 = 0.513, \gamma h_1 = 2.5.$$

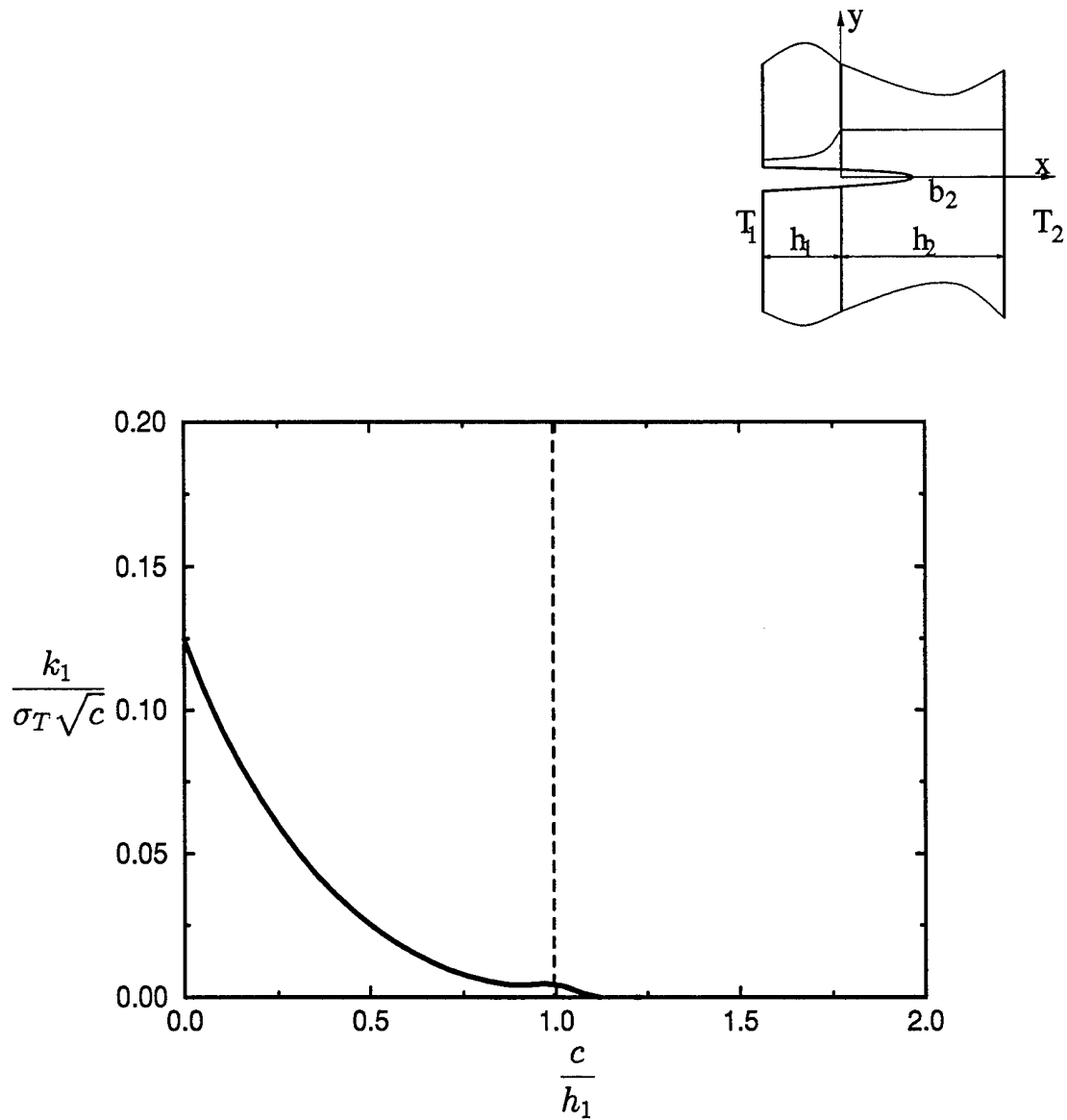


Figure 5.66 The effect of temperature fall at one boundary on normalized stress intensity factor for an edge crack passing through the interface.

$$c = \text{crack length, } b_1 = h_1, \frac{h_2}{h_1} = 1.0, \sigma_T = \frac{8\mu_0\alpha_0(T_0 - T_1)(1 + \nu)}{(1 + \kappa)},$$

$$T_2 = T_0, T_1 < T_0, \frac{\mu_0}{\mu_1} = e^{\beta h_1}, \frac{\alpha_0}{\alpha_1} = e^{\alpha h_1}, \frac{k_0}{k_c} = e^{\gamma h_1},$$

$$\beta h_1 = 0.375, \alpha h_1 = 0.513, \gamma h_1 = 2.5 \text{ (PSZ-René41).}$$

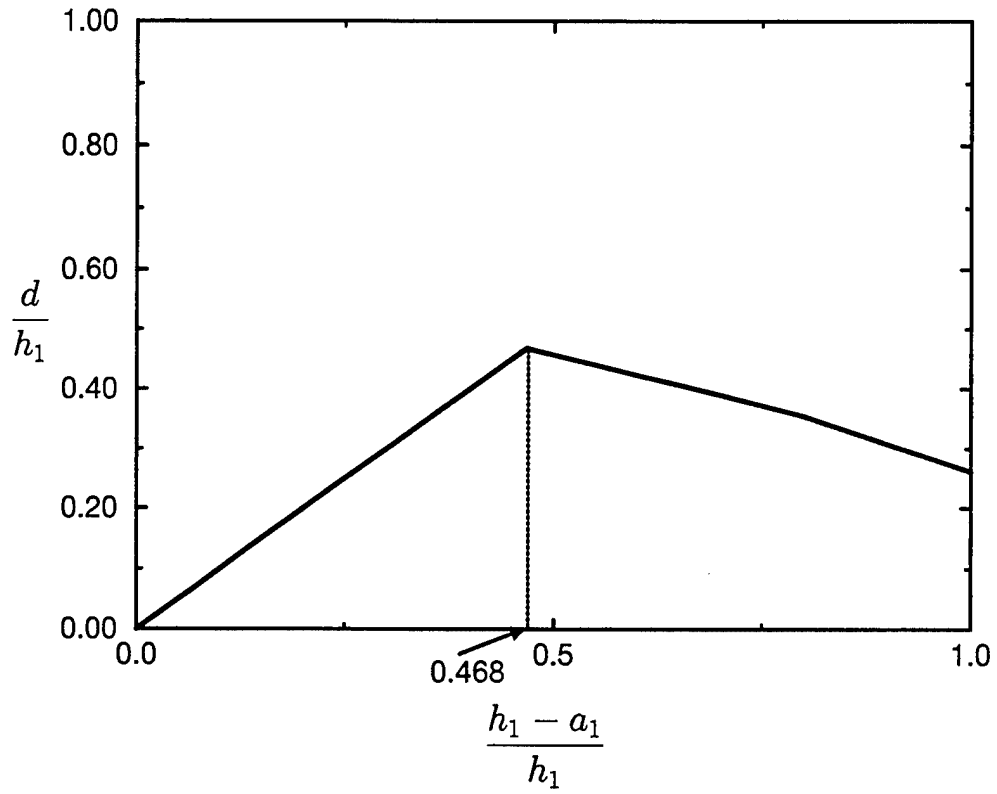
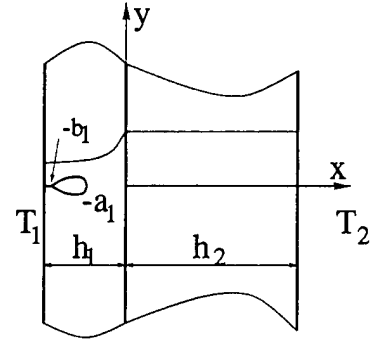


Figure 5.67 Crack closure length as a function of the location of the open crack tip

for an edge crack under uniform temperature rise. $T_1 = T_2 = T > T_0$,

$$d = \frac{h_1 - b_1}{h_1}, \frac{h_2}{h_1} = 1.0, \frac{\mu_0}{\mu_1} = e^{\beta h_1}, \frac{\alpha_0}{\alpha_1} = e^{\alpha h_1}, \frac{k_0}{k_c} = e^{\gamma h_1},$$

$$\beta h_1 = -0.2576, \alpha h_1 = -0.0513, \gamma h_1 = 1.2777 \text{ (PSZ-Ti-6Al-4V).}$$

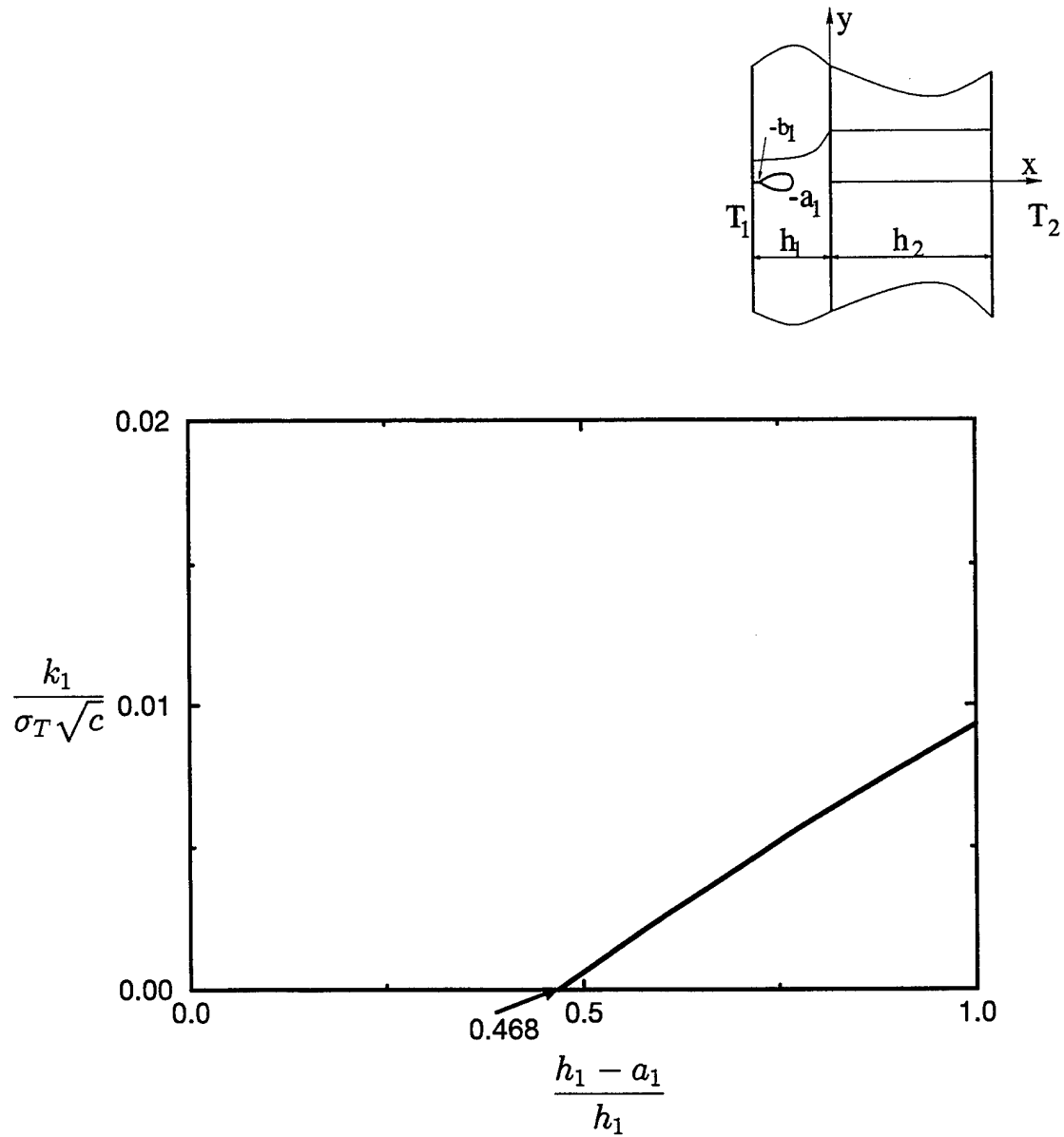


Figure 5.68 The effect of uniform temperature rise on normalized stress intensity

factor for an edge crack located in the nonhomogeneous layer.

$$c = \frac{(b_1 - a_1)}{2}, b_1 \text{ determined from Fig. 5.67,}$$

$$\frac{h_2}{h_1} = 1.0, T_1 = T_2 = T > T_0,$$

$$\sigma_T = \frac{8\mu_0\alpha_0(T - T_0)(1 + \nu)}{(1 + \kappa)}, \frac{\mu_0}{\mu_1} = e^{\beta h_1}, \frac{\alpha_0}{\alpha_1} = e^{\alpha h_1}, \frac{k_0}{k_c} = e^{\gamma h_1},$$

$$\beta h_1 = -0.2576, \alpha h_1 = -0.0513, \gamma h_1 = 1.2777 \text{ (PSZ-Ti-6Al-4V).}$$

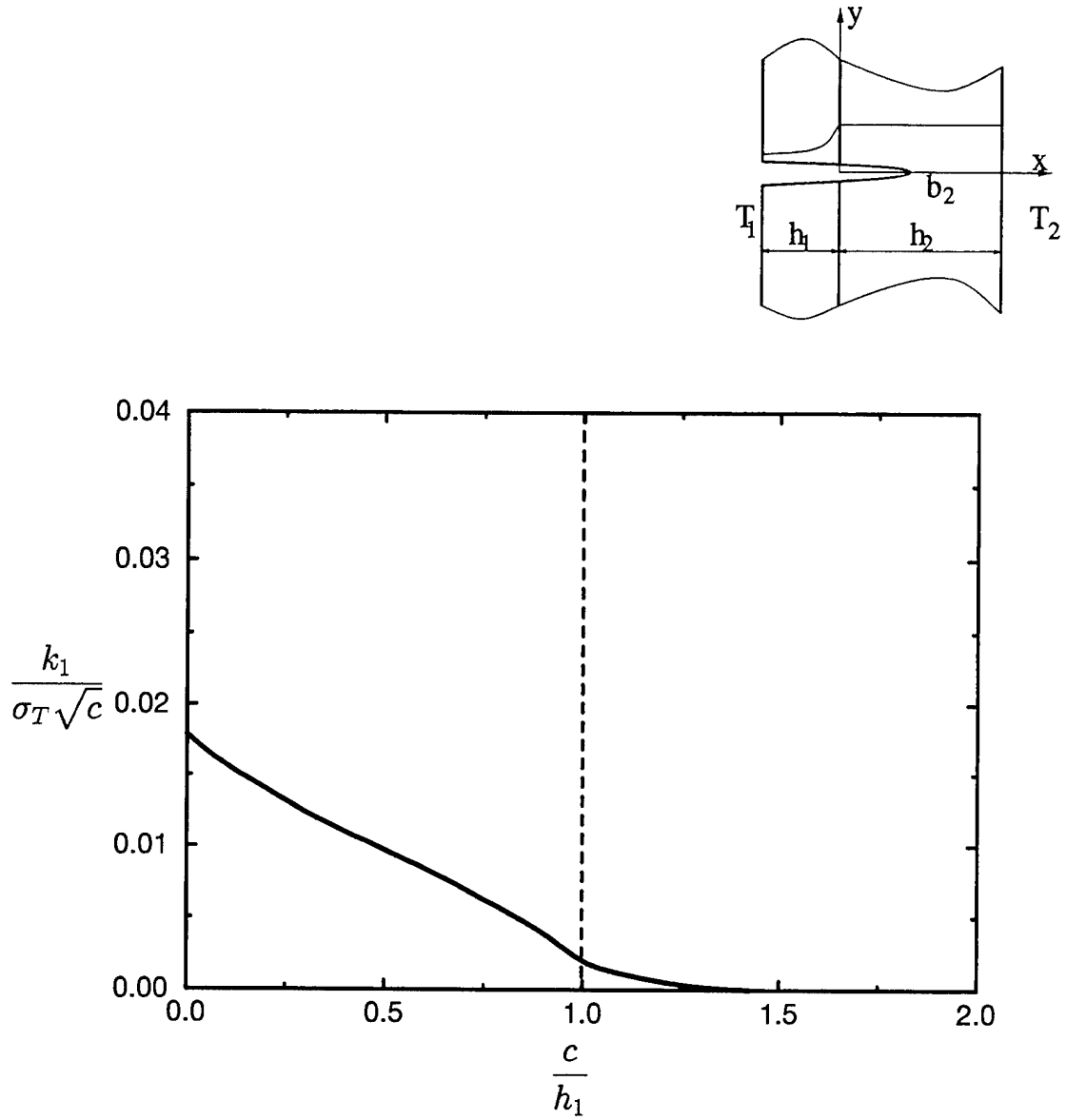


Figure 5.69 The effect of uniform temperature fall on normalized stress intensity

factor for an edge crack passing through the interface.

$$c = \text{crack length, } b_1 = h_1, \frac{h_2}{h_1} = 1.0, \sigma_T = \frac{8\mu_0\alpha_0(T_0 - T)(1 + \nu)}{(1 + \kappa)},$$

$$\frac{\mu_0}{\mu_1} = e^{\beta h_1}, \frac{\alpha_0}{\alpha_1} = e^{\alpha h_1}, \frac{k_0}{k_c} = e^{\gamma h_1}, T_1 = T_2 = T < T_0,$$

$$\beta h_1 = -0.2576, \alpha h_1 = -0.0513, \gamma h_1 = 1.2777 \text{ (PSZ-Ti-6Al-4V).}$$

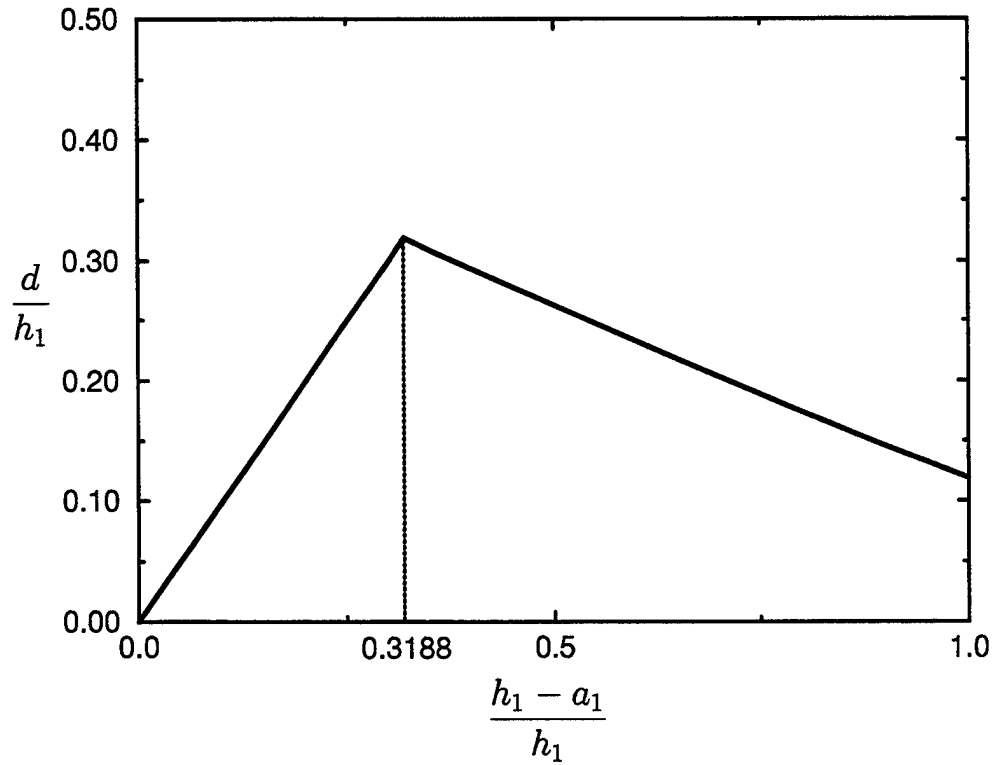
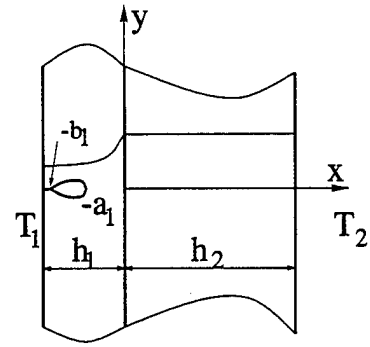


Figure 5.70 Crack closure length as a function of the location of the open crack tip

for an edge crack loaded thermally. $T_2 = T_0, T_1 > T_0$,

$$d = \frac{h_1 - b_1}{h_1}, \frac{h_2}{h_1} = 1.0, \frac{\mu_0}{\mu_1} = e^{\beta h_1}, \frac{\alpha_0}{\alpha_1} = e^{\alpha h_1}, \frac{k_0}{k_c} = e^{\gamma h_1},$$

$$\beta h_1 = -0.2576, \alpha h_1 = -0.0513, \gamma h_1 = 1.2777 \text{ (PSZ-Ti-6Al-4V).}$$

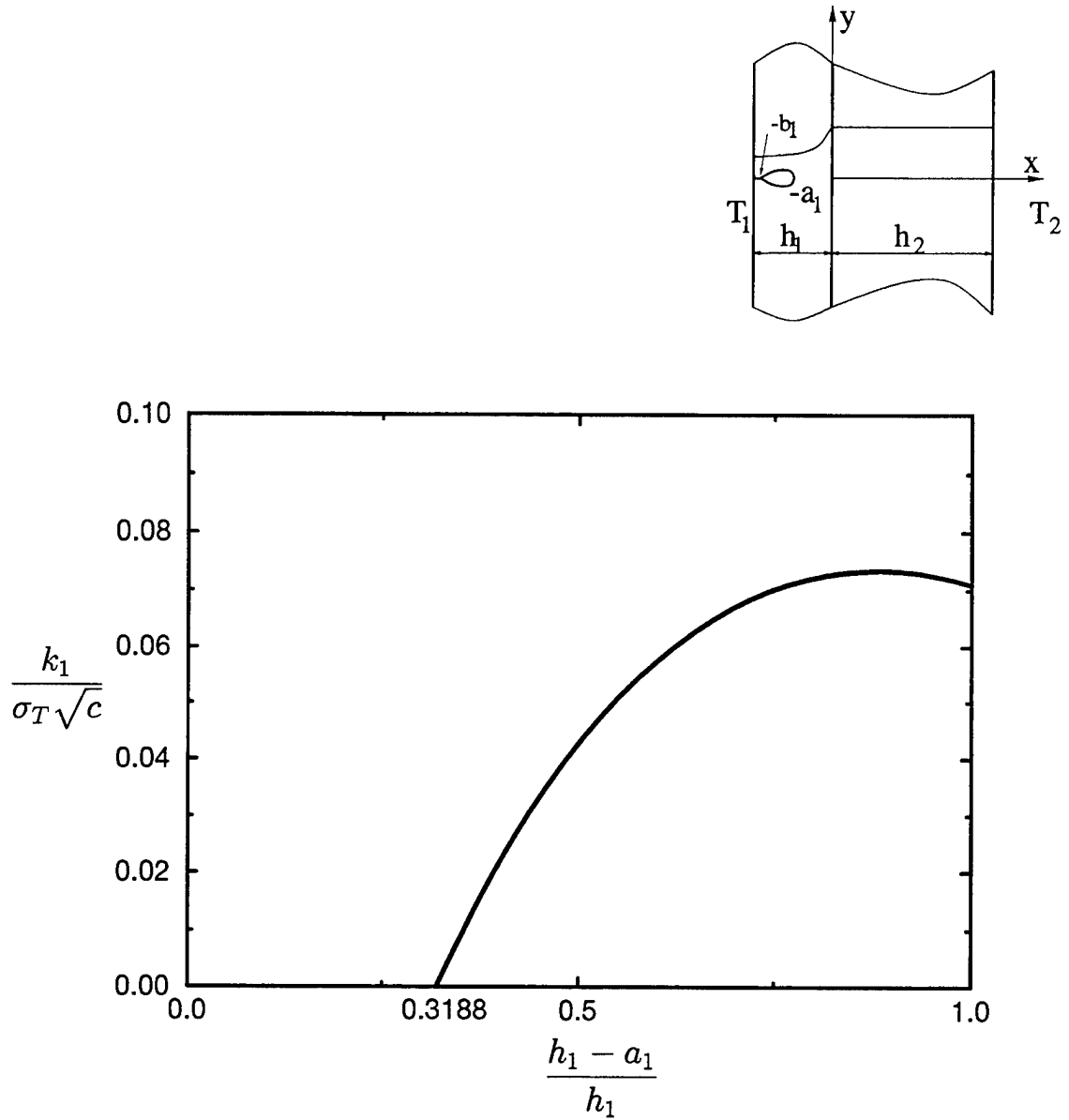


Figure 5.71 The effect of temperature rise at one boundary on normalized stress

intensity factor for an edge crack located in the nonhomogeneous layer.

$$c = \frac{(b_1 - a_1)}{2}, b_1 \text{ determined from Fig. 5.70, } \frac{h_2}{h_1} = 1.0, T_2 = T_0, T_1 > T_0,$$

$$\sigma_T = \frac{8\mu_0\alpha_0(T_1 - T_0)(1 + \nu)}{(1 + \kappa)}, \frac{\mu_0}{\mu_1} = e^{\beta h_1}, \frac{\alpha_0}{\alpha_1} = e^{\alpha h_1}, \frac{k_0}{k_c} = e^{\gamma h_1},$$

$$\beta h_1 = -0.2576, \alpha h_1 = -0.0513, \gamma h_1 = 1.2777 \text{ (PSZ-Ti-6Al-4V).}$$

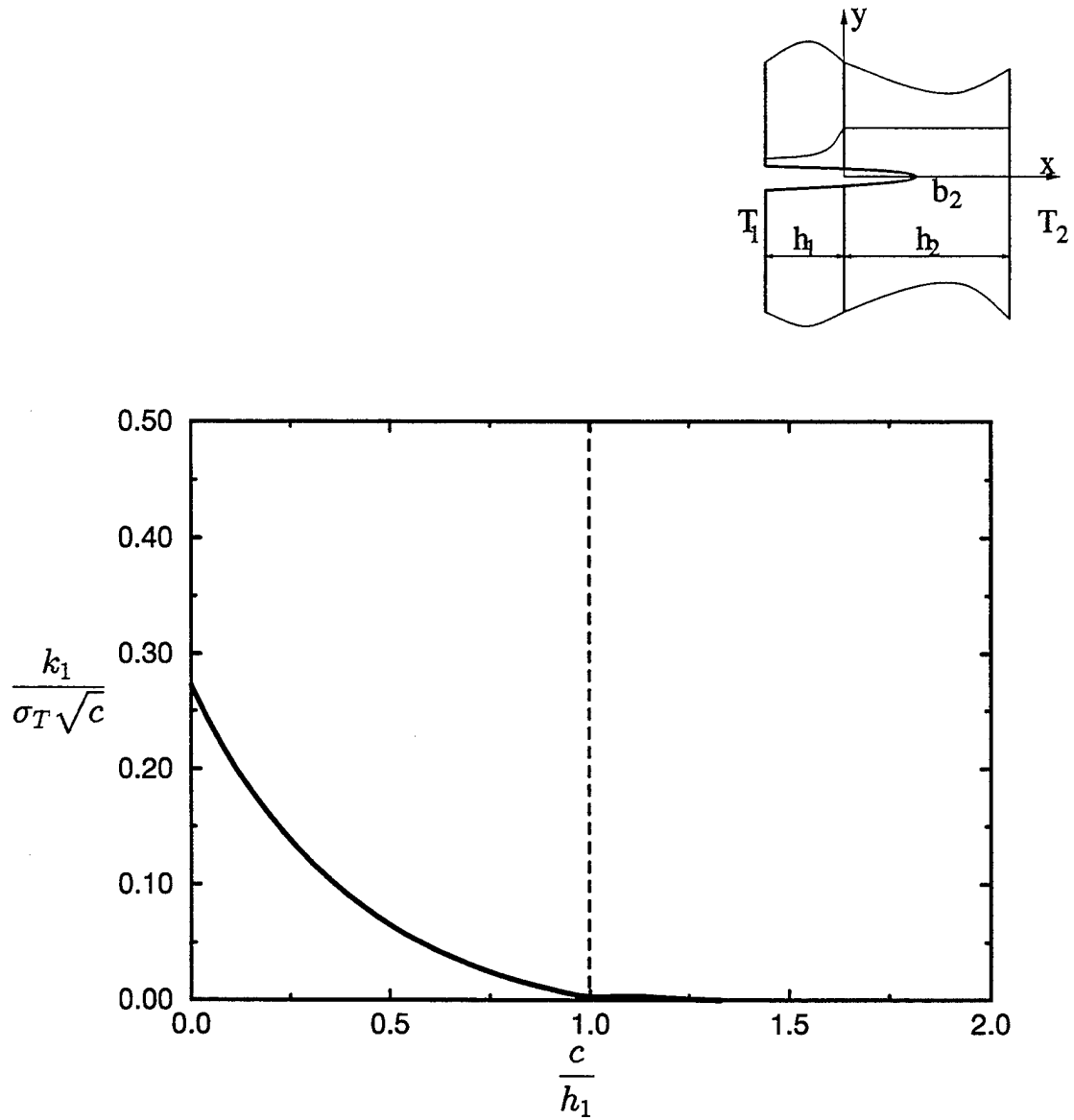


Figure 5.72 The effect of temperature fall at one boundary on normalized stress intensity factor for an edge crack passing through the interface.

$$c = \text{crack length}, b_1 = h_1, \frac{h_2}{h_1} = 1.0, \sigma_T = \frac{8\mu_0\alpha_0(T_0 - T_1)(1 + \nu)}{(1 + \kappa)},$$

$$\frac{\mu_0}{\mu_1} = e^{\beta h_1}, \frac{\alpha_0}{\alpha_1} = e^{\alpha h_1}, \frac{k_0}{k_c} = e^{\gamma h_1}, T_2 = T_0, T_1 < T_0,$$

$$\beta h_1 = -0.2576, \alpha h_1 = -0.0513, \gamma h_1 = 1.2777 \text{ (PSZ-Ti-6Al-4V).}$$

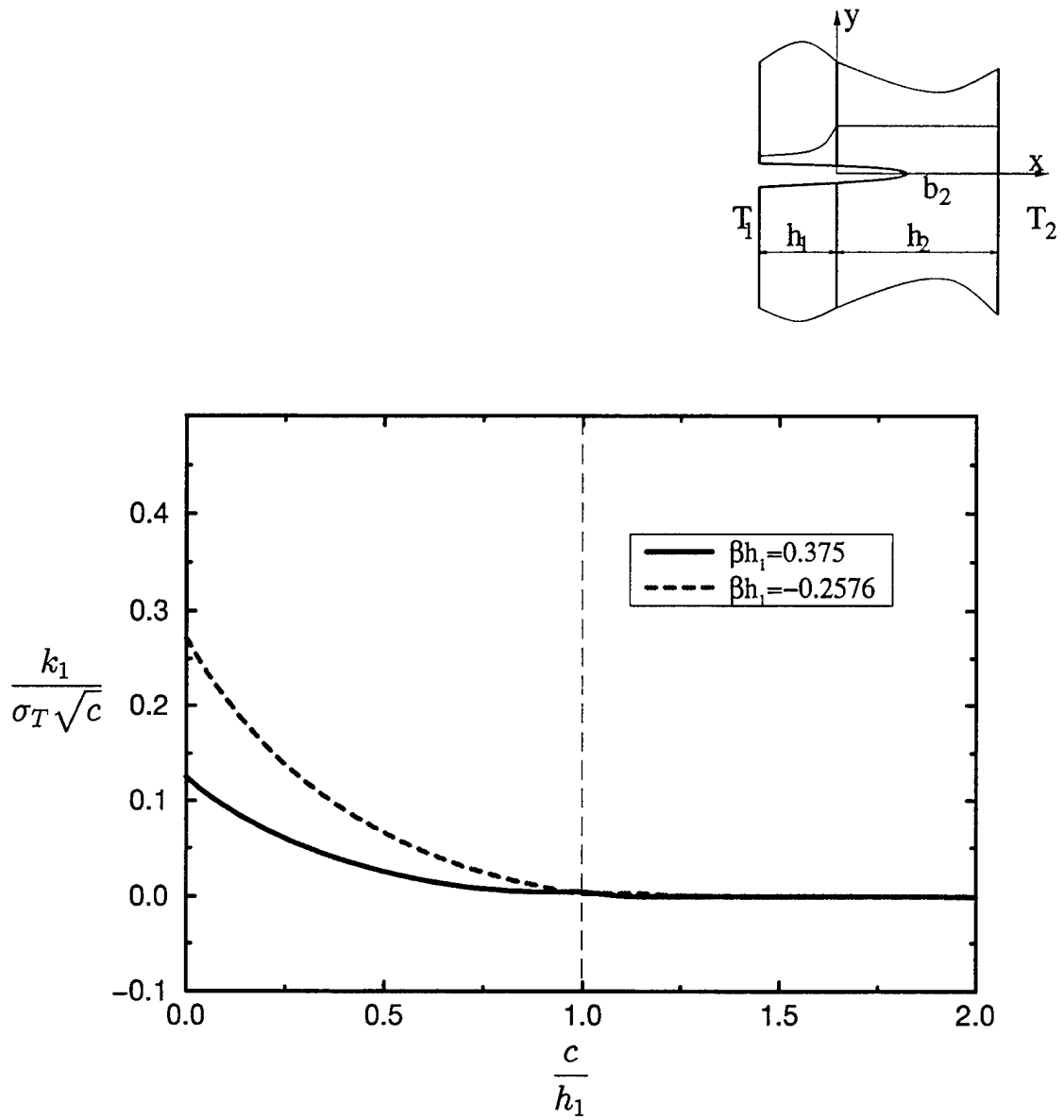


Figure 5.73 Comparative effect of temperature fall at one boundary on normalized stress intensity factor for an edge crack passing through the interface.

$$c = \text{crack length, } b_1 = h_1, \frac{h_2}{h_1} = 1.0, \sigma_T = \frac{8\mu_0\alpha_0(T_0 - T_1)(1 + \nu)}{(1 + \kappa)},$$

$$\frac{\mu_0}{\mu_1} = e^{\beta h_1}, \frac{\alpha_0}{\alpha_1} = e^{\alpha h_1}, \frac{k_0}{k_c} = e^{\gamma h_1}, T_2 = T_0, T_1 < T_0.$$

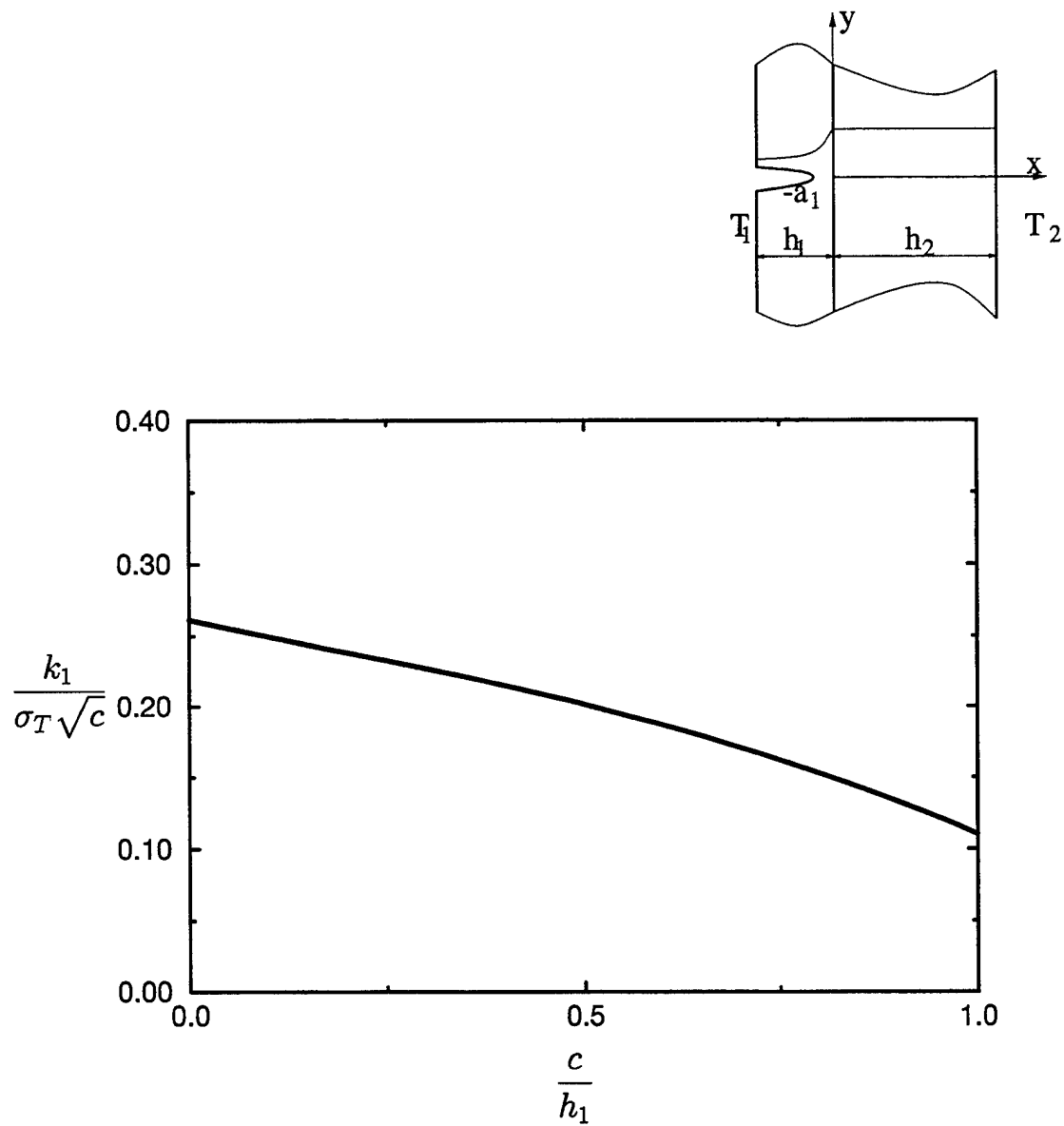


Figure 5.74 The effect of uniform temperature rise on normalized stress intensity factor for an edge crack located in the nonhomogeneous layer.

$$c = (b_1 - a_1), b_1 = h_1, \frac{h_2}{h_1} = 10.0, \sigma_T = \frac{8\mu_0\alpha_0(T - T_0)(1 + \nu)}{(1 + \kappa)},$$

$$\frac{\mu_0}{\mu_1} = e^{\beta h_1}, \frac{\alpha_0}{\alpha_1} = e^{\alpha h_1}, \frac{k_0}{k_c} = e^{\gamma h_1}, T_1 = T_2 = T > T_0,$$

$$\beta h_1 = 0.375, \alpha h_1 = 0.513, \gamma h_1 = 2.5 \text{ (PSZ-René41).}$$

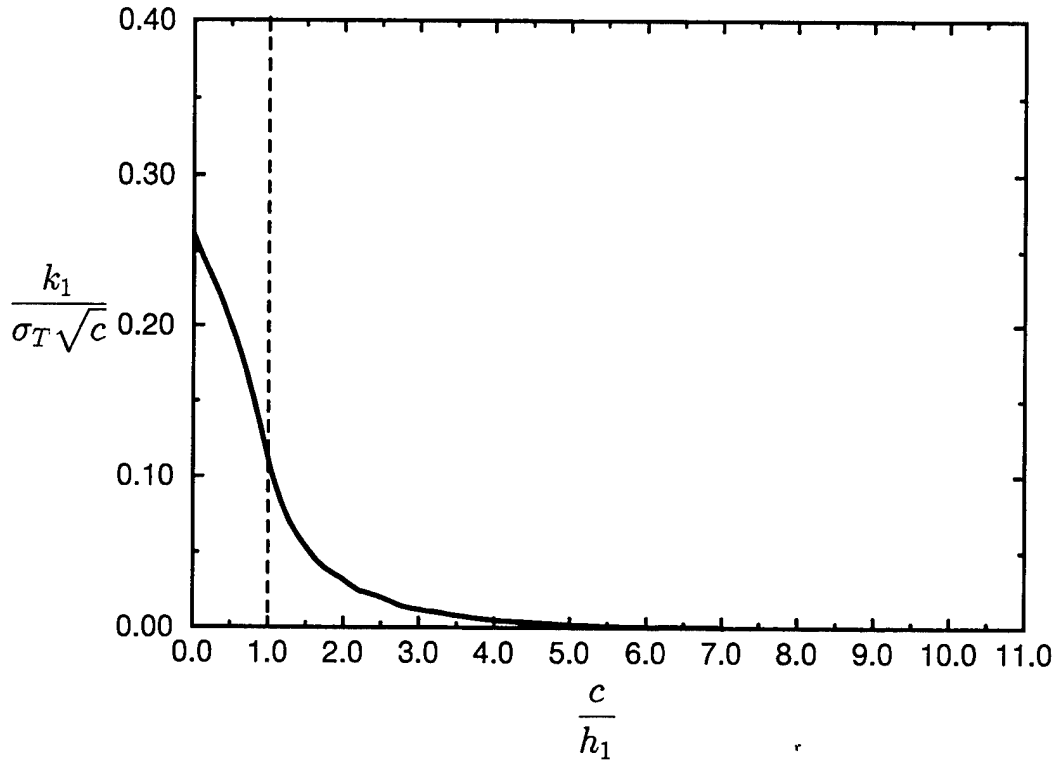
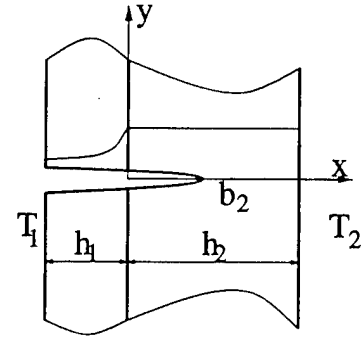


Figure 5.75 The effect of uniform temperature rise on normalized stress intensity

factor for an edge crack passing through the interface.

$$c = \text{crack length}, b_1 = h_1, \frac{h_2}{h_1} = 10.0, \sigma_T = \frac{8\mu_0\alpha_0(T - T_0)(1 + \nu)}{(1 + \kappa)},$$

$$\frac{\mu_0}{\mu_1} = e^{\beta h_1}, \frac{\alpha_0}{\alpha_1} = e^{\alpha h_1}, \frac{k_0}{k_c} = e^{\gamma h_1}, T_1 = T_2 = T > T_0,$$

$$\beta h_1 = 0.375, \alpha h_1 = 0.513, \gamma h_1 = 2.5 \text{ (PSZ-René41).}$$

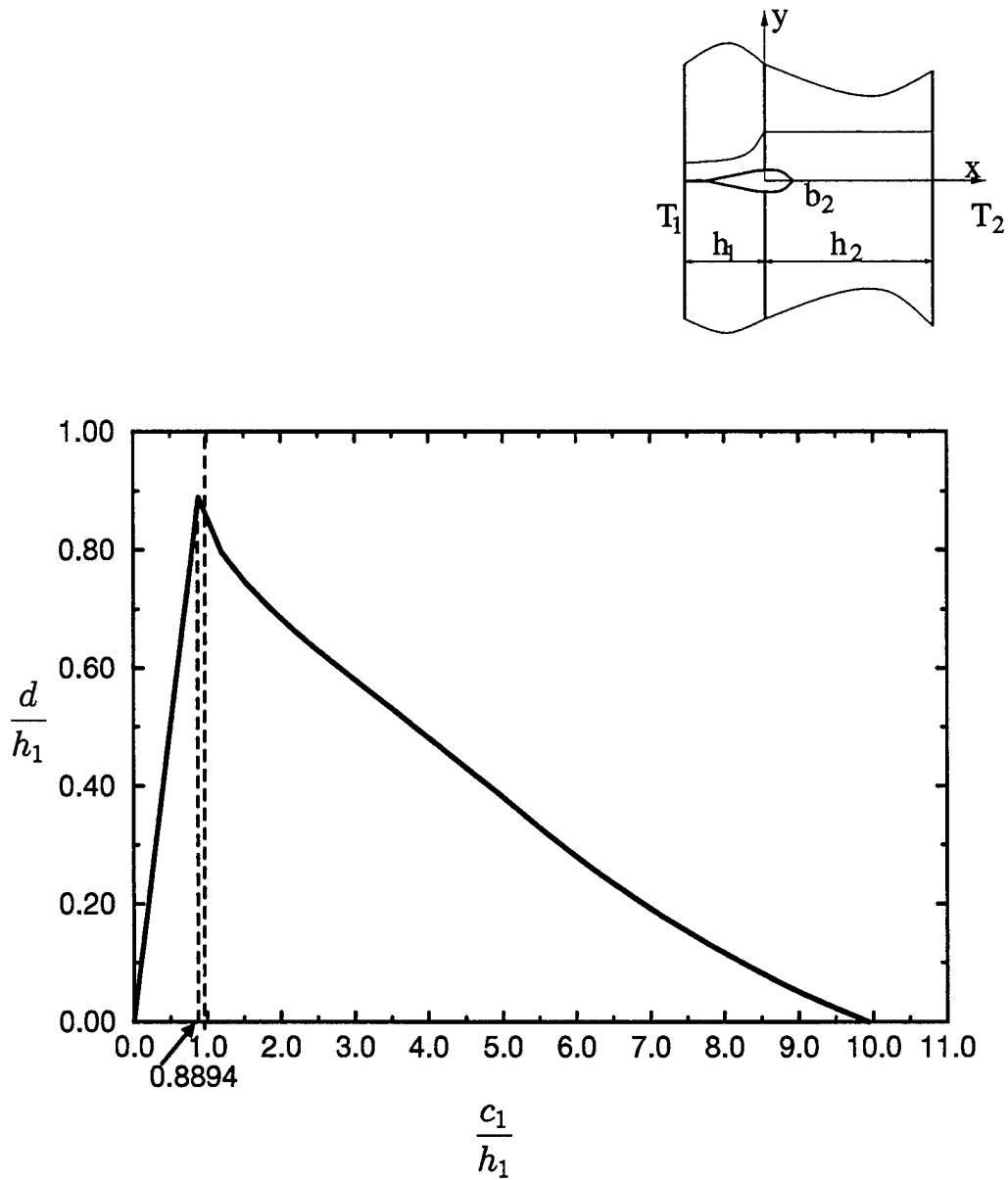


Figure 5.76 Crack closure length as a function of the location of the open crack tip

for an edge crack passing through the interface under uniform temperature

fall. $T_1 = T_2 = T < T_0$, $d = h_1 - b_1$, $\frac{h_2}{h_1} = 10.0$,

$$\frac{\mu_0}{\mu_1} = e^{\beta h_1}, \frac{\alpha_0}{\alpha_1} = e^{\alpha h_1}, \frac{k_0}{k_c} = e^{\gamma h_1},$$

$\beta h_1 = 0.375$, $\alpha h_1 = 0.513$, $\gamma h_1 = 2.5$ (PSZ-René41),

$c_1 = h_1 - a_1$ for crack in coating, $c_1 = h_1 + b_2$ for through crack.

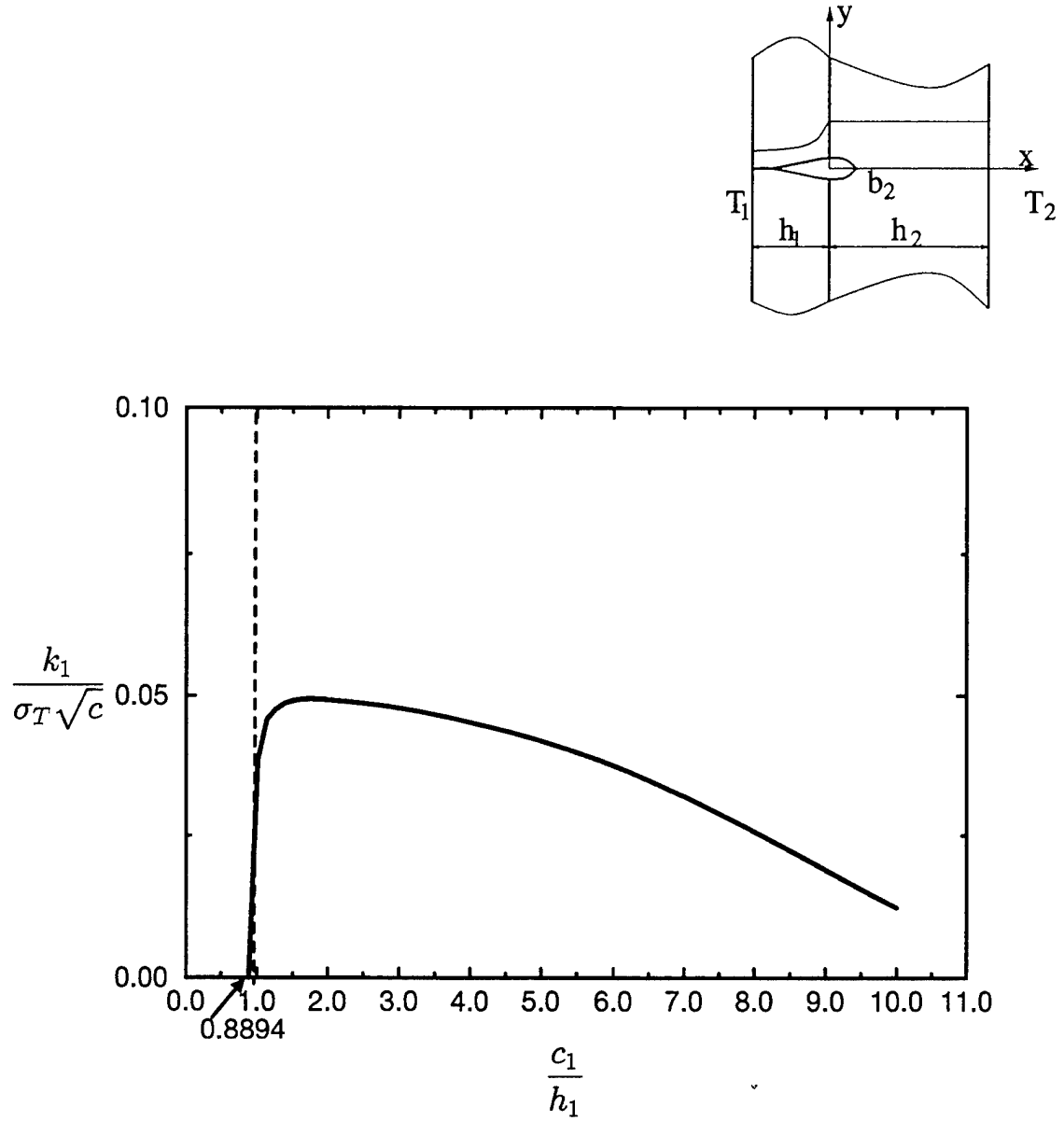


Figure 5.77 The effect of uniform temperature fall on normalized stress intensity

factor for an edge crack passing through the interface. c = half crack

length, b_1 determined from Fig. 5.76, $\frac{h_2}{h_1} = 10.0$, $T_1 = T_2 = T < T_0$,

$$\sigma_T = \frac{8\mu_0\alpha_0(T_0 - T)(1 + \nu)}{(1 + \kappa)}, \quad \frac{\mu_0}{\mu_1} = e^{\beta h_1}, \quad \frac{\alpha_0}{\alpha_1} = e^{\alpha h_1}, \quad \frac{k_0}{k_c} = e^{\gamma h_1},$$

$$\beta h_1 = 0.375, \quad \alpha h_1 = 0.513, \quad \gamma h_1 = 2.5 \text{ (PSZ-René41),}$$

$$c_1 = h_1 - a_1 \text{ for crack in coating, } c_1 = h_1 + b_2 \text{ for through crack.}$$

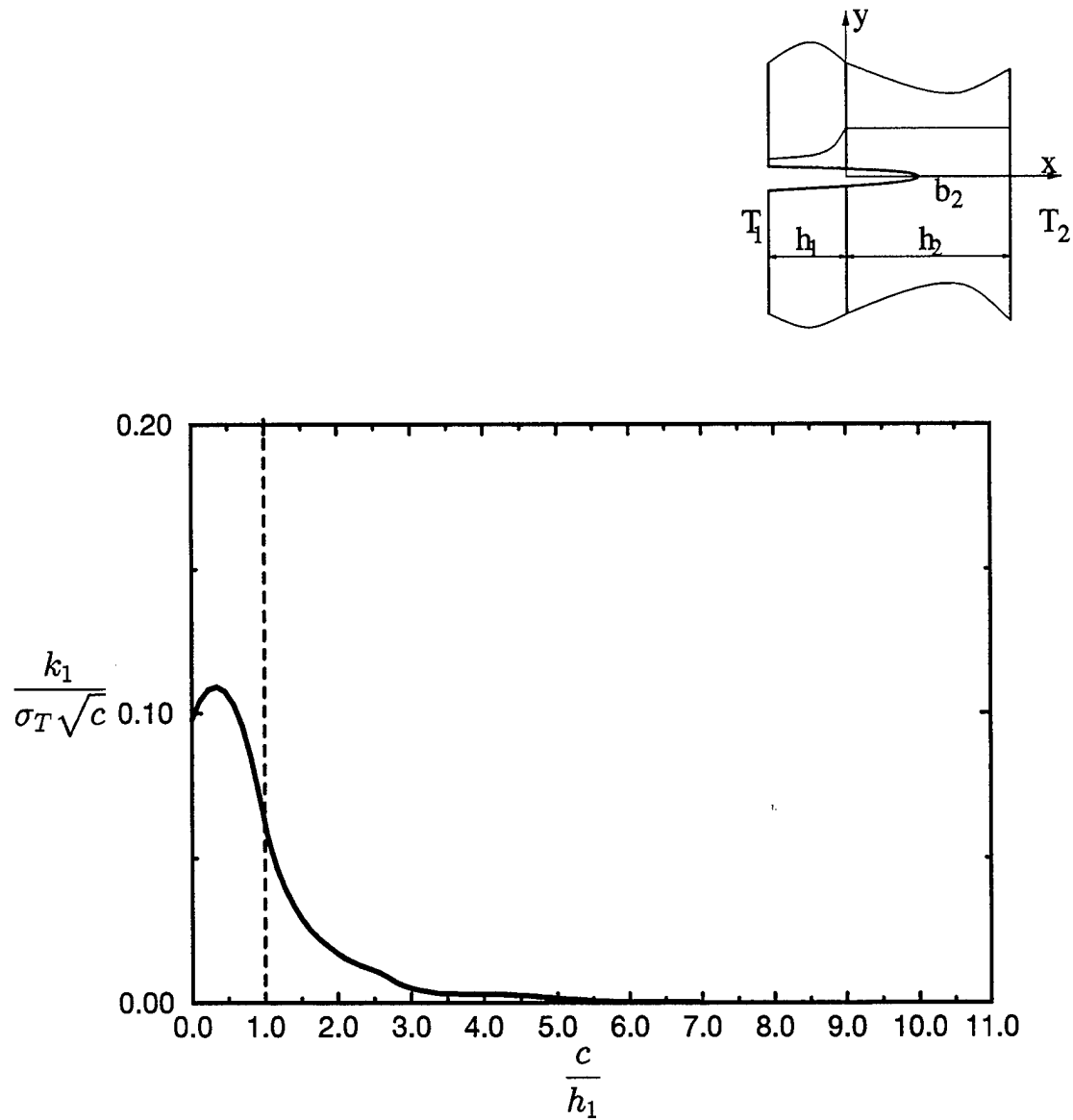


Figure 5.78 The effect of temperature rise at one boundary on normalized stress intensity factor for an edge passing through the interface.

$$c = \text{crack length}, b_1 = h_1, \frac{h_2}{h_1} = 10.0, \sigma_T = \frac{8\mu_0\alpha_0(T_1 - T_0)(1 + \nu)}{(1 + \kappa)},$$

$$\frac{\mu_0}{\mu_1} = e^{\beta h_1}, \frac{\alpha_0}{\alpha_1} = e^{\alpha h_1}, \frac{k_0}{k_c} = e^{\gamma h_1}, T_2 = T_0, T_1 > T_0$$

$$\beta h_1 = 0.375, \alpha h_1 = 0.513, \gamma h_1 = 2.5 \text{ (PSZ-René41).}$$

CHAPTER 6

CONCLUSIONS AND FUTURE WORK

6.1 Conclusions

In the work presented in this dissertation, the basic mode I crack problems of Functionally Graded Material coatings were studied. The substrate was assumed to be homogenous and of finite thickness. This allowed a parametric study to determine the influence of the substrate thickness on crack propagation. The model developed in this work can accommodate internal as well as edge cracks. Also, the problem of crack crossing the interface has been investigated.

From a theoretical point of view, the most important feature of this study is the determination of the singularity at the interface when a crack either touches the interface or when a crack passes through the interface. In all previous works published in literature on this subject, it was assumed that there is no singularity at the interface. The assumption is based on the physical nature of FGMs. Because the material property remains continuous through the interface, it was assumed that there will not be any singularity at the interface. Finite element programs based on this assumption lead to logical results. Hence the assumption has been widely accepted. But no mathematical proof of it was provided. The "kink" in the material property arising from the discontinuity in the first derivative, though, always raises some questions as to whether the assumption is well-founded. In [43], it was shown that if a crack in the homogeneous medium touches the interface, there is no singularity due to the interface. This is only one half of the problem, though. The real challenge is if the crack lies in the nonhomogeneous medium. In this study, an elaborate asymptotic analysis was performed at the interface. After rigorous manipulations and after some very meticulous algebra, it was shown conclusively that, in fact, there is no singularity at the interface. It does not matter whether the crack is in the

homogeneous medium or the nonhomogeneous medium or whether the crack is crossing the interface.

From a practical point of view, the most important question is the prediction of the life of the coating under various loading conditions. Hence a comprehensive fracture study of the FGM coating bonded to the homogeneous substrate was performed. The model provided is very flexible for the fracture study. It can accommodate a range of crack configurations. This has facilitated a systematic parametric fracture study for internal cracks, surface cracks and combination of two collinear cracks. Also, a range of loading conditions were considered. The applied loads were chosen so as to model the loading conditions in practical situations. Both mechanical and thermal loadings were considered. The results of interest are the stress intensity factors and the crack opening displacements.

It was shown that the stress intensity factors tend to increase as the crack enters the stiffer part of the graded material. This effect was previously observed in [42, 43, 46]. The increase in the stress intensity factor, though, should not be automatically assumed to lead to crack propagation. Crack propagation depends not only on the stress intensity factor (driving force) but also on the material toughness (resisting force). In the case of metal-ceramic Functionally Graded Materials, the material toughness is thought to increase with the metal content. An elaborate metallurgical analysis of the material toughness is required to determine the exact relation between the driving force and the resisting force.

Another parameter of interest was the substrate thickness. It was observed that the stress intensities were considerably lower for thicker substrates. This indicates that the coating could be made to last longer if the substrate thickness is relatively higher. In the case of edge cracks, it was observed that doubling the coating thickness reduced the stress intensity factor for a crack reaching the interface to almost half. Hence it is suggested that the ratio of substrate thickness to coating thickness $\frac{h_2}{h_1}$ should be maintained at safe levels

of 4 or higher. Fortunately, this is the case in most practical situations. The ratio $\frac{h_2}{h_1}$ is greater than 5 in most industrial applications.

During thermal loadings, a peculiar feature of crack closure was observed. It is an important feature when considering pure thermal loadings. It gives a characteristic length of the compressive zone where an existing flaw can remain dormant. Surface cracks in this zone will always remain suppressed. The length of the compressive zone is determined by a simple stress analysis of the uncracked specimen. Details of this analysis are provided in Section 5.2. If the characteristic surface flaw size is smaller than the length of the compressive zone, an elaborate fracture analysis may not be even necessary. It should, however, be noted that there might be other loadings superposed over the thermal loadings when considering practical situations. In that case, the flaw might propagate. The resultant stress intensity factor due to all loadings should be considered. In any case, the compressive part of the thermal loading will help reduce the stress intensities for surface cracks.

The analysis performed in this study is linear elastic. As such, the stress intensity factors due to various loadings can be added to obtain the resultant stress intensity factors. In this study, the stress intensity factors for individual loadings are provided. To apply these results in practical situations with multiple loadings, one needs to only add up the different stress intensity factors. It should, however, be noted that the results in this study are given in the normalized form. Care should be taken to take these normalizations in account before adding up the stress intensity factors.

In this study, it is assumed that the crack always propagates perpendicular to the nominal interface. This assumption has to be considered carefully in case of FGMs. For homogeneous materials under symmetric loading, the cleavage plane would be the plane of symmetry. This is the plane where the strain energy release rate G is maximum. As G_c , the critical strain energy release rate is same in all directions, the plane of symmetry would be

the preferred plane of crack propagation. In FGMs, though, the situation is different. G again is maximum along the plane of symmetry. G_c has to be determined carefully. This problem can be looked in two different ways. In the first case, we assume that the crack growth is infinitesimal. In this case, the material being isotropic, critical strain energy release rate G_c is the same in all directions. Hence, again, the crack propagation would be along the plane of symmetry. The assumption of infinitesimal crack growth is, however, not very practical. At the crack tip, the crack propagation will be in finite jumps which usually are of the dimension of the grain size. Though the grain size of ceramics can be very small, the grain size of metals can be large. If we consider the average grain size to be about $10\ \mu$, we can no longer assume infinitesimal crack growth. This leads to the possibility of varying G_c in different directions. Depending on the material, G_c might be lower in a direction not perpendicular to the interface. Crack propagation will take place in a direction where $G - G_c$ is maximum and it is possible that this direction might not be the plane of symmetry. Again, a careful metallurgical analysis is required to determine G_c accurately.

Another limitation of this analysis is that plasticity has not been considered. It is readily acknowledged that plasticity may play a major role in the metal-rich region of the FGM and in the substrate. However, it is assumed that the crack growth considered here is subcritical where the small scale yielding at the crack tip does not affect the large scale K -field. This analysis is useful in creep and fatigue studies. Rapid crack propagation affected by plasticity will, however, be out of consideration here. The reason plasticity has not been included in the analysis is because of the complexity it introduces. A pure continuum analysis including plasticity for a problem of the scale considered in this study is analytically intractable. It is suggested that such problems be solved using Finite Element Analysis. The results of this study would be good benchmarks for Finite Element community.

6.2 Future work

The discussions in the previous section leads to the future work to be done in this field. The following problems are some of the problems to be considered.

1. Introduction of plasticity

As discussed before, plasticity would play a major role in stress analysis and fracture characterization of FGMs. It is, however, very difficult, if not impossible, to introduce plasticity in a continuum model for this problem. The purely linear elastic problem itself is highly complex. The analysis is very involved and time-consuming. It is therefore suggested that Finite Element Analysis be used to address the problems involving plasticity. The results in the work presented in this dissertation will be of use in elastic FEM analysis. For example, the crack tip singularities are only square root singularities. Hence only such elements need to be used at the crack tip. The bimaterial interface is only a nominal one. No singularity needs to be embedded in the elements at the interface.

2. Determination of direction of propagation of crack

This problem has also been discussed in Section 6.1. For every crack length, it is necessary to assume a finite crack increment. For every crack increment, the difference $G - G_c$ can be evaluated. The maximum value will determine the direction of the crack increment. Though this problem can be solved analytically, it is much easier to attempt it by Finite Element Analysis. The problem will be a mixed mode problem. That will introduce more complexity but will be a better model of practical situations.

REFERENCES

1. Bunk, W.G.J., "Advanced aerospace materials", FGM '90 Proceedings of the 1st International Symposium on Functionally Gradient Materials, Functionally Gradient Materials Forum, Sendai, Japan, pp. 1-2, 1990.
2. Koizumi, M., "Challenging to the inhomogeneous materials production-status and aspects", FGM '90 Proceedings of the 1st International Symposium on Functionally Gradient Materials, Functionally Gradient Materials Forum, Sendai, Japan, pp. 3-4, 1990.
3. Lee, W.Y., Bae, Y.W., Berndt, C.C., Erodogan, F., Lee, Y.-D., Mutasim, Z., "The concept of functionally gradient materials for advanced thermal barrier coating applications; a review", *Journal of the American Ceramic Society*, Vol. 79, No. 3, pp., 1996
4. Nissley, D.M., "Thermal barrier coating life modeling in aircraft gas turbine engines", Thermal Barrier Coating Workshop, Proceedings of a conference held at NASA Lewis Research Center, Cleveland, Ohio, pp. 265-281, March 1995.
5. Hirano, T., Yamada, T., Teraki, J., Niino, M., Kumakawa, A., "A study of functionally gradient material design system for a thrust chamber", Proceedings of the 16th International Symposium of Space Technology and Science, Sapporo, Japan, May 1988.
6. Kurihara, K., Sasaki, K., Kawarada, M., "Adhesion improvement of diamond films", FGM'90, pp. 65-69, 1990.

7. Yamanouchi,M., Koizumi,M.,Hirai,T.,Shiota,I.(Eds), FGM '90 Proceedings of the 1st International Symposium on Functionally Gradient Materials, Functionally Gradient Materials Forum, Sendai, Japan,1990.
8. Hirano,T., Teraki,J., Yamada,T.," On the design of functionally gradient materials", FGM '90 Proceedings of the 1st International Symposium on Functionally Gradient Materials, Functionally Gradient Materials Forum, Sendai, Japan,pp. 5-10, 1990.
9. Hirano,T., Yamada,T., "Multi-paradigm expert system architecture based upon the inverse design concept". International workshop on Artificial Intelligence for Industrial Applications, Hitachi, Japan, 1988.
10. Bunshah,R.F., Blocher,J.M., Mattox,D.M., Bonifield,T.D., McGuire,G.E., Fish,J.G., Schwartz,M., Ghate,P.B., Thorton,J.A., Jacobson,B.E., Tucker,R.C., Deposition Technologies for Films and Coatings, Noyes Publications, New Jersey, U.S.A., 1982.
11. Hirai,T., Sasaki,M.,"Vapor-deposited functionally gradient materials", *JSME International Journal*, Series I, Vol. 34, No.2, pp.123-129,1990.
12. Fukui,Y.,"Fundamental investigation of functionally gradient material manufacturing system using centrifugal force", *JSME International Journal*, Series I, Vol. 34, No.2, pp. 144-148,1990.
13. Tanihata,K., Miyamoto,Y., Matsuhita,K., Ma,X., Kawasaki,A., Watanabe,R., Hirano,K.,"Fabrication of CrC/Ni functionally gradient materials by gaspressure

combustion sintering", submitted to 2nd International Symposium on FGM, San Francisco, Nov. 2-4, 1992.

14. Miyamoto, Y., "New ceramic processing approaches using combustion synthesis under gas pressure", *The American Ceramics Society Bulletin*, Vol. 69, No. 4, pp. 686-690, 1990.

15. Steffens, H., Dvorak, M., Wewel, M., "Plasma sprayed functionally gradient materials", FGM '90 Proceedings of the 1st International Symposium on Functionally Gradient Materials, Functionally Gradient Materials Forum, Sendai, Japan, pp. 139-144, 1990.

16. Hirai, T., "Functionally gradient materials", *Processing of Ceramics*, Part 2, Brook, R.J. (Ed), pp 295-341.

17. Benien, H., Meyer, M., Sucentrunk, R., "Application of functionally gradient materials in the aerospace industry", FGM '90 Proceedings of the 1st International Symposium on Functionally Gradient Materials, Functionally Gradient Materials Forum, Sendai, Japan, pp. 135-138, 1990.

18. Stewart, D.A., Leiser, D.B., Kolodziej, P., Smith, M., "Thermal response of integral multi-component composite thermal protection system", *Journal of Spacecraft and Rockets*, Vol. 23, pp. 420-427, 1986.

19. Shiau, F.Y., Zuo, Y., Zeng, X.Y., Lin, J.C., Chang, Y.A., "Interfacial reactions between Co and GaAs", *Adhesion in Solids*, Material Research Society Symposium Proceedings, Vol. 119, pp. 171-176, MRS, Pittsburgh, PA, 1988.

20. Hruban,K., "The semi-infinite solid with variable modulus of elasticity", *Bulletin of International Academy of Tcheque. Sciences*, Vol. 13, pp.46, 1944.
21. Olszak,W.(Ed), "Non-homogeneity in elasticity and plasticity", IUTAM Symposium, Warsaw, 1958, Permagon Press Ltd.,1959.
22. Golecki,J., " On the foundations of the theory of elasticity of plane incompressible non-homogeneous bodies", Non-homogeneity in elasticity and plasticity, Olszak,W.(Ed), IUTAM Symposium, Warsaw, 1958, Permagon Press Ltd., pp. 39-51,1959.
- 23.Erdogan,F., Gupta,G.D., "Layered composites with an interface flaw", *International Journal of Solids and Structures*, Vol. 7, pp.1089-1107,1971.
24. Rice,J.R., "Elastic fracure mechanics concepts for interfacial cracks", *ASME Journal of Applied Mechanics*, Vol. 55, pp.98-103, 1988.
25. Suo,Z., Hutchinson,J.W., "Interface crack between two elastic layers", *International Journal of Fracture*, Vol 43, pp.1-18, 1990.
26. Lu,M., Erdogan,F., "Stress intensity factors in two bonded elastic layers containing cracks perpendicular to and on the interface-I Analysis", *Engineering Fracutue Mechanics*, Vol. 18, pp.491-506, 1983.

27. Lu,M., Erdogan,F., "Stress intensity factors in two bonded elastic layers containing cracks perpendicular to and on the interface-II Solution and results", *Engineering Fracture Mechanics*, Vol. 18, pp.507-528, 1983.
28. Khrapkov,A.A., "Firat fundamental problem for a piecewise-homogeneous plane with a slit perpendicular to the line of separation", *Journal of Applied Mathematics and Mechanics*, Vol. 32, pp.666-678, 1972.
29. Cook,T.S., Erdogan,F., "Stresses in bonded materials with a crack perpendicular to the interface", *International Journal of Engineering Sciences*, Vol. 10, pp.677-697, 1972.
30. Gupta,G.D., "A layered composite with broken laminate", *International Journal of Solids and Structures*, Vol. 9, pp.1141-1154, 1973.
31. Erdogan,F., Cook,T.S., "Antiplane shear cracks terminating at and going through a bimaterial interface", *International Journal of Fracture*, Vol. 10, pp.227-240, 1974.
32. Cannon,R.M., Fisher,R.M., Evans,A.G., "Decohesion of thin films from ceramics", *Material Research Society Symposium Proceedings*, Vol. 54, pp. 799-804, 1986.
33. Torquato,S., "Random heterogeneous media: Microstructure and improved bounds on effective properties", *Applied Mechanics Review*, Vol. 44, No 2, pp. 37-76, 1991
34. Hashin,Z., Strickman,S., "A variational approach to the theory of the elastic behaviour of multiphase materials", *Journal of Mechanics and Physics of Solids*, Vol. 11, pp. 127-140, 1963.

35. Varley,E., Saymour,B.A., "A method for obtaining exact solutions to partial differential equations with variable coefficients", *Studies in Applied Mathematics*, Vol. 78, pp. 183-225, 1988.
36. Kassir,M.K., "Boussinesq problem for nonhomogeneous solids", *Journal of Engineering Mechanics*, Vol. 98, pp. 457-470, 1972.
37. Kassir,M.K., Chauprasert,M.A., "A rigid punch in contact with a nonhomogeneous solid", *ASME Journal of Applied Mechanics*, Vol. 41, pp. 1019-1024, 1974.
38. Bakirtas,I., "The problem of a rigid punch on a nonhomogeneous elastic half space", *International Journal of Engineering Sciences*, Vol. 18, pp. 597-610, 1980.
39. Konda,N., Erdogan,F., "The mixed mode crack problem in a nonhomogeneous elastic plane", Report to the Office of Naval Research, 1989.
40. Delale,F., Erdogan,F., "Interface crack in a nonhomogeneous elastic medium", *International Journal of Engineering Sciences*, Vol. 26, pp. 559-568, 1988b.
41. Chen,Y., Erdogan,F., "The interface crack problem in nonhomogeneous bonded materials of finite thickness", Report to the Office of Naval Research, 1992.
42. Erdogan,F., "The crack problem for bonded nonhomogeneous materials under antiplane shear loading", *ASME Journal of Applied Mechanics*, Vol. 52, pp. 823-828, 1985.

43. Erdogan,F., Kaya.A.C., Joseph,P.F., "The crack problem in bonded nonhomogeneous materials", *ASME Journal of Applied Mechanics*, Vol. 58, No. 2, pp. 410-418, 1991.
44. Erdogan,F., Kaya.A.C., Joseph,P.F., "The mode III crack problem in bonded materials with a nonhomogeneous interfacial zone", *ASME Journal of Applied Mechanics*, Vol. 58, No. 2, pp. 419-427, 1991.
45. Erdogan,F., Ozturk,M., "Diffusion problems in bonded nonhomogeneous materials with an interface cut", *International Journal of Engineering Sciences*, Vol. 30, pp. 1507-1523, 1992.
46. Erdogan,F., Wu,B.H., "The surface crack problem for a plate with functionally graded properties", Report to Air Force Office of Scientific Research, Grant F49620-93-1-0252, 1994.
47. Miller,C.J., Millavec,W.A., Kicher,T.P., "Thermal stress analysis of layered cylindrical shells", *American Institute of Aeronautics and Astronautics Journal*, Vol. 19, No. 4, pp. 523-530, 1981.
48. Venkataramana, J., "Thermal stresses in heterogeneous thick isotropic shells", *Nuclear Engineering and Design*, Vol. 30, pp. 369-378, 1974.
- 49 Fuchiyama,T., Noda,N., Tsuji,T., Obata,Y., "Analysis of thermal stress and stress intensity factor of functionally gradient materials", *Ceramic Transactions: Functionally*

Gradient Materials, Eds.:Holt,J.B., Koizuni,M., Hirai,T., Munir,Z.A., The American Ceramic Society, Westerville, Ohio, Vol. 34, pp. 425-432, 1993.

50. Schneider,G.A., Petzow,G.,"Thermal shock evaluation of functionally gradient materials", FGM '90 Proceedings of the 1st International Symposium on Functionally Gradient Materials, Functionally Gradient Materials Forum, Sendai, Japan, pp. 327-332, 1990.

51. Noda,N., Tsuji,T.,"Steady thermal stresses in a plate of functionally gradient material", FGM '90 Proceedings of the 1st International Symposium on Functionally Gradient Materials, Functionally Gradient Materials Forum, Sendai, Japan, pp. 339-344, 1990.

52. Obata,Y., Noda,N.,"Transient thermal stresses in a plate of functionally gradient material", Ceramic Transactions: Functionally Gradient Materials, Eds.:Holt,J.B., Koizuni,M., Hirai,T., Munir,Z.A., The American Ceramic Society, Westerville, Ohio, Vol. 34, pp.403-410, 1993.

53. Erdogan,F., Wu,B.H.,"Crack problems in FGM layers under thermal stresses", Report to Air Force Office of Scientific Research, Grant F49620-93-1-0252, 1994.

54. Zhang,Q.-J., Zhang,L.-M., Yuan,R.-Z.,"A coupled thermoelasticity model of functionally gradient materials under sudden high surface heating", Ceramic Transactions: Functionally Gradient Materials, Eds.:Holt,J.B., Koizuni,M., Hirai,T., Munir,Z.A., The American Ceramic Society, Westerville, Ohio, Vol. 34, pp.99-106, 1993.

55. Kaya,A.C., Erdogan,F., "Stress intensity factors and COD in an orthotropic strip", *International Journal of Fracture*, Vol. 16, No. 2, pp.171-190, 1980.
- 56.Erdogan,F., "Slow crack growth in glasses and ceramics under residual and applied stresses", *Journal of Electronic Packaging*, Vol. 111, pp.61-67, 1989.
57. Bakioglu,M., Erdogan,F., "The crack-contact and the free-end problem for a strip under residual stress", *ASME Journal of Applied Mechanics*, Vol. 44., pp. 41-46, 1976.
58. Bakioglu,M., Erdogan,F., Hasselman,D.P.H., "Fracture mechanical analysis of self-fatigue in surface compression strengthened glass plates", *Journal of Materials Science*, Vol. 11, pp. 1826-1834, 1976.
59. Erdogan,F., Cook,T.S., "Antiplane shear crack terminating at and going through a bimaterial interface", *International Journal of Fracture*, Vol. 10, No. 2, pp. 227-240, 1974.
60. Erdogan,F., "Mixed boundary value problems", *Mechanics Today*, Ed.: S.Nemat-Nasser, Pergamon Press, Oxford, Vol. 14, pp. 1-86, 1978.
61. Erdogan,F., "Complex function technique", *Continuum Physics*, Ed.: A.C. Eringen, Academic Press, pp. 524-603, 1975.
62. Erdogan,F., Gupta,G.D., Cook,T.S., "Numerical solution of singular integral equations", *Methods of Analysis and Solutions of Crack Problems*, Ed.: G.C.Sih, Noordhoff International Publishing, Leyden, pp. 368-425, 1973.

63. Joseph,P., "Plates and shells containng a surface crack under general loading conditions", Ph.D. Dissetation, Lehigh University, 1987.
64. Stroud,A.H., Secrest,D., "Gaussian Quadrature Formula", Prentice Hall, Englewood Cliffs, New Jersey, 1986.
65. Abramovitz,M., Stegun,I.A., "Handbook of Mathematical Functions", Dover Publications, Inc., New York, 1965.
66. Muskhelishvili,N.I., "Singular Integral Equations", Noordhoff International, Leyden, 1977.
67. Rizk,A.E.A., "Cracking of a layered medium on an elastic foundation under thermal shock", Ph.D. Disseratation, Lehigh University, 1988.
68. Gatewood, B.E., "Thermal stresses with applications to airplanes, missiles, turbines and nuclear reactors", McGraw-Hill Book Company, Inc., New York, 1957.
69. Lee, Y.-D., Erdogan, F., "Interface cracking of graded coatings", to appear in *International Journal of Fracture*.

APPENDIX A
EXPRESSIONS FOR VARIOUS KERNELS

$$\delta = \beta \sqrt{\left(\frac{3-\kappa}{1+\kappa}\right)} \quad (A1)$$

$$p_1 = -\frac{\beta}{2} - \frac{\sqrt{\beta^2 + 4\alpha^2 + 4i\alpha\delta}}{2},$$

$$p_2 = -\frac{\beta}{2} - \frac{\sqrt{\beta^2 + 4\alpha^2 - 4i\alpha\delta}}{2},$$

$$p_3 = -\frac{\beta}{2} + \frac{\sqrt{\beta^2 + 4\alpha^2 + 4i\alpha\delta}}{2},$$

$$p_4 = -\frac{\beta}{2} + \frac{\sqrt{\beta^2 + 4\alpha^2 - 4i\alpha\delta}}{2}. \quad (A2 - A5)$$

$$q_1 = \frac{(\kappa-1)(p_1^2 + \beta p_1) - (\kappa+1)\alpha^2}{2\alpha p_1 + (\kappa-1)\alpha\beta},$$

$$q_2 = \frac{(\kappa-1)(p_2^2 + \beta p_2) - (\kappa+1)\alpha^2}{2\alpha p_2 + (\kappa-1)\alpha\beta},$$

$$q_3 = \frac{(\kappa-1)(p_3^2 + \beta p_3) - (\kappa+1)\alpha^2}{2\alpha p_3 + (\kappa-1)\alpha\beta},$$

$$q_4 = \frac{(\kappa-1)(p_4^2 + \beta p_4) - (\kappa+1)\alpha^2}{2\alpha p_4 + (\kappa-1)\alpha\beta}. \quad (A6 - A9)$$

$$\theta_1 = (\kappa+1)q_1 p_1 + (3-\kappa)\alpha,$$

$$\theta_2 = (\kappa+1)q_2 p_2 + (3-\kappa)\alpha,$$

$$\theta_3 = (\kappa+1)q_3p_3 + (3-\kappa)\alpha,$$

$$\theta_4 = (\kappa+1)q_4p_4 + (3-\kappa)\alpha. \quad (A10 - A13)$$

$$\Gamma_1 = p_1 - \alpha q_1,$$

$$\Gamma_2 = p_2 - \alpha q_2,$$

$$\Gamma_3 = p_3 - \alpha q_3,$$

$$\Gamma_4 = p_4 - \alpha q_4, \quad (A14 - A17)$$

$$\phi_1 = \frac{\theta_1}{(\kappa-1)},$$

$$\phi_2 = \frac{\theta_2}{(\kappa-1)},$$

$$\phi_3 = \frac{\theta_3}{(\kappa-1)},$$

$$\phi_4 = \frac{\theta_4}{(\kappa-1)}. \quad (A18 - A21)$$

$$c^* = \alpha^2 + \frac{\beta^2}{4},$$

$$d^* = \sqrt{(\alpha^2 + \frac{\beta^2}{4})^2 + \alpha^2\delta^2},$$

$$c = \sqrt{\frac{d^* - c^*}{4}},$$

$$d = \sqrt{\frac{d^* + c^*}{4}}. \quad (A22 - A25)$$

$$R_1^* = \int_{-b_1}^{-a_1} g_1(t_1) R_1(\alpha, t_1) dt_1,$$

$$R_1 = -\frac{\kappa-1}{\kappa+1} \alpha^2 \frac{-c\beta \cos(c(t_1+h_1)) + (2c^2+2d^2-d\beta) \sin(c(t_1+h_1))}{cd(c^2+d^2)} e^{(-(t_1+h_1)(d-\frac{\beta}{2}))} \quad (A26 - A27)$$

$$R_2^* = \int_{-b_1}^{-a_1} g_1(t_1) R_2(\alpha, t_1) dt_1,$$

$$R_2 = \frac{2}{\kappa+1} \alpha \frac{-c(d^2+c^2+\frac{\beta^2}{4}) \cos(c(t_1+h_1)) + d(c^2+d^2-\frac{\beta^2}{4}) \sin(c(t_1+h_1))}{cd(c^2+d^2)} e^{(-(t_1+h_1)(d-\frac{\beta}{2}))} \quad (A28 - A29)$$

$$R_3^* = \int_{-b_1}^{-a_1} g_1(t_1) R_{3a}(\alpha, t_1) dt_1 + \int_{a_2}^{b_2} g_2(t_2) R_{3b}(\alpha, t_2) dt_2,$$

$$R_{3a} = \frac{1}{\kappa+1} \alpha^2 \frac{c\beta \cos(ct_1) - (2c^2+2d^2+d\beta) \sin(ct_1)}{cd(c^2+d^2)} e^{(t_1(d+\frac{\beta}{2}))},$$

$$R_{3b} = \frac{2\alpha t_2}{\kappa+1} e^{-\alpha t_2}. \quad (A30 - A32)$$

$$R_4^* = \int_{-b_1}^{-a_1} g_1(t_1) R_{4a}(\alpha, t_1) dt_1 + \int_{a_2}^{b_2} g_2(t_2) R_{4b}(\alpha, t_2) dt_2,$$

$$R_{4a} = -\frac{2}{\kappa+1} \alpha \frac{c(d^2+c^2+\frac{\beta^2}{4}) \cos(ct_1) + d(c^2+d^2-\frac{\beta^2}{4}) \sin(ct_1)}{cd(c^2+d^2)} e^{(t_1(d+\frac{\beta}{2}))},$$

$$R_{4b} = \frac{-2(\alpha t_2 - 1)}{\kappa + 1} e^{-\alpha t_2}. \quad (A33 - A35)$$

$$R_5^* = \int_{-b_1}^{-a_1} g_1(t_1) R_{5a}(\alpha, t_1) dt_1 + \int_{a_2}^{b_2} g_2(t_2) R_{5b}(\alpha, t_2) dt_2,$$

$$R_{5a} = -\frac{1}{4} e^{(t_1(d + \frac{\beta}{2}))}$$

$$\left(\frac{\{(c^3 + cd^2 + 3c\frac{\beta^2}{4})(\frac{\kappa-3}{\kappa+1}) + c\delta^2 + c\alpha^2\} \cos(ct_1)}{cd(c^2 + d^2)} \right. \\ \left. - \frac{\{(-c^2d - d^3 + d^2\beta + c^2\beta + 3d\frac{\beta^2}{4})(\frac{\kappa-3}{\kappa+1}) + d\delta^2 + d\alpha^2\} \sin(ct_1)}{cd(c^2 + d^2)} \right),$$

$$R_{5b} = \frac{2\alpha t_2 - 1 + \kappa}{2\alpha(\kappa + 1)} e^{-\alpha t_2}. \quad (A36 - A38)$$

$$R_6^* = \int_{-b_1}^{-a_1} g_1(t_1) R_{6a}(\alpha, t_1) dt_1 + \int_{a_2}^{b_2} g_2(t_2) R_{6b}(\alpha, t_2) dt_2,$$

$$R_{6a} = R_{6a1} + R_{6a2} + R_{6a3},$$

$$R_{6a1} = \alpha(\delta^2 + \alpha^2) \frac{(4cd + c\beta)\cos(ct_1) + (2c^2 - 2d^2 - d\beta)\sin(ct_1)}{8cd(c^2 + d^2)^2 + (c^2 + d^2)\beta(d + \frac{\beta}{4})} e^{(t_1(d + \frac{\beta}{2}))},$$

$$R_{6a2} = \frac{\alpha\beta}{2} \frac{c \cos(ct_1) - d \sin(ct_1)}{cd(c^2 + d^2)} e^{(t_1(d + \frac{\beta}{2}))},$$

$$R_{6a3} = -\frac{\alpha}{8} \frac{\kappa + 5}{\kappa + 1} \frac{c\beta \cos(ct_1) - (2c^2 + 2d^2 + d\beta) \sin(ct_1)}{cd(c^2 + d^2)} e^{(t_1(d + \frac{\beta}{2}))},$$

$$R_{6b} = R_{6b1} + R_{6b2},$$

$$R_{6b1} = \frac{e^{-\alpha t_2}}{2\alpha},$$

$$R_{6b2} = \frac{-e^{-\alpha t_2} t_2}{\kappa+1}. \quad (A39 - A46)$$

$$R_7^* = \int_{a_2}^{b_2} g_2(t_2) R_7(\alpha, t_2) dt_2,$$

$$R_7 = \frac{2\alpha(t_2 - h_2)}{\kappa+1} e^{\alpha(t_2 - h_2)}. \quad (A47 - A48)$$

$$R_8^* = \int_{a_2}^{b_2} g_2(t_2) R_8(\alpha, t_2) dt_2,$$

$$R_8 = -\frac{2(1+\alpha(t_2 - h_2))}{\kappa+1} e^{\alpha(t_2 - h_2)}. \quad (A49 - A50)$$

$$e_1 = -(2\alpha h_2 - k) e^{(-2\alpha h_2)},$$

$$e_2 = -\frac{(1 + (2\alpha h_2 + k)(2\alpha h_2 - k))}{2\alpha} e^{(-2\alpha h_2)}. \quad (A51 - A52)$$

$$R_{01}^* = \int_{a_2}^{b_2} g_2(t_2) R_{01b}(\alpha, t_2) dt_2,$$

$$R_{01b} = \frac{(R_7 + R_8) + (2\alpha h_2 - \kappa)(R_7 - R_8)}{4\alpha} e^{-\alpha h_2}. \quad (A53 - A54)$$

$$f_1 = 2\alpha e^{(-2\alpha h_2)},$$

$$f_2 = (2\alpha h_2 + k) e^{(-2\alpha h_2)}. \quad (A55 - A56)$$

$$R_{02}^* = \int_{a_2}^{b_2} g_2(t_2) R_{02b}(\alpha, t_2) dt_2,$$

$$R_{02b} = \frac{(R_8 - R_7)}{2} e^{-\alpha h_2}. \quad (A57 - A58)$$

$$\delta^* = \kappa - 2\alpha e_2 - \kappa e_2 f_1 + \kappa e_1 f_2 + \kappa f_2 + \kappa e_1. \quad (A59)$$

$$\gamma_1 = \frac{\kappa(1+f_2) - \alpha(1+q_1)e_2}{\delta^*},$$

$$\gamma_2 = \frac{\kappa(1+f_2) - \alpha(1+q_2)e_2}{\delta^*},$$

$$\gamma_3 = \frac{\kappa(1+f_2) - \alpha(1+q_3)e_2}{\delta^*},$$

$$\gamma_4 = \frac{\kappa(1+f_2) - \alpha(1+q_4)e_2}{\delta^*}. \quad (A60 - A63)$$

$$R_{03}^* = \int_{-b_1}^{-a_1} g_1(t_1) R_{03a}(\alpha, t_1) dt_1 + \int_{a_2}^{b_2} g_2(t_2) R_{03b}(\alpha, t_2) dt_2,$$

$$R_{03a} = \frac{-\kappa R_{6a}(1+f_2) + \alpha e_2(R_{5a} + R_{6a})}{\delta^*},$$

$$R_{03b} = \frac{-\kappa R_{01b}(1+f_2) - \kappa R_{6b}(1+f_2) + \alpha e_2(R_{5b} + R_{6b}) + \kappa e_2 R_{02b}}{\delta^*}. \quad (A64 - A66)$$

$$\delta_1 = \frac{(q_1-1)\alpha + \alpha(1+q_1)e_2 - \kappa f_1}{\delta^*},$$

$$\delta_2 = \frac{(q_2-1)\alpha + \alpha(1+q_2)e_2 - \kappa f_1}{\delta^*},$$

$$\delta_3 = \frac{(q_3-1)\alpha + \alpha(1+q_3)e_2 - \kappa f_1}{\delta^*},$$

$$\delta_4 = \frac{(q_4-1)\alpha + \alpha(1+q_4)e_2 - \kappa f_1}{\delta^*}. \quad (A67 - A70)$$

$$R_{04}^* = \int_{-b_1}^{-a_1} g_1(t_1) R_{04a}(\alpha, t_1) dt_1 + \int_{a_2}^{b_2} g_2(t_2) R_{04b}(\alpha, t_2) dt_2,$$

$$R_{04a} = \frac{\kappa R_{6a} f_1 - \alpha(R_{5a} - R_{6a}) - \alpha e_1(R_{5a} + R_{6a})}{\delta^*},$$

$$R_{04b} = \frac{\kappa R_{6b} f_1 - \alpha(R_{5b} - R_{6b}) - \alpha e_1(R_{5b} + R_{6b}) + R_{01b}(2\alpha + \kappa f_1) - \kappa R_{02b}(1 + e_1)}{\delta^*} \quad (A71 - A73)$$

$$\omega_3 = \frac{\Gamma_2 \theta_3 - \Gamma_3 \theta_2}{\Gamma_1 \theta_2 - \Gamma_2 \theta_1} e^{-(p_3 - p_1)h_1},$$

$$\omega_4 = \frac{\Gamma_2 \theta_4 - \Gamma_4 \theta_2}{\Gamma_1 \theta_2 - \Gamma_2 \theta_1} e^{-(p_4 - p_1)h_1}. \quad (A74 - A75)$$

$$R_{11}^* = \int_{-b_1}^{-a_1} g_1(t_1) R_{11}(\alpha, t_1) dt_1,$$

$$R_{11a} = \frac{R_2 \theta_2 - R_1 \Gamma_2}{\Gamma_1 \theta_2 - \Gamma_2 \theta_1} e^{(p_1)h_1}. \quad (A76 - A77)$$

$$\rho_3 = \frac{\Gamma_3 \theta_1 - \Gamma_1 \theta_3}{\Gamma_1 \theta_2 - \Gamma_2 \theta_1} e^{-(p_3 - p_2)h_1},$$

$$\rho_4 = \frac{\Gamma_4 \theta_1 - \Gamma_1 \theta_4}{\Gamma_1 \theta_2 - \Gamma_2 \theta_1} e^{-(p_4 - p_2)h_1}. \quad (A78 - A79)$$

$$R_{12}^* = \int_{-b_1}^{-a_1} g_1(t_1) R_{12}(\alpha, t_1) dt_1,$$

$$R_{12a} = \frac{R_1 \Gamma_1 - R_2 \theta_1}{\Gamma_1 \theta_2 - \Gamma_2 \theta_1} e^{(p_2 h_1)}. \quad (A80 - A81)$$

$$j_1^* = 2\alpha + 2\alpha e_1 - (\kappa + 1)f_1,$$

$$j_2^* = (\kappa + 1) + 2\alpha e_2 - (\kappa + 1)f_2,$$

$$k_1^* = \phi_1 + j_1^* \gamma_1 + j_2^* \delta_1,$$

$$k_2^* = \phi_2 + j_1^* \gamma_2 + j_2^* \delta_2. \quad (A82 - A85)$$

$$\hat{R}_{3a} = R_{3a} - j_1^* R_{03a} - j_2^* R_{04a} - k_1^* R_{11a} - k_2^* R_{12a},$$

$$\hat{R}_{3b} = R_{3b} - j_1^* R_{03b} - j_2^* R_{04b} - 2\alpha R_{01b} + (\kappa + 1)R_{02a}. \quad (A86 - A87)$$

$$l_1^* = 2\alpha - 2\alpha e_1 + (\kappa - 1)f_1,$$

$$l_2^* = (\kappa - 1) - 2\alpha e_2 + (\kappa - 1)f_2,$$

$$m_1^* = \Gamma_1 + l_1^* \gamma_1 + l_2^* \delta_1,$$

$$m_2^* = \Gamma_2 + l_1^* \gamma_2 + l_2^* \delta_2. \quad (A88 - A91)$$

$$\widehat{R}_{4a} = R_{4a} - l_1^* R_{03a} - l_2^* R_{04a} - m_1^* R_{11a} - m_2^* R_{12a},$$

$$\widehat{R}_{4b} = R_{4b} - l_1^* R_{03b} - l_2^* R_{04b} + 2\alpha R_{01b} - (\kappa - 1) R_{02b}. \quad (A92 - A93)$$

$$k_3^* = \phi_3 + j_1^* \gamma_3 + j_2^* \delta_3,$$

$$k_4^* = \phi_4 + j_1^* \gamma_4 + j_2^* \delta_4,$$

$$m_3^* = \gamma_3^* + l_1^* \gamma_3 + l_2^* \delta_3,$$

$$m_4^* = \gamma_4^* + l_1^* \gamma_4 + l_2^* \delta_4. \quad (A94 - A97)$$

$$p_1^* = k_1^* \omega_3 + k_2^* \rho_3 + k_3^*,$$

$$p_2^* = k_1^* \omega_4 + k_2^* \rho_4 + k_4^*,$$

$$q_1^* = m_1^* \omega_3 + m_2^* \rho_3 + m_3^*,$$

$$q_2^* = m_1^* \omega_4 + m_2^* \rho_4 + m_4^*. \quad (A98 - A101)$$

$$R_{13}^* = \int_{-b_1}^{-a_1} g_1(t_1) R_{13a}(\alpha, t_1) dt_1 + \int_{a_2}^{b_2} g_2(t_2) R_{13b}(\alpha, t_2) dt_2,$$

$$R_{13a} = \frac{\widehat{R}_{3a} q_2^* - \widehat{R}_{4a} p_2^*}{p_1^* q_2^* - p_2^* q_1^*},$$

$$R_{13b} = \frac{\widehat{R}_{3b} q_2^* - \widehat{R}_{4b} p_2^*}{p_1^* q_2^* - p_2^* q_1^*}. \quad (A102 - A104)$$

$$R_{14}^* = \int_{-b_1}^{-a_1} g_1(t_1) R_{14a}(\alpha, t_1) dt_1 + \int_{a_2}^{b_2} g_2(t_2) R_{14b}(\alpha, t_2) dt_2,$$

$$R_{14a} = \frac{\widehat{R}_{4a} p_1^* - \widehat{R}_{3a} q_1^*}{p_1^* q_2^* - p_2^* q_1^*},$$

$$R_{14b} = \frac{\widehat{R}_{4b} p_1^* - \widehat{R}_{3b} q_1^*}{p_1^* q_2^* - p_2^* q_1^*}. \quad (A105 - A107)$$

$$\begin{aligned} \Phi_1^* &= \left\{ - \left(-(3-\kappa)m_1 i\alpha + (\kappa+1)n_1 \right) e^{n_1 y} \frac{m_2 n_2 - i\alpha}{m_1 n_1 - m_2 n_2} \right. \\ &\quad \left. + \left(-(3-\kappa)m_2 i\alpha + (\kappa+1)n_2 \right) e^{n_2 y} \right\} e^{-i\alpha x} \Big|_{y \rightarrow 0} \end{aligned} \quad (A108)$$

$$z_1 = \{(1+\kappa)\alpha + (3-\kappa)p_1 q_1\} e^{(p_1 x_1)},$$

$$z_2 = \{(1+\kappa)\alpha + (3-\kappa)p_2 q_2\} e^{(p_2 x_1)},$$

$$z_3 = \{(1+\kappa)\alpha + (3-\kappa)p_3 q_3\} e^{(p_3 x_1)},$$

$$z_4 = \{(1+\kappa)\alpha + (3-\kappa)p_4 q_4\} e^{(p_4 x_1)}. \quad (A109 - A112)$$

$$R_{21}^* = \int_{-b_1}^{-a_1} g_1(t_1) R_{21a}(\alpha, x_1, t_1) dt_1 + \int_{a_2}^{b_2} g_2(t_2) R_{21b}(\alpha, x_1, t_2) dt_2,$$

$$R_{21a}(\alpha, x_1, t_1) = 2 \operatorname{Re} \left\{ R_{11a} z_1 + R_{13a} (z_3 + \omega_3 z_1 + \rho_3 z_2) \right\},$$

$$R_{21b}(\alpha, x_1, t_2) = 2 \operatorname{Re} \left\{ R_{13a}(z_3 + \omega_3 z_1 + \rho_3 z_2) \right\}. \quad (\text{A113} - \text{A115})$$

$$\begin{aligned} \hat{k}_1 &= \left\{ - \left(-(3-\kappa)m_1 i \alpha + (\kappa+1)n_1 \right) e^{n_1 y} \frac{m_2 n_2 - i \alpha}{m_1 n_1 - m_2 n_2} \right. \\ &\quad \left. + \left(-(3-\kappa)m_2 i \alpha + (\kappa+1)n_2 \right) e^{n_2 y} \right\} \Big|_{y \rightarrow 0} \frac{(m_1 n_1 - i \alpha)}{(m_1 n_1 - m_2 n_2)} \frac{i}{\alpha} \quad (\text{A116}) \end{aligned}$$

$$\begin{aligned} K_{11}(\alpha, x_1) &= \left\{ \int_0^A \left\{ \operatorname{Re}(\hat{k}_1(\alpha, y)) \cos(\alpha(t_1 - x_1)) \right. \right. \\ &\quad \left. \left. - \left(\operatorname{Im}(\hat{k}_1(\alpha, y)) + 4 \left(\frac{\kappa-1}{k+1} \right) \right) \sin(\alpha(t_1 - x_1)) \right\} d\alpha \right. \\ &\quad + \int_A^\infty \left\{ \left(\operatorname{Re}(\hat{k}_1(\alpha, y) - \operatorname{Re}(\hat{k}_{1\infty h}(\alpha, y))) \cos(\alpha(t_1 - x_1)) \right. \right. \\ &\quad \left. \left. - \left(\operatorname{Im}(\hat{k}_1(\alpha, y)) + 4 \left(\frac{\kappa-1}{k+1} \right) - \right. \right. \right. \\ &\quad \left. \left. \left. \operatorname{Im}(\hat{k}_{1\infty h}(\alpha, y)) \right) \sin(\alpha(t_1 - x_1)) \right\} d\alpha \right. \\ &\quad + \int_A^\infty \left\{ \operatorname{Re}(\hat{k}_{1\infty h}(\alpha, y)) \cos(\alpha(t_1 - x_1)) \right. \\ &\quad \left. \left. - \operatorname{Im}(\hat{k}_{1\infty h}(\alpha, y)) \sin(\alpha(t_1 - x_1)) \right\} d\alpha \right. \\ &\quad \left. + 2 \int_0^\infty R_{21a}(\alpha, x_1, t_1) d\alpha \right\} \left(\frac{k+1}{4(\kappa-1)} \right) \quad (\text{A117}) \end{aligned}$$

$$K_{12}(\alpha, x_1) = 2 \int_0^\infty R_{21b}(\alpha, x_1, t_2) d\alpha \left(\frac{k+1}{4(\kappa-1)} \right) \quad (\text{A118})$$

$$\Phi_2^* = 2i \left(\frac{|\alpha|}{\alpha} + \alpha y \right) e^{-i\alpha x} e^{-|\alpha|y} \Big|_{y \rightarrow 0} \quad (A119)$$

$$\hat{k}_2 = - \frac{4i}{(1+\kappa)} \left(\frac{|\alpha|}{\alpha} + \alpha y \right) e^{-|\alpha|y} \Big|_{y \rightarrow 0} \quad (A120)$$

$$n_1^* = 2\alpha(2\alpha(x_2 - h_2) + 3) e^{\alpha(x_2 - 2h_2)} + 2\alpha e^{\alpha x_2},$$

$$n_2^* = ((2\alpha h_2 + \kappa)(2\alpha(x_2 - h_2) + 3) - 1) e^{\alpha(x_2 - 2h_2)} + (2\alpha x_2 + \kappa - 3) e^{\alpha x_2},$$

$$o_1^* = \omega_3(\gamma_1 n_1^* + \delta_1 n_2^*) + \rho_3(\gamma_2 n_1^* + \delta_2 n_2^*) + \gamma_3 n_1^* + \delta_3 n_2^*,$$

$$o_2^* = \omega_4(\gamma_1 n_1^* + \delta_1 n_2^*) + \rho_4(\gamma_2 n_1^* + \delta_2 n_2^*) + \gamma_4 n_1^* + \delta_4 n_2^*. \quad (A121 - A124)$$

$$R_{22}^* = \int_{-b_1}^{-a_1} g_1(t_1) R_{22a}(\alpha, x_2, t_1) dt_1 + \int_{a_2}^{b_2} g_2(t_2) R_{22b}(\alpha, x_2, t_2) dt_2,$$

$$R_{21}(\alpha, x_2, t_1) = R_{11a}(\gamma_1 n_1^* + \delta_1 n_2^*) + R_{12a}(\gamma_2 n_1^* + \delta_2 n_2^*)$$

$$+ R_{13a} o_1^* + R_{14a} o_2^* + R_{03a} n_1^* + R_{04a} n_2^*,$$

$$R_{22}(\alpha, x_2, t_2) = \frac{(R_7 + R_8) + (2\alpha h_2 - \kappa)(R_7 - R_8)}{2} e^{-\alpha(h_2 - x_2)}$$

$$+ \frac{(2\alpha x_2 - \kappa + 3)(R_8 - R_7)}{2} e^{-\alpha(h_2 - x_2)}$$

$$+ R_{13b} o_1^* + R_{14b} o_2^* + R_{03b} n_1^* + R_{04b} n_2^*. \quad (A125 - A127)$$

$$K_{21}(\alpha, x_2) = 2 \int_0^\infty R_{21a}(\alpha, x_2, t_1) d\alpha \left(\frac{k+1}{4} \right) \quad (A128)$$

$$K_{22}(\alpha, x_2) = 2 \int_0^\infty R_{21b}(\alpha, x_2, t_2) d\alpha \left(\frac{k+1}{4} \right) \quad (A129)$$

APPENDIX B

ASYMPTOTIC EXPRESSIONS FOR KERNELS

The expressions for the various variables used in Chapter 3 in the asymptotic expansions of the integrands of the Fredholm kernels are given here.

$$\underline{R_{21a}(\alpha, x_1, t_1)}$$

$$R_{21a}(\alpha, x_1, t_1) \sim \left(c_1^* \alpha^2 + c_2^* \alpha + c_3^* + \frac{c_4^*}{\alpha} \right) e^{-(x_1+t_1+2h_1)\alpha} \\ + \left(e_1^* \alpha + e_2^* + \frac{e_3^*}{\alpha} + \frac{e_4^*}{\alpha^2} \right) e^{(x_1+t_1)\alpha} \quad (B1)$$

where

$$c_1^* = 16 \left(\frac{\kappa-1}{3-\kappa} \right) \frac{1}{\beta^2} \sin(\zeta_1) \sin(\zeta_2) e^{\left(\frac{\beta(t_1-x_1)}{2} \right)} \quad (B2)$$

$$c_2^* = -4 \frac{\kappa-1}{(3-\kappa)(1+\kappa)} \frac{1}{\beta} \left(2\xi_1 \sin(\zeta_1) \sin(\zeta_2) + \Delta \cos(\zeta_2) \sin(\zeta_1) (1+\kappa) \right. \\ \left. + 3\Delta \sin(\zeta_2) \cos(\zeta_1) (1+\kappa) + 6\sin(\zeta_2) \sin(\zeta_1) (1+\kappa) \right) e^{\left(\frac{\beta(t_1-x_1)}{2} \right)} \quad (B3)$$

$$c_3^* = 2 \frac{\kappa-1}{(3-\kappa)(1+\kappa)^2} \left(\xi_1^2 \sin(\zeta_1) \sin(\zeta_2) \right. \\ \left. + \xi_1 (1+\kappa) \left\{ \Delta \cos(\zeta_2) \sin(\zeta_1) + 3\Delta \sin(\zeta_2) \cos(\zeta_1) + 6\sin(\zeta_2) \sin(\zeta_1) \right\} \right. \\ \left. + (1+\kappa) \left\{ -2(\kappa-3) \cos(\zeta_2) \cos(\zeta_1) + \Delta (1+\kappa) \cos(\zeta_2) \sin(\zeta_1) \right\} \right)$$

$$\begin{aligned}
& + 5\Delta(1+\kappa)\sin(\zeta_2)\cos(\zeta_1) + 6(1+\kappa)\sin(\zeta_2)\sin(\zeta_1) + 16\sin(\zeta_2)\sin(\zeta_1) \Big\} \\
& - 2\xi_3\Delta\sin(\zeta_2)\cos(\zeta_1) - 2\xi_2\Delta\cos(\zeta_2)\sin(\zeta_1) \Big) e^{\left(\frac{\beta(\zeta_1-\pi_1)}{2}\right)} \tag{B4}
\end{aligned}$$

$$c_4^* = - \frac{\kappa-1}{(3-\kappa)(1+\kappa)^3} \frac{\beta}{6}$$

$$\begin{aligned}
& \left(2\xi_1^3\sin(\zeta_2)\sin(\zeta_1) \right. \\
& + 3\xi_1^2(1+\kappa) \Big\{ \Delta\cos(\zeta_2)\sin(\zeta_1) + 3\Delta\sin(\zeta_2)\cos(\zeta_1) + 6\sin(\zeta_2)\sin(\zeta_1) \Big\} \\
& + 6\xi_1(1+\kappa) \Big\{ -2(\kappa-3)\cos(\zeta_2)\cos(\zeta_1) + \Delta(1+\kappa)\cos(\zeta_2)\sin(\zeta_1) \\
& + 5\Delta(1+\kappa)\sin(\zeta_2)\cos(\zeta_1) + 2(7+4\kappa)\sin(\zeta_2)\sin(\zeta_1) \\
& - 2\xi_3\Delta\sin(\zeta_2)\cos(\zeta_1) - 2\xi_2\Delta\cos(\zeta_2)\sin(\zeta_1) \Big\} \\
& + 6(1+\kappa) \Big\{ \Delta\cos(\zeta_2)\cos(\zeta_1) + 16\Delta(1+\kappa)\sin(\zeta_2)\cos(\zeta_1) \\
& + (k+41)(1+\kappa)\sin(\zeta_2)\sin(\zeta_1) + \xi_3(\kappa-3)\cos(\zeta_2)\cos(\zeta_1) \\
& - \xi_2(\kappa-3)\sin(\zeta_2)\sin(\zeta_1) + 3\xi_2(\kappa-3)\cos(\zeta_2)\cos(\zeta_1) \\
& - 3\xi_3(\kappa-3)\sin(\zeta_2)\sin(\zeta_1) - 6\xi_2(1+\kappa)\Delta\cos(\zeta_2)\sin(\zeta_1) \\
& - 6\xi_3(1+\kappa)\Delta\sin(\zeta_2)\cos(\zeta_1) \Big\} \Big) e^{\left(\frac{\beta(\zeta_1-\pi_1)}{2}\right)} \tag{B5}
\end{aligned}$$

where

$$\Delta = \sqrt{\frac{3-\kappa}{1+\kappa}} \quad (B6)$$

$$\xi_1 = (2h_1 + x_1 + t_1)\beta,$$

$$\xi_2 = (h_1 + t_1)\beta,$$

$$\xi_3 = (h_1 + x_1)\beta. \quad (B7 - B9)$$

$$\zeta_1 = \frac{1}{2} \Delta \beta (h_1 + x_1),$$

$$\zeta_2 = \frac{1}{2} \Delta \beta (h_1 + t_1),$$

$$\zeta_3 = \frac{1}{2} \Delta \beta (x_1),$$

$$\zeta_4 = \frac{1}{2} \Delta \beta (t_1). \quad (B10 - B13)$$

$$e_1^* = -8 \frac{\kappa-1}{(3-\kappa)(1+\kappa)} \frac{1}{\beta} \sin(\zeta_3) \sin(\zeta_4) e^{\left(\frac{-(x_1-t_1)\beta}{2}\right)} \quad (B14)$$

$$e_2^* = -4 \frac{\kappa-1}{(3-\kappa)(1+\kappa)^2} \sin(\zeta_4)$$

$$\left(\sin(\zeta_3) (\xi_5 + 2\kappa) + \Delta \cos(\zeta_3) (1+\kappa) \right) e^{\left(\frac{-(x_1-t_1)\beta}{2}\right)} \quad (B15)$$

$$e_3^* = -\frac{\kappa-1}{(3-\kappa)(1+\kappa)^3} \frac{\beta}{2}$$

$$\begin{aligned}
& \left(\sin(\zeta_3)\sin(\zeta_4) \{ 2\xi_5^2 + 8\kappa\xi_5 + \kappa^3 - \kappa^2 + 7\kappa + 25 \} \right. \\
& - \cos(\zeta_3)\cos(\zeta_4) \{ (1+\kappa)^2(\kappa-3) \} - \sin(\zeta_3)\cos(\zeta_4)\Delta(1+\kappa)^3 \\
& - \cos(\zeta_3)\sin(\zeta_4)\Delta(1+\kappa)(\kappa^2-2\kappa+5) \\
& \left. - 4\sin(\zeta_3-\zeta_4)\Delta(1+\kappa)\beta t_1 \right) e^{\left(\frac{-(x_1-t_1)\beta}{2}\right)} \tag{B16}
\end{aligned}$$

$$\begin{aligned}
e_4^* &= -\frac{\kappa-1}{(3-\kappa)(1+\kappa)^4} \frac{\beta^2}{12} \\
& \left(\sin(\zeta_3)\sin(\zeta_4) \left\{ 2\xi_5^3 + 12\kappa\xi_5^2 + 3\beta t_1(\kappa^3 - \kappa^2 + 7\kappa + 25) \right. \right. \\
& \quad \left. \left. + 3\beta x_1(\kappa^3 - 5\kappa^2 + 15\kappa + 37) + 3(\kappa^4 - 2\kappa^3 - 4\kappa^2 + 10\kappa - 21) \right\} \right. \\
& - \cos(\zeta_3)\cos(\zeta_4) \left\{ 3\beta t_1(1+\kappa)(\kappa-3)^2 + 3\beta x_1(1+\kappa)^2(\kappa-3) \right. \\
& \quad \left. \left. + 3(\kappa^2-1)(\kappa-3)(1+\kappa) \right\} \right. \\
& - \sin(\zeta_3)\cos(\zeta_4)\Delta \left\{ 12\beta^2 x_1 t_1(1+\kappa) + 12\beta^2 t_1^2(1+\kappa) \right. \\
& \quad \left. \left. + 3\beta t_1(1+\kappa)(\kappa^2 + 10\kappa + 1) + 3\xi_5(1+\kappa)^3 + 3(1+\kappa)^2(\kappa^2 + 3) \right\} \right. \\
& - \cos(\zeta_3)\sin(\zeta_4)\Delta \left\{ 6\beta^2 x_1^2(1+\kappa) - 6\beta^2 t_1^2(1+\kappa) + 3\beta t_1(1+\kappa)(\kappa^2 - 2\kappa + 5) \right. \\
& \quad \left. \left. + 3\xi_5(1+\kappa)^2(5+\kappa) + 3(\kappa^2-1)(\kappa^2+6\kappa+13) \right\} \right) e^{\left(\frac{-(x_1-t_1)\beta}{2}\right)} \tag{B17}
\end{aligned}$$

where

$$\xi_5 = (x_1 + t_1)\beta. \quad (B18)$$

$$\underline{R_{21b}(\alpha, x_1, t_2)}$$

$$R_{21b}(\alpha, x_1, t_2) \sim \left(r_1^* \alpha + r_2^* + \frac{r_3^*}{\alpha} + \frac{r_4^*}{\alpha^2} \right) e^{(x_1 - t_2)\alpha} \quad (B19)$$

where

$$r_1^* = \frac{2}{\beta \Delta (1 + \kappa)^2} \left(\sin(\zeta_3) (t_2 \beta (\kappa - 1)^2 + 2(\kappa^2 - 1)) - \cos(\zeta_3) t_2 \beta (\kappa^2 - 1) \right) e^{\left(\frac{-x_1 \beta}{2} \right)} \quad (B20)$$

$$\begin{aligned} r_2^* = \frac{1}{\Delta (1 + \kappa)^3} & \left(\beta x_1 \left\{ \sin(\zeta_3) (t_2 \beta (\kappa - 1)^2 + 2(\kappa^2 - 1)) - \cos(\zeta_3) t_2 \beta (\kappa^2 - 1) \right\} \right. \\ & \left. + \sin(\zeta_3) \left\{ 2t_2 \beta (\kappa + 3)(\kappa - 1) + 2(\kappa^2 - 1)(1 + \kappa) \right\} \right. \\ & \left. - \cos(\zeta_3) \Delta \left\{ 2t_2 \beta (\kappa^2 - 1) - 4(\kappa^2 - 1)(1 + \kappa) \right\} \right) e^{\left(\frac{-x_1 \beta}{2} \right)} \end{aligned} \quad (B21)$$

$$\begin{aligned} r_3^* = \frac{\beta}{2\Delta (1 + \kappa)^4} & \left(\beta^2 x_1^2 \left\{ \sin(\zeta_3) (t_2 \beta (\kappa - 1)^2 + 2(\kappa^2 - 1)) - \cos(\zeta_3) t_2 \beta (\kappa^2 - 1) \right\} \right. \\ & + 2\beta x_1 \left\{ \sin(\zeta_3) (t_2 \beta (\kappa^2 + 3) \frac{(\kappa - 1)}{2} + (\kappa^2 - 1)(1 + \kappa)) \right. \\ & \left. + \cos(\zeta_3) (-t_2 \beta (\kappa^2 - 1) \frac{(\kappa + 1)}{2} + (\kappa^2 - 1)(1 + \kappa)) \right\} \\ & + \sin(\zeta_3) \left\{ 2t_2 \beta (\kappa^2 + 3\kappa - 2)(\kappa - 1) + (\kappa^2 - 1)(1 + \kappa)^2 \right\} \\ & \left. + \cos(\zeta_3) \Delta \left\{ -2t_2 \beta (\kappa^2 - 1)(\kappa - 1) + (\kappa^2 - 1)(1 + \kappa)^2 \right\} \right) e^{\left(\frac{-x_1 \beta}{2} \right)} \end{aligned} \quad (B22)$$

$$\begin{aligned}
r_4^* &= \frac{\beta^2}{4\Delta(1+\kappa)^5} \left(\beta^3 x_1^3 \left\{ \sin(\zeta_3)(t_2\beta(\kappa-1)^2+2(\kappa^2-1)) - \cos(\zeta_3)t_2\beta(\kappa^2-1) \right\} \right. \\
&\quad + 2\beta^2 x_1^2 \left\{ \sin(\zeta_3)(t_2\beta(\kappa^2+3)\frac{(\kappa-1)}{2}+(\kappa^2-1)(1+\kappa)) \right. \\
&\quad \left. \left. + \cos(\zeta_3) (-t_2\beta(\kappa^2-1)\frac{(\kappa+1)}{2}+(\kappa^2-1)(1+\kappa)) \right\} \right. \\
&\quad + \beta x_1 \left\{ \sin(\zeta_3)(2t_2\beta(2\kappa^2+\kappa-5)(\kappa-1)-(\kappa^2-1)(1+\kappa)(3\kappa-13)) \right. \\
&\quad \left. \left. + \cos(\zeta_3)\Delta(4t_2\beta(\kappa^2-1)(\kappa+1)+(\kappa^2-1)(1+\kappa)^2) \right\} \right. \\
&\quad + \sin(\zeta_3) \left\{ 2t_2\beta(\kappa^3+\kappa^2-11\kappa-3)(\kappa-1)-(\kappa^2-5)(\kappa^2-1)(1+\kappa) \right\} \\
&\quad \left. - \cos(\zeta_3)\Delta \left\{ 2t_2\beta(\kappa^2-1)(\kappa-1)^2+(\kappa^2-1)^2(1+\kappa) \right\} \right) e^{\left(\frac{-x_1\beta}{2}\right)}
\end{aligned} \tag{B23}$$

$$\underline{R_{22a}(\alpha, x_2, t_1)}$$

$$R_{22a}(\alpha, x_2, t_1) \sim \left(t_1^* \alpha + t_2^* + \frac{t_3^*}{\alpha} + \frac{t_4^*}{\alpha^2} + \frac{t_5^*}{\alpha^3} \right) e^{-(x_2-t_1)\alpha} \tag{B24}$$

where

$$t_1^* = -\frac{1}{\beta\Delta(\kappa+1)^2} \left(-2\cos(\zeta_4)\Delta x_2\beta(\kappa+1) + \sin(\zeta_4)(2x_2\beta(\kappa-1) + 4(\kappa+1)) \right) \tag{B25}$$

$$\begin{aligned}
t_2^* &= -\frac{2}{\Delta(\kappa+1)^3} \left(\frac{\beta t_1}{4} \left\{ -2\cos(\zeta_4)\Delta x_2\beta(\kappa+1) + \sin(\zeta_4)(2x_2\beta(\kappa-1) + 4(\kappa+1)) \right\} \right. \\
&\quad \left. + 2\cos(\zeta_4)\Delta(\kappa+1)^2 + \sin(\zeta_4)(2x_2\beta + (1-\kappa^2)) \right) e^{(\frac{t_1\beta}{2})} \\
&\hspace{15em} (B26)
\end{aligned}$$

$$\begin{aligned}
t_3^* &= -\frac{\beta}{4\Delta(\kappa+1)^4} \left(\beta^2 t_1^2 \left\{ -2\cos(\zeta_4)\Delta x_2\beta(\kappa+1) + \sin(\zeta_4)(2x_2\beta(\kappa-1) + 4(\kappa+1)) \right\} \right. \\
&\quad \left. + 4\beta t_1 \left\{ 2\cos(\zeta_4)\Delta(\kappa+1)^2 + \sin(\zeta_4)(2x_2\beta + (1-\kappa^2)) \right\} \right. \\
&\quad \left. - 2\cos(\zeta_4)\Delta(\kappa+1)^3 - 2\sin(\zeta_4)x_2 t_1 \Delta^2 \beta^2 (\kappa+1)^2 \right. \\
&\quad \left. + \sin(\zeta_4)(4x_2\beta(\kappa-3) - 2(\kappa+1)(\kappa^2 - 2\kappa + 5)) \right. \\
&\quad \left. - \cos(\zeta_4)\Delta t_1 \beta(\kappa+1)(2x_2\beta(\kappa-1) + 4(\kappa+1)) \right) e^{(\frac{t_1\beta}{2})} \\
&\hspace{15em} (B27)
\end{aligned}$$

$$\begin{aligned}
t_4^* &= -\frac{\beta^2}{8\Delta(\kappa+1)^5} \left(\beta^3 t_1^3 \left\{ -2\cos(\zeta_4)\Delta x_2\beta(\kappa+1) + \sin(\zeta_4)(2x_2\beta(\kappa-1) + 4(\kappa+1)) \right\} \right. \\
&\quad \left. + 4\beta^2 t_1^2 \left\{ 2\cos(\zeta_4)\Delta(\kappa+1)^2 + \sin(\zeta_4)(2x_2\beta + (1-\kappa^2)) \right\} \right. \\
&\quad \left. + \beta t_1 \left\{ -2\cos(\zeta_4)\Delta(\kappa+1)^3 + \sin(\zeta_4)(4x_2\beta(\kappa-3) - 2(\kappa+1)(\kappa^2 - 2\kappa + 5)) \right\} \right. \\
&\quad \left. + 2\cos(\zeta_4)\Delta(\kappa+1)^2(2x_2\beta + (\kappa^2 - 1)) \right. \\
&\quad \left. + \sin(\zeta_4)(4x_2\beta(\kappa^2 - 8\kappa - 1) + 2(\kappa^2 - 1)(\kappa^2 - 2\kappa - 11)) \right)
\end{aligned}$$

$$\begin{aligned}
& -\sin(\zeta_4)(2x_2t_1^2\beta^3\Delta^2(\kappa+1)^2-8\Delta^2\beta t_1(\kappa+1)^3 \\
& -\cos(\zeta_4)\left\{t_1^2\beta^2\Delta(\kappa+1)(2x_2\beta(\kappa-1)+4(\kappa+1))\right. \\
& \left.+4(\kappa+1)t_1\beta\Delta(1-\kappa^2+2x_2\beta)\right\}\Big)e^{\left(\frac{t_1\beta}{2}\right)} \tag{B28}
\end{aligned}$$

$$\begin{aligned}
t_5^* &= -\frac{\beta^3}{16\Delta(\kappa+1)^6}\left(\beta^4t_1^4\left\{-2\cos(\zeta_4)\Delta x_2\beta(\kappa+1)+\sin(\zeta_4)(2x_2\beta(\kappa-1)+4(\kappa+1))\right\}\right. \\
& +4\beta^3t_1^3\left\{2\cos(\zeta_4)\Delta(\kappa+1)^2+\sin(\zeta_4)(2x_2\beta+(1-\kappa^2))\right\} \\
& +\beta^2t_1^2\left\{-2\cos(\zeta_4)\Delta(\kappa+1)^3+\sin(\zeta_4)(4x_2\beta(\kappa-3)-2(\kappa+1)(\kappa^2-2\kappa+5))\right\} \\
& +\beta t_1\left\{2\cos(\zeta_4)\Delta(\kappa+1)^2(2x_2\beta+(\kappa^2-1))\right. \\
& \left.+\sin(\zeta_4)(4x_2\beta(\kappa^2-8\kappa-1)+2(\kappa^2-1)(\kappa^2-2\kappa-11))\right\} \\
& +2\cos(\zeta_4)\Delta(\kappa(\kappa+1)^3(\kappa-3)-2x_2\beta(\kappa^2-1)(\kappa+1) \\
& +2\sin(\zeta_4)(4x_2\beta(5\kappa^2-8\kappa-5)+(\kappa+1)(\kappa^4-5\kappa^3+3\kappa^2-7\kappa+16)) \\
& +\cos(\zeta_4)\left\{x_2t_1^2\Delta^3\beta^3(\kappa+1)^2+4t_1^2\Delta\beta^2(1-\kappa^2+2x_2\beta)\right. \\
& \left.+t_1\Delta\beta(\kappa+1)(4x_2\beta(\kappa-2)-(\kappa+1)(\kappa-1)^2)\right\}
\end{aligned}$$

$$\begin{aligned}
& + \sin(\zeta_4) \left\{ t_1^2 \Delta^2 \beta^2 (\kappa+1)^2 (x_2 \beta (\kappa-1) - 6(\kappa+1)) \right. \\
& \quad \left. + 2t_1 \Delta^2 \beta (\kappa+1)^4 + 2t_1^3 x_2 \Delta^2 \beta^3 (\kappa+1)^2 \right\} e^{\left(\frac{t_1 \beta}{2}\right)}
\end{aligned} \tag{B29}$$

$R_{22b}(\alpha, x_2, t_2)$

$$\begin{aligned}
R_{22b}(\alpha, x_2, t_2) \sim & \left(o_1^* \alpha + o_2^* + \frac{o_3^*}{\alpha} + \frac{o_4^*}{\alpha^2} + \frac{o_5^*}{\alpha^3} \right) e^{-(x_2+t_2)\alpha} \\
& + \left(p_1 \alpha^2 + p_2 \alpha + p_3 \right) e^{(x_2+t_2-2h_2)\alpha}
\end{aligned} \tag{B30}$$

where

$$o_1^* = \frac{2x_2 t_2 \beta}{(\kappa+1)^2} \tag{B31}$$

$$o_2^* = -\frac{2t_2 \beta}{(\kappa+1)^2} + \frac{x_2 t_2 \beta^2 (\kappa-1)}{(\kappa+1)^3} \tag{B32}$$

$$o_3^* = \frac{\beta}{2(\kappa+1)} + \frac{t_2 \beta^2 (1-\kappa)}{(\kappa+1)^3} + \frac{x_2 t_2 \beta^3 \kappa (\kappa-3)}{2(\kappa+1)^4} \tag{B33}$$

$$\begin{aligned}
o_4^* = & \frac{\beta^2 (1-\kappa^2)}{4(\kappa+1)^3} - \frac{t_2 \beta^3 (1-\kappa)^2}{2(\kappa+1)^4} - \frac{x_2 \beta^3}{2(\kappa+1)^3} + \frac{x_2 t_2 \beta^4 (\kappa-1)(\kappa^2-5\kappa-2)}{4(\kappa+1)^5}
\end{aligned} \tag{B34}$$

$$\begin{aligned}
o_5^* = & \frac{\beta^3 \kappa (\kappa-3)}{8(\kappa+1)^3} - \frac{t_2 \beta^4 (\kappa^2-1)(\kappa^2-4\kappa-1)}{4(\kappa+1)^6} - \frac{x_2 \beta^4 (\kappa-1)}{4(\kappa+1)^4} \\
& + \frac{x_2 t_2 \beta^5 (\kappa^4-10\kappa^3+14\kappa^2+10\kappa+1)}{8(\kappa+1)^6}
\end{aligned} \tag{B35}$$

$$p_1^* = -4 \frac{(h_2 - x_2)(h_2 - t_2)}{(\kappa + 1)},$$

$$p_2^* = 2 \frac{(h_2 - x_2) + 3(h_2 - t_2)}{(\kappa + 1)},$$

$$p_3^* = -\frac{4}{(\kappa + 1)}. \quad (B36 - B38)$$

APPENDIX C **RIGHT HAND SIDES AND NORMALIZATIONS** **FOR DIFFERENT LOADINGS**

As can be seen from equations (3.28), (3.36) in Chapter 3, the right hand side of the singular integral equation is

$$RHS = p_1(x) \frac{(\kappa+1)}{4\mu(x)} \quad (C1)$$

where $p_1(x)$ is the crack surface loading corresponding to different far-field loadings. Due to superposition, it turns out that this $p_1(x)$ is nothing but the negative of the normal stress produced at the plane of the crack in an uncracked specimen. In this appendix, the expressions for right hand sides and the normalization for the stress intensity factors are derived for fixed grip loading, far-field tension, far-field bending and thermal loading. All strains and stresses are evaluated at $y = 0$ plane.

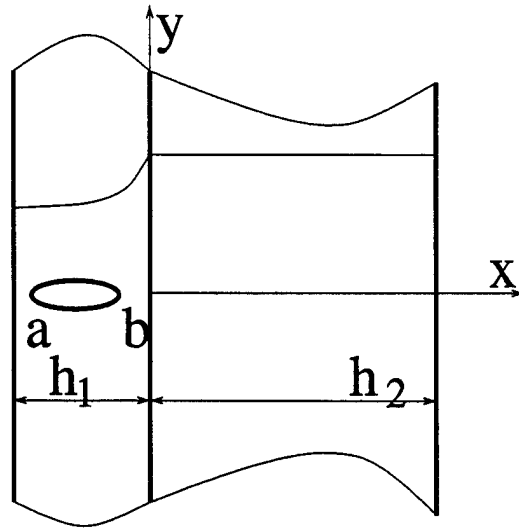


Figure C.1 Nonhomogeneous strip bonded to homogeneous strip. Internal crack in nonhomogeneous strip.

Consider a strip as shown in Fig (C.1). The strip is homogeneous on positive side of x and nonhomogeneous on the negative. Let it have a crack extending from a to b . An edge crack can be obtained by letting a go to zero. Let the unknown function (derivative of the displacement) be $g(t)$ and the corresponding function in normalized coordinates be $\hat{g}(r)$. Let $\hat{g}(r)$ be defined as

$$\hat{g}(r) = F(r)w(r) \quad (C2)$$

where $w(r)$ is some weight function. $F(r)$ in general will be a summation of the sort

$$F(r) = \sum_n A_n X_n \quad (C3)$$

where X_n is some orthogonal polynomial and A_n 's are the unknowns.

Fixed grip loading

In this case, we apply a uniform strain ϵ_0 at infinity. Stress-strain relation gives us,

$$\epsilon_{yy} = \frac{(\kappa+1)}{8\mu(x)} (\sigma_{yy} - \frac{3-\kappa}{1+\kappa} \sigma_{xx}). \quad (C4)$$

For this loading,

$$\epsilon_{zz} = \sigma_{xx} = 0. \quad (C5)$$

Hence, using equation (C4)

$$\sigma_{yy} = \frac{8\mu(x)}{(\kappa+1)} \epsilon_0 = -p_1(x). \quad (C6)$$

Substituting into (C1)

$$RHS = -2\epsilon_0 \quad (C7)$$

and

$$k_1(a) = \frac{4\mu(a)}{(\kappa+1)} \sqrt{\frac{b-a}{2}} F(-1), \quad (C8)$$

$$k_1(b) = -\frac{4\mu(b)}{(\kappa+1)} \sqrt{\frac{b-a}{2}} F(1). \quad (C9)$$

It should be noted that for an edge crack, the expression $\sqrt{\frac{b-a}{2}}$ is replaced by \sqrt{b} .

Dividing the entire equation by $2\epsilon_0$, we can now normalize the stress intensity factors with respect to

$$\sigma_0 = \frac{8\mu_0}{(\kappa+1)} \sqrt{\frac{b-a}{2}} \epsilon_0. \quad (C10)$$

Then we obtain,

$$RHS = -1, \quad (C11)$$

$$k_{1n}(a) = \frac{\mu(a)}{\mu_0} F(-1), \quad (C12)$$

$$k_{1n}(b) = -\frac{\mu(b)}{\mu_0} F(1). \quad (C13)$$

It should be noted when a goes to zero, we have an edge crack at the left. For an edge crack, the normalization is usually done with respect to the shear modulus μ_1 . This yields the benchmark value of 1.1215222 for the normalized stress intensity factor in the limiting case when the crack length goes to zero. To obtain normalization with respect to μ_1 , it is necessary to multiply eqn (C13) by a factor of $\frac{\mu_0}{\mu_1}$.

Far-field tension and bending

Usually any far-field loading can be resolved into a far-field tension (N) acting along the midplane of the specimen and a far-field moment (M). If the crack is sufficiently away from the loading, by St. Venant's principle, the stresses produced by the resultant

force and moment will be the same as those produced by the specific loading for all practical purposes. Under such loading, due to compatibility, we have,

$$\epsilon_{yy} = Ax + B. \quad (C14)$$

Equilibrium equation states that

$$\int_{-h_1}^{h_2} \sigma_{yy}(x) dx = N \quad (C15)$$

while moment equation gives,

$$\int_{-h_1}^{h_2} (x - \frac{h_2 - h_1}{2}) \sigma_{yy}(x) dx = M. \quad (C16)$$

Using Hooke's law,

$$\sigma_{yy}(x) = \frac{8\mu(x)}{(\kappa+1)} \epsilon_{yy} \quad (C17)$$

and equations (C14), (C15) and (C16), some simple algebra yields,

$$c_1 A + c_2 B = \frac{N}{\frac{8\mu_0}{(\kappa+1)} h_1} = \hat{N}, \quad (C18)$$

$$c_3 A + c_4 B = \frac{M + \frac{h_2 - h_1}{2} N}{\frac{8\mu_0}{(\kappa+1)} h_1^2} = \hat{M} \quad (C19)$$

where

$$c_1 = \left(\frac{e^{-\beta h_1}}{\beta} - \frac{1}{h_1 \beta^2} + \frac{e^{-\beta h_1}}{h_1 \beta^2} + \frac{h_2^2}{2h_1} \right), \quad (C20)$$

$$c_2 = \left(\frac{1}{h_1 \beta} - \frac{e^{-\beta h_1}}{h_1 \beta} + \frac{h_2}{h_1} \right), \quad (C21)$$

$$c_3 = \left(-\frac{e^{-\beta h_1}}{\beta} - \frac{2e^{-\beta h_1}}{h_1 \beta^2} + \frac{2}{h_1^2 \beta^3} - \frac{2e^{-\beta h_1}}{h_1^2 \beta^3} + \frac{h_2^3}{3h_1^2} \right), \quad (C22)$$

$$c_4 = \left(\frac{e^{-\beta h_1}}{h_1 \beta} - \frac{1}{h_1^2 \beta^2} + \frac{e^{-\beta h_1}}{h_1^2 \beta^2} + \frac{h_2^2}{2h_1^2} \right). \quad (C23)$$

Solving (C18) and (C19) we get,

$$A = \frac{\hat{N}c_4 - \left(\hat{M} + \frac{h_2-h_1}{2}\hat{N}\right)c_2}{c_1c_4 - c_3c_2}, \quad (C24)$$

$$B = \frac{\left(\hat{M} + \frac{h_2-h_1}{2}\hat{N}\right)c_1 - \hat{N}c_3}{c_1c_4 - c_3c_2} \quad (C25)$$

Using (C14) and (C17) we get

$$p_1(x) = \frac{8\mu(x)}{(\kappa+1)}(Ax + B) \quad (C26)$$

where A and B are given by (C24), (C25).

Special Cases

(I) $\hat{M} = 0$, Pure farfield tension (membrane loading)

$$A = \frac{\hat{N}c_4 - \frac{h_2-h_1}{2}\hat{N}c_2}{c_1c_4 - c_3c_2}, \quad (C27)$$

$$B = \frac{\frac{h_2-h_1}{2}\hat{N}c_1 - \hat{N}c_3}{c_1c_4 - c_3c_2}. \quad (C28)$$

(II) $\hat{N} = 0$, Pure bending

$$A = \frac{-\hat{M}c_2}{c_1c_4 - c_3c_2}, \quad (C29)$$

$$B = \frac{\hat{M}c_1}{c_1c_4 - c_3c_2}. \quad (C30)$$

Substituting (C26) into (C1) we have

$$RHS = 2(Ax + B). \quad (C31)$$

In case (I) $\hat{M} = 0$, dividing the entire equation by $2\hat{N}$, we can normalize the stress intensity factor with respect to

$$\sigma_N = \frac{8\mu_0}{(\kappa+1)} \sqrt{\frac{b-a}{2}} \hat{N} = \frac{N}{h_1} \sqrt{\frac{b-a}{2}} \quad (C32)$$

giving,

$$RHS = \frac{Ax + B}{\hat{N}}, \quad (C33)$$

$$k_{1n}(a) = \frac{\mu(a)}{\mu_0} F(-1), \quad (C34)$$

$$k_{1n}(b) = -\frac{\mu(b)}{\mu_0} F(1). \quad (C35)$$

In case (II) $\hat{N} = 0$, dividing the entire equation by $2\hat{M}$, we can normalize the stress intensity factor with respect to

$$\sigma_M = \frac{8\mu_0}{(\kappa+1)} \sqrt{\frac{b-a}{2}} \hat{M} = \frac{M}{h_1^2} \sqrt{\frac{b-a}{2}} \quad (C36)$$

giving,

$$RHS = \frac{Ax + B}{\hat{M}}, \quad (C37)$$

$$k_{1n}(a) = \frac{\mu(a)}{\mu_0} F(-1), \quad (C38)$$

$$k_{1n}(b) = -\frac{\mu(b)}{\mu_0} F(1). \quad (C39)$$

Thermal Loading

The thermal stress problem has been discussed in detail in Section 5.2. The expressions for $c_i (i = 1, \dots, 4)$ are as given in (C20 – C23). For uniform temperature change and for conduction case, the expressions for R_1 and R_2 are different. Hence the two cases are considered separately.

Uniform temperature change

R_1 and R_2 are given as,

$$R_1 = \frac{\alpha_0 \Delta T}{(\alpha + \beta) h_1} \left(1 - e^{-(\alpha + \beta) h_1} \right) + \alpha_0 \Delta T \frac{h_2}{h_1}, \quad (C40)$$

$$R_2 = \frac{\alpha_0 \Delta T}{h_1^2 (\alpha + \beta)} \left(h_1 e^{-(\alpha + \beta) h_1} - \frac{1 - e^{-(\alpha + \beta) h_1}}{(\alpha + \beta)} \right) + \alpha_0 \Delta T \frac{h_2^2}{2 h_1^2}. \quad (C41)$$

The right hand side can now be written as

$$RHS = \begin{cases} 2\alpha_0 \Delta T \left(-e^{\alpha x} + \frac{Ax+B}{\alpha_0 \Delta T} \right), & x < 0 \\ 2\alpha_0 \Delta T \left(\frac{Ax+B}{\alpha_0 \Delta T} \right), & x > 0 \end{cases} \quad (C42)$$

Dividing the entire equation by $2\alpha_0 \Delta T$ the stress intensity factor can now be normalized with respect to

$$\sigma_T = \frac{8\mu_0\alpha_0\Delta T}{1 + \kappa} \quad (C43)$$

giving,

$$RHS = \begin{cases} \left(-e^{\alpha x} + \frac{Ax+B}{\alpha_0\Delta T} \right), & x < 0 \\ \left(\frac{Ax+B}{\alpha_0\Delta T} \right), & x > 0 \end{cases} \quad (C44)$$

$$k_{1n}(a) = \frac{\mu(a)}{\mu_0} F(-1), \quad (C45)$$

$$k_{1n}(b) = -\frac{\mu(b)}{\mu_0} F(1). \quad (C46)$$

Steady state heat conduction

R_1 and R_2 are given as,

$$\begin{aligned} R_1 = & \frac{\alpha_0(\Delta T_1 - \Delta T_i)}{h_1(\alpha + \beta - \gamma)} \left(\frac{1 - e^{-(\alpha+\beta-\gamma)h_1}}{e^{\gamma h_1} - 1} \right) + \alpha_0 \left(\frac{\Delta T_i - \Delta T_1}{e^{\gamma h_1} - 1} + \Delta T_i \right) \left(\frac{1 - e^{-(\alpha+\beta)h_1}}{h_1(\alpha + \beta)} \right) \\ & + \alpha_0(-\Delta T_i) \frac{h_2}{2h_1} + \alpha_0(\Delta T_i) \frac{h_2}{h_1} \end{aligned} \quad (C46)$$

$$\begin{aligned} R_2 = & \frac{\alpha_0(\Delta T_1 - \Delta T_i)}{h_1^2(\alpha + \beta - \gamma)(e^{\gamma h_1} - 1)} \left(h_1 e^{-(\alpha+\beta-\gamma)h_1} - \frac{1 - e^{-(\alpha+\beta-\gamma)h_1}}{(\alpha + \beta - \gamma)} \right) \\ & + \alpha_0 \left(\frac{\Delta T_i - \Delta T_1}{e^{\gamma h_1} - 1} + \Delta T_i \right) \left(\frac{e^{-(\alpha+\beta)h_1}}{h_1(\alpha + \beta)} - \frac{1 - e^{-(\alpha+\beta)h_1}}{h_1^2(\alpha + \beta)^2} \right) \\ & + \alpha_0(-\Delta T_i) \frac{h_2^2}{3h_1^2} + \alpha_0(\Delta T_i) \frac{h_2^2}{2h_1^2} \end{aligned} \quad (C47)$$

The right hand side can now be written as

$$RHS = \begin{cases} 2\alpha_0\Delta T_1 \left(-e^{\alpha x} \frac{\Delta T(x)}{\Delta T_1} + \frac{Ax+B}{\alpha_0 T_1} \right), & x < 0 \\ 2\alpha_0\Delta T_1 \left(\frac{Ax+B}{\alpha_0 T_1} \right), & x > 0 \end{cases} \quad (C48)$$

Dividing the entire equation by $2\alpha_0\Delta T_1$ the stress intensity factor can now be normalized with respect to

$$\sigma_T = \frac{8\mu_0\alpha_0\Delta T_1}{1 + \kappa} \quad (C49)$$

giving,

$$RHS = \begin{cases} \left(-e^{\alpha x} \frac{\Delta T(x)}{\Delta T_1} + \frac{Ax+B}{\alpha_0 T_1} \right), & x < 0 \\ \left(\frac{Ax+B}{\alpha_0 T_1} \right), & x > 0 \end{cases} \quad (C50)$$

$$k_{1n}(a) = \frac{\mu(a)}{\mu_0} F(-1) \quad (C51)$$

$$k_{1n}(b) = -\frac{\mu(b)}{\mu_0} F(1) \quad (C52)$$

APPENDIX D

SOME USEFUL INTEGRATIONS

During the numerical analysis performed for this dissertation, some integrations were evaluated in the closed form. Closed form solutions have an advantage over numerical solutions in that the time spent during the numerical phase is considerably less. Also, the accuracy is much higher. In this appendix, the expressions for these closed form solutions are given.

In the analysis of internal cracks (Chapter 3), the following expressions were used:

$$\frac{1}{\pi} \int_{-1}^1 \frac{T_n(r)}{(r-s)\sqrt{1-r^2}} dr = U_{n-1}(s), \quad n \geq 1 \quad (D1)$$

$$\frac{1}{\pi} \int_{-1}^1 [\log|r-s|] \frac{T_n(r)}{\sqrt{1-r^2}} dr = -\frac{T_n(s)}{n}, \quad n \geq 1 \quad (D2)$$

In the analysis of edge cracks (Chapter 3), the following expressions were used:

$$\frac{1}{\pi} \int_{-1}^1 \frac{1}{(r-s)\sqrt{1-r^2}} dr = 0 \quad (D3)$$

$$\frac{1}{\pi} \int_{-1}^1 [\log|r-s|] \frac{1}{\sqrt{1-r^2}} dr = -\log(2) \quad (D4)$$

$$\frac{1}{\pi} \int_{-1}^1 \frac{1}{(r-s)\sqrt{1-r^2}} dr = \frac{\log|B|}{\sqrt{1-s}}, \quad |s| < 1 \quad (D5)$$

$$\frac{1}{\pi} \int_{-1}^1 \left[\log|r-s| \right] \frac{1}{\sqrt{1-r}} dr = -4\sqrt{2} + 2\sqrt{2} \log|1+s| + 2\sqrt{1-s} \log|B|, \quad (D6)$$

$$|s| < 1$$

where

$$B = \frac{1 + \sqrt{\frac{1-s}{2}}}{1 - \sqrt{\frac{1-s}{2}}} \quad (D7)$$

APPENDIX E

MATERIAL PROPERTIES

This appendix gives a table of material properties used in the numerical calculations in this dissertation. The values are taken from Noda et.al. [51]

	$k, W/mK$	E, MPa	$\alpha \times 10^6, 1/K$
<i>PSZ</i>	2.09	151	10
<i>Ti - 6Al - 4V</i>	7.5	116.7	9.5
<i>SUS304</i>	11.9	193	18.7
<i>Rene - 41</i>	25.5	219.7	16.7
<i>Molybdenum</i>	14.2	310	5.1
<i>Tungsten</i>	16.5	400	6.0

Table E.1 Thermal and mechanical properties for some commonly used materials

APPENDIX F
INTERNAL AND EDGE CRACK IN
NONHOMOGENEOUS HALF-PLANE

The geometry of this problem is shown in Fig *F.1*. The crack is located on the $y = 0$ plane from $x = a$ to $x = b$. If $a > 0$, we obtain an internal crack. If on the other hand $a = 0$, we obtain an edge crack.

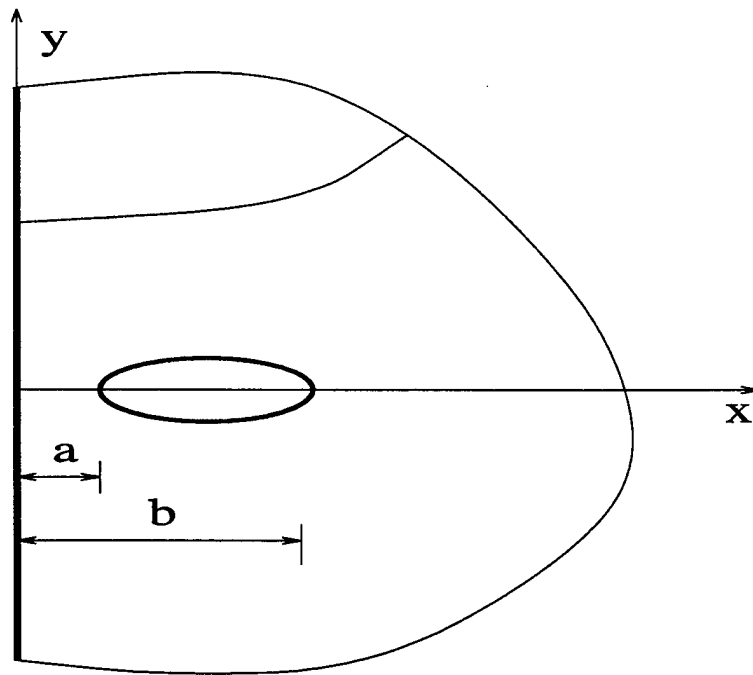


Figure *F.1* Geometry of the problem

Formulation of the problem

The governing equations for the nonhomogenous medium were developed in Section 2.3.1. They are as follows :

$$(1+\kappa)\frac{\partial^2 u}{\partial x^2} + (\kappa-1)\frac{\partial^2 u}{\partial y^2} + 2\frac{\partial^2 v}{\partial x \partial y} + \beta(1+\kappa)\frac{\partial u}{\partial x} + \beta(3-\kappa)\frac{\partial v}{\partial y} = 0, \quad (F1)$$

$$(\kappa-1)\frac{\partial^2 v}{\partial x^2} + (1+\kappa)\frac{\partial^2 v}{\partial y^2} + 2\frac{\partial^2 u}{\partial x \partial y} + \beta(\kappa-1)\frac{\partial v}{\partial x} + \beta(\kappa-1)\frac{\partial u}{\partial y} = 0 \quad (F2)$$

where β is the nonhomogeneity parameter. We use the superposition technique to find expressions for stresses and displacements in a manner similar to that discussed in Section 2.3.3. We superpose the solutions obtained from a nonhomogeneous plane with crack and those obtained from a nonhomogeneous half-space without a crack. The expressions for stresses and displacements thus obtained are as follows:

$$u = \frac{1}{2\pi} \int_{-\infty}^{\infty} \sum_{j=1}^2 m_j D_j(\alpha) e^{n_j y} e^{-i\alpha x} d\alpha + \frac{2}{\pi} \int_0^{\infty} \sum_{j=1}^2 q_j A_j(\alpha) e^{p_j x} \cos(\alpha y) d\alpha, \quad (F3)$$

$$v = \frac{1}{2\pi} \int_{-\infty}^{\infty} \sum_{j=1}^2 D_j(\alpha) e^{n_j y} e^{-i\alpha x} d\alpha + \frac{2}{\pi} \int_0^{\infty} \sum_{j=1}^2 A_j(\alpha) e^{p_j x} \sin(\alpha y) d\alpha, \quad (F4)$$

$$\sigma_{xx} = \frac{\mu_0 e^{(\beta x)}}{\kappa-1} \frac{1}{2\pi} \int_{-\infty}^{\infty} \sum_{j=1}^2 \left\{ -(\kappa+1)m_j i\alpha + (3-\kappa)n_j \right\} D_j(\alpha) e^{n_j y} e^{-i\alpha x} d\alpha + \frac{\mu_0 e^{(\beta x)}}{\kappa-1} \frac{2}{\pi} \int_0^{\infty} \sum_{j=1}^2 \left\{ (\kappa+1)q_j p_j + (3-\kappa)\alpha \right\} A_j(\alpha) e^{p_j x} \cos(\alpha y) d\alpha, \quad (F5)$$

$$\begin{aligned}\sigma_{yy} = & \frac{\mu_0 e^{(\beta x)}}{\kappa-1} \frac{1}{2\pi} \int_{-\infty}^{\infty} \sum_{j=1}^2 \left\{ -(3-\kappa)m_j i\alpha + (\kappa+1)n_j \right\} D_j(\alpha) e^{n_j y} e^{-i\alpha x} d\alpha + \\ & \frac{\mu_0 e^{(\beta x)}}{\kappa-1} \frac{2}{\pi} \int_0^{\infty} \sum_{j=1}^2 \left\{ (3-\kappa)q_j p_j + (\kappa+1)\alpha \right\} A_j(\alpha) e^{p_j x} \cos(\alpha y) d\alpha,\end{aligned}\quad (F6)$$

$$\begin{aligned}\tau_{xy} = & \mu_0 e^{(\beta x)} \frac{1}{2\pi} \int_{-\infty}^{\infty} \sum_{j=1}^2 \left\{ -i\alpha + m_j n_j \right\} D_j(\alpha) e^{n_j y} e^{-i\alpha x} d\alpha + \\ & \mu_0 e^{(\beta x)} \frac{2}{\pi} \int_0^{\infty} \sum_{j=1}^2 \left\{ p_j - q_j \alpha \right\} A_j(\alpha) e^{p_j x} \sin(\alpha y) d\alpha.\end{aligned}\quad (F7)$$

Expressions for p_j 's, q_j 's, m_j 's and n_j 's are provided in Appendix A and in Chapter 2. The unknowns A_1 , A_2 , D_1 and D_2 are evaluated from the boundary conditions which can be expressed as

$$\sigma_{xx}(0, y) = 0, \quad (F8)$$

$$\tau_{xy}(0, y) = 0, \quad (F9)$$

$$\tau_{xy}(x, 0) = 0, \quad 0 < x < \infty, \quad (F10)$$

$$\sigma_{yy}(x, 0) = p(x), \quad a < x < b, \quad (F11)$$

$$v(x, 0) = 0, \quad 0 < x < a, \quad b < x < \infty. \quad (F12)$$

Development of the Integral Equation

Using (F7) and (F10), it may be seen that,

$$\begin{aligned}\mu_0 e^{(\beta x)} \frac{1}{2\pi} \int_{-\infty}^{\infty} \sum_{j=1}^2 \left\{ -i\alpha + m_j n_j \right\} D_j(\alpha) e^{n_j y} e^{-i\alpha x} d\alpha \Big|_{y \rightarrow 0} + \\ \mu_0 e^{(\beta x)} \frac{2}{\pi} \int_{-\infty}^{\infty} \sum_{j=1}^2 \left\{ p_j - q_j \alpha \right\} A_j(\alpha) e^{p_j x} \sin(\alpha y) d\alpha \Big|_{y \rightarrow 0} = 0.\end{aligned}\quad (F13)$$

Taking now the Fourier inverse transform, we have,

$$D_1(\alpha) = -\frac{(m_2 n_2 - i\alpha)}{(m_1 n_1 - i\alpha)} D_2(\alpha). \quad (F14)$$

We define new unknown function,

$$g(x) = \frac{\partial v}{\partial x}(x, 0) \quad a < x < b. \quad (F15)$$

Now taking Fourier inverse transform of (F4) and using (F14), (F15) we obtain

$$D_2(\alpha) = \frac{(m_1 n_1 - i\alpha)}{(m_1 n_1 - m_2 n_2)} \frac{i}{\alpha} \int_a^b g(t) e^{i\alpha t} dt. \quad (F16)$$

By using the two homogeneous boundary conditions (F8) and (F9) and the expressions from (F5) and (F7), after taking the appropriate Sine or Cosine transforms we can write a system of two algebraic equations in two unknowns. The system of equations we obtain is as follows:

$$a_{11} A_1 + a_{12} A_2 = R_1^*, \quad (F17)$$

$$a_{21} A_1 + a_{22} A_2 = R_2^* \quad (F18)$$

where

$$a_{11} = (\kappa + 1)q_1 p_1 + (3 - \kappa)\alpha, \quad (F19)$$

$$a_{12} = (\kappa + 1)q_2 p_2 + (3 - \kappa)\alpha, \quad (F20)$$

$$a_{21} = p_1 - q_1 \alpha, \quad (F21)$$

$$a_{22} = p_2 - q_2 \alpha, \quad (F22)$$

$$R_1^* = \int_a^b g(t) R_1(\alpha, t) dt, \quad (F23)$$

$$R_1 = -\frac{\kappa - 1}{\kappa + 1} \alpha^2 e^{(-t(d - \frac{\epsilon}{2}))} \left(\frac{-c\beta \cos(ct) + (2c^2 + 2d^2 - d\beta) \sin(ct)}{cd(c^2 + d^2)} \right), \quad (F24)$$

$$R_2^* = \int_a^b g(t) R_2(\alpha, t) dt, \quad (F25)$$

$$R_2 = \frac{2}{\kappa+1} \alpha e^{(-t(d-\frac{\beta}{2}))} \left(\frac{-c(d^2+c^2+\frac{\beta^2}{4})\cos(ct)+d(c^2+d^2-\frac{\beta^2}{4})\sin(ct)}{cd(c^2+d^2)} \right), \quad (F26)$$

$$c = \sqrt{\frac{d^*-c^*}{4}}, \quad (F27)$$

$$d = \sqrt{\frac{d^*+c^*}{4}}, \quad (F28)$$

$$c^* = \alpha^2 + \frac{\beta^2}{4}, \quad (F29)$$

$$d^* = \sqrt{(\alpha^2 + \frac{\beta^2}{4})^2 + \alpha^2 \delta^2}, \quad (F30)$$

$$\delta = \sqrt{\left(\frac{3-\kappa}{1+\kappa}\right)} \beta. \quad (F31)$$

The pair of algebraic equations in (F16) and (F17) can be solved using Cramer's rule.

The solution thus obtained can be expressed as

$$A_1 = \frac{a_{22}R_1 - a_{12}R_2}{a_{11}a_{22} - a_{12}a_{21}}, \quad (F32)$$

$$A_2 = \frac{a_{11}R_2 - a_{21}R_1}{a_{11}a_{22} - a_{12}a_{21}}. \quad (F33)$$

By using the mixed boundary condition in (F11), and using (F14), (F16), (F31), (F32) we can now write the integral equation as

$$\begin{aligned}
& \frac{1}{\pi} \int_a^b g(t) dt \int_0^\infty \left\{ \text{Re}(\widehat{k}_1) \cos(\alpha(t-x)) - \text{Im}(\widehat{k}_1) \sin(\alpha(t-x)) \right\} d\alpha \\
& + \frac{1}{\pi} \int_a^b g(t) dt \int_0^\infty \widehat{k}_2(\alpha, x, t) d\alpha = p(x) \frac{\kappa - 1}{\mu_0 e^{\beta x}}
\end{aligned} \tag{F34}$$

where

$$\begin{aligned}
\widehat{k}_1(\alpha, x, t) = & - \frac{\left((1 + \kappa)n_1 - (3 - \kappa)i\alpha m_1 \right) (m_2 n_2 - i\alpha)}{i\alpha(m_2 n_2 - m_1 n_1)} \\
& + \frac{\left((1 + \kappa)n_2 - (3 - \kappa)i\alpha m_2 \right) (m_1 n_1 - i\alpha)}{i\alpha(m_2 n_2 - m_1 n_1)},
\end{aligned} \tag{F35}$$

$$\begin{aligned}
\widehat{k}_2(\alpha, x, t) = & \frac{\left((1 + \kappa)\alpha + (3 - \kappa)q_1 p_1 \right) (a_{22} R_1 - a_{12} R_2) e^{p_1 x}}{a_{11} a_{22} - a_{12} a_{21}} \\
& + \frac{\left((1 + \kappa)\alpha + (3 - \kappa)q_2 p_2 \right) (a_{11} R_2 - a_{21} R_1) e^{p_2 x}}{a_{11} a_{22} - a_{12} a_{21}}.
\end{aligned} \tag{F36}$$

Extracting the singular part of the kernel in a manner identical to that in Section 3.1.3, we obtain,

$$\frac{1}{\pi} \int_a^b \left[\frac{1}{t-x} + K(x, t) \right] g(t) dt = p(x) \frac{\kappa + 1}{4\mu_0 e^{\beta x}} \tag{F37}$$

where

$$\begin{aligned}
K(x, t) = & \frac{1}{4} \left(\frac{\kappa + 1}{\kappa - 1} \right) \left(\int_0^\infty \left\{ \text{Re}(\widehat{k}_1) \cos(\alpha(t-x)) \right. \right. \\
& \left. \left. - (\text{Im}(\widehat{k}_1) + 4 \left(\frac{\kappa - 1}{\kappa + 1} \right) \sin(\alpha(t-x)) + 2\widehat{k}_2(\alpha, x, t)) \right\} d\alpha \right).
\end{aligned} \tag{F38}$$

It should be noted here that $K(x, t)$ contains a generalized Cauchy kernel as was found in Chapter 3. To extract the generalized Cauchy kernel, we need to perform asymptotic analysis on $\hat{k}_2(\alpha, x, t)$ as $\alpha \rightarrow \infty$. The behavior of $\hat{k}_2(\alpha, x, t)$ as $\alpha \rightarrow \infty$ can be expressed as

$$\hat{k}_2(\alpha, x, t) \sim \left(c_1^* \alpha^2 + c_2^* \alpha + c_3^* + \frac{c_4^*}{\alpha} \right) e^{(x+t)\alpha}. \quad (F39)$$

The expressions for c_i^* 's are as given in Appendix B where $x_1 + h_1$ is now replaced by x and $t_1 + h_1$ is replaced by t .

Singularities at crack tips

Internal crack

For $a > 0$, we obtain an internal crack. This case is identical to that discussed in Section 3.3.1. It should be noted here that the coordinate axis is shifted in this analysis. But that does not affect the evaluation of the singularities in any way. We find that,

$$\alpha_1 = \beta_1 = \frac{1}{2} \quad (F40)$$

and the unknown function can be expressed as

$$g(t) = \frac{g^*(t)}{(t-a)^{\frac{1}{2}}(b-t)^{\frac{1}{2}}} \quad (F41)$$

where $g^*(t)$ is a bounded function.

Edge crack

For $a = 0$, we obtain an edge crack. This case is similar to the case discussed in Section 3.3.4. The singularities obtained are as follows:

$$\alpha_1 = 0, \beta_1 = \frac{1}{2}. \quad (F42)$$

We can now express the unknown function as

$$g(t) = \frac{g^*(t)}{(b-t)^{\frac{1}{2}}} \quad (F43)$$

where again $g^*(t)$ is a bounded function.

Numerical Procedure

Internal crack

We normalize the singular integral equation in (F36) using

$$t = \frac{b-a}{2}r + \frac{b+a}{2}, \quad (F44)$$

$$x = \frac{b-a}{2}s + \frac{b+a}{2}. \quad (F45)$$

Thus we obtain,

$$\frac{1}{\pi} \int_{-1}^1 \left[\frac{1}{(r-s)} + \tilde{K}(s, r) \right] \tilde{g}(r) dr = \tilde{p}(s) \frac{\kappa+1}{4\mu_0} \quad (F46)$$

where

$$\tilde{K}(s, r) = \left(\frac{b-a}{2} \right) K \left(\frac{b-a}{2}s + \frac{b+a}{2}, \frac{b-a}{2}r + \frac{b+a}{2} \right), \quad (F47)$$

$$\tilde{g}(r) = g \left(\frac{b-a}{2}r + \frac{b+a}{2} \right), \quad (F48)$$

$$\tilde{p}(s) = p \left(\frac{b-a}{2}s + \frac{b+a}{2} \right). \quad (F49)$$

Using (F40), (F43) and (F44), we can express the unknown function as follows:

$$\tilde{g}(r) = \frac{F(r)}{\sqrt{1-r^2}} \quad (F50)$$

where $F(r)$ is a bounded function. It may be expressed as

$$F(r) = \sum_{n=0}^N A_n T_n(r). \quad (F51)$$

Substituting (F49) and (F50) into (F45) we obtain,

$$\frac{1}{\pi} \sum_{n=0}^N A_n \int_{-1}^1 \left[\frac{1}{(r-s)} + \tilde{K}(s, r) \right] \frac{T_n(r)}{\sqrt{1-r^2}} dr = \tilde{p}(s) \frac{\kappa+1}{4\mu_0}. \quad (F52)$$

The single valuedness condition dictates that $A_0 = 0$. Converting equation (F51) into a set of algebraic equations as explained in Chapter 4 we obtain,

$$\frac{1}{\pi} \sum_{n=1}^N A_n \int_{-1}^1 \left[\frac{1}{(r-s_k)} + \tilde{K}(s_k, r) \right] \frac{T_n(r)}{\sqrt{1-r^2}} dr = \tilde{p}(s_k) \frac{\kappa+1}{4\mu_0} \quad (k = 1..N) \quad (F53)$$

where the collocation points are chosen as follows:

$$s_k = \frac{(2k-1)\pi}{2N} \quad (k = 1..N). \quad (F54)$$

Edge crack

Normalizing the singular integral equation in (F36) using

$$t = \frac{b}{2}r + \frac{b}{2}, \quad (F55)$$

$$x = \frac{b}{2}s + \frac{b}{2}. \quad (F56)$$

we obtain,

$$\frac{1}{\pi} \int_{-1}^1 \left[\frac{1}{(r-s)} + \tilde{K}(s, r) \right] \tilde{g}(r) dr = \tilde{p}(s) \frac{\kappa+1}{4\mu_0} \quad (F57)$$

where

$$\tilde{K}(s, r) = \left(\frac{b}{2}\right) K\left(\frac{b}{2}s + \frac{b}{2}, \frac{b}{2}r + \frac{b}{2}\right), \quad (F58)$$

$$\tilde{g}(r) = g\left(\frac{b}{2}r + \frac{b}{2}\right), \quad (F59)$$

$$\tilde{p}(s) = p\left(\frac{b}{2}s + \frac{b}{2}\right). \quad (F60)$$

Using (F42), (F55) and (F56) we can express the unknown density function as follows:

$$\tilde{g}(r) = \frac{F(r)}{\sqrt{1-r}} \quad (F61)$$

where $F(r)$ is a bounded function. It may be expressed as

$$F(r) = \sum_{n=0}^N A_n T_n(r). \quad (F62)$$

Substituting (F60) and (F61) into (F56) we obtain,

$$\frac{1}{\pi} \sum_{n=0}^N A_n \int_{-1}^1 \left[\frac{1}{(r-s)} + \tilde{K}(s, r) \right] \frac{T_n(r)}{\sqrt{1-r}} dr = \tilde{p}(s) \frac{\kappa+1}{4\mu_0}. \quad (F63)$$

We can convert this integral equation into a set of linear algebraic equations as discussed in Chapter 4. Thus we obtain

$$\frac{1}{\pi} \sum_{n=0}^N A_n \int_{-1}^1 \left[\frac{1}{(r-s_k)} + \tilde{K}(s_k, r) \right] \frac{T_n(r)}{\sqrt{1-r}} dr = \tilde{p}(s_k) \frac{\kappa+1}{4\mu_0} \quad (k = 1..N) \quad (F64)$$

where the collocation points are chosen as follows:

$$s_k = \frac{(2k-1)\pi}{2(N+1)} \quad (k = 1..N+1). \quad (F65)$$

Numerical Results

Table *F.1* provides the normalized stress intensity factors for an edge crack in a nonhomogeneous half-space subjected to fixed grip loading. The results are evaluated for various values of the normalized nonhomogeneity parameter βb where b is the crack length. These results have also been plotted in Fig *F.1*.

βb	$\frac{k_1}{\sigma\sqrt{b}}$	βb	$\frac{k_1}{\sigma\sqrt{b}}$
0.0001	1.121523	− 0.0001	1.1215
0.1	1.1550	− 0.1	1.1139
0.2	1.2039	− 0.2	1.1185
0.3	1.2635	− 0.3	1.1293
0.4	1.3324	− 0.4	1.1440
0.5	1.4103	− 0.5	1.1611
0.6	1.4971	− 0.6	1.1796
0.7	1.5931	− 0.7	1.1989
0.8	1.6987	− 0.8	1.2185
0.9	1.8146	− 0.9	1.2377
1.0	1.9413	− 1.0	1.2561

Table *F.1* Normalized stress intensity factors for edge crack in nonhomogeneous half space subjected to fixed grip loading.

$$\sigma = \frac{8\mu_0\epsilon_0}{1 + \kappa}.$$

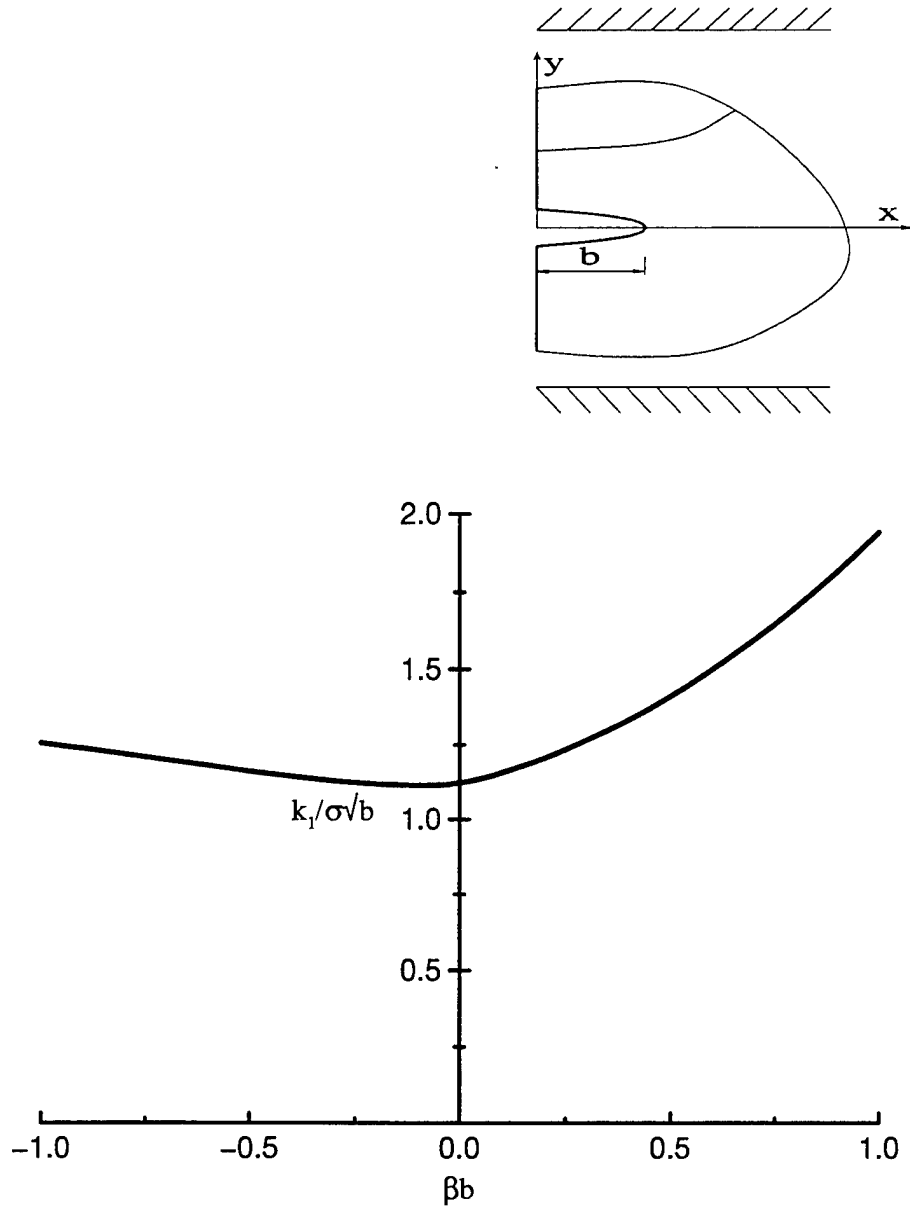


Figure *F.2* Normalized stress intensity factor for a nonhomogeneous half-plane as a function of normalized nonhomogeneity parameter βb under fixed grip loading.

$$\sigma = \frac{8\mu_0\epsilon_0}{1 + \kappa}.$$